Fundamental Study and Development of 0-3 Dielectric Composites with High Dielectric Constant

by

Lin Zhang

A dissertation submitted to the Graduate Faculty of
Auburn University
in partial fulfillment of the
requirements for the Degree of
Doctor of Philosophy

Auburn, Alabama
August 3, 2013

Keywords: Dielectric, composite, conducting polymer, ferroelectric polymer, percolation theory, dielectric loss

Approved by

Zhongyang Cheng, Chair, Professor of Materials Engineering
Barton C. Prorok, Professor of Materials Engineering
Dong-Joo Kim, Associate Professor of Materials Engineering
Xinyu Zhang, Assistant Professor of Polymer and Fiber Engineering

Abstract

Dielectric composites are promising materials for many applications. Polymer-based 0-3 composites with a high dielectric constant represent an important category of dielectric composites being studied in research.

Different conductors were used as filler for 0-3 dielectric composites. By combining solution casting and hot-pressed processing, two nanocomposites with nano-sized Ni particles embedded into copolymer poly (vinylidene fluoride-co-trifluoroethylene) [P(VDF-TrFE)70/30 mol%] and poly (vinylidene fluoride-co-chlorotrifluoroethylene) [P(VDF-TrFE) 88/12 mol%] have been prepared. Uniform dispersion of nanoparticles in nanocomposite materials was achieved by improvement of processing conditions. Dielectric constants of more than 1000 with relatively low loss were obtained in both systems. Both composites had a high percolation threshold (φ_c>50 vol.%), making the material reproducible for practical applications.

Novel all-organic dielectric composites based on polypyrrole (PPy) nanoclips were prepared by the same process as Ni-polymer composites. Due to their 2D structure and large surface area, the composites were highly flexible with a high dielectric constant and a low φ_c (φ_c<8 wt.%). Dielectric constant more than 1000 was obtained in PPy-P(VDF-TrFE) composites. The dielectric constant of a composite with 8 wt.% of

PPy is more than 100 times higher than that of the P(VDF-TrFE)70/30 matrix, rising to 1200 at room temperature.

From study of Ni-polymer composites and PPy-polymer composites, a new dielectric process was observed in both composites, which was a relaxation process with a very low relaxation frequency. There are three mechanisms in this conductor-polymer composite: 1) the dielectric relaxation process from the polymer matrix, 2) the new dielectric relaxation process from the composite, and 3) the conductivity of the conducting filler.

From study of Ni-polymer composites and PPy-polymer composites, the φ_c and critical value (s) of composite are different with the selecting data at different frequency and temperature. This conclusion was confirmed using six reported systems with different conducting fillers from literature. High length-to-width ratio may cause much of the difference in φ_c and s with different frequencies.

The mechanism behind the dielectric properties of conductor-dielectric composites was explained in this dissertation by introducing the dielectric loss (or conductivity). In this research, the contribution of the loss to the effective dielectric constant (ε_{eff}) is dependent on the microstructure of the composite. Three different models were studied: the series model is for 2-2 composite, Maxwell model is for 0-3 composite and Lichtenecker's logarithmic mixing model leads itself to 0-0 composite. The conductivity of matrix and filler both have much effect on the dielectric constant and loss. A way to develop composites with high dielectric constant and low loss was introduced.

Acknowledgments

I would like to express my deepest and sincere appreciation to my advisor Prof. Zhongyang Cheng for his expert guidance, support and persistent encouragement during my graduate studies at Auburn University. I would like to emphasize that his influence on me was not only with regards to scientific knowledge but also as a person.

I would like to give my sincere thanks to my committee members and university reader, Dr. Barton C. Prorok, Dr. Dong-Joo Kim, Dr. Xinyu Zhang, and Dr. Minseo Park for their generous guidance and insightful suggestions. Special thanks to Mr. Roy Howard, Mr. L.C. Mathison, and Mr. Steven Moore for their general technical support.

Special thanks also go to all my graduate friends, especially group members: Dr. Suiqiong Li, Dr. Xiaobing Shan, Dr. Liling Fu, Dr. Kewei Zhang, Dr. Peixuan Wu, Dr. Anxue Zhang, Wei Wang, Koichi Yamaguchi, Zhizhi Sheng, Patrick Bass, Yang Tong, Wenya Du, Naved Siddiqui, and Victor Agubra. Thanks also go to Dr. Zhen Liu for preparation of the conducting polymers, Dr. Xiaogang Wang for preparation of the composites, Dr. Zhimin Dang for providing their experimental data, Dr. Xu Lu and Dr. Li Jin for measurement of dielectric properties at low temperature. I also would like to thank some of my friends: Dr. Wen Shen, Dr. Dan Liu, Dr. Yu Zhao, Dr. Zijie Cai, Dr. Yingjia Liu, Dr. Xiaoyun Yang, Dr. Yajiao Yu, Jing Dai, Yating Chai,

Honglong Wang, Xiaolong Wang, Naved Siddiqui and Victor Agubra. My time in this PhD program has been more fun and interesting with them together.

Most importantly, I wish to express my love and gratitude to my father, my mother, and my brother for their great love, emotional support, and encouragement which inspire me all the time during my studies and also throughout my life.

Table of Contents

List of Tables

List of Figures

CHAPTER 1

Introduction and Literature Review

1.1. Fundamentals of Dielectrics

Dielectrics are widely used in electronic and electrical devices/systems [1-3]. The performance of a dielectric material is characterized by their complex permittivity (ε^*) for the dielectrics used under weak electric field, by their polarization-electric field (*P-E*) relationship and their breakdown field (i.e., dielectric strength, E_b) for dielectrics used under a high electric field. Based on the applications, there are different needs for dielectric materials. For some applications, such as insulation materials of integrated circuit, dielectrics with a low dielectric constant (i.e., low-k materials) are highly desirable, while for some other applications, such as gate dielectrics in field-effect transistors, dielectrics with a high dielectric constant are preferred. Dielectrics used under a high electric field generally require a high E_b with low loss at the applied electric field.

1.1.1. Dielectrics and Capacitance

A dielectric is an electrical insulator which can respond to an external stimulation, electrical field, $\vec{E}$, with electrical polarization, $\vec{P}$, which reflects the induced dipole moments $\vec{p}$ as [4, 5]:

$$\vec{P} = \frac{\sum_{i=1}^{N} \vec{p}}{dv} \tag{1-1}$$

The permittivity ε^* is defined by:

$$\vec{D} = \varepsilon_0 \vec{E} + \vec{P} \tag{1-2}$$

$$\vec{D} = \varepsilon^* \vec{E} = \varepsilon_r^* \varepsilon_0 \vec{E} \tag{1-3}$$

where $\vec{D}$ is electric displacement, ε_0 is the permittivity of vacuum (8.8542×10^{-12} $C^2/J\cdot m$), ε^* is permittivity of the material, ε_r^* is relative permittivity ($= \varepsilon^*/\varepsilon_0 = \varepsilon'_r - j\varepsilon''_r$). ε'_r is typically called the dielectric constant. Combining equations (1-2) and (1-3), results that:

$$\vec{P} = (\varepsilon_r^* - 1)\varepsilon_0 \vec{E} \tag{1-4}$$

Due to the complex nature of ε_r^*, there is a phase difference between $\vec{D}$ and $\vec{E}$. The phase difference defines the dielectric loss ($tan\delta$) as:

$$\tan\delta = \frac{\varepsilon''_r}{\varepsilon'_r} \tag{1-5}$$

where δ reflects the phase difference 90-δ between the $\vec{D}$ and $\vec{E}$.

When an AC electric field with a sinusoidal wave function at an angular frequency, ω, (i.e. $E(t)=E_0 sin(\omega t)$, where E_0 is a constant and t is the time) is applied onto a dielectric, there is a displacement current going through the dielectric, the density of displacement current is

$$J_D = \frac{\partial D(t)}{\partial t} = j \cdot \omega \cdot \varepsilon_0 \cdot \varepsilon_r^* \cdot E(t) \tag{1-6}$$

If the dielectric has a non-zero electric conductivity, σ, there will be a conducting current, the density of the conducting current is

$$J_C = \sigma \cdot E(t) \tag{1-7}$$

Therefore, the total current going through a real dielectric would be

$$J_T = J_D + J_C = \left[j\omega\varepsilon_0 \varepsilon_r^*(\omega) + \sigma \right] \cdot E(t) \tag{1-8}$$

That is, if a dielectric with non-zero electric conductivity is experimentally characterized, the response includes both the dielectric and electric conductive response. If the measured response is treated as the dielectric response only, the electric conductivity would contribute to the measured imaginary part of the permittivity as

$$\varepsilon_{con}^{''} = \frac{\sigma}{\varepsilon_0 \cdot \omega} \tag{1-9}$$

In this case, the measured permittivity and its imaginary part are

$$\varepsilon_{r,meas}^{*}(\omega) = \varepsilon_r'(\omega) - j\left[\varepsilon_r''(\omega) + \frac{\sigma}{\varepsilon_0 \omega}\right] \tag{1-10a}$$

$$\varepsilon_{r,meas}''(\omega) = \varepsilon_r''(\omega) + \frac{\sigma}{\varepsilon_0 \omega} \tag{1-10b}$$

The corresponding dielectric loss is

$$\tan\delta = \frac{\varepsilon_r'' + \dfrac{\sigma}{\varepsilon_0 \omega}}{\varepsilon_r'} \tag{1-11}$$

If the dielectric is treated as a conductor,

$$\sigma_{\mathrm{Re}al}(\omega) = \sigma_0 + \varepsilon_0 \cdot \omega \cdot \varepsilon_{r,meas}''(\omega)$$

(1-12)

1.1.2. Mechanism of Polarization

The dielectric response, $\vec{P}$, in a dielectric material may originate from different mechanisms [4, 5]. For a homogeneous material, the dielectric responses have, in general, four mechanisms (as illustrated in **Figure 1-1**).

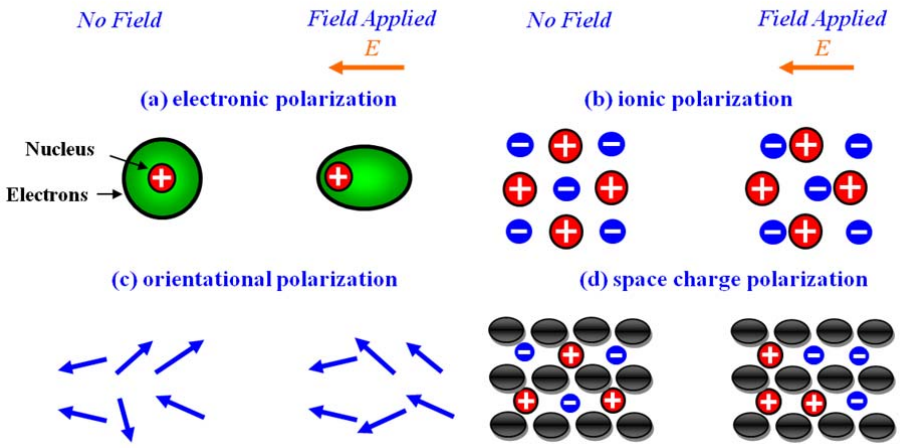

Figure 1-1. Schematic of (a) electronic polarization, (b) ionic polarization, (c) orientational polarization, (d) space charge polarization.

(1) *Electronic polarization*: The electric field causes the displacement of the outer electron cloud from the inner positive nucleus. This polarization has a response time of 10^{-14}~10^{-16} *s* and is independent of temperature.

(2) *Ionic polarization*: Ions response to an electric field with a change in the relative distance in between ions. The response time is about 10^{-12}~10^{-13} *s* and is almost independent of temperature.

(3) *Orientational Polarization*: If there are dipoles existing in a material, the electric field $\vec{E}$ would generate a torque on each dipole and the torque would cause the dipoles align along the electric field direction. The response time is about 1~10^{-8} *s* and is strongly dependent on temperature.

(4) *Space charge polarization*: When the space charge appears in the dielectric material, the electric field, $\vec{E}$, generates a force on the particle, which separate the positive and negative charges. Therefore, there are some dipole moments formed. The response time is large than 10^{-5}~1 *s* which is strongly

dependent on temperature.

The dielectric response of each polarization mechanism changes with frequency *f*, but with different patterns. The electronic and ionic polarization result in a dielectric response, while the response of the orientational and space charge is relaxation polarization. The ε^* versus frequency for a dielectric with all four polarization mechanisms is shown in **Figure 1-2**.

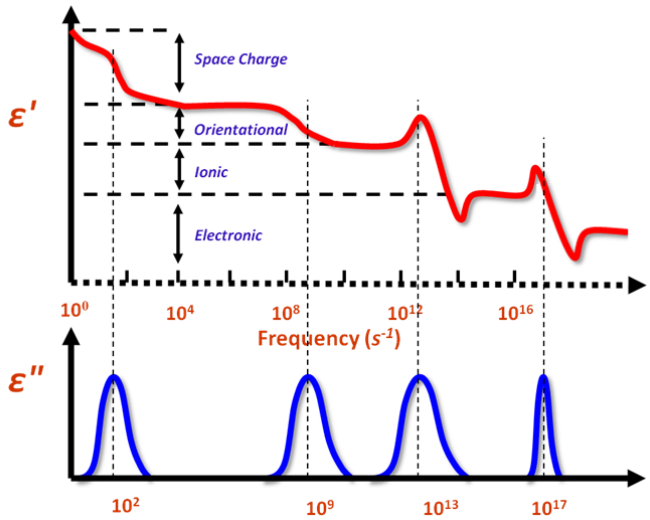

Figure 1-2. Frequency dependence of the permittivity for a dielectric with four different types of dielectric responses: (a) real part and (b) imaginary part.

1.1.3. Dielectric Relaxation

In classical physics, the dielectric relaxation is often described using simple Debye equation as:

$$\varepsilon^*_r(\omega) = \varepsilon_\infty + \frac{\varepsilon_s - \varepsilon_\infty}{1 + j\omega\tau_0} \tag{1-13}$$

$$\varepsilon'_r = \varepsilon_\infty + \frac{\varepsilon_s - \varepsilon_\infty}{1 + \omega^2\tau_0^2} \tag{1-14}$$

$$\varepsilon''_r = \frac{(\varepsilon_s - \varepsilon_\infty)\omega\tau_0}{1 + \omega^2\tau_0^2} \tag{1-15}$$

$$\tan\delta = \frac{\varepsilon''_r}{\varepsilon'_r} = \frac{(\varepsilon_s - \varepsilon_\infty)\omega\tau_0}{\varepsilon_s + \varepsilon_\infty\omega^2\tau_0^2} \tag{1-16}$$

where τ_0 is the so-called relaxation time of the relaxation process ($f_0=\omega_0/2\pi = 1/2\pi\tau_0$ is called the relaxation frequency), ε_s is the static permittivity (ω=0), ε_∞ is the permittivity at high frequency limit ($\omega=\infty$). The "ε_s-ε_∞" reflects the contribution of the relaxation process to the static dielectric constant and is also called as the permittivity strength of the relaxation process. The schematic dependence of ε'_r, ε''_r and $tan\delta$ on the angular frequency, ω, based on Debye equation is shown in **Figure 1-3**. At the relaxation frequency, the imaginary part of the permittivity reaches its maximum, while the dielectric loss reaches its maximum at a frequency, $(\varepsilon_{rs}/\varepsilon_{r\infty})^{1/2}(\tau_0)^{-1}$ ($>\omega_0$).

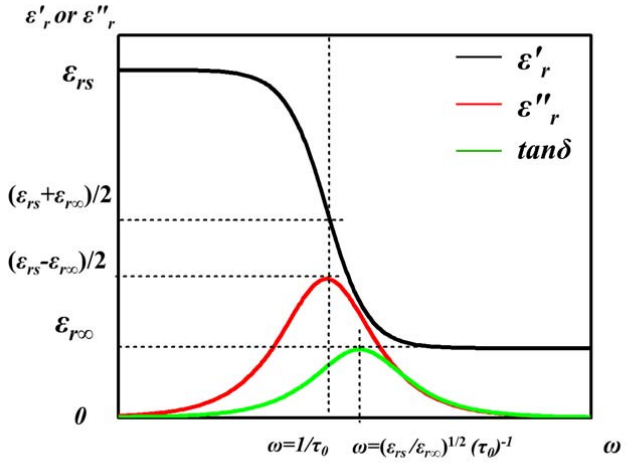

Figure 1-3. Frequency dependence of ε'_r, ε''_r and $tan\delta$ calculated using Debye equation.

It should be mentioned that the Debye equation describes the dielectric response of the simplest case of a relaxation process. For a real material, the frequency dependence of the permittivity is usually much more complicated. In these cases, the concept of multiple relaxation times is used. That is, Eq. (1-13) becomes:

$$\varepsilon^*_r(\omega) = \sum_{i=1}^{n}\left[\varepsilon_{\infty,i} + \frac{\Delta\varepsilon_i}{1 + j\omega\tau_{0,i}}\right] \quad (i=1, 2, 3\ldots n) \tag{1-17}$$

where $\tau_{0,i}$ is the relaxation times of the i^{th} relaxation process, $\Delta\varepsilon_i$ is the permittivity strength of the i^{th} relaxation process, $\varepsilon_{s,i}$ is the multiple static permittivity (ω=0). When there are too many relaxation times, a distribution of relaxation time is usually used. All of these relaxation processes make the frequency dependence of the dielectric constant much more complicated.

In 1980s, Johnscher took a new approach to study the dielectric response [6]. In his approach, the imaginary part of the permittivity is used and plotted versus frequency as shown in **Figure 1-4**.

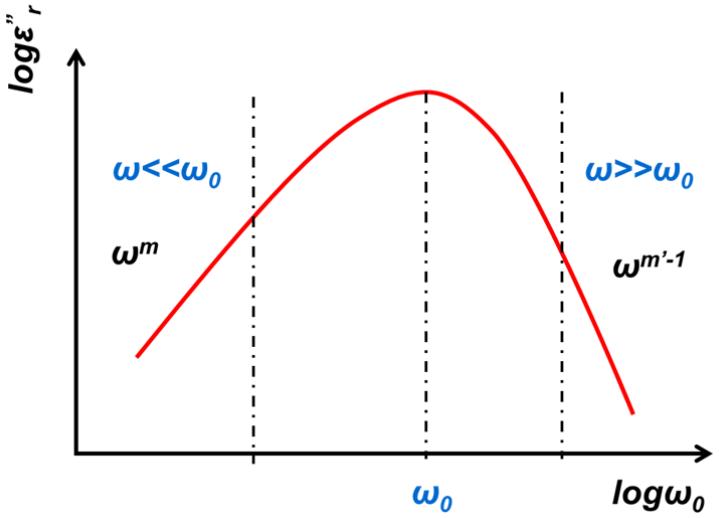

Figure 1-4. The schematic of ε''_r as a function of ω in log-log relationship.

It is observed that $\log\varepsilon''_r \sim \log\omega$ shows a linear relationship when the frequency is much higher or lower than the relaxation frequency, ω_0. That is,

$$\varepsilon''_r \propto \omega^m \quad (\omega << \omega_0) \tag{1-18}$$

$$\varepsilon''_r \propto \omega^{m'-1} \quad (\omega >> \omega_0) \tag{1-19}$$

Based on this approach and the results from many dielectrics, it is concluded that $0<m<1$ and $0<m'<1$. Actually, for a simple Debye process described by Debye equation Eq. (1-12), $m=1$ and $m'=0$.

Considering the conductivity discussed in Section 1.1.1, the electrical conductivity will contribute to the measured ε''_r. When Johnscher's approach is used, the imaginary part of the measured permittivity can be written as

$$\varepsilon''_{r,meas}(\omega) = \omega^m + \frac{\sigma_0}{\varepsilon_0 \omega} \tag{1-20}$$

If the measured electric conductivity is used, one can get that the real part of the measured electrical conductivity is dependent on the frequency as:

$$\sigma_{meas}(\omega) = \sigma_0 + A \cdot \omega^{m+1} = \sigma_0 + A \cdot \omega^n \tag{1-21}$$

where σ_0 is electric conductivity (a constant), A and n are constants.

1.2. Dielectric Materials

Various dielectrics, such as gases, liquids, and solids, are widely used in the current industry for different applications based on their different and unique dielectric properties [7-12]. All dielectric materials can be classified either by its structure or its composition.

By the structure, dielectrics can be classified into two major categories: nonpolar materials and polar materials [1]. A nonpolar material is a material whose molecule or unit cell does not have a permanent dipole moment. A polar material is a material possessing a permanent dipole moment which is associated with its molecule or unit cell. In some of the polar materials, the interaction among these dipoles is so

strong that these dipoles align along the same direction, which results in a spontaneous polarization P_s (i.e. the material has a polarization without an electric field applied on it). These materials are named as pyroelectric materials. The pyroelectric materials have a critical temperature (i.e. Curie temperature). The material is pyroelectric when the temperature is lower than the Curie temperature, while the material is paraelectric (PE) when the temperature is higher than the Curie temperature. If the P_s in a pyroelectric material can be switched by an external electric field, the material is called as ferroelectric (FE) material. Since the electric field can switch the P_s in a ferroelectric, FE materials usually exhibit a very high dielectric constant, especially at temperature around the FE-to-PE phase transition temperature.

By the composition, dielectrics can be classified into inorganic and organic materials. With regard to solid dielectrics, both polymers and inorganic compounds are widely used. In general, polymers have a low processing temperature, are flexibility with the ability to withstand a high mechanical impact, and exhibit a high breakdown field, but exhibit a lower dielectric constant. Inorganic dielectrics exhibit a high dielectric constant, but require a high process temperature and are brittle with a lower breakdown field. All of these materials are of interest for many applications.

1.2.1. Inorganic Dielectric Materials

For the nonpolar inorganic materials, they usually have a low dielectric constant, such as $\varepsilon_{\text{silicon}}\approx 3.7$, $\varepsilon_{\text{diamonds}}\approx 5.5\sim 10$, $\varepsilon_{\text{parfin}}\approx 1.9\sim 2.5$, $\varepsilon_{\text{carbon tetrachloride}}\approx 2.0$ and $\varepsilon_{\text{Quartz}} \approx 4.4$ [1]. R. F. Cava *et al.* reported a dielectric material $(Ta_2O_5)_{0.92}$-$(TiO_2)_{0.08}$ which has a relative high dielectric constant (~126 at room temperature) [11].This is

the highest dielectric constant found to date in a nonpolar material.

The polar inorganic materials such as the ferroelectric ceramics and crystals, usually exhibit a high dielectric constant (~10^3). For example, the widely studied/used ferroelectric $BaTiO_3$ (BT) exhibits a dielectric constant of 1500. The dielectric constant of other ceramics $Pb(Mg_{1/3}Nb_{2/3})O_3$(PMN) and $Pb(Zr_{0.52}Ti_{0.48})O_3$(PZT) at 1 kHz are larger than 1000, such as ε_{PMN}=5500, ε_{PZT}=1300, etc [12, 13]. Although these ferroelectrics exhibited a high dielectric constant, their dielectric constant is strongly dependent on temperature. For example, their dielectric constant shows a maximum at the FE-to-PE phase transition temperature as shown in **Figure 1-5(a)**. At temperature higher than this phase transition temperature, the dielectric constant is dependent on the temperature by the Curie-Weiss law as [12]:

$$\varepsilon'_r = \frac{C}{T - T_c} \tag{1-22}$$

where T_c is the Curie temperature and C is the Curie constant.

Some ferroelectric based solid solution ceramics/crystals, such as PMN, exhibit a so-called relaxor ferroelectric behavior. The relaxor ferroelectrics have a weaker temperature dependence on the dielectric constant than the ferroelectrics at temperatures around Curie temperature. And they exhibit a very high dielectric constant in a broad temperature range as shown in **Figure 1-5(a)**. However, the dielectric constant of the relaxor ferroelectrics is still strongly dependent on the temperature, and more importantly, their dielectric constant is strongly dependent on the frequency as shown in **Figure 1-5(b)**.

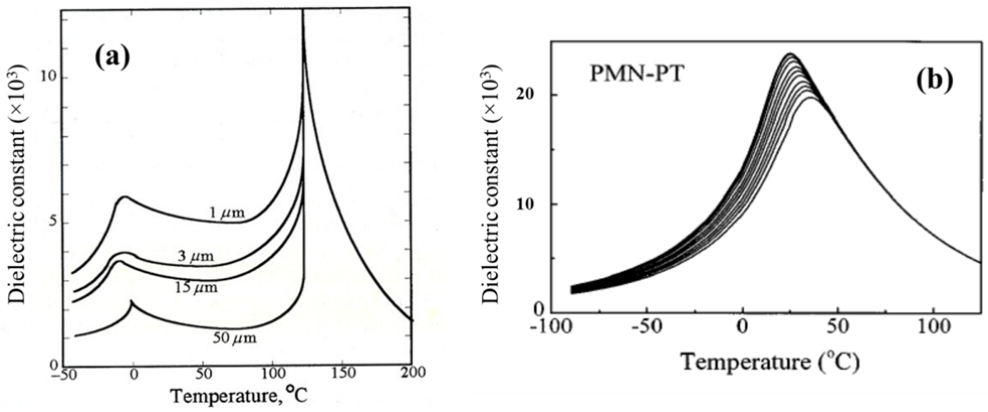

Figure 1-5. Dielectric constant versus temperature. (a) $BaTiO_3$ FE ceramics with different grain sizes at frequency of 1 kHz [13]; (b) 0.9PMN-0.1PT Relaxor FE ceramics different frequencies from 100 Hz to 100 kHz [14].

In the last 15 years, some inorganic non-ferroelectric materials with very high dielectric constant (~10^4) have been developed, such as $CaCu_3Ti_4O_{12}$ (CCTO), $Bi_{2/3}Cu_3Ti_4O_{12}$ or in the $ACu_3Ti_4O_{12}$ family. These materials are very interesting for dielectric study and applications. Among these materials, CCTO is of interest since it exhibits a high dielectric constant that is nearly independent of the temperature over a broad temperature range from 100 to 400 K at frequencies below 1 MHz [15, 16].

1.2.2. Dielectric Polymers

Various polymers, such as epoxy, polyethylene (PE), polyester (PS), poly(methyl methacrylate) (PMMA), poly(vinyl chloride) (PVC), polyurethanes (PU), and Polytetrafluoroethylene (PTFE) have been studied as dielectrics based on their processibility, flexibility, dielectric response, dielectric strength, melting temperature and glass transition temperature for different applications. The non-polar polymers exhibit a small dielectric constant. For example, ε_{epoxy}=4, ε_{PE}=2.2~2.4, ε_{PS}=2.8~4.5, ε_{PTFE}=2.1, etc [7-13].

To achieve a high dielectric constant in polymers, polar polymers have been

widely studied and used as dielectrics. Ferroelectric poly(vinylidene fluoride) (PVDF) is the most studied polar polymer. PVDF homopolymer and PVDF-based copolymers and terpolymers, such as poly(vinylidene fluoride-trifluoroethylene) [P(VDF-TrFE)], poly(vinylidene fluoride-chlorotrifluoroethylene) [P(VDF-CTFE)], poly(vinylidene fluoride-hexafluoropropylene) [P(VDF-HFP)] and P(VDF-TrFE-CFE), have been developed and studied as dielectrics [17-25]. All these polymers exhibit a dielectric constant around 10 at room temperature and their dielectric constant can be as high as ~70 at their FE-to-PE phase transition temperature, as shown in **Figure 1-6(a)**. The PVDF-based ferroelectric polymer can also be modified into relaxor ferroelectrics by irradiation as shown in **Figure 1-6(b)**.

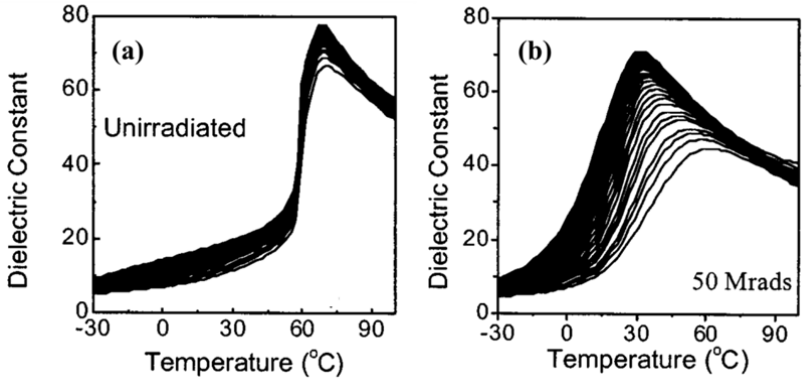

Figure 1-6. Dielectric constant at different frequencies versus temperature for P(VDF-TrFE) films during cooling with a rate of 2 °C/min: (a) unirradiated and (b) irradiated under 50 Mrads [18].

The ferroelectricity in polymers originates from the dipole associated with the configuration of polymer chain, such as (-CH_2-CF_2-) in PVDF has a dipole moment of about 7.06×10^{-30} Cm. For PVDF-based copolymers, TrFE and CTFE are very interesting since these copolymers exhibit a high electromechanical response and have a high energy storage capability. The difference and similarity among VDF, TrFE, and

CTFE monomers are shown in **Figure 1-7**.

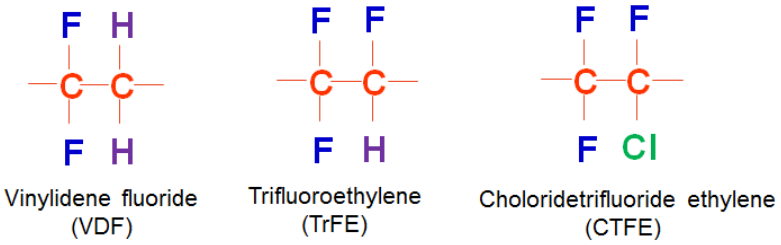

Figure 1-7. The chemical units of VDF, TrFE and CTFE.

1.3. Dielectric Composites

A composite is a mixture of materials with significantly different physical or chemical properties in an attempt to obtain some advanced properties. The physical properties of a composite can be the sum, combination, and product of the properties of its constituents based on their physical properties and connectivity. For example, the total mass of a composite is simply the sum of the mass of each constituent. The connectivity was first classified by Newnham *et al* [26]. For the composites with two constituents, their connectivity can be defined as 0-0, 1-0, 2-0, 3-0, 1-1, 2-1, 3-1, 2-2, 3-2, and 3-3 as shown in **Figure 1-8**, where 0/1/2/3 represent the number of dimension in continuity for each component in the composite [27-31]. For example, a 0-3 composite is defined as 0-dimention (i.e. isolated) of a particle is embedded in 3-dimention of a continuous media. The matrix is the "glue" that holds the composite together and usually the softer phase compared to filler [6, 31].

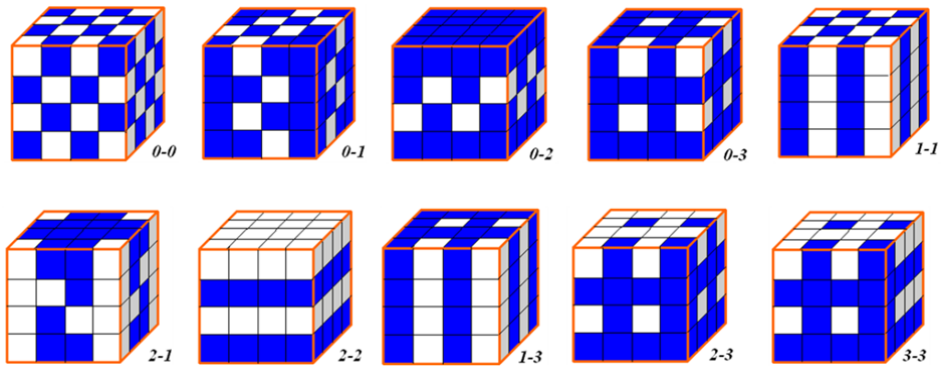

Figure 1-8. Ten connectivity patterns in diphasic composite [27].

Dielectric materials which are flexible with a low processing temperature, exhibit a high dielectric constant, and have a high breakdown field, are required for many applications. To meet these different needs dielectric composites, especially 0-3 composites using dielectric polymer as matrix, have been widely studied in last three decades.

Based on the fillers used, the polymer-based 0-3 composites can be classified into two types: one is dielectric-dielectric composites in which the fillers are dielectric materials; the other is conductor-dielectric composites where the fillers are conducting materials as shown in **Figure 1-9** [32, 33].

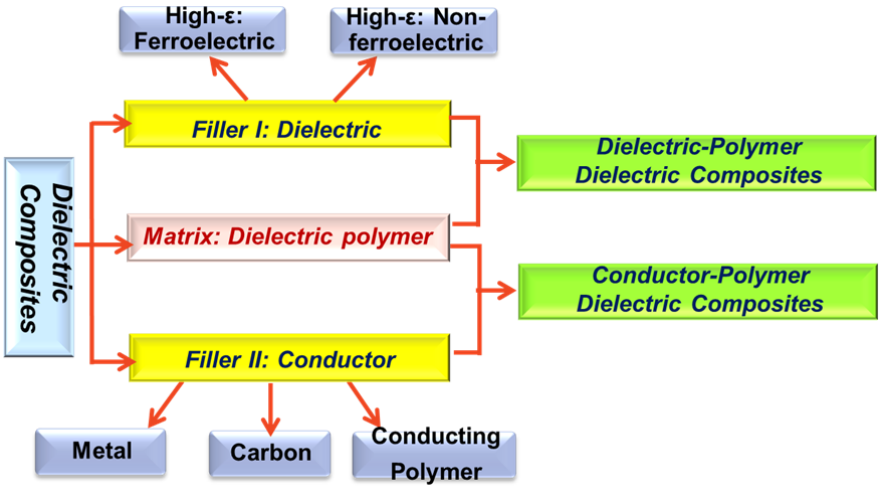

Figure 1-9. Schematic of two types of polymer-based 0-3 composites.

In both types of composites, the polymer matrix plays a key role in the dielectric performance of the composites. For example, the breakdown field of a composite is mainly dependent on the polymer matrix; the dielectric constant of a composite is strongly dependent on the dielectric constant (ε_m) of the polymer matrix. Therefore, many polymers, such as PMMA, PVC, PU, PVDF and its co/ter-polymer, have been used in the development of composites [21-25].

The dielectric property of a conductor-dielectric composite is determined by the percolation phenomenon [32]. That is, when the volumetric content of conducting filler is lower than a certain value (i.e. percolation threshold φ_c), the composite is an insulator/dielectric and the dielectric constant increases with increasing filler content. As the filler content approaches the φ_c, the dielectric constant increases with increasing filler content very rapidly so that a giant dielectric constant may be obtained in the composites close to φ_c. If the filler content is higher than the φ_c, the composite is a conductor. Therefore, the φ_c is very critical for a conductor-dielectric composite. The φ_c is dependent on the geometry, shape, size, distribution of the conducting fillers [33, 34]. Therefore, conducting fillers with various shapes (spherical, core-shell, tube, and bar/wire like) ranging in size from micrometers to nanometers have been studied [35-38]. Semiconductors have also been used as fillers [39-41]. It should be mentioned that it has been experimentally demonstrated/found that the φ_c is also strongly dependent on the process used to prepare the composite. This is related to the distribution of the filler, since for the same composite system, different process can result in different distribution of the filler, which can have

different φ_c.

For dielectric-dielectric composites, it is extremely important to find fillers with a high dielectric constant. Therefore, many ferroelectric and relaxor ferroelectrics have been widely used in the development of dielectric-dielectric composites due to the fact that these materials exhibit a high dielectric constant as described in Section 1.2.1[42-47]. Since the discovery on high dielectric constant in CCTO [48, 49], it has been of interest in utilizing CCTO for the development of composites. This is a new avenue for the development of dielectric composites [50].

The effective dielectric property, ε_{eff}, of a composite is certainly dependent on the volumetric fraction (φ) of the filler and the properties of the filler and matrix. However, the exact relationship between the dielectric property of the composite and each constitutes can be very different.

1.4. Polymer Based 0-3 Conductor-Dielectric Composites

1.4.1. Percolation Theory

The effective dielectric constant of a 0-3 conductor-dielectric composite is dependent on the volumetric content of conductor filler as shown in **Figure 1-10**. At the lower concentration of filler, conductive particles are separated from each other and randomly distributed into the matrix. The corresponding electric properties of the composites are dominated by the matrix. With increasing filler concentration, local clusters of particles begin to form and the dielectric constant increases. As the filler content approaches a certain value, the pattern of conductive particles creates the infinite conductive cluster and a network of channels connected by the conductive

fillers. At the same time, the dielectric constant increases abruptly, reaching a very high value. This critical value of filler content is the so-called percolation threshold, where the φ_c is the composition at which the conductor particles form channels through the composite [32, 36]. The φ_c is dependent of many factors, such as size, shape, as well as their distribution of filler particles, microstructure of the composite. For a real conductor-dielectric composite, the φ_c is dependent on the microstructure of the composite.

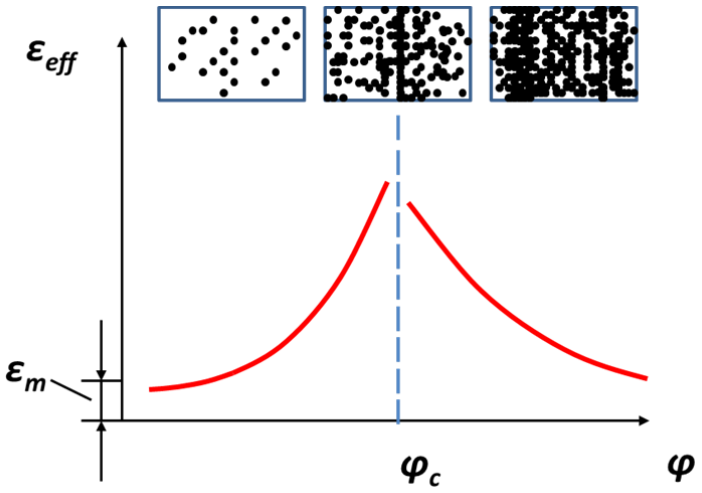

Figure 1-10. Effective dielectric constant of a 0-3 conductor-dielectric composite versus the volumetric content of conducting filler (φ), where φ_c is the percolation threshold (dashed blue line). The insets show the microstructure of the composite.

For ordered binary composites, if the filler particles are spherical with the same diameter, a φ_c of 74%, 68% and 52% can be obtained for the filler particles with an ordered face centered cubic (FCC), body centered cubic (BCC), and simple cubic (SC) structure, respectively. For a truly random distribution of the filler, the φ_c is one third [51]. Certainly, the size and shape of the conducting filler particles as well as their orientation also have a strong influence on the φ_c [32]. For a real composite,

determining the φ_c can be a challenge.

The shape of filler can be roughly classified into two types: one is spherical fillers and another is ellipsoidal fillers (including bar, tube, fiber etc.). If the composite is treated as a random mixture of two types of spherical particles, the particle size of the matrix is R_1 and the particle size of the filler is R_2, It is obtained that the φ_c is about ~0.16 for R_1/R_2~1 and larger than 0.16 if R_1/R_2>>1 [36, 52]. A continuous percolating cluster of the minor phase is formed at φ_c<0.16. The φ_c of the composites with spherical filler can be smaller than 0.1 by use of this approach. For ellipsoidal fillers, because it is easy for ellipsoidal fillers to connect with each other, the φ_c value may decrease to much less than 0.16. For ellipsoidal fillers with a large aspect ratio [i.e., p = (length of the long axis)/(length of the short axis)], it was obtained that $\varphi_c \propto 1/p$, (i.e., φ_c decreases with an increase in the aspect ratio), as shown in **Figure 1-11**[32, 53].

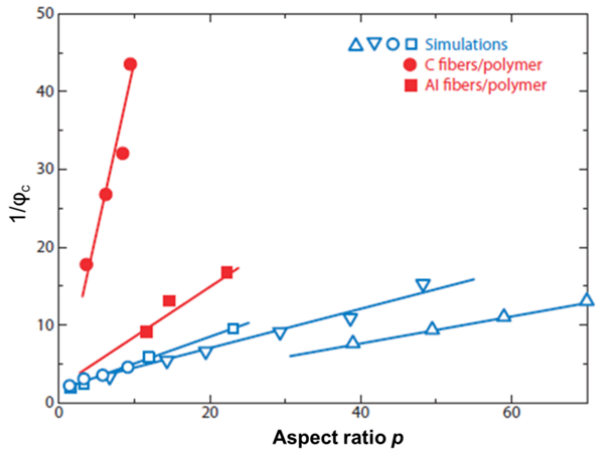

Figure 1-11. Dependence of φ_c on the aspect ratio p of the fillers in composites filled with randomly oriented C and Al fibers [32, 55].

For the composites in the insulator regime ($\varphi<\varphi_c$), the dependence of the effective dielectric constant on the filler content has been an interesting topic in last three

decades. Actually, the influence of the conducting metal filler on the dielectric response of a dielectric was first recognized, independently by Cavendish in 1773 and Faraday in 1837 when they connected a dielectric with a metal in series [54, 55]. Maxwell showed the residual-charge effect which can be accounted for different materials connected by a parallel pattern having different dielectric properties and conductivities [55]. The effective dielectric response of this series connection of an ideal dielectric and an ideal conductor is:

$$\frac{1}{\varepsilon^*_{eff}(\omega)} = \sum_{k=1}^{n} \frac{\varphi_k}{\left[\varepsilon'_k - j\left(\frac{\sigma_k}{\omega\varepsilon_0}\right)\right]} \tag{1-23}$$

where φ_k, ε_k, σ_k are the volume fraction, dielectric constant and conductivity of the k^{th} component, respectively (k=1, 2, 3…n). For a real composite, it can be a challenge to simulate the effective dielectric response of a composite. For example, the conductivity of the filler and the connectivity/microstructure of the composite as well as the size and shape of the filler particles will play some role.

For a typical binary mixture, a dielectric sphere with radius a and relative dielectric constant, ε_1, are surrounded by a spherical shell with outer radius b and relative dielectric constant, ε_2. The volume fraction φ is $(a/b)^3$. The effective dielectric constant of this system is

$$\varepsilon_{eff} = \varepsilon_2 \frac{\left[1 - 2\varphi\frac{\varepsilon_2 - \varepsilon_1}{2\varepsilon_2 + \varepsilon_1}\right]}{\left[1 + \varphi\frac{\varepsilon_2 - \varepsilon_1}{2\varepsilon_2 + \varepsilon_1}\right]} \tag{1-24}$$

Wagner considered a sphere as a conductor with a conductivity σ dispersed in a non-conducting media with relative dielectric constant, ε,

$$\varepsilon_1 = -j\frac{\sigma}{\omega\varepsilon_0} \quad \text{and} \quad \varepsilon_2 = \varepsilon \tag{1-25}$$

Combining Eq. (1-25) with Eq. (1-24),

$$\varepsilon_{eff}(\omega) = \varepsilon_\infty(\omega) + \frac{\left[\varepsilon_{eff}(0) - \varepsilon_{eff}(\infty)\right]}{\left[1 + j\omega\tau\right]} \tag{1-26}$$

In which

$$\varepsilon_{eff}(\infty) = \lim_{\omega\to\infty}\varepsilon_{eff}(\omega) = \frac{2\varepsilon(1-\varphi)}{2+\varphi} \tag{1-27a}$$

$$\varepsilon_{eff}(0) = \frac{\varepsilon(1+2\varphi)}{1-\varphi} \tag{1-27b}$$

$$\tau = \frac{\varepsilon_0\varepsilon(2+\varphi)}{\sigma(1-\varphi)} \tag{1-27c}$$

Based on a random resistance network model [56], it was concluded that the ε_{eff} at low frequency can be approximately expressed as

$$\varepsilon_{eff} \propto \left[A(\varphi_c - \varphi)^\alpha + B(\varphi_c - \varphi)^\beta\right]^{-1} \tag{1-28}$$

where $\varphi < \varphi_c$, $A > 0$, $B > 0$, $\alpha > 0$, and $\beta > 0$. For a random binary system, it was obtained as

$$\varepsilon_{eff} \propto \varepsilon_m(\varphi_c - \varphi)^{-s} \tag{1-29}$$

where $\varphi < \varphi_c$ and s (> 0) are constants [57]. A numerical simulation was used to determine the value of s. It was concluded that $s \approx 0.7$ [58].

Equation (1-29) is much simpler than Eq. (1-28). Therefore, Eq. (1-29) is widely used in the literature to fit experimental results [32-37]. In the literature, Eq. (1-29) is normalized as:

$$\varepsilon_{eff} = \varepsilon_m\left(\frac{\varphi_c - \varphi}{\varphi_c}\right)^{-s} \tag{1-30}$$

since the dielectric constant of the composite should be ε_m when $\varphi = 0$.

It was also found that the ε_{eff} of a conductor-dielectric composite with φ close to φ_c is strongly dependent on the frequency. For example, it was showed that [56]:

$$\varepsilon_{eff} \propto \omega^{\gamma-1} \tag{1-31}$$

where γ (<1) is a constant and ω is the angular frequency. Based on numerical simulations, the value of γ has been proposed. For a random resistance networks, it was indicated that $\gamma \approx 0.73 \pm 0.05$ [56], while for a random binary medium, it was indicated that $\gamma = 0.75 \pm 0.05$ [57]. It should be mentioned that, in reality, the composite with a composition close to φ_c may have a much higher conductivity than what has been obtained from theory research since quantum mechanical tunneling through the insulating barriers may not be ignorable.

The conductor-dielectric composite has been widely studied for the development of composites with high a dielectric constant since the 1980s [38, 39, 55, 57]. In last 30 decades, conductor-dielectric composites using dielectric polymers as matrix have been extensively studied due to the composites flexibility. The polymer based conductor-dielectric composites studied so far can be classified into three categories based on the conductor filler: 1) metal; 2) carbon-based filler; 3) conducting polymer (CP). Metal particles are the most commonly used as conductor filler due to the fact that these particles can be easily prepared.

1.4.2. Metal Particles Embedded in Polymer

Metal-polymer composites have been widely studied and employed for different applications, such as for static or electromagnetic interference (EMI) shielding [59,

60]. Particles of various metals have been used in the development of composites with high a dielectric constant, such as Ni, Ag, Cu, and Al, which are the most commonly used for metals, as shown in **Table 1-1** [61-70]. For example, a dielectric constant as high as 2000 has been reported for an epoxy filled with 10 μm silver flakes [65]. It was experimentally found that the composites with nano-sized metal particles have a lower dielectric constant and a low dielectric loss than that with micro-sized metal particles. In an Al-epoxy composite [68], a dielectric constant around 100 and loss tangent around 0.02 were also observed. This could be attributed to tunneling network composed of the self-passivated Al particles with thick outside Al_2O_3 shells.

Ni is one of the more popular metals that have been studied by different groups [61-64]. *Panda* et al [61] observed a threshold composition of 0.278 in cold compacted Ni-PVDF. Further, they also prepared composites using 20μm Ni particles. In this case, the percolation threshold increased to 0.57 vol.% of Ni [62]. The mixture pressed at room temperature under 30 MPa for nano-size composites and 8 MPa for micro-size composites, respectively. The φ_c obtained in the composites with nano-sized fillers was lower than with micro-sized fillers. This indicated that the size, shape of the filler, and its volume fraction in the composite actually play a significant role in the dielectric constant and the percolation threshold by affecting the distance between particles and the interfacial area between filler and matrix.

Table 1-1. The dielectric properties of conductor-polymer composites

Filler	Matrix	Filler's size	Dielectric properties			Parameters			*Freq* (Hz)	Ref
			φ_m	$\varepsilon_{r\,max}$	$tan\delta$	φ_c	s	γ		
Metal										
Ni	PVDF	20-30nm	28%	1273	2.04	27.8%	0.82		1k	[61]
Ni	PVDF	20μm	57%	995	~1	57.2%	0.72		1k	[62]
Ni	PVDF	5μm	20%	400	0.18	17%	0.89		100	[63]
Ni	PVDF	50nm	20%	70	<0.1	20%	-		1k	[64]
Ag flake	epoxy	10 μm	11.4%	2000	0.24				10k	[65]
Ag	PVDF	D: 100nm L: 20μm	2%	379	0.25	20%	0.89		1k	[66]
Ag	PI	0.5μm	12.5%	400	-	12.2%	0.27			[67]
Al	epoxy	3μm	80%	30	0.02				1k	[68]
Cu	PE	20-25μm	20%	50	0.04				1k	[69]
Steel	PVDF	D:30μm L:500μm	10%	427	800	9.4%	0.36		50	[70]
Carbon										
CF	PE	D: 2-8μm L: 100μm	30%	35	<0.2	30%	1	0.82	200k	[71]
CF	PVDF	D: 8μm L: 100μm	7.4%	80	<0.1	6.6%	0.86	0.82	1k	[72]
Carbon	PU	130nm	10%	2000	1000	10%	1.78		129	[73]
MWCNT	PVDF	-	2%	300	<0.8	1.6%	0.31		1k	[74]
MWCNT	PVDF	D:10-20nm L:30μm	6%	1500	<2	3.8%	1.05		1k	[75]
MWCNT	PVDF	D:10-30nm L:10μm	15%	5000	<2	8%	1.63		1k	[76]
MWCNT	PVDF	D:20-40nm L:15μm	12%	2000	1	10.4%	1.06		1k	[77]
Graphite	PVDF	D:0.5-25μm T:20-60μm	2.34%	$>10^7$	>200	1.01%	0.76		100	[78]
Graphite	HDPE	10-20μm	10%	4000	>800	4%	0.76	0.78	50k	[79]
MWCNT	LDPE	D:20-40nm L:5-15μm	10%	400		9.6%			1	[80] [81]
MWCNT	PVDF	D:20-40nm L:5-15μm	13%	6000		9.2%			1	[81]
Conducting polymer										
PANI	P(VDF-TrFE-CFE)	<1 μm	25.1%	5500	0.6	25.9%	0.95	0.79	1k	[82]
PANI	PVDF	D:20-50nm L:0.1-0.2μm	2.9wt%	700	<1	2.9wt%	-		100	[83]
PANI	PVDF	100nm	5%	400	<1	4.2%	0.3		1k	[84]
PANI	PVDF	100nm	20wt%	170	0.8	27%	0.48		100	[85]

Compared to Panda, Dang *et al.* demonstrated ideal percolative behavior in hot-molded Ni (micro-size)-PVDF composites with a percolation threshold Ni vol%=0.17 [63]. They hot pressed the composite under 10MPa at 200^{o}C instead of room temperature. Again, it is demonstrated that composites with nano-sized metal particles have a lower dielectric constant (ε_r~70) with a low dielectric loss (<0.1) compared to those with micro-sized metal particles (ε_r~400) [63]. Xu *et al.* used a solution method, KH550 coupling agent and pressed under 18MPa at 200^{o}C to improve the dispersion and affinity of Ni particles in the PVDF matrix [64]. The dielectric constant was found to be 70 with a loss smaller than 0.1 at 1 kHz with the Ni vol% is 20%. All of these results indicate that dielectric properties of the metal-polymer composite are dependent on processing conditions and size.

1.4.3. Carbon Filler Embedded in Polymer

Percolation thresholds can be significantly reduced by using a conductor fiber, as shown in **Table 1-1** [71-81]. For example, composites made of carbon fiber filling PVDF resulted in the φ_c smaller than 10% [72, 74-76]. Additionally, fiber-based composites should have a better flexibility than the particle-based composites. Although different fibers have been studied, most of efforts were given to carbon fiber and carbon nanotube (CNT) due to the fact that they can be easily prepared with a larger length(L)/diameter(D) ratio. This aspect ratio can be tuned over a great range [76-78]. Carbon fillers have a higher intrinsic conductivity (10^5~10^8 S/m) and a significantly lower density than metals. More importantly, carbon-based fillers have a high compatibility with polymer matrices. CNT has a higher aspect ratio and a much

higher conductivity and flexibility compared to carbon fibers. Therefore, a higher dielectric response is expected and obtained in CNT-based composites. For example, a dielectric constant of 1000 has been reported in several composites [75-78]. Unfortunately, the composites using a conducting fiber as a filler exhibited a very high loss.

1.4.4. Conducting Polymer Embedded in Polymer

Recently, all-organic composites have been developed using conducting polymers (CP) as filler which have a high dielectric constant [82-85]. There are three main reasons that the conducting polymer is a good candidate filler for the development of composites with high dielectric constant. Firstly, the CP have an inherent advantage that the conductivity can be adjusted by very simple inorganic/organic acid doping. Secondly, CP-dielectric polymer composites are all-organic composites which may be prepared as homogeneous films resulting in good mechanical properties. Thirdly, the organic interface bonding between two polymers may be prepared in polymerization at one time. The polyaniline (PANI)-PVDF composites have been studied over the wide ranges of temperatures and frequencies. Huang *et al.* reported that the composite had a very high dielectric constant (>5000) and low loss (0.6) at 1 kHz [82]. Moreover, this composite was very flexible which show high electromechanical response. To improve the interface bonding between two polymers, organic acid was used as a doping agent, (Dodecylbenzene sulfonic acid (DBSA) [83, 85] and perfluorosulfonic acid (PFSA) [83]). The PFSA can improve the performance of the PANI because it serves as a surface passivation layer for the conductive fillers. The dielectric

properties and parameters of percolation characterizations are listed in **Table 1-1**. It can be concluded that the CP-polymer composites are promising. However, their development is limited by the size and shape of CP available fillers.

1.4.5. Summary of Conductor-Polymer Composites

The conductor-dielectric composites can exhibit a high dielectric constant when the filler concentration is close to the φ_c (can be as small as 10 vol.%). Unfortunately, these composites exhibit a high dielectric loss and a low E_b. This can be reduced by using a high insulating barrier between the filler and matrix. For example, core-shell particles, which have a thin insulator shell, show some promises [86-90]. However, further research is needed.

As discussed in Section 1.4.1, the φ_c is dependent of many factors, especially the microstructure of the composite, which is strongly dependent on preparation process. If the conducting fillers disperse homogeneously in the matrix, the clusters in percolation theory have a high φ. That is, a high φ_c can be achieved by improving the filler distribution using different processes.

However, it is very risky to prepare composite with a low φ_c due to the abrupt variation of dielectric constant near the threshold. A small deviation from the φ_c could result in significant drop of the dielectric constant, making it rather difficult to control the parameters of the preparation process. That is, low φ_c composites require not only the precise control of filler loading but extremely uniform distribution of the filler in the matrix. Compared to composites with low φ_c, composites with high φ_c have a wider "safe" range of volume fraction, which makes the material reproducible for

application, and can achieve higher dielectric constants.

CP based composites are promising due to their good mechanical properties. However, the availability of CP particles is limited. Their size and shape are not well controlled and most CP are spheres or fibers.

1.5. Dielectric-Dielectric Composites

Understanding the dielectric response of a composite (or heterogeneous dielectrics) has been an interesting topic for fundamental research and applications. Actually, the dielectric property of a heterogeneous dielectric is one of earliest researched topics for the physics of dielectrics. For reasons of mathematical analogy, all the results are valid for dielectric constant, electric conductivity, heat conductivity, and diffusivity of such materials. Actually, many of models/formulas presented below for the calculation of the dielectric property of a composite were originally developed for the calculation of the conductivity or diffusivity of a mixture

To determine the dielectric constant of a real composite, the polarization response to an electric field of a region that is filled with different dielectrics in some arbitrary way has to be calculated. This is an impossible task even if the detailed information about the dielectric constant and spatial distribution of each constitute is given [51]. Therefore, various models have been introduced to simulate the composites and many formulas have been proposed to describe the composition dependence of the dielectric constant for 0-3 composites. Some of these formulas are purely empirical, while some are based on simplified models of a composite/mixture with approximations in their derivation. In all these formulas, the dielectric property (i.e. the effective dielectric

constant ε_{eff}) of the composite is expressed as a function of composite's composition (i.e. the content of fillers or volume fraction of fillers, φ), dielectric constant, ε_m, of matrix and the dielectric constant, ε_f, of the filler materials. In some models/formulas, one more parameter related to the filler particles, such as shape and orientation were also used.

1.5.1. Dielectric Physics of Composite with Simple Configuration

The most known models/formulas are two extremely simplified cases: parallel and series models/cases as shown in **Figure 1-12**, in which two dielectrics are used. The ε_{eff} of the mixture can be simply written as:

$$\varepsilon_{eff}^{\ n} = \varphi_1 \varepsilon_1^{\ n} + \varphi_2 \varepsilon_2^{\ n} \tag{1-32}$$

where φ_1 and φ_2 ($\varphi_1 + \varphi_2 = 1$) are the volume fraction of the dielectric 1 and dielectric 2, respectively, ε_1 and ε_2 are the dielectric constant of dielectric 1 and dielectric 2, respectively, and the n is either +1 for parallel case or -1 for series case. The dependence of ε_{eff} on the volume fraction of the dielectric 1 or dielectric 2 is plotted for series and parallel in **Figure 1-13**.

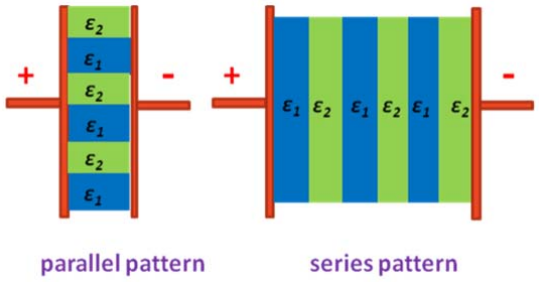

Figure 1-12. Schematic of parallel pattern and series pattern**.**

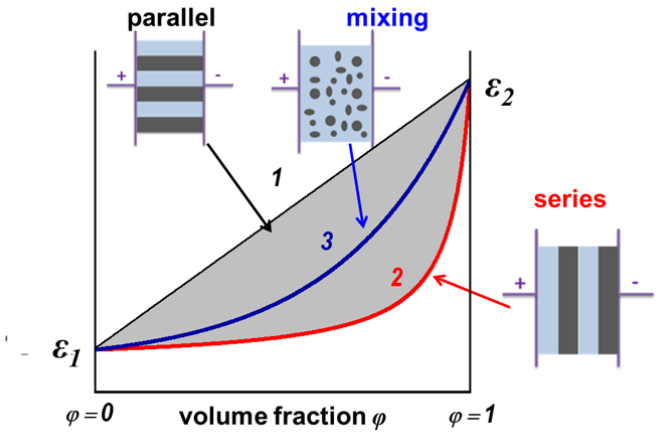

Figure 1-13. Schematic of dielectric constant of two phases 1 and 2 vs. volume fraction in the mixture: 1, parallel connection; 2, series connection; 3, real composite.

Equation (1-32) has been extended as a general formula with the n representing a variable related to the composite. Various n values/expressions have been introduced. For example, n = 1/2 (refractive index model) was proposed by Birchak *et al*. based on the study of refractive index [91] and n = 1/3 was derived by Landau and Lifshitz [92] and Looyenga [93], respectively, using different approaches. Based on the results obtained using Monte Carlo simulation and finite element methods for spherical particles randomly dispersed in a mixture, Wakino suggested that $n = \varphi - \varphi_0$ [94]. Here φ_0 is the critical volume fraction at which the curves of the dielectric constant predicted by the new equation and the logarithmic mixing rule intercept each other. The simulation results also indicate that $\varphi_0 \approx 0.35$. Using the results obtained from the simulation based on Maxwell's equation, Stölzle *et al.* [95] proposed $1.55\varphi + 0.25 \le n \le 1.65\varphi + 0.27$ for $\varphi < 0.25$. A more complicated modification was proposed as [96]

$$\varepsilon_{eff}^{\ n} = z \cdot \varphi_1 \varepsilon_1^{\ n} + (1 - z \cdot \varphi_1)\varepsilon_2^{\ n} \tag{1-33}$$

where z is a new correction factor which is dependent on frequency and $n=A\varphi+B$ with

both A and B as constants which are dependent on frequency.

As shown in **Figure 1-13**, Wiener proposed that for a real composite, the ε_{eff} follows,

$$\left(\varphi_1 \cdot \varepsilon_1^{-1} + \varphi_2 \cdot \varepsilon_2^{-1}\right)^{-1} \le \varepsilon_{eff} \le \varphi_1 \cdot \varepsilon_1 + \varphi_2 \cdot \varepsilon_2 \tag{1-34}$$

Eq. (1-34) is named as the Wiener limits. It should be mentioned that the Wiener limits are not physically proven but only assumption.

Lichtenecker recognized the Wiener limits and proposed a formula [97]:

$$\varepsilon_{eff} = \frac{\left(\varphi_1 \cdot \varepsilon_1 + \varphi_2 \cdot \varepsilon_2\right)^u}{\left(\varphi_1 \cdot \varepsilon_1^{-1} + \varphi_2 \cdot \varepsilon_2^{-1}\right)^{1-u}} \tag{1-35}$$

where u is the relative weight of parallel connection and "*1-u"* is the relative weight of series connection. The limits in the dielectric response of a mixture are important for the development of new dielectrics. Various theorems have been established and applied to derive/determine the limits of dielectric response of a mixture. Hashin and Shtrikman gave the following limits for a 0-3 composite [98]:

$$\varepsilon_1 + \varphi_2\left(\frac{1}{\varepsilon_2 - \varepsilon_1} + \frac{\varphi_1}{3\varepsilon_1}\right)^{-1} \le \varepsilon_{eff} \le \varepsilon_2 + \varphi_1\left(\frac{1}{\varepsilon_1 - \varepsilon_2} + \frac{\varphi_2}{3\varepsilon_2}\right)^{-1} \tag{1-36}$$

Lichtenecker logarithmic mixing law: Lichtenecker treated mixtures/composites using statistics and proposed [97]:

$$\log\varepsilon_{eff} = \varphi_1 \log\varepsilon_1 + \varphi_2 \log\varepsilon_2 \qquad \text{or} \qquad \varepsilon_{eff} = \varepsilon_1^{\varphi_1} \cdot \varepsilon_2^{\varphi_2} \tag{1-37}$$

This is the Lichtenecker's logarithmic mixing law, which is the most known model and has been widely used in literature to calculate the effective dielectric constant of a mixture/composite. It was also recognized by Lichtenecker that Eq. (1-35) and (1-37) have the same result when $\varphi_1=\varphi_2=1/2$ and $u=1/2$.

Similar with Eq. (1-32), the Lichtenecker's logarithmic mixture law is symmetric with respect to its constituents. It is generally considered as a quasiempirical formula. The assumption used in its derivation was that each component has a random distribution of particle shapes and orientation so that the charge density within a component can be replaced by the mean charge density of the mixture [99]. This is different with 0-3 composites. That is, the Lichtenecker's logarithmic law can only be used for the mixture in which the spatial distribution of shapes and orientations of the inclusions can be treated as statistically random. Therefore, the success (or failure) of the Lichtenecker's logarithmic law in predicting the effective dielectric constant of a dielectric-dielectric composite is most likely allied to how well this condition is satisfied [99].

Modifications were introduced soon after the Lichtenecker's logarithmic mixing law was proposed. One of these is

$$\log\varepsilon_{eff} = (1-u\varphi_2)\varphi_1 \log\varepsilon_1 + (1+u\varphi_1)\varphi_2 \log\varepsilon_2$$

$$or \quad \varepsilon_{eff} = \varepsilon_1^{\varphi_1(1-u\varphi_2)} \cdot \varepsilon_2^{\varphi_2(1+u\varphi_1)} \tag{1-38}$$

where u is a parameter introduced to modify the Lichtenecker's logarithmic mixing law. It was believed that the Lichtencker's logarithmic mixing law Eq. (1-37) is good for the ratio of $\varepsilon_2/\varepsilon_1$ less than 4, while the modified mixture law Eq. (1-33) extends the useful range of the ratio of $\varepsilon_2/\varepsilon_1$ to less than 10. However, the value of u is unknown. Later on, Bruggeman showed that the value of u is dependent on both ε_1 and ε_2 as [100]: $u = \frac{3}{2}\frac{\varepsilon_2 - \varepsilon_1}{\left(2\sqrt{\varepsilon_2} + \sqrt{\varepsilon_1}\right)\left(\sqrt{\varepsilon_2} + 2\sqrt{\varepsilon_1}\right)}$.

1.5.2. Models for 0-3 Composites

Considering its success in many cases, the Lichtenecker's logarithmic mixing law was also modified to be used for 0-3 composite. That is,

$$\log \varepsilon_{eff} = \log \varepsilon_m + (1-u)\varphi \log(\frac{\varepsilon_f}{\varepsilon_m})$$

$$or \quad \varepsilon_{eff} = \varepsilon_m{}^{1-\varphi} \cdot \varepsilon_f{}^{\varphi} \cdot \left(\frac{\varepsilon_m}{\varepsilon_f}\right)^{u\varphi} \tag{1-39}$$

where the parameter u represents the shape of the fillers. This was also widely used in literature for 0-3 composites. It was experimentally found that the value of u is about 0.3 for most well dispersed ceramic-polymer composites. It should be mentioned that Eq. (1-39) is used for 0-3 composites, in which the volume fraction of the polymer matrix cannot be too small. Actually, it is easy to find that Eq. (1-39) gives an unreasonable results for φ=1.

Rayleigh Models: In Rayleigh's study in 1890s, the composites were treated as a medium in which the same dielectric spheres were embedded in a rectangular order in the dielectric [101]. The calculation resulted in an infinite series, of which each term represented an order of approximation. For the simplest case, the dielectric spheres were embedded in a cube order in air (dielectric constant=1). Rayleigh's calculation showed that the ε_{eff} for a moderate value of φ can be approximately calculated by

$$\varepsilon_{eff} = 1 + \frac{3\varphi}{\frac{\varepsilon_f + 2}{\varepsilon_f - 1} - \varphi - 1.65\frac{\varepsilon_f - 1}{\varepsilon_f + 4/3}\varphi^{10/3}} \tag{1-40}$$

For a small value of φ, it becomes:

$$\frac{\varepsilon_{eff}-1}{\varepsilon_{eff}+2}=\varphi\frac{\varepsilon_f-1}{\varepsilon_f+2} \tag{1-41}$$

If the air is replaced with a dielectric with a dielectric constant ε_m, Eqs. (1-40) and (1-41) become:

$$\varepsilon_{eff}=\varepsilon_m+\frac{3\varphi}{\frac{\varepsilon_f+2\varepsilon_m}{\varepsilon_f-\varepsilon_m}-\varphi-1.65\frac{\varepsilon_f-\varepsilon_m}{\varepsilon_f+\frac{4}{3}\varepsilon_m}\varphi^{10/3}} \tag{1-42}$$

$$\frac{\varepsilon_{eff}-\varepsilon_m}{\varepsilon_{eff}+2\varepsilon_m}=\varphi\frac{\varepsilon_f-\varepsilon_m}{\varepsilon_f+2\varepsilon_m} \qquad (\varphi<<1) \tag{1-43}$$

Equation (1-43) is also called in the literature as the Maxwell Garnett equation [102]. Considering Eqs. (1-41) and (1-43), Wiener proposed [103]

$$\frac{\varepsilon_{eff}-\varepsilon_m}{\varepsilon_{eff}+u\varepsilon_m}=\varphi\frac{\varepsilon_f-\varepsilon_m}{\varepsilon_f+u\varepsilon_m} \tag{1-44}$$

where u ($0<u<\varphi$) is named as "form number." It was assumed that the u is dependent on the shape and size of the filler particles, but not the value of φ. Later on, it was also proposed that the value of u is also dependent on ε_m and ε_f [103].

Maxwell-Wagner equation: If filler particles are spherical in shape, the composite can be treated as a dielectric sphere (filler) surrounded by a concentric spherical shell (matrix) as shown in **Figure 1-14**. Therefore, the effective dielectric constant of the composite can be calculated as [99, 102, 104],

$$\begin{aligned}\varepsilon_{eff}&=\varepsilon_m\frac{2\varepsilon_m+\varepsilon_f+2\varphi(\varepsilon_f-\varepsilon_m)}{2\varepsilon_m+\varepsilon_f-\varphi(\varepsilon_f-\varepsilon_m)}\\&=\varepsilon_m\left[1+\frac{3\varphi(\varepsilon_f-\varepsilon_m)}{(2+\varphi)\varepsilon_m+(1-\varphi)\varepsilon_f}\right]=\varepsilon_m\left[1+\frac{\varphi}{\varepsilon_m/(\varepsilon_f-\varepsilon_m)+(1-\varphi)/3}\right]\end{aligned} \tag{1-45}$$

This is the Maxwell-Wagner (also named as Maxwell-Garnett) mixing rule. It has

been widely employed for calculation of the dielectric constant of 0-3 composites. Based on the assumptions used, the interaction between the disposed spheres is ignored. Therefore, this result is only effective for infinite dilution of the dispersed phase. That is, the spherical filler particles are well separated by distances greater than their characteristic size. It is also argued that this mixing rule is an approximation of the Lichtenecker's logarithmic law [99]. Although Eq. (1-45) was originally derived under static field, this equation was also derived later on by Webman *et al.* [57] using effective medium theory for the dielectric behavior of microscopically inhomogeneous materials at optical and microwave frequency and by Skipetrov [105] for a random media in which the heterogeneities of the dielectric constant are much smaller than the wavelength of the electromagnetic wave.

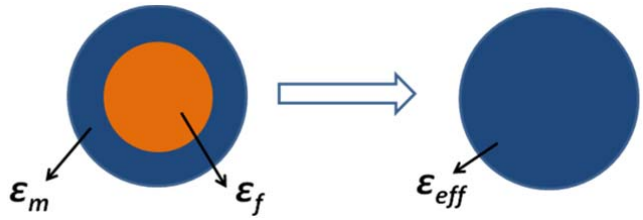

Figure 1-14. Schematic of Maxwell-Wagner equation.

Bruggeman model: Rayleigh's calculation was further expended by Bruggeman to different cases. For a composite made of particles of two dielectrics (this is lightly different with 0-3 composites but more close to 0-0 composites), it is obtained for a composite of two inter-dispersed materials,

$$\varphi\left(\frac{\varepsilon_f-\varepsilon_{eff}}{\varepsilon_f+2\varepsilon_{eff}}\right)+(1-\varphi)\left(\frac{\varepsilon_m-\varepsilon_{eff}}{\varepsilon_m+2\varepsilon_{eff}}\right)=0 \qquad (1\text{-}46)$$

In the derivation, it was assumed: 1) all particles are very small compared to the

dimension of the sample/composite, 2) the shape, size, and the locations of all particles are randomly distributed, 3) the number of particles is large, and 4) all particles are closely packaged together so that there is no gap between particles [68].

Equation (1-46) is widely used in literatures as Bruggeman mixing rule (this is also called as Polder-Van Santeen in literature as it was also proposed in [106]). This expression was also derived based on the study of conductivity for a random mixture in which each constituent (spherical particles) acts as if surrounded by a homogenous medium whose properties are those of the mixture [107]. Actually, this is a direct result of an effective medium approximation or self-consistent approximation [57].

To fit the experimental results better, the Bruggeman mixing rule was modified. For example, considering Eq. (1-43) and the modification of Eq. (1-44) into Eq. (1-46), it was proposed [108-110]

$$\varphi\left(\frac{\varepsilon_f-\varepsilon_{eff}}{\varepsilon_f+u\varepsilon_{eff}}\right)+(1-\varphi)\left(\frac{\varepsilon_m-\varepsilon_{eff}}{\varepsilon_m+u\varepsilon_{eff}}\right)=0 \tag{1-47}$$

where u is a constant. Based on the conductivity of a composite, McLachian proposed a general effective medium formula based on the effective media theory and consideration of percolation features in a composite [108-110]. When the percolation phenomenon is considered, it was proposed that u equals to the critical volume fraction (φ_c) of the filler where the filler particles first forms a continuous percolation path across the medium. This general formula for the dielectric property of a composite is

$$\varphi\left(\frac{{\varepsilon_f}^{1/t}-{\varepsilon_{eff}}^{1/t}}{{\varepsilon_f}^{1/t}+u\cdot{\varepsilon_{eff}}^{1/t}}\right)+(1-\varphi)\left(\frac{{\varepsilon_m}^{1/t}-{\varepsilon_{eff}}^{1/t}}{{\varepsilon_m}^{1/t}+u\cdot{\varepsilon_{eff}}^{1/t}}\right)=0 \tag{1-48}$$

where $u=\varphi_c/(1-\varphi_c)$ is dependent on the critical volume fraction of filler particles, and t is parameter characterizing the microstructure (including size and shape) or distribution and interconnectivity of the components in a composite material.

Based on Rayleigh's results and assumptions, Bruggeman further introduced a change in the volume fraction of the filler and derived the following equation for a random distribution of dielectric spheres in a matrix with a low concentration [100].

$$1-\varphi=\left(\frac{\varepsilon_f-\varepsilon_{eff}}{\varepsilon_f-\varepsilon_m}\right)\left(\frac{\varepsilon_m}{\varepsilon_{eff}}\right)^{1/3} \tag{1-49}$$

This is the Bruggeman equation. This is also named as the Hanai equation since Hanai derived this equation for complex permittivity [111].

The Bruggeman equation Eq. (1-49) has been modified based on different considerations to fit the experimental results. For example, the left side of Eq. (1-49) was modified as [112]:

$$1-\varphi\left[u-(u-1)\varphi\right]=\left(\frac{\varepsilon_f-\varepsilon_{eff}}{\varepsilon_f-\varepsilon_m}\right)\left(\frac{\varepsilon_m}{\varepsilon_{eff}}\right)^{1/3} \tag{1-50}$$

where u is a constant. It was experimentally found that the value of u can be either positive or negative. Another widely used modification of Bruggeman equation Eq. (1-49) is [113, 114]

$$1-\varphi=\left(\frac{\varepsilon_f-\varepsilon_{eff}}{\varepsilon_f-\varepsilon_m}\right)\left(\frac{\varepsilon_m}{\varepsilon_{eff}}\right)^{1/\alpha} \tag{1-51}$$

where α is an empirically determined value (≥3) to fit the experimental data.

Knott equation: In the study of plastic foams, Knott introduced a model, in which the filler particles (i.e. air) are treated as small cubes that are surrounded by the matrix (i.e. foam) with the same thickness [115]. Therefore, the effective capacitance (i.e. the

effective dielectric constant) of the foam is simulated using the capacitance of the cubes and the matrix. In the model, the capacitance of all these elements (i.e. cubes and slabs) is calculated using the parallel-plate mode. Based on these assumptions, it was obtained that

$$\varepsilon_{eff} = \varepsilon_m \left[1 - \frac{(\varepsilon_m - \varepsilon_f)\cdot\varphi}{\varepsilon_f + (\varepsilon_m - \varepsilon_f)\cdot\varphi^{1/3}} \right] \tag{1-52}$$

Yamada equation: In a study of dielectric and piezoelectric properties of 0-3 composite, Yamada et al. introduced the following formula using the static field condition [116],

$$\varepsilon_{eff} = \varepsilon_m \left(1 + \frac{\alpha\varphi(\varepsilon_f - \varepsilon_m)}{\alpha\varepsilon_m + (1-\varphi)(\varepsilon_f - \varepsilon_m)} \right) \tag{1-53}$$

where α is the parameter attributed to the shape and orientation of the ellipsoidal filler particles. Based on the experimental results, the value of α for ceramic particles is bigger than one (mostly about 10).

Reverse composite: Due to the assumptions and simplifications used in each of the above models, some (i.e. Eqs. (1-39), (1-44), and (1-47)) are symmetrical in terms of their constituents, and others are asymmetrical. The asymmetric result is more closely related to a real 0-3 composite. For a real random 0-3 composite, it is likely that the filler becomes the matrix and the matrix may be separated into isolated particles when the volume fraction of the filler is high. When the matrix and filler are exchanged, the ε_{eff} is clearly different, as illustrated in **Figure 1-15**, where Maxwell-Wagner equation (Eq. (1-45)) is used. For a real composite, when φ is small, the matrix is most likely to be the matrix so the ε_{eff} should follow the curve I, while when φ is big, the matrix is

most likely to be the filler and the filler becomes matrix so the ε_{eff} should follow curve II. Therefore, at certain composition, the ε_{eff} changes from curve I to curve II as illustrated in the figure as the curve III (blue cross). Therefore, a rapid increase in the ε_{eff} with increasing φ will be observed. This is somehow similar to the percolation phenomenon observed in conductor-dielectric composites discussed in Section 1.4.1.

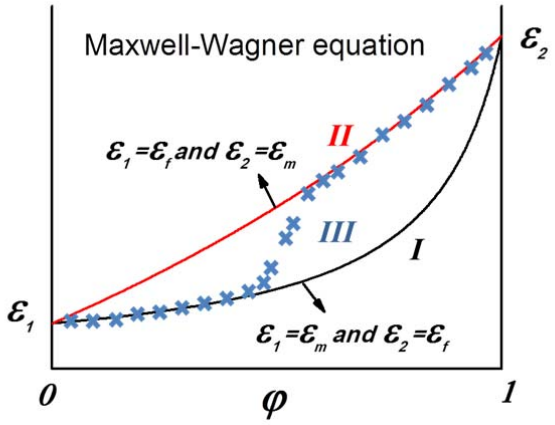

Figure 1-15. Schematic of reverse model for the composite. The black (I) curve is the result obtained using dielectric-1 as matrix and dielectric-2 as filler, while the red (II) curve is obtained using dielectric-1 as filler and dielectric-2 as matrix. The III curve (blue cross) is presented as possible real case.

1.5.3. Limitation

The ε_{eff} of a composite was simulated using the six equations proposed for 0-3 composites as shown in **Figure 1-16**, where ε_f =1000 and ε_m =10 are used. In the figure, the results for parallel and series connections are also presented for comparison. For modified Lichtenecker's logarithmic law, Eq. (1-39), the u=0.3 was used. For Yamada Model, Eq. (1-53), the shape factor α=10 was used. It is easy to conclude that: (1) the ε_{eff} of composites always increases with the volume content of filler, in other words, the ε_{eff} monotonically changes with φ; (2) ε_{eff} falls in between area of curve of parallel (black) and series (blue) connection. That is, the Wiener

limits from Eq. (1-34) are valid as:

$$\varepsilon_{seri} \le \varepsilon_{eff} \le \varepsilon_{para} \tag{1-54}$$

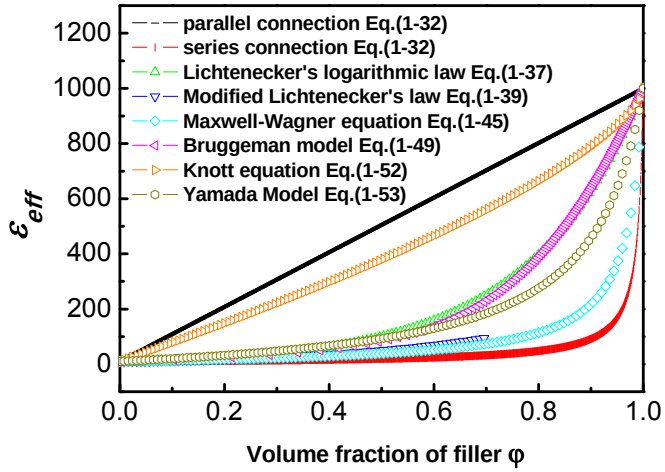

Figure 1-16. Schematic of dielectric constant of different models.

As more and more experimental results are being reported, some experimental results have been shown contradict with the current understanding. For example, based on the dielectric constant at 100 Hz of BT/PVDF composites at room temperature, Dang *et al* reported that the ε_{eff} increases with increasing φ for φ_{BT}<0.5, then decreases, as shown in **Figure 1-17**[118]. The composites were prepared by a simple blending and hot-molding procedure. The BT powders are a nearly spherical shape with grain sizes of about 1 μm. The appearance of a maximum-like curve on ε_{eff} vs. φ contradicts with the monotonically change expected for the composite. This was simply explained by the possible pores in the composites with high content of fillers without solid experimental data on the porosity.

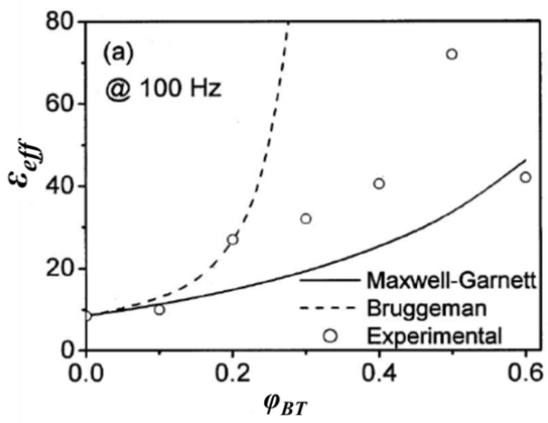

Figure 1-17. Variation of the dielectric constant of the BT/PVDF composites with the volume fraction of BT particles. For comparison, the calculations by using Maxwell–Garrett and Bruggeman equations are also shown [118].

Yang *et al*. reported CCTO/PVDF composites using micro-CCTO powders (CCTO-2, micro-size) [119]. The CCTO with PVDF powder were thoroughly mixed for 20 min then molded by hot pressing at about 200^{o}C under a pressure of 50 MPa to get tablet-shaped samples that were 12 mm in diameter and about 0.8 mm in thickness. As shown in **Figure 1-18**, the ε_{eff} vs. φ exhibited a peak-like curve. The ε_{eff} increased with increasing CCTO volume content then decreases. The author concluded that the micro-sized CCTO exhibited "insulating" boundaries in the matrix.

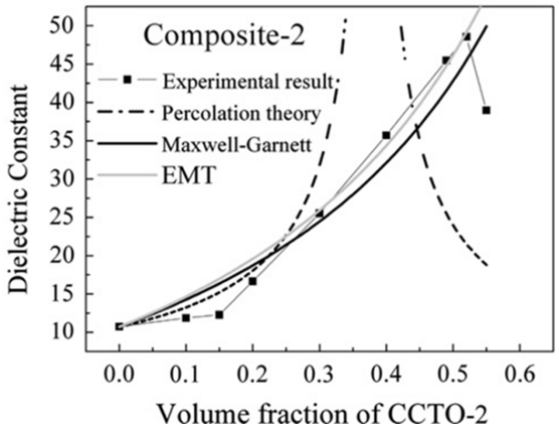

Figure 1-18. Comparison of experimental and theoretical dielectric constants of micro-size CCTO/ PVDF at 100 Hz and room temperature [119].

Murugaraj *et al* reported the dielectric enhancement in composites, where nano-sized alumina (dielectric constant is 9.8) were embedded in polyimide (PI) with a dielectric constant of 3.5. As shown in **Figure 1-19**, the ε_{eff} monotonically increases with the content of filler to a value that is higher than the dielectric constant of the filler [120]. This cannot be explained by any model and breaks the Wiener limits. This oxide-polymer precursor suspension was cast on a flat glass at 100 °C for an hour to remove the solvent. These films were then cured in the temperature range of 180-300°C in an inert atmosphere to obtain robust and stress-free nanocomposite thin films. The average particle size of alumina was in the range of 10-15nm and the agglomeration of particles was limited to 100-150nm cluster sizes.

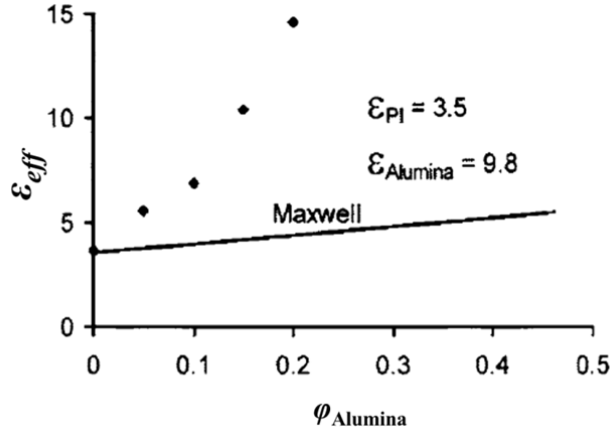

Figure 1-19. Variation of composite dielectric constant with PI-alumina at 100 kHz and solid line is fitted by Maxwell equation [120].

1.5.4. Interfacial Layer

All the models/equations proposed for 0-3 composites are based on only the properties of matrix and filler. In real 0-3 composites, especially polymer-based composites, an interfacial layer between the filler and polymer matrix may exist. The

interfacial layer has different properties than the filler and matrix. Therefore, the interfacial layer has been considered as the reason responsible for the experimental results. Due to its difficulty in determining thickness and dielectric property of the interfacial layer, there are not many quantified results [121-127]. In the literature, whenever there are some phenomena that are difficult to be understood using two constituents, it is generally explained as the results of the interfacial layer. This is in general correct, but lacks the quantified results.

The volume fraction of the interfacial layer in a composite is dependent on the thickness of the interfacial layer and the surface area of the filler particles as shown in **Figure 1-20**, where three thicknesses are assumed for the interfacial layer and the filler particles are treated as spheres with the same diameter. Clearly, as the particle size decreases, the volume fraction of the interfacial layer increases. The thicker the interfacial layer is, the more the volume fraction of the interfacial layer is.

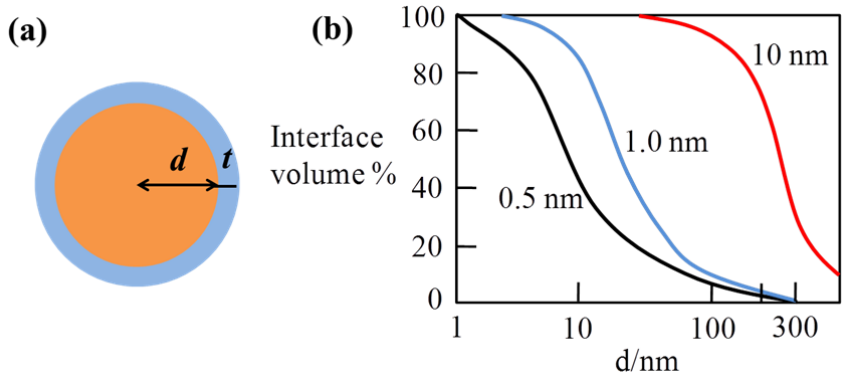

Figure 1-20. Volume fraction of interfacial layer as the function of the diameter (d) of the spherical filler particles, where the thickness of the interfacial layer is assumed as 0.5 nm, 1.0 nm, and 10 nm respectively. [128].

Table 1-2. Volume fraction of interfacial layer with different size of filler and thickness of interfacial layer for APF structure

radius of filler (nm)	Thickness of interfacial layer (nm)					
	0.1	0.5	1	5	10	20
5	4.26%	18.40%	31.18%	64.75%	71.26%	73.41%
10	2.18%	10.08%	18.40%	52.07%	64.75%	71.26%
20	1.10%	5.28%	10.08%	36.11%	52.07%	64.75%
50	0.44%	2.18%	4.27%	18.40%	31.18%	47.03%
100	0.22%	1.10%	2.18%	10.08%	18.40%	31.18%
200	0.11%	0.55%	1.10%	5.28%	10.08%	18.40%
500	0.04%	0.22%	0.44%	2.18%	4.27%	8.21%

Certainly, the volume fraction of the interface cannot be 100%. As mentioned in Section 1.4.1, the most tightly packed crystal with the same size spheres has an atomic packing factor (APF) of only 74%. Assuming that the particles are the same spheres and the interfacial layer is uniformly coated on the surface of the filler particles, the volume fraction of the filler plus interfacial layer in a composite is about 74%. The volume fraction of the interfacial layer can be estimated for the filler with different diameters, as listed in **Table 1-2**.

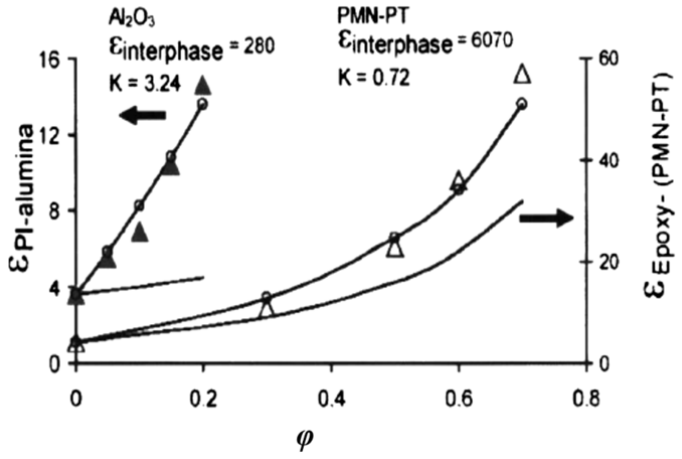

Figure 1-21. Comparison of Vo-Shi model prediction with experiment data on PI-alumina composite and epoxy-(PMN-PT) composite [120].

To quantify the contribution of the interfacial layer to the ε_{eff}, the interfacial

layer has been treated as a single phase of material. When the interfacial layer is treated as a new phase with a well-defined dielectric property, a two-phase composite becomes a three-phase composite. In this way, the experimentally observed ε_{eff} can be fitted well as shown in **Figure 1-21**, where the thickness of the interfacial layer and the interface interaction are presented by the value of *K* [129, 130]. The Vo-Shi model is an empirical three phase model that recognizes a distinct interphase region surrounding the filler of these polymer composites. The thickness of the interfacial layer depended on the degree of interaction between the polymer and the particle, which results in a nonmonotonic relationship of the dielectric constant with particle volume fraction [120, 129, 130]. As shown in **Figure 1-18**, the so-called dielectric constant of interphase can be as high as 280 for PI-Alumina composites. It is also obtained that the thickness of the interfacial layer is about 4 nm. For another epoxy-(PMN-PT) composite, the dielectric constant of interphase is calculated more than 6000. The average size of PMN-PT is around 900nm. The $\varepsilon_{interface}/\varepsilon_m$ is around 1000 times [131].

By considering interfacial layer/phase, the experimental results can be fitted well, it fails to explain for interfacial layer itself. As mentioned above, the processing temperature of polymer-based composites is pretty low, ~ 200 ^{o}C. At this temperature there is no change to be anticipated for the ceramic filler, which are prepared at temperatures higher than 1000 ^{o}C. That is, the so-called interfacial layer should be the polymer matrix itself with a different microstructure than the bulk polymer matrix. Based on the dielectric physics, it would be very difficult to understand that by

changing microstructure, the dielectric constant of interfacial layer can be 100 times of the bulk polymer matrix.

1.5.5. Dielectric Loss of Composite

Most of the models/formulas given in the section 1.5.1 and 1.5.2 were initially derived only for the effective dielectric constant of a composite. Some of them can be used for complex permittivity. For example, Eq. (1-49) was obtained by Bruggeman for the dielectric constant only, but later on extended to complex permittivity by Hanai. However, in most of literatures, it is still the case that only the dielectric constant is fitted/simulated using these formulas/equations since by using the complex permittivity these formulas become too complicated. For the case, when the dielectric loss is really needed to be considered, the general practice has been: (1) analyzing the dielectric constant using the formulas previous defined for only the dielectric constant; (2) analyzing the dielectric loss, using the formulas for complex permittivity with the ε_{eff} obtained in (1). For example, when using the Bruggeman equation, Eq. (1-49), for complex permittivity, the imaginary part is calculated using

$$\varepsilon''_{eff} = \frac{(\varepsilon_f - \varepsilon_{eff})(\varepsilon_f + 2\varepsilon_m)\varepsilon_{eff}}{(\varepsilon_f - \varepsilon_m)(\varepsilon_f + 2\varepsilon_{eff})\varepsilon_m}\varepsilon''_m + \frac{3(\varepsilon_{eff} - \varepsilon_f)\varepsilon_{eff}}{(\varepsilon_f - \varepsilon_m)(\varepsilon_f + 2\varepsilon_{eff})}\varepsilon''_f \qquad (1\text{-}55)$$

where ε''_{eff}, ε''_f and ε''_m are the imaginary part of complex relative permittivity (i.e. the dielectric constant is the real part of complex relative permittivity) of the composite, the filler, and the matrix, respectively [132]. The volume fraction of the filler is represented by the ε_{eff}, where ε_{eff} is obtained using Eq. (1-49) only for the real part of the complex relative permittivity.

In other words, the important limitation in these models is that they do not take the dielectric loss into account. Additionally, all above discussions are based on ideal dielectrics (i.e. zero electrical conductivity). Actually, all dielectrics have non-zero conductivities. As discussed in Section 1.1.3, Eq. (1-10), the electrical conductivity contributes to the imaginary part of the measured permittivity. For a composite, the conductivity of its constituent would make dielectric response much more complete. Besides the contribution to dielectric loss, the electrical conductivity may result in the charge accumulation on the interface between two constitutes of a composite, which in turn will change the distribution of electrical field in the material. That is, the electrical conductivity would respond with some kinds of the dielectric responses.

1.5.6. Dielectric-Polymer 0-3 Composites

Table 1-3 shows some of the high-dielectric-constant 0-3 composites reported in the literature and the commercially available composites. BT is widely used as filler because BT is relatively inexpensive and easy to prepare in different sizes from nm to μm. For BT-based composites, a linear relationship between BT volume fraction and the effective dielectric constant was observed in PMMA and BT composite and the dielectric constant is about 40 for the composites with 60 vol.% BT [19]. A dielectric constant of 44 was obtained in composites with 40 vol.% BT using epoxy as matrix [133]. Other polymers, such as PVDF and PS, have also been used to prepare 0-3 composites with BT as fillers with dielectric constant as high as 100 was obtained [134, 135]. It has to be mentioned that it is well known that the dielectric constant of BT ceramics is strongly dependent on the grain size. That is, the dielectric constant of

BT particles is strongly dependent on the size of the particles. This is one of the reasons that the dielectric property of the BT-based composite varies over a large range. However, the BT has phase transitions, one around 120^{o}C and the other around 0^{o}C, as shown in **Figure 1-5(a)**. At the phase transition temperature, there is a big change in the dielectric constant, which is not desirable for the most of the dielectric applications.

PMN-PT exhibits a much higher dielectric constant at room temperature than the BT and does not show a phase transition. Therefore, PMN-PT is also widely used as filler for the development of high-dielectric-constant composites as shown in **Table 1-3** [138, 139]. PZT is a widely used piezoelectric ceramic has also been used as fillers in the development of high-dielectric constant composites due to the fact that PZT exhibits a high dielectric constant and is easy to prepare [140-142]. Another widely used ceramic system is BST due to the fact that the BST can exhibit a high dielectric constant at temperature around room temperature [143]. The high-energy electron irradiation was carried out on a composite system using PMN-PT ceramic powders as the filler and P(VDF-TrFE) copolymer as the matrix. The irradiation composite exhibited a much higher dielectric constant (~200) than other composites at room temperature due to the enhancement of ε_m [139]. The irradiated also made the BST-P(VDF-TrFE) composites exhibit a high dielectric constant (~150) at room temperature [143].

Table 1-3 The dielectric properties of ceramic-polymer composites at room temperature [33]

Dielectric fillers	Polymers	filler's size	composites				Ref.
			φ(vol%)	ε_{eff}	*tanδ*	*Freq.*	
$BaTiO_3$	PMMA	-	60%	40	0.012	1kHz	[19]
$BaTiO_3$	Epoxy	-	40%	44	0.2	1kHz	[133]
$BaTiO_3$	PVDF	0.1μm	70%	152.3	<0.1	1kHz	[134]
$BaTiO_3$	Polystyrene	0.7μm	70%	100	<1	1kHz	[135]
$BaTiO_3$	PVC	6.8-0.3μm	40%	18	-	100kHz	[136]
$BaTiO_3$	polyamide (PA)	17-100nm	70%	80	0.02	1MHz	[137]
(Bi,Na)$BaTiO_3$*	P(VDF-TrFE)70/30	-	30%	30	<0.02	1kHz	[132]
PMN	Epoxy	-	40%	24	0.05	100kHz	[133]
PMN-35PT	P(VDF-TrFE)70/30	-	40%	50	<0.1	1kHz	[138]
PMN-PT	P(VDF-TrFE)	0.5μm	50%	200	<0.1	10kHz	[139]
PZT	Polyurethane	-	30%	24	0.7	1kHz	[140]
PZT	PVDF	30nm	32%	40	-	100Hz	[141]
PZT	Polyvinyl-butyral	100μm	85%	155	0.05	1MHz	[142]
(Ba,Sr)TiO_3**	P(VDF-TrFE)70/30	1μm	50%	80	<0.2	1kHz	[143]
CCTO	P(VDF-TrFE)55/45	10μm	50%	610	<0.4	1kHz	[50]
CCTO	P(VDF-TrFE)55/45	<500nm	50%	60	0.05	1kHz	[144]
CCTO	Epoxy	0.3-0.5μm	40%	50	-	100Hz	[145]
CCTO	PVDF	1-7μm	55%	95	<0.24	100Hz	[146]
CCTO	Polystyrene	10-25μm	64%	80	-	100Hz	[147]
CCTO	Polyimide	1-4μm	40%	49	<0.2	100Hz	[148]
CCTO	polyethersulfone	-	50%	32.7	0.063	1kHz	[149]

*$(Bi_{0.5}Na_{0.5})_{0.94}Ba_{0.06}TiO_3$ **$(Ba_{0.65}Sr_{0.35})TiO_3$

Since the discovery of CCTO in the 2000s, a great deal of attention has been given to CCTO since it is a non-ferroelectric ceramic with a high dielectric constant and a weak electromechanical coupling effect as discussed in Section 1.2.1. Different

composite systems have been developed using CCTO as the filler [50, 144-150]. For temperature dependency concerns, the CCTO/P(VDF-CTFE) composite using nano-sized CCTO exhibited a dielectric constant of 100 that is almost independent of temperature (up to 120 ^{o}C) [150]. It was also found that the dielectric behavior of the composites is strongly dependent on the size of the CCTO particles. For micro-sized CCTO particles, a dielectric constant of more than 200 was obtained at room temperature [50]. For composites using nano-sized CCTO particles, a composite at room temperature exhibited a dielectric constant of 60 and loss of about 0.05 at 1 kHz [144].

1.6. Research Objectives

In this work, conducting filler-polymer nano-composites based on percolation phenomenon were studied, using nano-sized Ni and nanoclips Polypyrrole (PPy) as filler. Two different polymer matrices were used in this work: 1) P(VDF-TrFE) 55/45 mol% copolymer which exhibits a high dielectric constant and a phase transition around 110 ^{o}C; 2) P(VDF-CTFE) 88/12 mol% (VC88) which exhibits a high dielectric constant and a week piezoelectric effect with weak temperature dependence.

1. By combining the solution cast and hot pressing processes, Ni-polymer nano-composites with high percolation was developed in Chapter 2, due to a more uniform distribution of metal powders inside the polymer matrix. The composites exhibit a high dielectric constant and relative low loss.
2. Using newly developed nanoclips, a new all-organic composite systems were developed and discussed in Chapter 3. Due to its 2D structure, the composites

show high flexibility with a high dielectric constant and a low percolation threshold.

3. From the study of Ni-polymer composites and PPy-polymer composites, the φ_c and s of composite are different with the selecting data at different frequencies and temperature. In Chapter 4, this conclusion was confirmed using six reported systems using different conducting fillers from literature are studied.
4. As discussed in Section 1.5.3, the ε_{eff} can be restricted by the Wiener limits. To investigate the contribution of dielectric loss to ε_{eff}, the loss of matrix and filler were considered in three different models which can represent three different microstructures. These results show the ε_{eff} of composites can be larger than the dielectric constant of both materials. However, the dielectric loss is between the values of dielectric loss of both materials. Therefore, a new approach to develop high performance composite was introduced.

References of Chapter 1

1. K. C. Kao, Dielectric Phenomena in Solids, Elsevier Academic Press, San Diego, CA 2004.
2. A. V. Hippel, Dielectric Materials and Applications, Technology Press of MIT, Cambridge, Boston 1954.
3. R. E. Hummel, Electronic Properties of Materials, Springer, Technology & Industrial Arts, 2001.
4. C. J. Dias, D. K. Das-Gupta, Ferroelectric Polymer and Ceramic-Polymer Composites, Trans Tech Publications Ltd., Switzerland, 1994.
5. R. E. Newnham, *Ann. Rev. Mat. Sci.* **16**, 47(1986).
6. A. K. Jonscher, *J. Phys. D: Appl. Phys*. **32**, R57 (1999).
7. H. Nalwa, Handbook of Low and High Dielectric Constant Materials and Their Applications, Academic Press, London, 1999.
8. Y. Rao, S. Ogitani, P. Kohl and C. P. Wong, *J. Appl. Poly. Sci*. **83**, 1084 (2002).
9. C. J. Dias and D.-K. Das Gupta, *IEEE Trans.Dielectr. Electr. Insul*. **3**, 706 (1996).
10. E. Reichmanis, H. Katz, C. Kloc, and A. Maliakal, *Bell Labs Tech. J.* **10**, 87 (2005).
11. R. F. Cava, W. F. Peck, and J. J. Krajewski, *Nature* **377**, 215(1995).
12. M. W. Barsoum, Fundamentals of Ceramics, Institute of Physics Publishing, Bristol and Philadelphia, 1997.

13. http://www.matweb.com/search/SearchSubcat.asp.

14. Z.-Y. Cheng, R.S. Katiyar, X. Yao, and A. S. Bhalla, *Phys. Rev. B* **57**, 8166 (1998).

15. C. C. Homes, T. Vogt, S. M. Shapiro, S. Wakimoto, and A. P. Ramirez *Science* **293**, 673 (2001).

16. M.A. Subramaniana, Dong Li, N. Duan, B.A. Reisner, and A.W. Sleight, *J. Solid State Chem*. **151**, 323 (2000).

17. Z.-Y. Cheng and Q. M. Zhang, *Mater. Res. Bull*.**33**, 183 (2008).

18. Z.-Y. Cheng, Q. M. Zhang and F. B. Bateman, *J. Appl. Phys*. **92**, 6749 (2002).

19. H. S. Nalwa, Ferroelectric Polymers: Chemistry, Physics, and Applications, Marcel Dekker Inc., New York, 1995.

20. S. H. Zhang, B. J. Chu, B. Neese, K. L. Ren, X. Zhou and Q. M. Zhang, *J. Appl. Phys*. **99**, 044107 (2006).

21. Q. M. Zhang, V. Bharti and X. Zhao, *Science* **280**, 2101 (1998).

22. Z. M. Li, S. Q. Li and Z.-Y. Cheng, *J. Appl. Phys*. **97**, 014102 (2005).

23. X. Zhou, X. H. Zhao, Z. G. Suo, C. Zou, J. Runt, S. Liu, S. H. Zhang and Q. M. Zhang, *Appl. Phys. Lett.* **94**, 162901 (2009).

24. M. Wegener and K. Arlt, *J. Phys. D: Appl. Phys.* **41**, 165409 (2008).

25. Z. M. Li, Y. H. Wang and Z.-Y. Cheng, *Appl. Phys. Lett.* **88**, 062904 (2006).

26. R. E. Newnham, D. P. Skinner and L. E. Cross, *Mater. Res. Bull*. **13**, 525 (1978).

27. D. P. Skinner, R. E. Newnham and L. E. Cross, *Mater. Res. Bull.* **13**, 599 (1978).

28. N. Jayasundere, B. V. Smith and J. R. Dunn, *J. Appl. Phys*. **76**, 2993 (1994).

29. C. K. Wong, Y. M. Poon and F. G. Shin, *J. Appl. Phys*. **90**, 4690 (2001).

30. S. M. Pilgrim and R. E. Newnham, *Mater. Res.Bull*. **21**, 1447 (1986).

31. M. T. Sebastian and H. Jantunen, *Int. J. Appl. Ceram. Technol*. **7**, 415 (2010).

32. C. W. Nan, Y. Shen and J. Ma, *Annu. Rev. Mater. Res*. **40**, 131 (2010).

33. L. Zhang and Z.-Y. Cheng, *J. Adv. Dielect*. **1**, 389 (2011).

34. D. Stauffer, Introduction to Percolation Theory (Taylor & Francis, London, 1992).

35. E. J. Garboczi, K. A. Snyder, J. F. Douglas and M. F. Thorpe, *Phys. Rev. E* **52**, 819 (1995).

36. C. W. Nan, *Prog. Mater. Sci*. **37**, 1 (1993).

37. J. Yacubowicz and M. Narkis, *Polymer Eng. Sci*. **26**, 1568 (1986).

38. D. Toker, D. Azulay, N. Shimoni, I. Balberg and O. Millo, *Phys. Rev. B* **68**, 041403 (2003).

39. Y. Shen, Z. X. Yue, M. Li and C. W. Nan, *Adv. Funct. Mater*. **15**, 1100 (2005).

40. G. S. Wang, Y. Deng, Y. Xiang and L. Guo, *Adv. Funct. Mater*. **18**, 2584 (2008).

41. Y. Deng, Y. J. Zhang, Y. Xiang, G. S. Wang and H. B. Xu, *J. Mater. Chem*. **19**, 2058 (2009).

42. Z. M. Dang, C. W. Nan, D. Xie, Y. H. Zhang and S. C. Tjong, *Appl. Phys. Lett*. **85**, 97 (2004).

43. D. N. Fang, A. K. Soh, C. Q. Li and B. Jiang, *J. Mater. Sci*. **36**, 5281 (2001).

44. S. Komarneni, *J. Mater. Chem*. **2**, 1219 (1992).

45. Z.-Y. Cheng, A.Q. Guo, and X. Yao, *Ferroelectrics* **190**, 167 (1997).

46. Z.-Y. Cheng, L. Y. Zhang and X. Yao, *J. Appl. Phys*. **79**, 8615 (1996).

47. M. E. Lines and A. M. Class, Principles and Applications of Ferroelectrics and Related Materials, Clarendon Press, Oxford, 1977.

48. A. N. Vasil'ev and O. S. Volkova, *Low Temp. Phys*. **33**, 895 (2007).

49. I. P. Raevski, S. A. Prosandeev, A. S. Bogatin, M. A. Malitskaya and L. Jastrabik, *J. Appl. Phys*. **93**, 4130 (2003).

50. M. D. Arbatti, X. B. Shan and Z.-Y. Cheng, *Adv. Mater*. **19**, 1369 (2007).

51. F. Carpi, D. De Rossi, R. Kornbluh, P. Perine, and P. Sommer-Larsen, dielectric elastomers as electromechanical transducers, Elsevier, Amsterdam, 2008.

52. R. Zallen, The Physics of Amorphous Solids, New York, Wiley, 1983.

53. J.Y. Yi and G. M. Choi, *J. Electroceram.* **3**:361(1999).

54. B. K. P. Scape, Principles of Dielectrics, Clarendon Press, Oxford, 1989.

55. J. C. Maxwell, Electricity and Magnetism, Clarendon Press, Oxford, 1892.

56. D. J. Bergman and Y. Imry, *Phys. Rev. Lett*. **39**, 1222 (1977).

57. I. Webman, J. Jortner and M. H. Cohen, *Phys. Rev. B* **15**, 5712 (1977).

58. M. T. Clarkson, *Phys. Rev. A* **37**, 2079 (1988).

59. D. C. Koskenmaki, C. D. Calhoun and B. E. Huff, US Patent (1991).

60. Q. Z. Xue, *Eur. Polym. J.* **40**, 323 (2004).

61. M. Panda, V. Srinivas, and A. K. Thakur, *Appl. Phys.Lett.* **92***,* 132905 (2008).

62. M. Panda, V. Srinivas, and A. K. Thakur, *Appl. Phys. Lett.* **93**, 242908 (2008).

63. Z.-M. Dang, Y. H. Lin, and C. W. Nan, *Adv. Mater.* **15**, 1625 (2003).

64. H. P. Xu, H. Q. Xie, D. D. Yang, Y. H. Wu, and J. R. Wang, *J. Appl. Polym. Sci.* **122**, 3466 (2011).

65. Y. Rao and C. P. Wong, *8th IEEE Proc. Electron. Compon. Technol. Conf.* 920 (2002).

66. L. Qi, B. I. Lee, S. H. Chen, W. D. Samuels and G. J. Exarhos, *Adv. Mater*. **17**, 1777 (2005).

67. Z. M. Dang, B. Peng, D. Xie, S. H. Yao, M. J. Jiang, and J. B. Bai, *Appl. Phys. Lett.* **92**, 112910 (2008).

68. J. W. Xu, K. S. Moon, C. Tison and C. P. Wong, *IEEE Trans. Adv. Packaging* **29**, 295 (2006).

69. Z. M. Dang, Y. H. Zhang and S.-C. Tjong, *Synth. Met*. **146**, 79 (2004).

70. Y. J. Li, X. Man, J. Q. Feng and Z. M. Dang, *Appl. Phys. Lett*. **89**, 072902 (2006).

71. Z. M. Dang, Y. Shen, L. Z. Fan, N. Cai and C. W. Nan, *J. Appl. Phys.* **93**, 5543 (2003).

72. Z. M. Dang, J. P. Wu, H. P. Xu, S. H. Yao, M. J. Jiang and J. B. Bai, *Appl. Phys. Lett.* **91**, 072912 (2007).

73. J. Macutkevic, D. Seliuta, G. Valušis, J. Banys, V. Kuznetsov, S. Moseenkov and O. Shenderova, *Appl. Phys. Lett*. **95**, 112901 (2009).

74. L. Wang and Z. M. Dang, *Appl. Phys. Lett*. **87**, 042903 (2005).

75. Q. Li, Q. Z. Xue, L. Z. Hao, X. L. Gao and Q. B. Zheng, *Compos. Sci. Technol*. **68**, 2290 (2008).

76. Z. M. Dang, L. Wang, Y. Yin, Q. Zhang and Q. Q. Lei, *Adv. Mater*. **19**, 852 (2007).

77. J. K. Yuan, S. H. Yao, Z. M. Dang, A. Sylvestre, M. Genestoux and J. B. Bai, *J. Phys. Chem. C* **115**, 5515 (2011).

78. F. He, S. Lau, H. L. Chan and J. T. Fan, *Adv. Mater*. **21**, 710 (2009).

79. V. Panwar, R. M. Mehra, J. O. Park and S. H. Park, *J. Appl. Polym. Sci*. **125**, E610 (2012).

80. J. K. Yuan, S. H. Yao, A. Sylvestre and J. B. Bai, *J. Phys. Chem. C*, **116**, 2051(2012)

81. J. K. Yuan, Z. M. Dang, S. H. Yao, J. W. Zha, T. Zhou, S. T. Li and J. B. Bai, *J. Mater. Chem*. **20**, 2441(2010)

82. C. Huang, and Q. M. Zhang, *Adv. Funct. Mater*. **14**, 501 (2004).

83. C. C. Wang, J. F. Song, H. M. Bao, Q. D. Shen, and C. Z. Yang, *Adv. Funct. Mater.* **18**, 1299 (2008).

84. J. K. Yuan, Z. M. Dang, S. H. Yao, J. W. Zha, T. Zhou, S. T. Li and J. B. Bai, *J. Mater. Chem*. **20**, 2441(2010)

85. K. Shehzad, A.Ul-Haq, S. Ahmad, M. Mumtaz, T. Hussain, A. Mujahid, A. T. Shah, M. Y. Choudhry, I. Khokhar, S. Ul-Hassan, F. Nawaz, F. Rahman, Y, Butt, and M. Pervaiz *J. Mater. Sci.* **48**, 3737 (2013).

86. J. W. Xu and C. P. Wong, *Appl. Phys. Lett*. **87**, 082907 (2005).

87. Y. Shen, Y. H. Lin, M. Li and C. W. Nan, *Adv. Mater*. **19**, 1418 (2007).

88. T. Y. Dai, K. Chen, X. T. Qing, Y. Lu, J. S. Zhu and F. Gao, *Macromol. Rapid Commun*. **31**, 484 (2010).

89. Z. M. Dang, Y. Q. Lin, H. P. Xu, C. Y. Shi, S. T. Li and J. B. Bai, *Adv. Funct. Mater.* **18**, 1509 (2008).

90. K. C. Li, H. Wang, F. Xiang, W. H. Liu and H. B. Yang, *Appl. Phys. Lett.* **95**, 202904 (2009).

91. J. R. Birchak, C. G. Gardner, J. E. Hipp and J. M. Victor, *Proc. IEEE* **62**, 93 (1974).

92. L. D. Landau and E. M. Lifshitz, Electrodynamics of Continuous Media, Lond Pergamon Press, London and New York, 1960.

93. H. Looyenga, *Physica* **31**, 401 (1965).

94. K. Wakino, *9th IEEE Int. Sym Appl. Ferro* 33 (1994)

95. S. Stölzle, A. Enders and G. Nimtz, *J. Phys. I Frace* **2**, 401 (1992).

96. J. B. Kim, T. W. Kim and C. G. Kim, *J. Appl. Polym. Sci.* **100**, 2189 (2006).

97. K. Lichtenecker, Physik. *Zeitschr*. **30**, 805 (1929).

98. Z. Hashin and S. Shtrikman, *J. Appl. Phys*. **33**, 3125 (1962).

99. R. Simpkin, *IEEE Trans. Microwave Theory Tech*. **58**, 545 (2010).

100. D. A. G. Bruggeman, *Ann. Phys. (Leipzig)* **24**, 636 (1935).

101. J. W. Rayleigh, *Phil. Mag*. **34**, 481 (1892).

102. A. H. Sihvola, *IEEE Trans. Geosci. Remote Sens.* **29**, 679 (1991).

103. J. C. Maxwell, Electricity and Magnetism, Clarendon Press, Oxford, 1892.

104. K. W. Wagner, Die Isolierstoffe der Elektrotechnik, Springer, Berlin, 1924.

105. S. E. Skipetrov, *Phys. Rev. B* **60**, 12705 (1999).

106. D. Polder and J. H. van Santeen, *Physica* **12**, 257(1946).

107. R. Landauer, *J. Appl. Phys*. **23**, 779 (1952).

108. D. S. McLachlan, *J. Phys. C*. **19**, 1339 (1986).

109. D. S. McLachlan, *J. Phys. C*. **20**, 865 (1987).

110. D. S. McLachlan, *J. Phys. C*. **21**, 1521 (1988).

111. T. Hanai, Kolloid, Z. **171**, 23 (1960).

112. S. M. Puranik, A. C. Kunbharkhane and S. C. Mehrotra, *J. Mol. Liq*. **59**, 173 (1994).

113. E. tuncer, S. M. Gubanski and B. Nettelblad, *J. Appl. Phys*. **89**, 8092 (2001).

114. J. P. Calame, *J. Appl. Phys*. **104**, 114108 (2008).

115. E. F. Knott, *IEEE Trans. Antennas Propag*. **41**, 1167 (1993)

116. T. Yamada, T. Ueda and T. Kitayama*, J. Appl. Phys*. **53**, 4328 (1982).

117. T. K. H. Starke, C. Johnston, S. Hill, P. Dobson and P. S. Grant, *J. Phys. D: Appl. Phys*. **39**, 1305(2005).

118. Z. M. Dang, Y. Shen and C.-W. Nan, *Appl. Phys. Lett.* **81**, 4814 (2002).

119. W.H. Yang, S.H. Yu, R. Sun, and E.X. Du, *Acta Mater*. **59**, 5593 (2011).

120. P. Murugaraj, D. Mainwaring and N. Mora-Huertas, *J. Appl. Phys* **98**, 054304 (2005).

121. E. Tuncer, Y. V. Serdyuk and S. M. Gubanski, *IEEE Trans. Dielectrics Electr. Insulation* **9**, 809 (2002).

122. C. Pecharroman and J. S. Moya, *Adv. Mater*. **12**, 294 (2000).

123. Z. M. Li, M. D. Atbatti and Z.-Y. Cheng, *Macromolecules* **37**, 79 (2004).

124. X. H. Zhao, Y. G. Wu, Z. G. Fan and F. Li, *J. Appl. Phys*. **95**, 8110 (2004).

125. J. P. Calame, *J. Appl. Phys*. **104**, 114108 (2008).

126. J. B. Kim, T. W. Kim and C. G. Kim, *J. Appl. Polym. Sci*. **100**, 2189 (2006).

127. Q. Xue, *Physica B* **344**, 129(2004).

128. T. J. Lewis, *J. Phys. D: Appl. Phys*. **38**, 202 (2005).

129. M. G. Todd and F. G. Shi, *J. Appl. Phys.* **94**, 4551 (2003).

130. H. T. Vo and F. G. Shi, *Microelectron. J.* **33**, 409 (2002).

131. Y. Rao, S. Ogitani, P. Kohl, and C. P. Wong, *J. Appl. Polym. Sci*. **83**, 1084 (2002).

132. X. X. Wang, K. H. Lam, X. G. Tang and H. L. W. Chan, *Solid State Commun*. **130**, 695 (2004).

133. D. H. Kuo, C. C. Chang, T. Y. Su, W. K. Wang and B. Y. Lin, *Mat. Chem.Phys.* **85**, 201 (2004).

134. Z. M. Dang, H. Y. Wang, B. Peng and C. W. Nan, *J. Electroceram*. **21**, 381 (2008).

135. Z. M. Dang, Y. Zheng and H. P. Xu, *J. Appl. Polym. Sci*. **110**, 3473 (2008).

136. M. Olszowy, Cz. Pawlaczyk, E. Markiewicz and J. Kułek, *Phys. Stat. Sol. (a)* **202**, 1848 (2005).

137. M. Kakimoto, A. Takahashi, T. Tsurumi and J. Hao, *Mater. Sci. Eng. B* **132**, 74 (2006).

138. K. H. Lam, H. L. W. Chan, H. S. Luo, Z. W. Yin and C. L. Choy, *Microelectron. Eng*. **66**, 792 (2003).

139. Y. Bai, Z.-Y. Cheng, V. Bharti, H. S. Xu and Q. M. Zhang, *Appl. Phys. Lett*. **76**, 3804 (2000).

140. K. S. Lam, Y. W. Wong, L. S. Tai, Y. M. Poon and F. G. Shin, *J. Appl. Phys.* **96**, 3896 (2004).

141. B. Hilczer, J. Kulek, E. Markiewicz, M. Kosec and B. Malic, *J. Non-Cryst. Sol.* **305**, 167 (2002).

142. L. J. Dong, C. X. Xiong, H. Y. Quan and G. Z. Zhao, *Scr. Mater*. **55**, 835 (2006).

143. S. U. Adikary, H. L. W. Chan, C. L. Choy, B. Sundaravel and I. H. Wilson, *Compos. Sci. Technol*. **62**, 2161 (2002).

144. L. Zhang, X. B. Shan, P. X. Wu and Z.-Y. Cheng, *Appl. Phys. A*, **405**, 92 (2012).

145. B. S. Prakash and K. B. R. Varma, *Compos. Sci. Technol*. **67**, 2363 (2007).

146. P. Thomas, K. T. Varughese, K. Dwarakanath and K. B. R. Varma, *Compos. Sci. Technol*. **70**, 539 (2010).

147. F. Amaral, C. P. L. Rubinger, F. Henry, L. C. Costa, M. A. Valente and A. Barros-Timmons, *J. Non-Cryst. Sol*. **354**, 5321 (2008).

148. Z. M. Dang, T. Zhou, S. H. Yao, J. K. Yuan, J. W. Zha, H. T. Song, J. Y. Li, Q. Chen, W. T. Yang and J. B. Bai, *Adv. Mater*. **21**, 2077 (2009).

149. F. J. Wang, D. X. Zhou and Y. X. Hu, *Phys. Status Solidi A* **206**, 2632 (2009).

150. X. B. Shan, Ph. D. Dissertation, Auburn University (2010).

CHAPTER 2

Metal-Polymer Dielectric Composites with High Percolation Threshold

2.1. Introduction

In this chapter, the Ni-polymer nano-composites with a high percolation threshold will be discussed, which used a new process of combining the solution casting and hot pressing. The percolation threshold larger than 50 vol.% has been obtained due to the a new process increases adhesiveness between the filler and the polymer, leading to a better homogeneity of filler dispersion. Two different polymer matrix systems, P(VDF-TrFE) and P(VDF-CTFE), were used since they both had a high dielectric constants and their dielectric constants exhibited a different temperature dependence.

2.2. Materials and Preparation

2.2.1. Materials

The nano Ni powder, with an average diameter of less than 100 nm, was purchased from Sigma Aldrich. Based on the manufacturers datasheet, the resistivity was around 6.97 μΩ·cm with a density of 8.9 g/cm^3 at 20 °C. **Figure 2-1** shows the identification of the phase of the nano Ni (D<100 nm) with XRD (Bruker D8) [1]. Three characteristic peaks for Ni (2θ = 44.8°, 52.0°, 76.7°) were observed, and peaks for the oxides were not observed. **Figure 2-2** shows the SEM of nano-sized Ni powder. P(VDF-CTFE) 88/12 mol% and P(VDF-TrFE) 70/30 mol% copolymers were

kindly provided by the Solvay company.

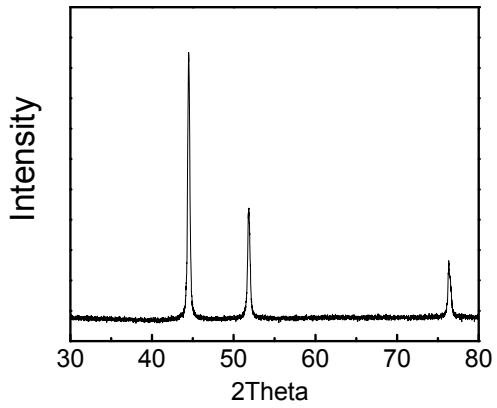

Figure 2-1. XRD pattern of Ni nano powder.

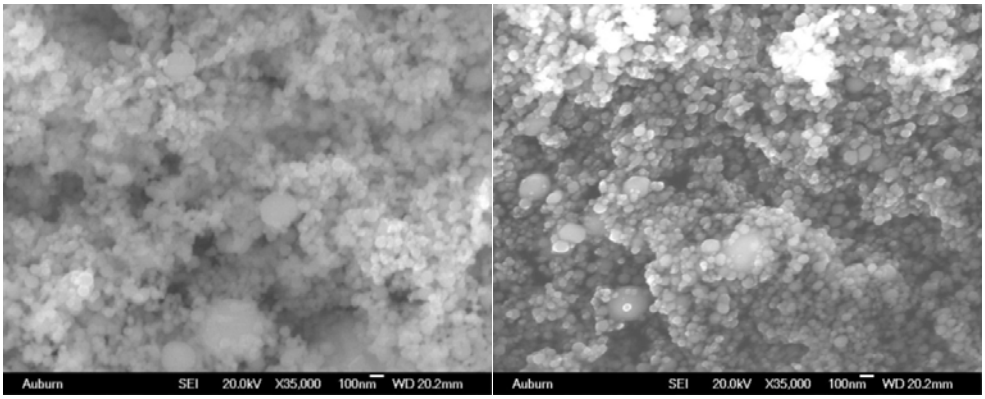

Figure 2-2. SEM of Ni nano powder.

2.2.2. Preparation of Composites

The overall process flowchart for the preparation of Ni-P(VDF-CTFE) 0-3 nanocomposite fabrication is shown in **Figure 2-3**. The first step was to make a solution-cast film. Compared with solid phase processes (mechanical approaches), the solution cast process is better for coating the surface of metal particles. This mixing process resulted in a good dispersion of fillers and a stronger interfacial interaction. P(VDF-CTFE) copolymer was dissolved in N, N-Dimethyl formamide (DMF) under

magnetic stirring for 12 hours. After the copolymer was dissolved in DMF, Ni particles were added into the solution.

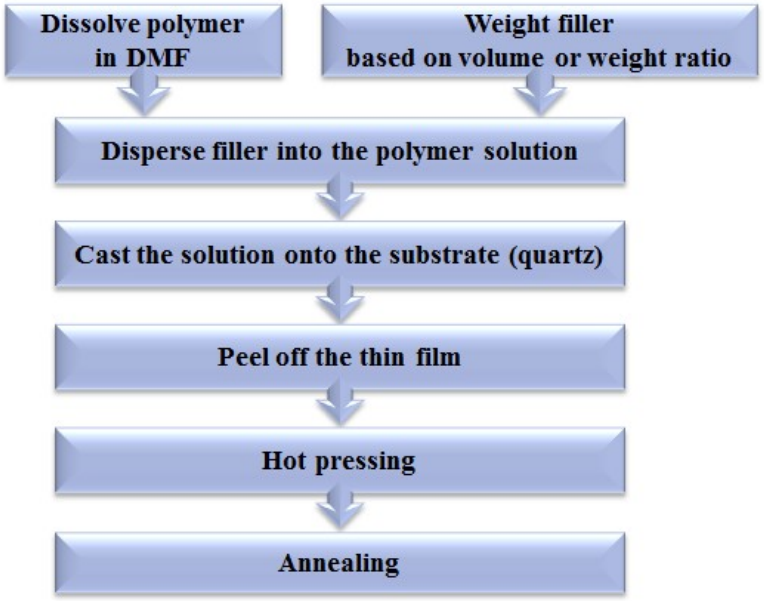

Figure 2-3. Process flowchart for hot-press solution casting composite.

Table 2-1 Volumetric ratios in Ni-P(VDF-CTFE) composites samples

	P(VDF-CTFE) weight(g)	P(VDF-CTFE) vol(cm^3)	Mix (vol.%)	Ni vol(cm^3)	Ni weight(g)
1	0.3	0.1705	10%	0.0189	0.1686
2	0.3	0.1705	20%	0.0426	0.3793
3	0.3	0.1705	30%	0.0731	0.6502
4	0.3	0.1705	40%	0.1136	1.0114
5	0.3	0.1705	45%	0.1395	1.2412
6	0.3	0.1705	50%	0.1705	1.5171
7	0.3	0.1705	55%	0.2083	1.8542
8	0.3	0.1705	60%	0.2557	2.2756

Ni-P(VDF-CTFE) nanocomposites with different Ni volume concentrations (10, 20, 30, 40, 50, 55, 60 vol.%) were prepared. A volumetric ratio table for Ni-P(VDF-CTFE) samples on a quartz substrate with 7.6×7.6 cm (3×3 in, Fisher Scientific) is given in **Table 2-1**. The weight of the polymer was fixed and the weight

of Ni was changed based on the volume ratio. As shown in **Table 2-1**, a fixed amount of solvent (10 ml) was used. In an attempt to achieve a uniform distribution of Ni powder in the polymer solution, a mixing procedure was taken. First, the solution was hand-stirred for 15 minutes as a premixing step. Then the solution was further dispersed by plating in an ultrasonic chamber for 1 hour. The final Ni-P(VDF-CTFE) solution was cast on a quartz plate at 70ºC for 8 hours. Finally, the cast film was released from the quartz substrate by immersing it into D.I. water. The final product was a flexible composite film.

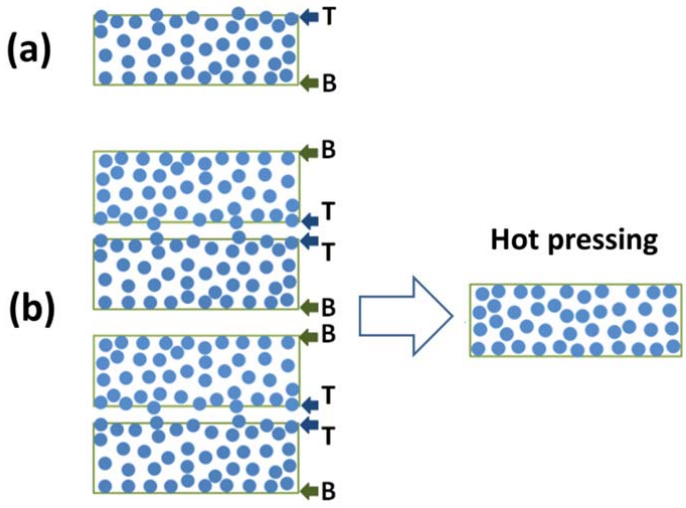

Figure 2-4. Process flowchart of hot-press solution casting composite: (a) as cast composite film (T: top and B: bottom), and (b) stack of four layers hot pressed into one layer.

Similar to previous works [1-3], it was found that the as-cast film had some porosity due to the evaporation of solvent. Therefore, a hot pressing procedure was used to improve the uniformity and the density of the composite. During the hot pressing process, a stack of four layers of as-cast composite were used with a configuration shown in **Figure 2-4**. That is, the stack was arranged that is the top of one as-cast film faced the top of another as-cast film and that the bottom of one

as-cast film faced the bottom of another as-cast film. Then, the stack was placed in plates and a force of 10 tons was applied at 150 ^{o}C. Finally, the hot-press composite films were placed between two glass plates and annealed at 140 ^{o}C for 8 hours in an oven. The thickness of one layer of the as-casted the film was around 50-60μm. After 4 layers were hot pressed, the thickness was around 110-150μm.

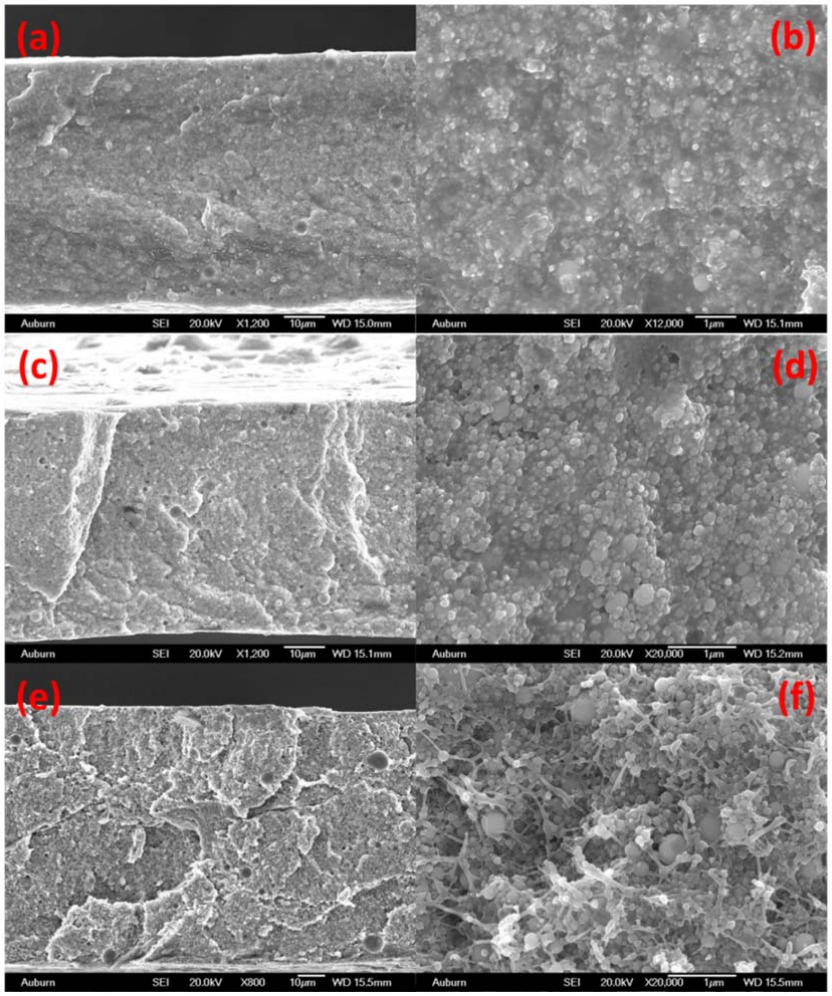

Figure 2-5. SEM of hot pressed Ni-P(VDF-CTFE) composites with different volume fractions of Ni: (a) and (b) 30 vol.%, (c) and (d) 55 vol.%, (e) and (f) 60 vol.%.

The morphologies and the uniformities of the composite films were examined using JEOL JSM 7000F FE-SEM (Scanning Electron Microscopy). The SEM pictures of hot pressed Ni-P(VDF-CTFE) composites with different volume fraction (30 vol.%,

55 vol.% and 60 vol.%) of Ni are shown in **Figure 2-5**. It indicates the hot-pressed composite films are dense and uniform.

2.2.3. Materials Characterization

For the characterization of the dielectric properties for the composite, the samples were sputtered with gold on top and bottom surfaces as electrodes using a PelcoSC-6 sputter coater. A special mask was used for coating the electrodes with a diameter of 3.2 mm. To obtain a uniform coating of gold for the electrode, four times of 30 second coating of each side is necessary, which resulted in a gold layer with a thickness about 40-60 nm. In this work, three individual samples for each concentration were measured. The Agilent 4294A impedance analyzer was employed to measure the dielectric property of the samples over a frequency range of 100 Hz to 1 MHz using Cp~D function. In order to characterize the temperature dependence of the dielectric response, the dielectric properties of the samples were characterized at frequencies of 1 kHz, 10 kHz, 100 kHz and 1 MHz over a temperature range from -70 ºC to 135 ºC in Xi'an Jiaotong University, China. The heating rate was 3 ^{o}C/min.

2.3. Dielectric Behavior of Ni-P(VDF-TrFE) Composites

2.3.1. Frequency Dependence of Dielectric Properties at Room Temperature

The dielectric properties of the composites with different Ni concentrations were measured at room temperature. **Figure 2-6** shows the dielectric properties and conductivity of the Ni-P(VDF-TrFE) nanocomposites with different Ni concentrations from 0 % to 53 vol.% [1].

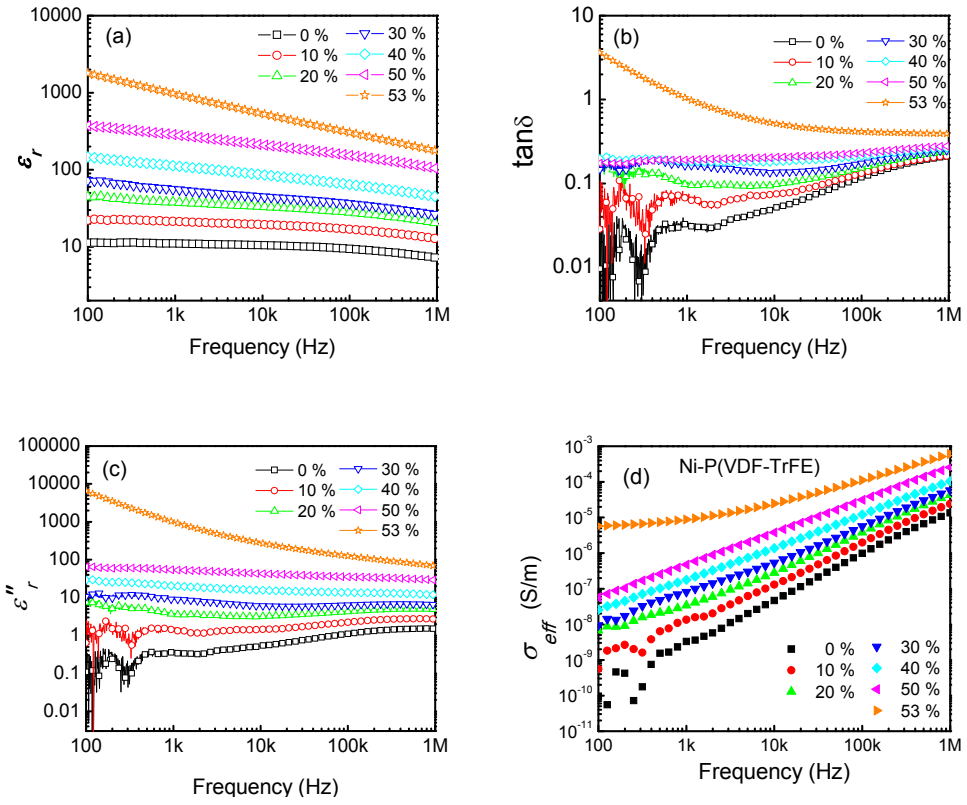

Figure 2-6. Frequency dependence of dielectric properties of Ni-P(VDF-TrFE) composites at room temperature : (a) dielectric constant, (b) dielectric loss, (c) imaginary part of dielectric constant and (d) conductivity.

As shown in the **Figure 2-6** (a), the dielectric constant of the composites increases with increasing filler content. This results in a giant dielectric constant in the composite with a high Ni concentration at low frequency. For example, the dielectric constant at 100 Hz and 1k Hz is 1790 and 967, respectively, for the composite with 53 vol.%. This is approximately 160 and 90 times that of the dielectric constant of the polymer matrix. From **Figure 2-6 (b)** and **(c)**, one can found that both $tan\delta$ and ε''_r increase with increasing frequency for the polymer matrix. However, $tan\delta$ and ε''_r observed in the composites from 10 vol.% to 30 vol.% show a different frequency dependence. At low frequencies, $tan\delta$ and ε''_r decrease with increasing frequency,

while at high frequencies, $tan\delta$ and ε''_r increase with increasing frequency. That is, there is a certain frequency at which they reach their minimum. This frequency separates the frequency range into two regimes: low and high frequency. This special frequency for $tan\delta$ is lower than that for ε''_r. From 40 vol.% to 53 vol.%, ε''_r decreases with increasing frequency continuously. All these indicate that there is a new dielectric process appearing in the composites. The contribution of this new dielectric process to the dielectric response of the composites increases with increasing Ni content.

To study this new dielectric process, the real part of electric conductivity of the composites is plotted in **Figure 2-6(d)**, where the real part of the conductivity is calculated from the imaginary part of the permittivity using Eq. (1-9). Clearly, the conductivity increases with increasing frequency, which indicates that the composites are still dielectric. It seems that the conductivity has a saturated value at low frequency, which means the samples have non-zero conductivity. That is, the conductivity of the composites, shown in **Figure 2-6(d)**, originates from a real conductivity and a dielectric process. The former should be independent of the frequency, while the latter is dependent on the frequency. If Johnscher's universal law, Eq. (1-21), is used to analyze the dielectric response (i.e. the ac conductivity), one can get,

$$\sigma_{meas} = \sigma_0 + A\omega^n \tag{2-1}$$

where σ_0 is the conductivity, ω is the angular frequency, and n is a constant.

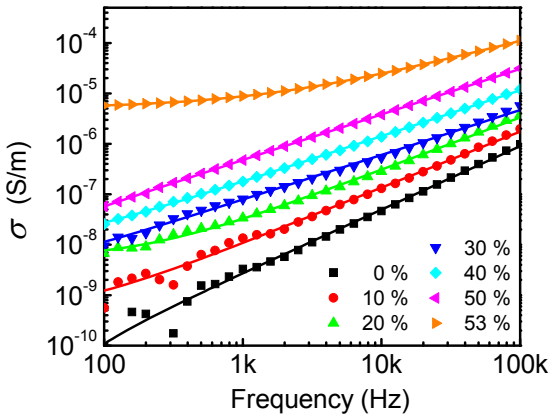

Figure 2-7. Real part of conductivity of composites versus frequency. The solid lines are the fitting results using Eq. (2-1). The Ni content is shown in the figure.

Equation (2-1) is used to fit the experimental results shown in **Figure 2-6 (d)**. Since the polymer matrix has a relaxation process with a relaxation frequency of 10^6 ~ 10^7 Hz and Johnscher's universal law is for the frequencies much higher or lower than the relaxation frequency, the data obtained at frequencies higher than 100 kHz was not used in the fitting. **Figure 2-7** shows the fitting results. Clearly, Eq. (2-1) fits the experimental results very well. All the fitting parameters are presented in **Table 2-2** and plotted in **Figure 2-8**.

Table 2-2 Parameters of Eq. (2-1) for fitting the conductivity of composites

Ni vol.%	Parameter in $\sigma_{meas} = \sigma_0 + A\omega^n$						
	σ_0	σ_0 error	A	A error	n	n error	R^2
0	1.69E-10	1.74E-11	5.76E-14	3.27E-15	1.2410	3.46E-3	0.9970
10	4.27E-10	6.23E-11	6.26E-13	5.11E-14	1.1117	7.25E-3	0.9899
20	5.16E-9	1.26E-10	3.09E-12	1.29E-13	1.0402	3.69E-3	0.9974
30	1.42E-9	2.75E-10	3.18E-11	1.11E-12	0.8913	3.13E-3	0.9975
40	5.94E-9	1.95E-10	6.09E-11	6.72E-13	0.9099	9.89E-4	0.9998
50	9.56E-9	1.50E-10	1.81E-10	7.36E-13	0.9155	3.65E-4	0.9999
53	5.08E-6	3.07E-9	6.26E-9	2.15E-11	0.7286	2.82E-4	0.9999

From the fitting results, it was found that the σ_0 of composites slowly increases with increasing Ni content for the composites with less than 50 vol.% of Ni, which were smaller than 1×10^{-8} S/m. When the Ni content is higher than 50 vol.%, the σ_0 increases rapidly with increasing φ. For example, the σ_0 of 53 vol.% is 530 times of conductivity of 50 vol.%, which means that the composite is close to the percolation threshold. The value of A increased with increasing Ni content. This means that the contribution of the new dielectric process in the composite to the dielectric response increased with the Ni content. This is consistent with the direct observation of the dielectric loss discussed above.

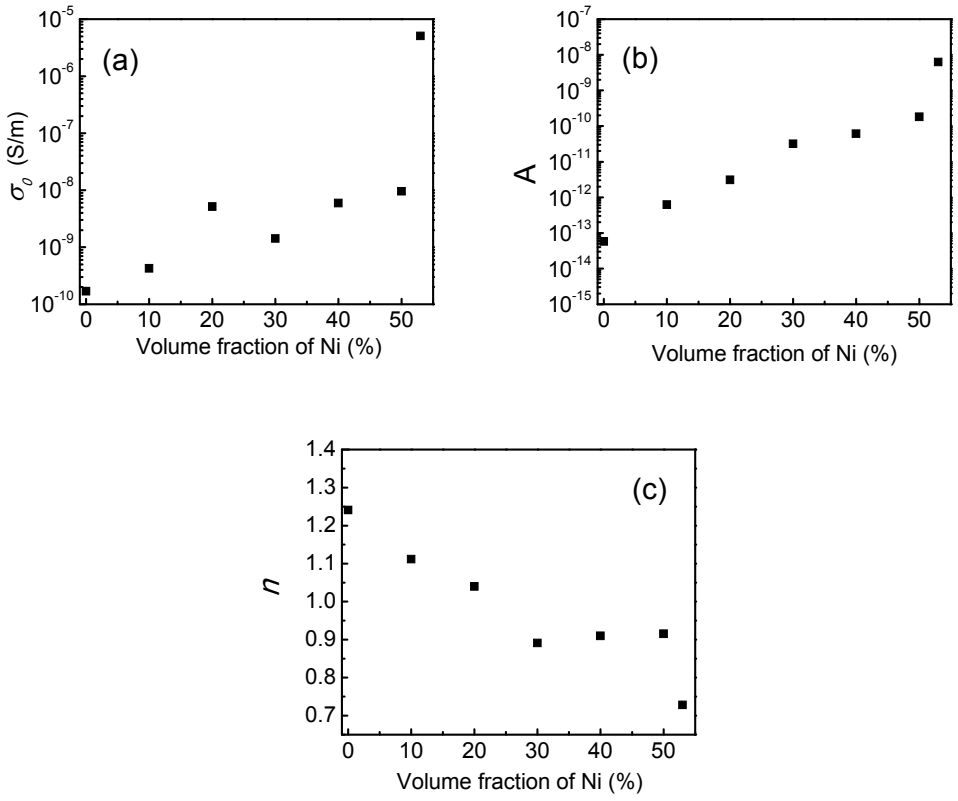

Figure 2-8. Fitting parameters, σ_0, A, and n, for different composites.

Regarding the value of n obtained from the fitting, one can find that n decreased

with increasing Ni concentration from 0 % to 30 vol.%, held value around 0.9 from 40 vol.% to 50 vol.%, then deceased at 53 vol.%. It was very interesting that the value of the *n* changes from larger than one for the composites with low Ni content to smaller than one for the composites with high Ni content. Based on the Johnscher's universal law, *n* larger than one means that the dielectric process has a relaxation frequency, which is much higher than the frequency range. For example, for the polymer matrix used, its relaxation frequency was higher than 10^6 Hz. Therefore, the *n* was 1.24 (>1) for the frequency range lower than 100 kHz. However, *n* smaller than one means the dielectric process had a relaxation frequency much lower than the frequency range. This means that the new dielectric process observed in the composites was a relaxation process with a very low relaxation frequency.

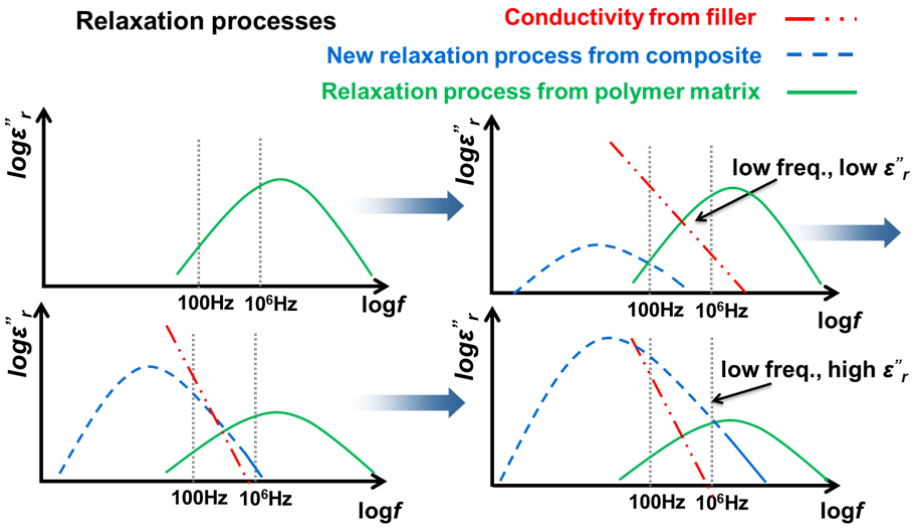

Figure 2-9. Schematic of the dielectric relaxation processes in conductor-polymer composites.

The schematic of the dielectric relaxation processes in conductor-polymer composites is shown in **Figure 2-9**. At the very beginning, if Ni concentration is 0, there is only dielectric process of polymer matrix. When Ni filler added in matrix,

there are three mechanisms in this conductor-polymer composite: 1) the dielectric relaxation process from the polymer matrix, 2) the new dielectric relaxation process from the composite, and 3) the conductivity of the conducting filler (Ni). Based on the results discussed before, the dielectric properties of the composites with less than 30 vol.% Ni content is dominated by the polymer matrix. With increasing Ni concentration, the value of ε''_r from new dielectric relaxation process will increase. With high Ni concentration, the dielectric properties obtained in the composites will be dominated by the new dielectric process.

2.3.2. Temperature Dependence of Dielectric Properties

The temperature dependence of the dielectric properties at different frequencies for pure polymer matrix is shown in **Figure 2-10**. Clearly, both $tan\delta$ and ε''_r show a peak at certain temperature (-20 ^{o}C to +20 ^{o}C). The higher the frequency is, the higher the peak temperature is and the higher the peak value is. This is a typical relaxation process due to the glass transition temperature (T_g). Above the T_g, There is a maximum value of dielectric constant which is related to the ferroelectric-to-paraelectric phase transition temperature (T_{max}) in the P(VDF-TrFE) polymer. T_{max} is around 100-110 ^{o}C. At high temperature, the dielectric loss increases with increasing temperature due to the conductivity.

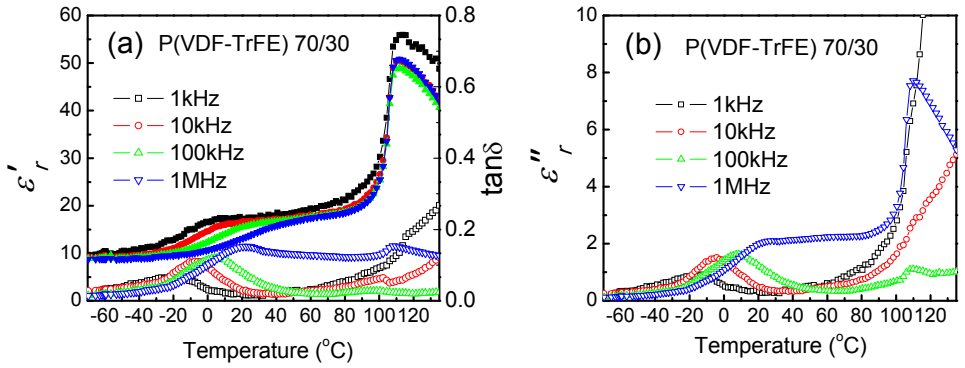

Figure 2-10. Temperature dependence of dielectric properties of pure P(VDF-TrFE): (a) real part(solid) and loss(open), (b) imaginary part.

Figure 2-11 to **Figure 2-16** show the temperature dependence of dielectric properties for Ni-P(VDF-TrFE) composites with different concentration of Ni at 1 kHz, 10 kHz, 100 kHz, and 1 MHz.

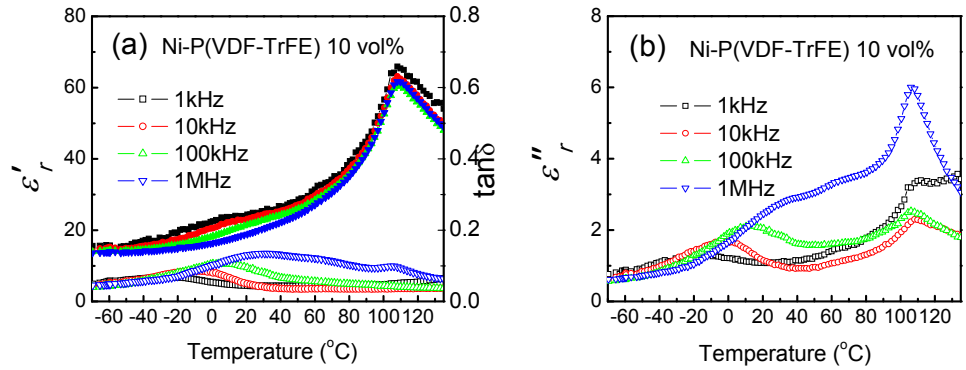

Figure 2-11. Temperature dependence of dielectric properties of the composite with 10 vol.% Ni: (a) real part(solid) and loss(open), (b) imaginary part.

The dielectric constant of the composite with 10 vol% of Ni shows the similar temperature dependence as the polymer matrix. Around T_{max}, the dielectric constant increases dramatically from 21 (at 80 °C) to 53 (at 109 °C) at 1 kHz for polymer matrix, however, the dielectric constant increases continuously and gradually from 39 (at 80 °C) to 65 (at 108 °C) at 1 kHz for 10 vol% of Ni. As discussed in **Figure 1-6**, the P(VDF-TrFE) polymer changed from the typical ferroelectric phase to relaxor

ferroelectric phase after irradiation, which indicated the Ni may decrease the crystallization of polymer matrix. The composite exhibited a lower loss at high temperature, which results in a weaker temperature dependence of the dielectric loss at high temperature than the polymer matrix. Regarding the glass transition process, similar to the polymer matrix, the higher the frequency, the higher the peak temperature for $tan\delta$ and ε''_r.

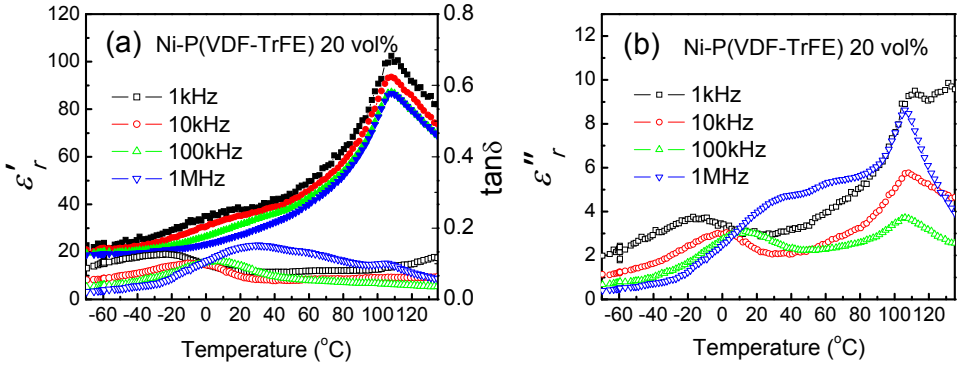

Figure 2-12. Temperature dependence of dielectric properties of the composite with 20 vol.% Ni: (a) real part(solid) and loss(open), (b) imaginary part.

The dielectric constant of the composite with 20 vol.% of Ni showed the similar temperature dependence as the composite with 10 vol.% of Ni. Again, the composite exhibited a lower loss at high temperature than the polymer matrix. Regarding glass transition process, although the ε''_r for the composite was higher than the composite with 10 vol.% Ni, the increase at low frequency was clearly higher than at high frequencies. For example, the peak of ε''_r at 100 kHz was 2.12 and 3.07, for the composites with 10 and 20 vol.%, respectively, while it at 1 kHz was 1.36 and 3.72, respectively. And the ε''_r of the composite at high temperature was also higher than the composite with 10vol.% Ni. All these may be the results of an increase in the DC

conductivity. This is consistent with the data shown in **Table 2-2**.

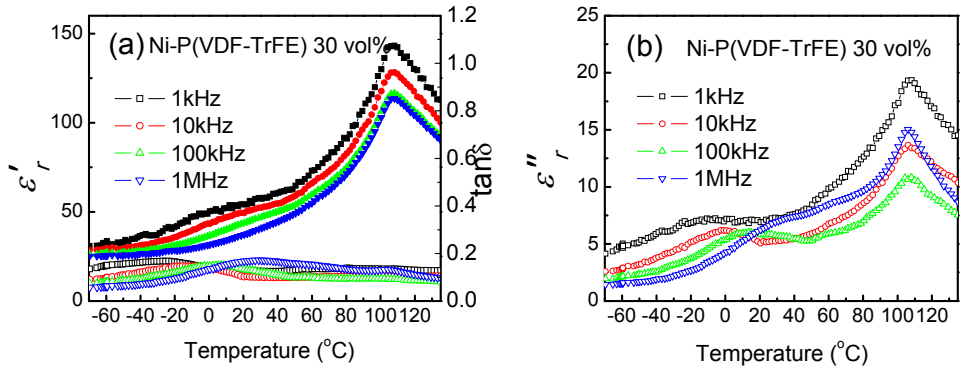

Figure 2-13. Temperature dependence of dielectric properties of the composite with 30 vol.% Ni: (a) real part(solid) and loss(open), (b) imaginary part.

The dielectric constant of the composite with 30 vol.% of Ni showed the similar temperature dependence as the composite with 20 vol.% of Ni. Again, the composite exhibited a lower loss at high temperature than the polymer matrix. For $\varepsilon''_{r,}$ the ε''_{r} at 1 kHz and 1 MHz peak value of T_{max} had the similar value for 20 vol.%. In 30 vol.% composite, the peak value of T_{max} at 1 kHz was larger than 1 MHz.

From a pure matrix to 30 vol%, it was easy to identify the glass transition temperature from imaginary part of dielectric constant. However, from 40 vol% to high volume fraction, the value of the "shoulder" between the peak of T_g and T_{max} in imaginary part increased due to the increasing loss. It was difficult to find the peak of glass transition temperature at high frequency. In 40 vol.% composite, the peak value of T_{max} at 1 kHz and 10 kHz both were larger than 1 MHz.

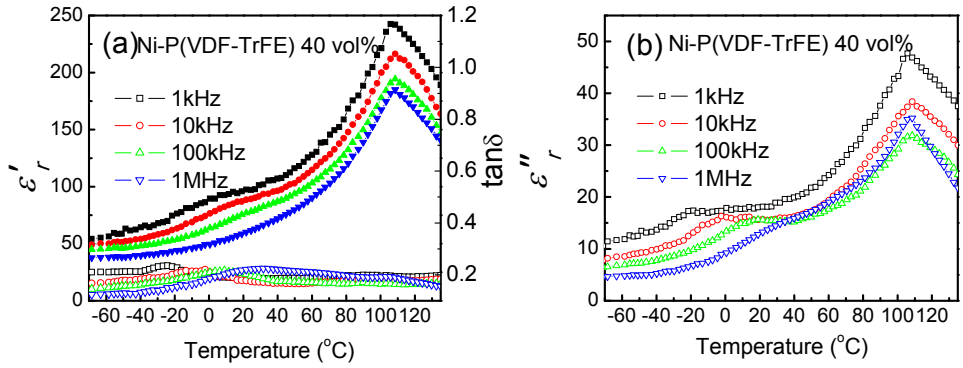

Figure 2-14. Temperature dependence of dielectric properties of the composite with 40 vol.% Ni: (a) real part(solid) and loss(open), (b) imaginary part.

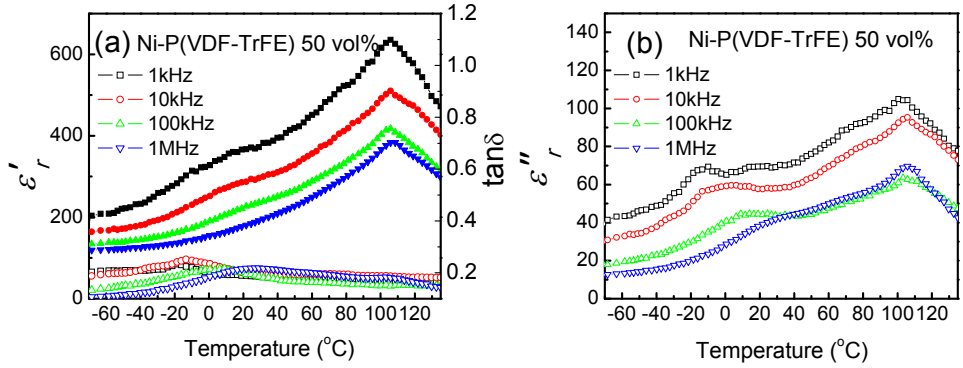

Figure 2-15. Temperature dependence of dielectric properties of the composite with 50 vol.% Ni: (a) real part(solid) and loss(open), (b) imaginary part.

The dielectric constant of the composite with 50 vol.% is around 600 at 1 kHz near the T_{max}, while the loss was around 0.2. Moreover, the dielectric constant of the composite with 53 vol.% was around 1500 at 1 kHz near T_{max}, while the loss was smaller than 0.2. High dielectric constant and low loss near T_{max} indicated this system may have good dielectric application. It is interesting to find that the loss at 1 kHz decreased with increasing temperature. It is possible that there is a new dielectric process in the low frequencies.

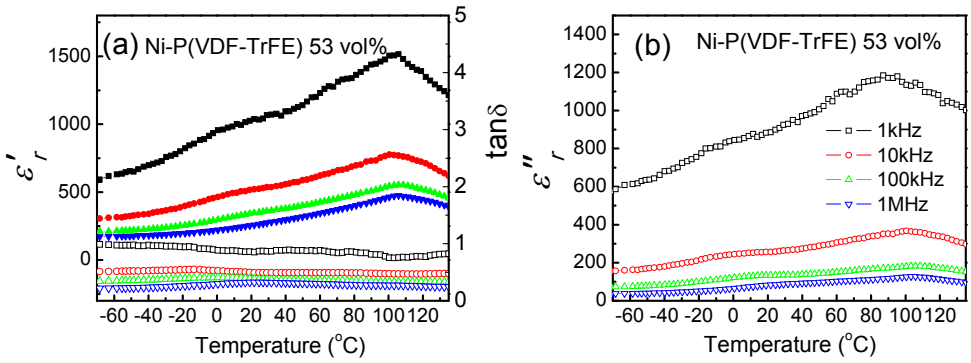

Figure 2-16. Temperature dependence of dielectric properties of the composite with 53 vol.% Ni: (a) real part(solid) and loss(open), (b) imaginary part.

For the composite with 53 vol.% Ni, the new dielectric relaxation process almost completely dominated the dielectric loss and the relaxation process was not easy to identify. The dielectric constant at peak position of 1 kHz was 2 times of which at 10 kHz, while the dielectric constant at peak position of 1 kHz was only 1.2 times of that at 10 kHz for 50 vol.%. The loss at 1 kHz was close to 1 but still smaller than 0.5 at 10 kHz, 100 kHz and 1 MHz.

To compare the dielectric properties of composites with different Ni volume fractions clearly, the ε'_r, ε''_r and *tanδ* at 1 kHz and 1 MHz are shown in **Figure 2-17**. As a short summary, ε'_r, and ε''_r increased with the increasing Ni content. The *tanδ* at low temperature increased with the increasing Ni content. At high temperature, except the composite with 53 vol.% of Ni, the composites exhibited a lower *tanδ* at low frequency. At high frequency, the new dielectric relaxation process almost completely dominated the dielectric properties. The peak of glass transition temperature slightly shifted to high temperature from 30vol% to 50 vol%. However, it was difficult to quantify the change of shifts for glass transition temperature.

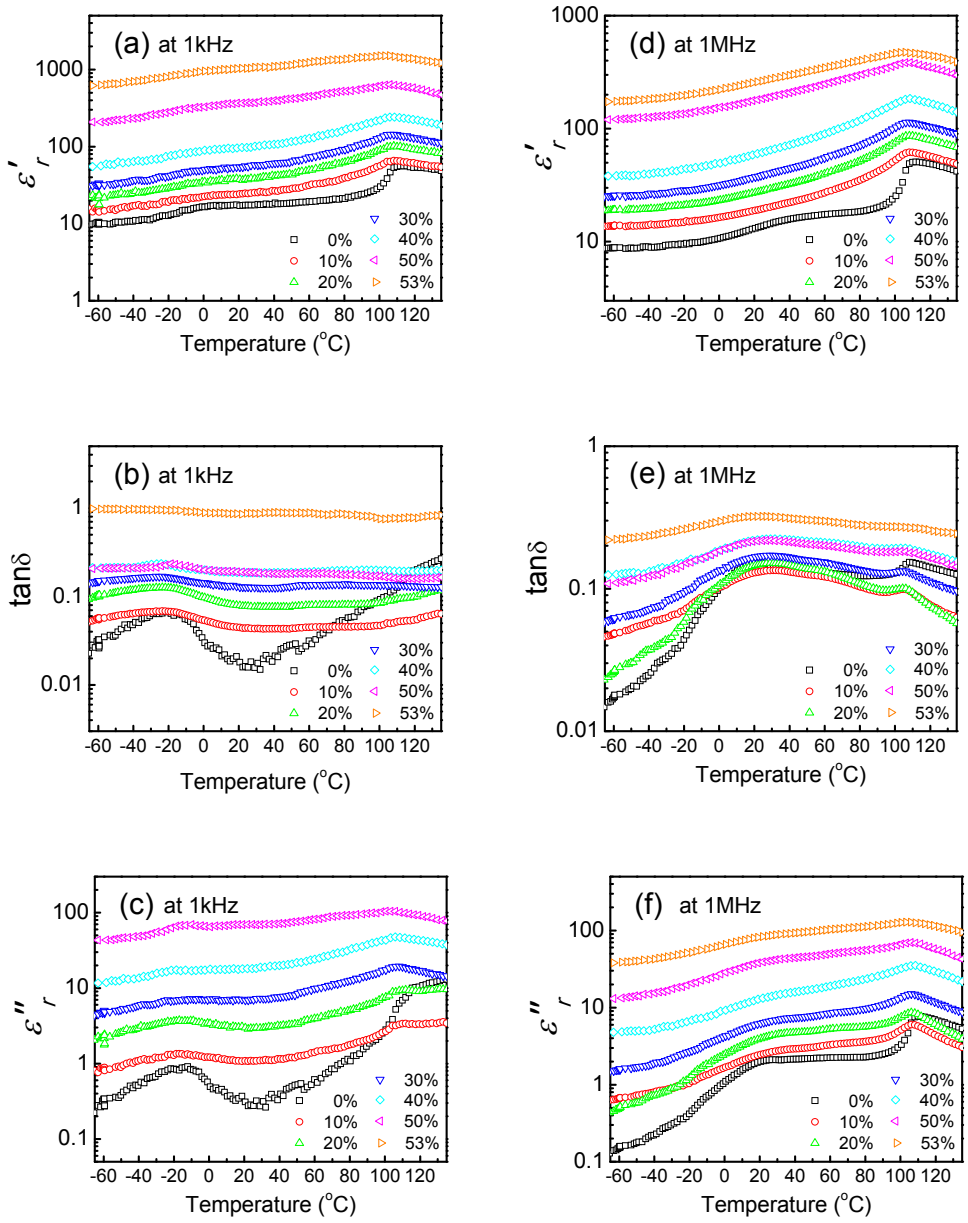

Figure 2-17. Temperature dependence of ε'_r, ε''_r and *tanδ* of composites: (a) to (c) at 1 kHz and (d) to (f) at 1 MHz.

In order to study the effect of Ni powder on the peak positions of T_{max} for the composites, the peak positions at different frequencies were fitted from **Figure 2-10** to **2-16**. The results are listed in **Table 2-7** and **Figure 2-18**. In each composite, the peak positions slightly increased with frequency when Ni content changed from 30%

to 53%. It can be explained that the new dielectric relaxation process dominated in the relaxation processes. With increasing Ni content, the peak positions of T_{max} decreased which is due to the size of crystal becoming smaller or crystallization of composite decreasing.

Table 2-3 The peak positions of T_{max} of composites at different frequencies

Freq.	0 vol.%	10 vol.%	20 vol.%	30 vol.%	40 vol.%	50 vol.%	53 vol.%
1kHz	113.53	110.81	109.89	108.89	108.76	105.05	102.28
10kHz	112.30	110.53	109.75	108.97	108.77	105.87	103.38
100kHz	112.65	110.64	110.16	109.29	108.84	107.07	105.27
1MHz	113.04	110.98	110.51	109.60	109.38	107.36	106.80

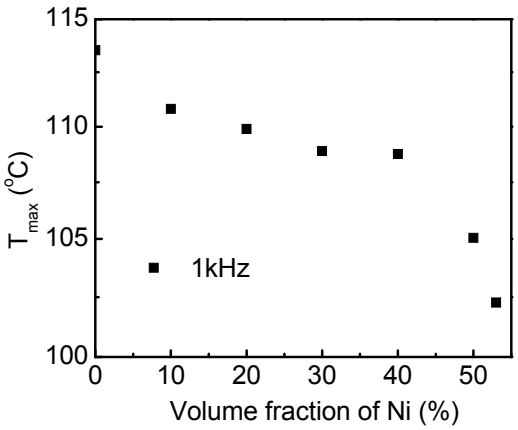

Figure 2-18. T_{max} of composites at 1 kHz.

2.4. Dielectric Behavior of Ni-P(VDF-CTFE) Composites

2.4.1. Frequency Dependence of Dielectric Properties at Room Temperature

The dielectric properties of Ni-P(VDF-TrFE) nano-composites show a high percolative threshold. It is interesting to confirm this by using another polymer as a matrix. In this section, P(VDF-CTFE) is used because of its following features. Firstly, similar with other PVDF-based polymers, P(VDF-CTFE) copolymer at room temperature also exhibits a dielectric constant around 10. Secondly, P(VDF-CTFE)

copolymers show that its dielectric constant is weakly dependent on the temperature. The dielectric properties and percolation behavior of the two composites can be compared and the new information about the dielectric mechanism can be realized.

The composites with different Ni concentration were measured at room temperature. **Figure 2-19** shows the dielectric properties and conductivity of the Ni-P(VDF-CTFE) nano-composites with different Ni concentration from 0 % to 60 vol.%.

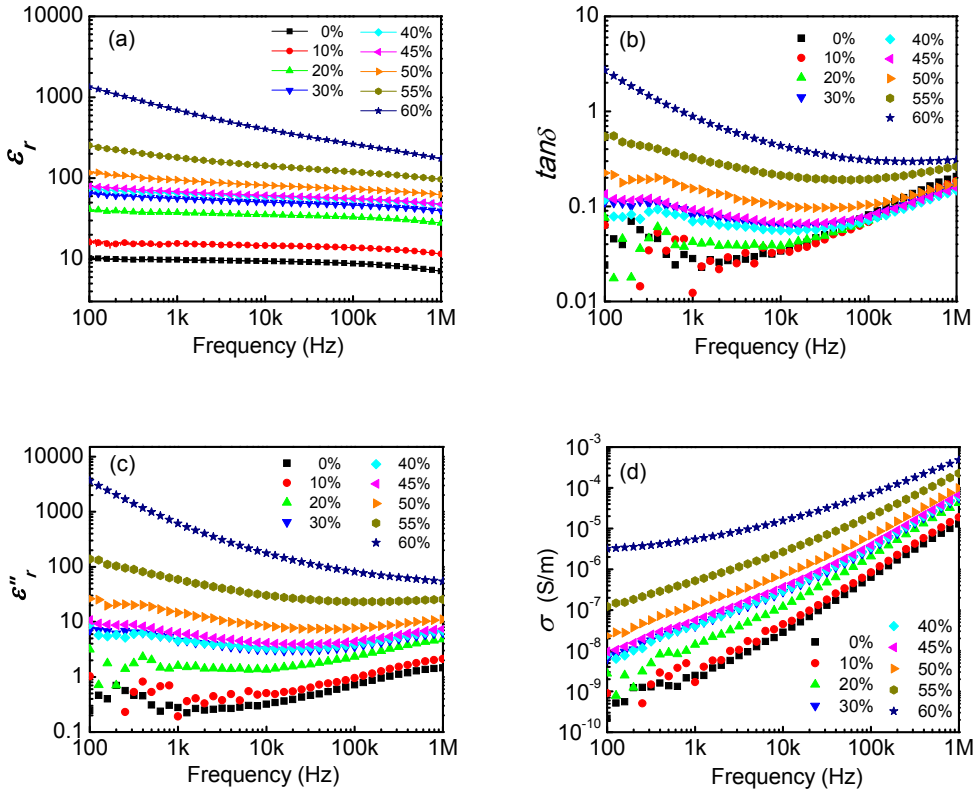

Figure 2-19. Dielectric responses: (a) dielectric constant, (b) dielectric loss, (c) imaginary part of dielectric constant and (d) conductivity varies with frequency for Ni -P(VDF-CTFE) composites with Ni concentrations from 0 % to 60 vol.%.

As shown in the **Figure 2-18 (a)**, the dielectric constant of the composites increased with increasing filler concentration. A high dielectric constant (>600) with a

loss less than one was observed at 1 kHz in the composite with 60 vol.% of Ni. This dielectric constant was more than 60 times that of the dielectric constant of the polymer matrix. The composites with low Ni concentration showed similar frequency dependence for the dielectric constant with the polymer matrix. For the composites with high Ni content, a stronger frequency dependence of the dielectric constant was observed. These are the same as what we observed in Ni-P(VDF-TrFE) composites. From **Figure 2-18 (b)** and **(c)**, it can be found that both $tan\delta$ and ε''_r increase with increasing frequency for polymer matrix. However, $tan\delta$ and ε''_r observed in the composites show a different frequency dependence. At low frequencies, they decrease with increasing frequency, while at high frequencies, they increase with increasing frequency. That is, there is a certain frequency, at which they reach their minimum. This frequency separates the frequency range into two regimes: low and high frequency. This certain frequency for $tan\delta$ is lower than that for ε''_r. All these indicate that there is a new dielectric process in the composites. The contribution of this new dielectric process to the dielectric response of the composites increased with increasing Ni concentration.

To study this new dielectric process, the real part of electric conductivity of the composites was plotted in **Figure 2-19 (d)**, where the real part of the conductivity from the imaginary part of the permittivity using Eq. (1-9). Clearly, the conductivity increases with increasing frequency. It seems that there is a saturated value for the conductivity at low frequency, which means the samples have non-zero conductivity. That is, the conductivity of the composites originated from the new dielectric process

and the dielectric relaxation from the composites. Similar to Section 2.3.1, Eq. (2-1) was used to analyze the dielectric response.

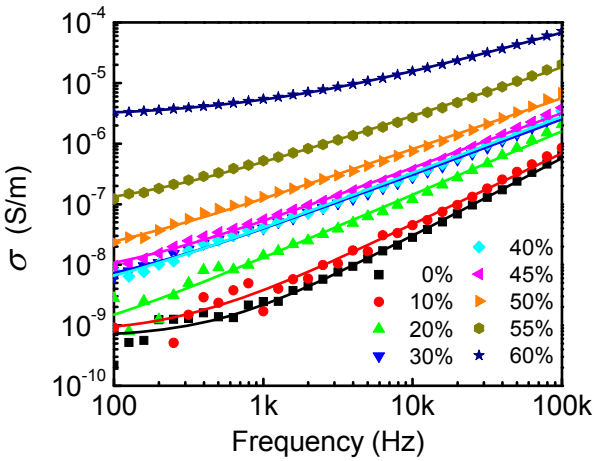

Figure 2-20. Real part of conductivity of composites versus frequency. The solid lines are the fitting results using Eq. (2-1).

Table 2-4. Parameters of Eq. (2-1) for fitting the conductivity of composites

Ni vol%	Parameter in $\sigma_{meas} = \sigma_0 + A\omega^n$						
	σ_0	σ_0 error	A	A error	n	n error	R^2
0	5.23E-10	1.85E-11	1.18E-14	7.56E-16	1.2503	5.53E-3	0.9969
10	7.48E-10	6.64E-11	1.05E-13	1.74E-14	1.1766	1.48E-2	0.9690
20	7.56E-10	1.14E-10	2.18E-12	1.51E-13	1.0490	6.26E-3	0.9918
30	2.87E-9	1.68E-10	1.19E-11	5.04E-13	0.9182	3.74E-3	0.9967
40	2.08E-9	1.84E-10	1.16E-11	2.25E-13	0.9275	4.16E-3	0.9959
45	4.83E-9	1.90E-10	1.69E-11	5.85E-13	0.9101	3.06E-3	0.9978
50	7.54E-9	5.31E-10	7.39E-11	2.82E-12	0.8415	3.38E-3	0.9971
55	6.65E-8	1.32E-9	3.57E-10	7.88E-12	0.8116	1.93E-3	0.9991
60	2.75E-6	7.09E-9	5.55E-9	6.57E-11	0.7023	9.82E-4	0.9998

Equation (2-1) was used to fit the experimental results shown in **Figure 2-19 (d)**. Since the polymer matrix had a relaxation process with a relaxation frequency of 10^6 ~ 10^7 Hz and Johnscher's universal law was used for the frequencies much higher or lower than the relaxation frequency. The data obtained at frequencies higher than 100

kHz was not used in the fitting. **Figure 2-20** shows the fitting results. Clearly, Equation (2-1) fits the experimental results very well. All the fitting parameters are presented in **Table 2-3** and plotted in **Figure 2-21**.

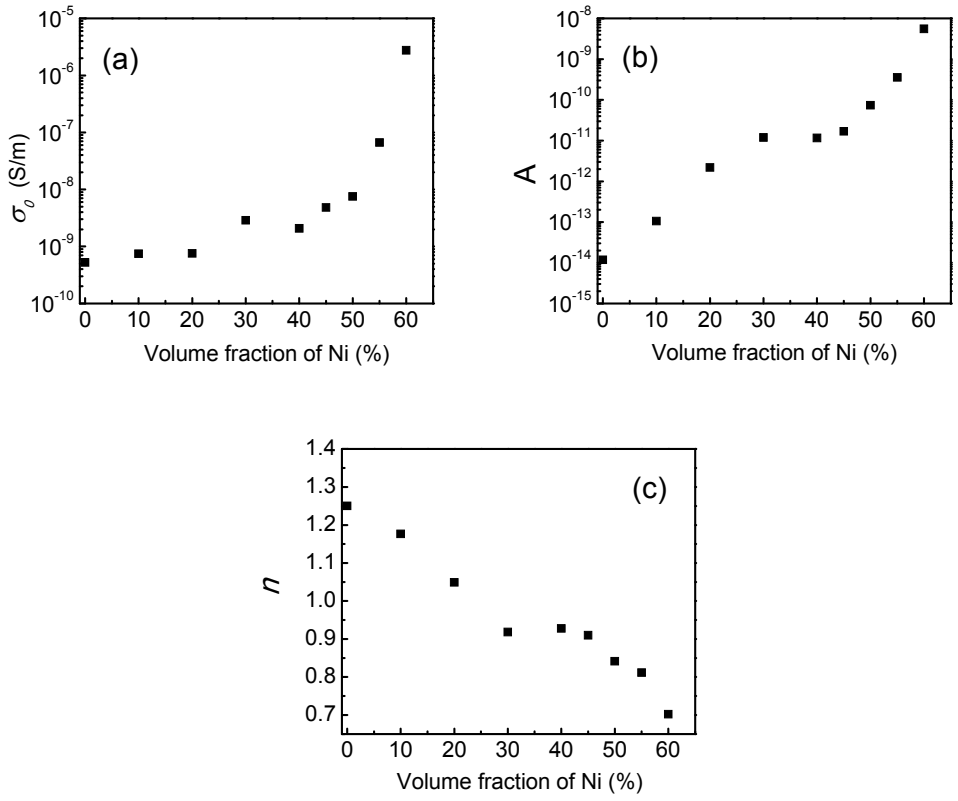

Figure 2-21. Fitting parameters, σ_0, A, and n, for different composites.

From the fitting results, it was found that the σ_0 of composites slowly increased with increasing Ni concentration for the composites with less than 50 vol.% of Ni. When the Ni content was higher than 50 vol.%, the σ_0 increase with the Ni concentration rapidly. For example, the σ_0 of the composites with 55 vol.% and 60 vol.% of Ni was more than 10 and 300 times, respectively, higher than that of the composite with 40 vol.% of Ni. The composites with 60 vol.% of Ni exhibited a high conductivity, which means that the composite was close to the φ_c. The value of A

increased with increasing Ni concentration. This means that the contribution of the new dielectric relaxation process in the composite to the dielectric response increases with the Ni concentration. This is consistent with the direct observation of the dielectric loss discussed above.

Regarding the value of *n* obtained from the fitting, one can find that *n* decreased with increasing Ni concentration. It is very interesting that the value of the *n* changes from larger than one for the composites with low Ni concentration to smaller than one for the composites with high Ni content. Based on the Johnscher's universal law, *n* larger than one means that the dielectric process has a relaxation frequency, which was much higher than the frequency range. For example, for the polymer matrix used, its relaxation frequency is higher than 10^6 Hz. Therefore, the *n* is 1.33 (>1) for the frequency range lower than 100 kHz. However, *n* smaller than one means the dielectric process has a relaxation frequency much lower than the frequency range. This means that the new dielectric process observed in the composites is a relaxation process with a very low relaxation frequency as discussed in Section 2.3.1.

2.4.2. Temperature Dependence of Dielectric Properties

The temperature dependence of the dielectric properties at different frequencies for pure polymer matrix is shown in **Figure 2-22**. Clearly, both $tan\delta$ and ε''_r show a peak at specific temperature (-20 ^oC to +20 ^oC). The higher the frequency is, the higher the peak temperature is and the higher the peak value is. This was a typical relaxation process due to the T_g. Above the T_g, the dielectric constant did not change much. At high temperatures, the dielectric loss increased with increasing temperature

due to the conductivity.

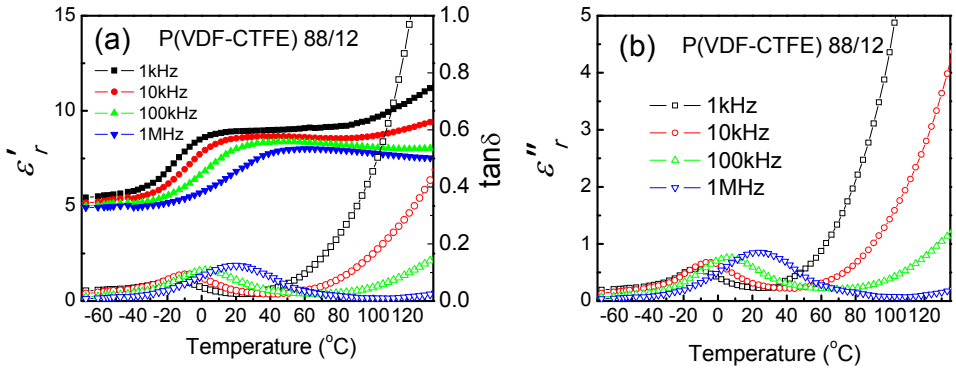

Figure 2-22. Temperature dependence of dielectric properties of pure P(VDF-CTFE): (a) real part(solid) and loss(open), (b) imaginary part.

Temperature dependence of the electrical conductivity can be written as [4, 5]:

$$\sigma = \sigma_0 \exp(-\frac{E_a}{k_B T}) \tag{2-2}$$

where σ_0 is the pre-exponential factor, E_a is an activation energy and k_B is the Boltzmann constant (=8.616×10^{-5}eV). According to Eq. (1-9), the imaginary part of dielectric constant also has the similar relationship with temperature,

$$\varepsilon_r'' = \frac{\sigma}{\varepsilon_0 \omega} \exp(-\frac{E_a}{k_B T}) \tag{2-3}$$

Then by taking the nature logarithm of both sides of the Eq. (2-3), we can get,

$$\ln \varepsilon_r'' = \ln\left(\frac{\sigma}{\varepsilon_0 \omega}\right) - \frac{E_a}{k_B}\left(\frac{1}{T}\right) \tag{2-4}$$

The imaginary part of dielectric constant of pure P(VDF-CTFE) versus 1000/T and the fitting results are shown in **Figure 2-23**, and the parameters are listed in **Table 2-5**.

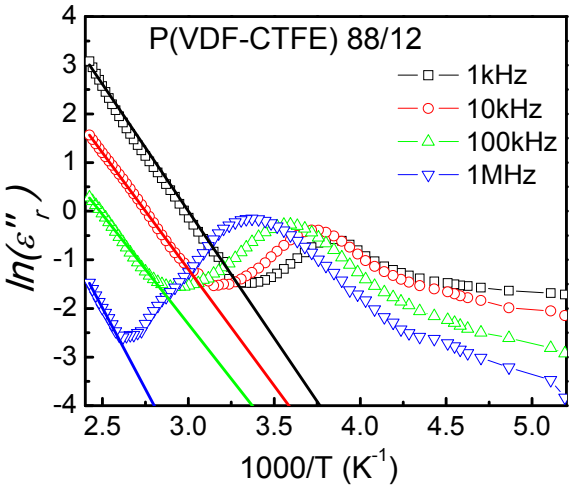

Figure 2-23. Imaginary part of dielectric constant of pure P(VDF-CTFE) versus 1000/T. The solid lines are the fitting results using Eq. (2-4).

Table 2-5. Parameters given by Eq. (2-4) fitting

Freq. (Hz)	$ln\varepsilon''_{r0}$	σ_0 (S/m)	E_a (eV)	R^2
1k	19.29	13.263	0.576	0.9999
10k	17.05	14.120	0.413	0.9997
100k	14.78	14.589	0.388	0.9992
1M	13.04	28.270	0.575	0.9982

Figure 2-24 to **Figure 2-31** show the temperature dependence of the dielectric properties at 1 kHz, 10 kHz, 100 kHz, and 1 MHz for the composites with different Ni concentrations.

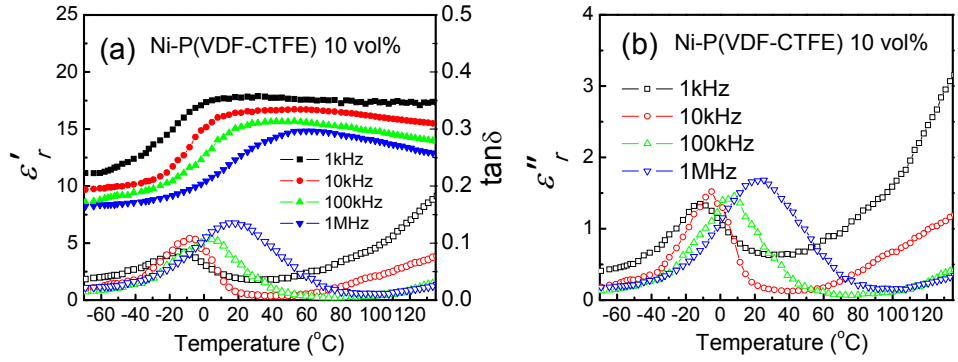

Figure 2-24. Temperature dependence of dielectric properties of the composite with 10 vol.% Ni: (a) real part (solid) and loss (open), (b) imaginary part.

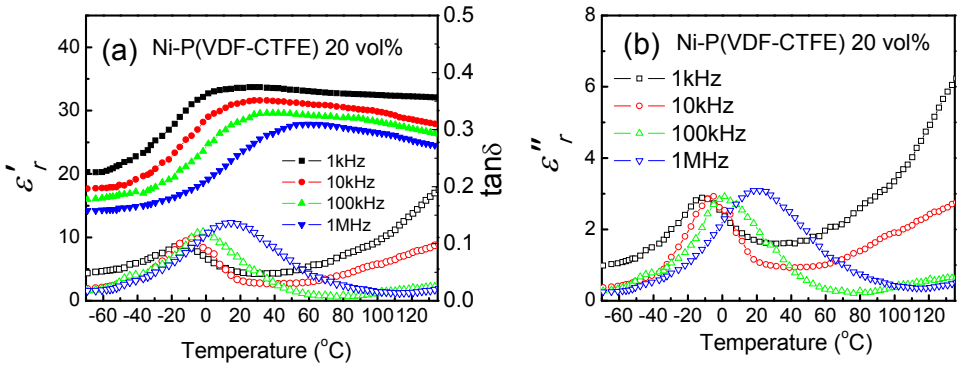

Figure 2-25. Temperature dependence of dielectric properties of the composite with 20 vol.% Ni: (a) real part(solid) and loss(open), (b) imaginary part.

The dielectric constant of the composite with 10 vol.% Ni showed the similar temperature dependence as the polymer matrix. However, the composite exhibited a lower loss at high temperature, which resulted in a weaker temperature dependence of the dielectric constant at high temperature than that of the polymer matrix. Regarding the glass transition process, similar to the polymer matrix, the higher the frequency, the higher the peak temperature for $tan\delta$ and ε''_r. However, the frequency dependence of the peak value changed some. For example, the peak value for 10 kHz was higher than that for 100 kHz. (1.52 for 10 kHz and 1.49 for 100 kHz). It was also interesting to find that there is a temperature range in which the loss is weakly dependent on the temperature. For example, at 10 kHz, this temperature range is about ~20 ^{o}C to ~60 ^{o}C. This means that in the composite there may be one more dielectric process besides the glass transition process.

The dielectric constant of the composite with 20 vol.% Ni showed the similar temperature dependence as the polymer matrix and composite with 10 vol.% Ni. Again, the composite exhibited a lower loss at high temperature than the polymer

matrix. Regarding glass transition process, although the ε''_r for the composite was higher than the composite with 10 vol.% Ni, the increase at low frequency is clearly higher than it at high frequency. For example, the peak of ε''_r at 1 MHz is 1.68 and 3.09, for the composites with 10 and 20 vol.%, respectively, while at 1 kHz it is 1.35 and 2.89, respectively. The ε''_r of the composite at high temperature was also higher than the composite with 10 vol.% Ni. All these may be the results of increase in the DC conductivity. This is consistent with the data shown in **Table 2-4**.

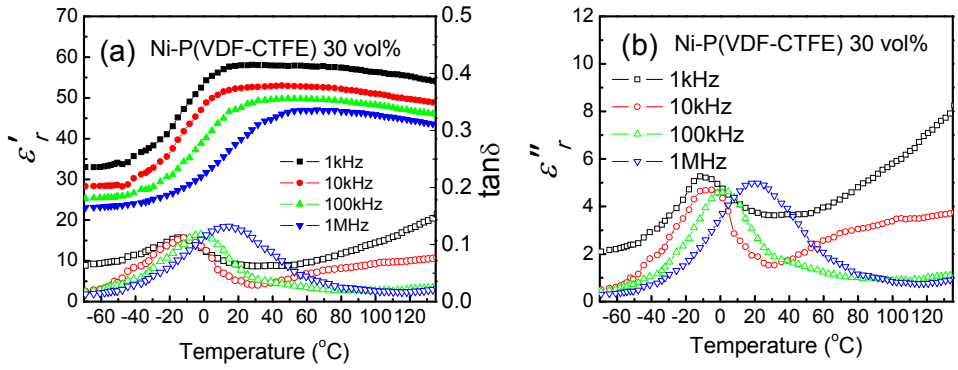

Figure 2-26. Temperature dependence of dielectric properties of the composite with 30 vol.% Ni: (a) real part(solid) and loss(open), (b) imaginary part.

For the composite with 30 vol% Ni, although the loss at high temperature was almost identical with the loss observed in the composite with 20 vol.% Ni, at the low temperature, especially at low frequency, clearly increased compared to the composite with 20 vol.% Ni. Here, the peak of ε''_r at 1 kHz was actually higher than it at 1 MHz. In other words, the conductivity of the composite was higher than the composite with 20 vol.%. This is consistent with the data shown in **Table 2-4**.

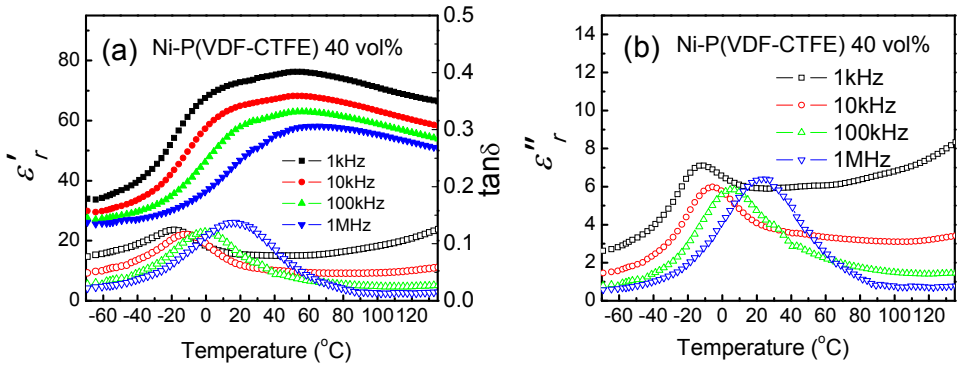

Figure 2-27. Temperature dependence of dielectric properties of the composite with 40 vol.% Ni: (a) real part(solid) and loss(open), (b) imaginary part.

For the composite with 40 vol.% Ni, the ε''_r was higher than that in composite with 30 vol.% Ni. Although the loss (*tanδ*) at low frequency at high temperature was lower than the composites with less Ni concentration, the loss at high frequency at high temperatures did not change much. At the glass transition temperature, the loss at low frequencies was higher than that of composites with less Ni concentration. All these indicate the composite had a higher conductivity than the composite with less Ni concentration. The peak of ε''_r at 1 kHz was again higher than it at 1 MHz. It is interest to find that the temperature dependence of the dielectric constant shown there was a new process which results in a peak like curve at ~60 ^{o}C. As discussed before, there were 3 different mechanisms in this system: 1) the dielectric relaxation process from the polymer matrix, 2) the new dielectric relaxation process from the composite, and 3) the conductivity of the conducting filler (Ni). With increasing Ni concentration, the dielectric constant of composites showed a new peak around 60 ^{o}C, which indicated the interfacial layer show a ferroelectric-like phase.

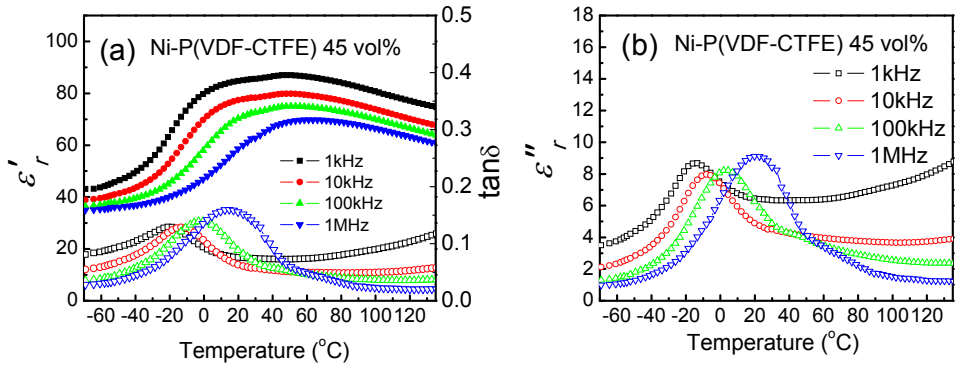

Figure 2-28. Temperature dependence of dielectric properties of the composite with 45 vol.% Ni: (a) real part(solid) and loss(open), (b) imaginary part.

For the composite with 45 vol.% Ni, temperature dependence of the dielectric constant was similar with that for 40 vol.% Ni. It was also interesting to find that the temperature dependence of the dielectric constant shown there was a new process which resulted in a peak like curve at ~60 ^{o}C. The loss at low frequency for the composite at high temperature was lower than composites with less Ni content, but it was higher than the composites with less Ni concentration at lower temperatures. It was found that ε''_r at the high frequencies was higher than that in composites with 40 vol.% Ni. Although the loss at low frequency at high temperature was lower than the composites with less Ni content, the loss at high frequency at high temperature did not change much. At the glass transition temperature, the loss at low frequency was higher than that of composites with less Ni concentration. All these indicate the composite had a higher conductivity than the composite with less Ni content. The peak of ε''_r at 1 kHz was again higher than it at 1 MHz.

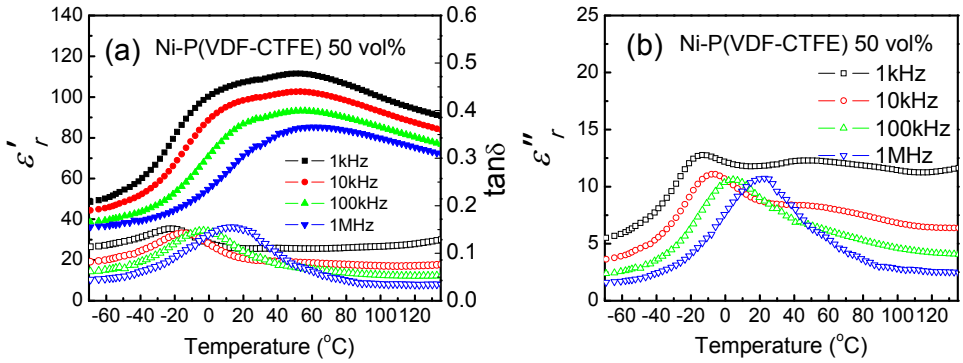

Figure 2-29. Temperature dependence of dielectric properties of the composite with 50 vol.% Ni: (a) real part(solid) and loss(open), (b) imaginary part.

For the composites with 50 vol.% Ni, temperature dependence of the dielectric constant was similar with that for 45 vol.% Ni. That is, there was peak like curve at 60°C. The loss at low frequency for the composite at high temperature was still lower than composites with less Ni concentration. The most important difference from composites with less Ni content was that the ε''_r of 50 vol.% at 1 kHz was larger than high frequency in the whole temperature range, which means the conductivity clearly dominate the dielectric loss at low frequency. At the glass transition temperature, the loss at low frequency was higher than that of composites with less Ni concentration. All these indicated the composite had a higher conductivity than the composite with less Ni concentration. The peak of ε''_r decreased with the increasing of frequency.

For the composite with 55 vol.% Ni, the temperature dependence of the dielectric constant had some difference compared to the composites with 50 vol.% Ni. Firstly, the value difference between each frequency became larger than composites with less Ni content. Secondly, the peak value of dielectric constant (~60°C) was only 1.6 times of that at low temperatures (-65°C). In 20 to 50 vol.% composites, the peak value of

dielectric constant is more than 2 times that compared to low temperatures. For the loss part, it was the first time that the loss at 1 kHz is larger than the high frequency response in the whole temperature range, which meant the conductivity clearly dominated the dielectric loss at low frequency. At glass transition temperature, the loss at low frequency was higher than that of composites with less Ni content. All these indicated the composite had a new dielectric relaxation process. The peak of ε''_r decreased with the increasing of frequency.

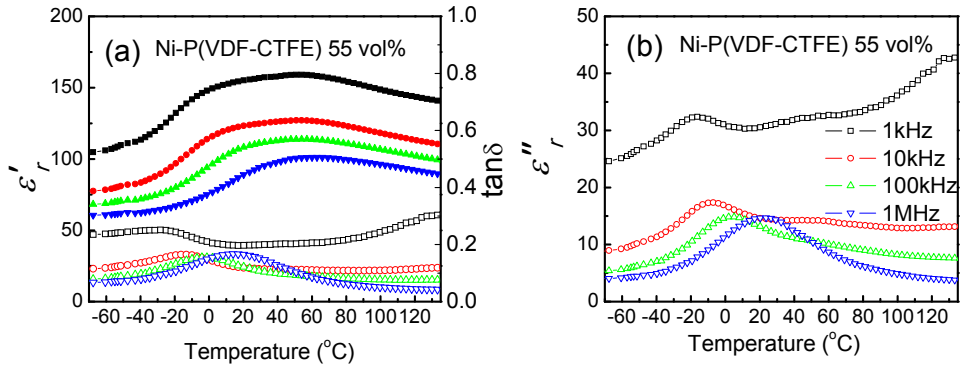

Figure 2-30. Temperature dependence of dielectric properties of the composite with 55 vol.% Ni: (a) real part(solid) and loss(open), (b) imaginary part.

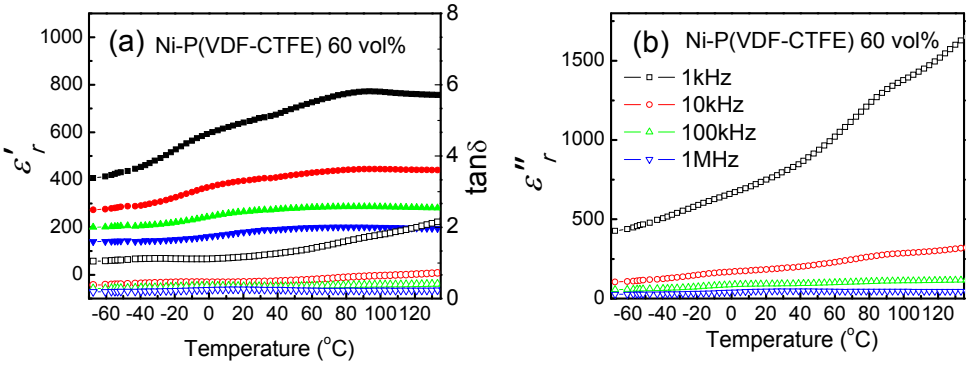

Figure 2-31. Temperature dependence of dielectric properties of the composite with 60 vol.% Ni: (a) real part, (b) loss and (c) imaginary part.

For the composites with 60 vol.% Ni, the new dielectric relaxation process almost completely dominated the dielectric loss and the relaxation process was not easy to

identify. The new process covered a larger temperature range and the peak of the dielectric constant was around 80 °C. The loss at 1 kHz was more than 1 but still smaller than 0.7 at 10 kHz, 100 kHz and 1 MHz.

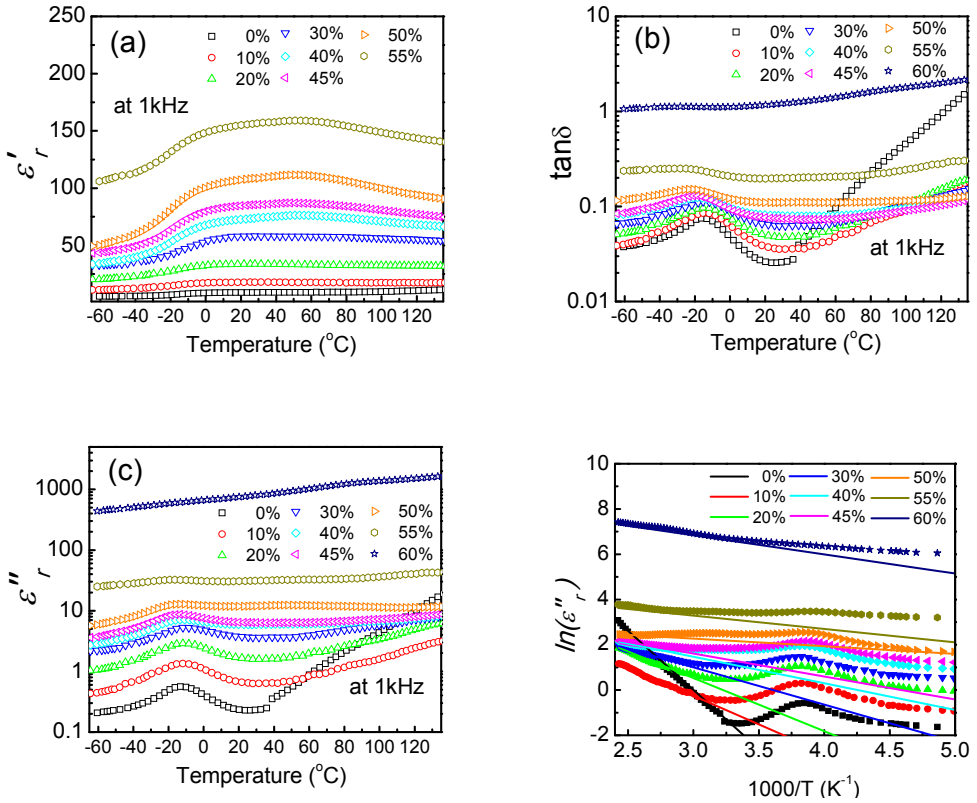

Figure 2-32. Temperature dependence of dielectric properties of composites: (a) ε'_r, (b) *tanδ*, (c) ε''_r and (d) $\ln\varepsilon''_r$ vs. 1000/T.

Table 2-6. Parameters given by Eq. (2-4) fitting at 1 kHz for composites

Ni vol.%	$ln\varepsilon''_{r0}$	σ_0 (S/m)	E_a (eV)	$ln\varepsilon''_{r0}$ at RT (S/m)	σ_0 at RT (S/m)	R^2
0	19.291	13.263	0.5767	-1.476	9.563×10^{-10}	0.9999
10	7.334	8.516×10^{-5}	0.2181	-0.438	1.769×10^{-8}	0.9752
20	7.571	1.079×10^{-4}	0.2024	0.483	4.132×10^{-8}	0.9851
30	5.942	2.116×10^{-5}	0.1420	1.107	8.497×10^{-8}	0.9745
40	4.998	8.236×10^{-6}	0.1013	1.772	1.603×10^{-7}	0.9978
45	4.657	5.856×10^{-6}	0.0875	1.855	1.949×10^{-7}	0.9992
50	3.272	1.466×10^{-6}	0.0288	2.473	4.786×10^{-7}	0.9873
55	5.210	1.018×10^{-5}	0.0509	3.431	1.221×10^{-6}	0.7586
60	9.467	2.962×10^{-5}	0.0727	6.657	3.898×10^{-5}	0.9949

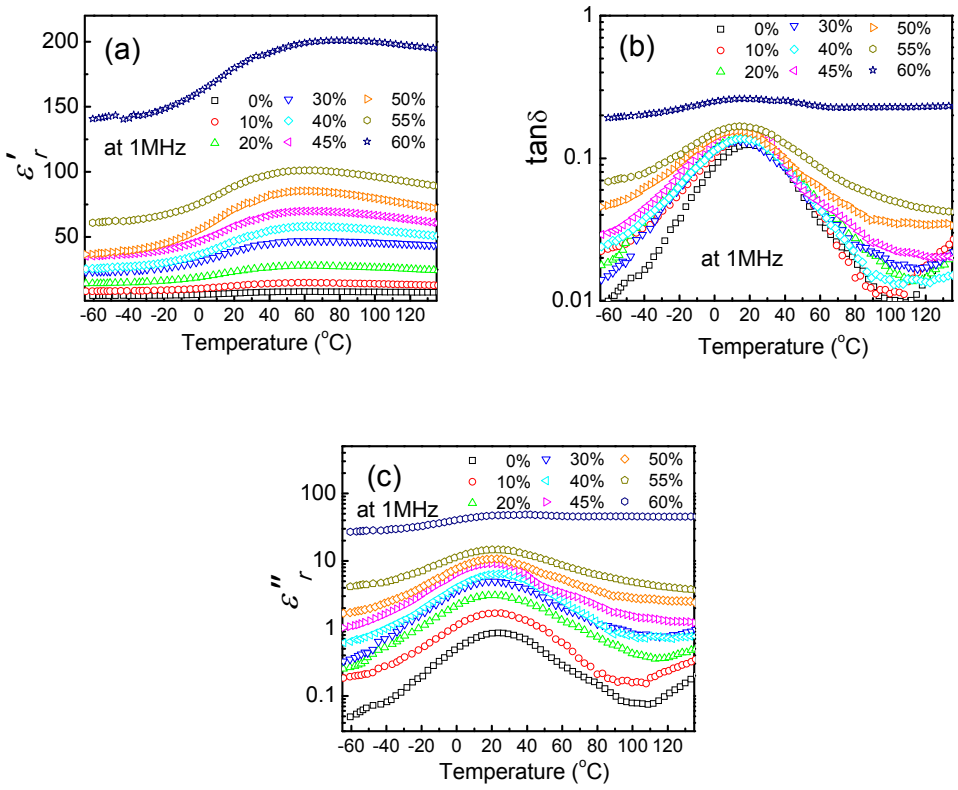

Figure 2-33. Temperature dependence of dielectric properties of composites: (a) ε'_r, (b) *tanδ* and (c) ε''_r.

To compare the dielectric properties with different Ni volume fraction clearly, the ε'_r, ε''_r and *tanδ* at 1 kHz and 1 MHz are shown in **Figure 2-32 and 2-33**. As a short summary, ε'_r, andε''_r increased with the increasing Ni content. The loss at low temperature increased with the increasing Ni content, while decreased firstly with the increasing Ni content then increased due to the higher conductivity at high temperature. The relationship between lnε''_r and 1000/T is shown in **Figure 2-32(d)** and the parameter is shown in **Table 2-6**. Compared with polymer matrix, it indicated that it is the new dielectric relaxation process not the conductivity contributed the ε''_rat low temperature.

Regarding the glass transition temperature, it was of interest to know whether the

filler had some influence on the T_g. The peak position of ε''_r firstly shifted to high temperature then back to a low temperature at 1 kHz. It then shifted to a low temperature then back to high temperature at 1 MHz. To quantify the analysis, the peak temperature of ε''_r was determined for all composites as shown in **Table 2-7** and **Figure 2-34**. All of the peak positions are fitted by peak fitting over a small temperature range from the imaginary parts of the dielectric constant. At 1 kHz and 10 kHz, the T_g slightly increased with increasing Ni content then decreased at 40 vol.%. The log*f* versus 1000/T_g is shown in **Figure 2-35(a)**.

Table 2-7 The glass transition temperature of relaxation behavior of Ni-P(VDF-CTFE) composites with different frequency (in K unit)

	0 vol.%	10 vol.%	20 vol.%	30 vol.%	40 vol.%	45 vol.%	50 vol.%	55 vol.%
1kHz	259.79	260.22	261.21	261.59	261.78	259.28	257.99	256.57
10kHz	268.22	266.89	266.98	266.05	266.74	265.5	264.77	264.75
100kHz	279.31	278.72	276.76	275.54	276.66	275.72	276.98	277.09
1MHz	296.82	295.28	295.18	295.66	293.31	292.56	294.1	296.38

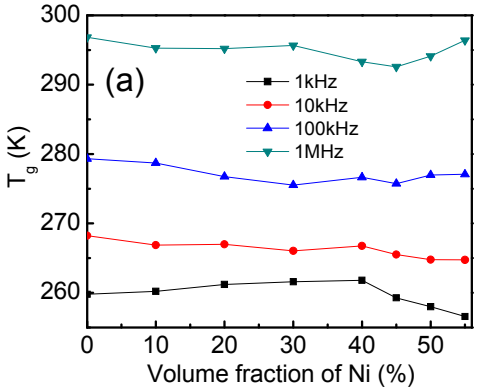

Figure 2-34. The glass transition temperature of relaxation behavior of Ni-P(VDF-CTFE) composites with different frequencies.

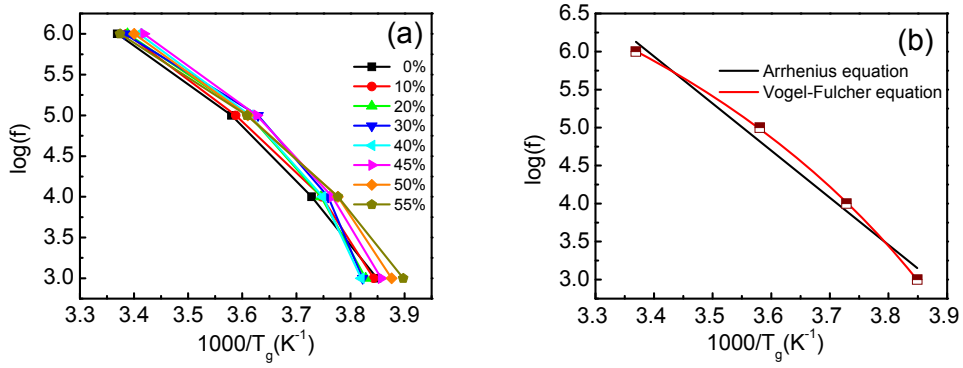

Figure 2-35. (a)Temperature dependence of the relaxation rate, and (b) temperature dependence of the relaxation rate for pure P(VDF-CTFE), black line: Arrhenius equation and red line: Vogel–Fulcher equation.

There are different relationships proposed for the relationship between log*f* and $1/T_g$. The simplest one is the Arrhenius relation:

$$f = f_0 \exp(-\frac{E_a}{k_B T}) \tag{2-5}$$

where f_0 is the pre-exponential factor, E_a is an activation energy and k_B is the Boltzmann constant (=8.616×10^{-5}eV). The Arrhenius relationship results in a linear relation between log*f* and $1/T_g$. This was clearly different with the experimental results shown in **Figure 2-35(b)**. Another model is the so-called Vogel–Fulcher (VF) relationship:

$$f = f_0 \cdot \exp\left(-\frac{E_a}{k_B (T_g - T_f)}\right) \tag{2-6}$$

where T_f is the static glass transition temperature and the other parameters have the same meaning as defined for Eq. (2-5). As shown in **Figure 2-35 (b)**, VF relationship can fit the experimental results well.

Table 2-8 Parameters given by fitting using Vogel–Fulcher equation

Ni vol.%	f_0 (Hz)	E_a (eV)	T_f(K)	R^2
0	1.12×10^{10}	0.03026	210.0	0.9996
10	1.23×10^{9}	0.01926	223.4	0.9966
20	1.33×10^{8}	0.01067	237.1	0.9998
30	2.51×10^{7}	0.00614	245.4	0.9977
40	1.05×10^{8}	0.00937	240.05	0.9963
45	4.81×10^{8}	0.01465	229.34	0.9996
50	1.03×10^{9}	0.01913	220.98	0.9962
55	1.99×10^{9}	0.02384	212.66	0.9999

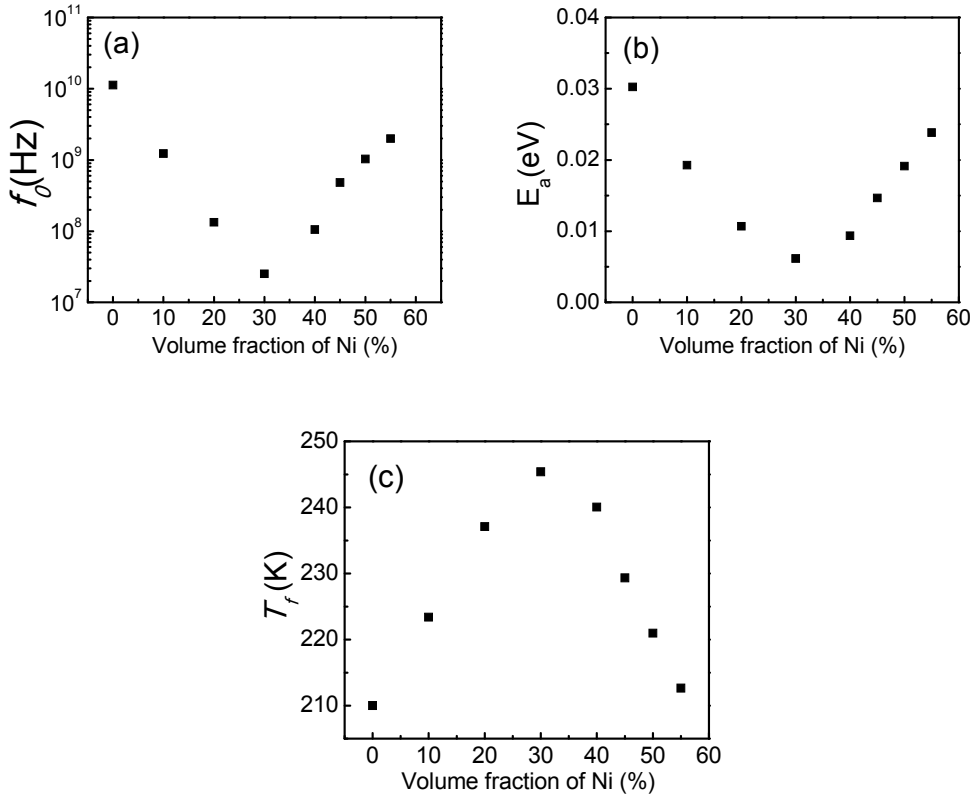

Figure 2-36. f_0, E_a, and $T_f$change with Ni concentrations from 0% to 60 vol.%.

The fitting parameters from VF relationship are listed in **Table 2-8** and plotted in **Figure 2-36**. Based on the parameters obtained for each composite, it was concluded that the activation energy decreased with increasing Ni content from 0 vol.% to 30 vol.%, then it increased with increasing Ni content from 30 vol.% to 55 vol.%. Regarding the T_g, it was found that T_g increased with Ni content from 0 % to 30 vol.%,

then decreased with increasing Ni content from 30 vol.% to 55 vol.%. The results shown in **Figure 2-36** are consistent with the results shown in **Figure 2-21**. That is, the composite with ~ 30 vol.% Ni corresponded to a special case. This phenomenon can be explained by the crystal-like interfacial layer in composites. From 0 vol.% to 30 vol.%, the T_g increased due to the volume of interfacial layer increasing. It can also be explained by **Table 1-2** in Section 1.5.4.

2.5. Matrix Effects on Percolative Behavior of Ni-Polymer Composites

Most researchers are focusing on the concentration of the filler approaching the φ_c from the low concentration side since the dielectric constant undergoes a sharp rise. The dielectric constant of the composite near this transition point often follows the percolation theory, as discussed in the Section 1.4.1, the percolation equation is selected to fit the experimental data is:

$$\frac{\varepsilon_{eff}}{\varepsilon_m} = \left(\frac{\varphi_c - \varphi}{\varphi_c} \right)^{-s} \tag{2-7}$$

where $\varphi < \varphi_c$ and s (> 0) is a constant.

2.5.1. Percolative Behavior of Ni-Polymer Composites at Room Temperature

The dependence of $\varepsilon_r/\varepsilon_m$ of the Ni-P(VDF-TrFE) and Ni-P(VDF-CTFE) composites on Ni volume fraction are plotted in **Figure 2-37**. **Figure 2-38** shows the relationship between $\varepsilon_r/\varepsilon_m$ and φ by fitting equation at 1 kHz and 1 MHz for the two systems as an example. To study the percolative behavior of the Ni-polymer composites at room temperature. The percolation threshold and critical value of Ni-P(VDF-TrFE) and Ni-P(VDF-CTFE) composites, which are determined by fitting

experimental results using Eq. (2-7), are listed in **Table 2-9** and plotted in **Figure 2-39**.

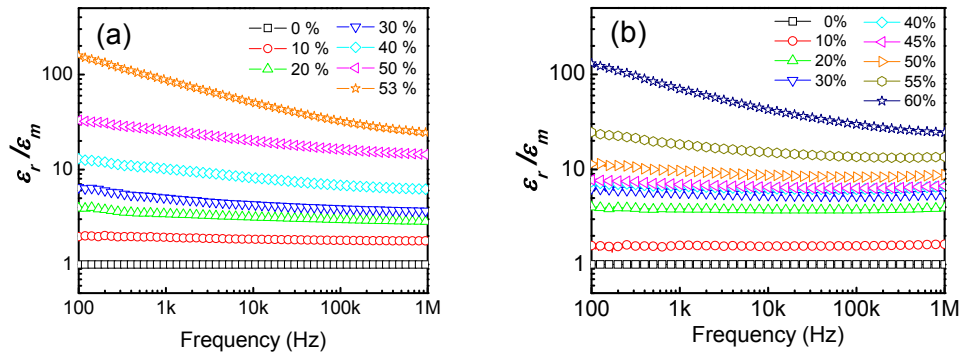

Figure 2-37. $\varepsilon_r/\varepsilon_m$ *vs.* frequency with different Ni volume fraction of (a) Ni-P(VDF-TrFE) and (b) Ni-P(VDF-CTFE) at room temperature.

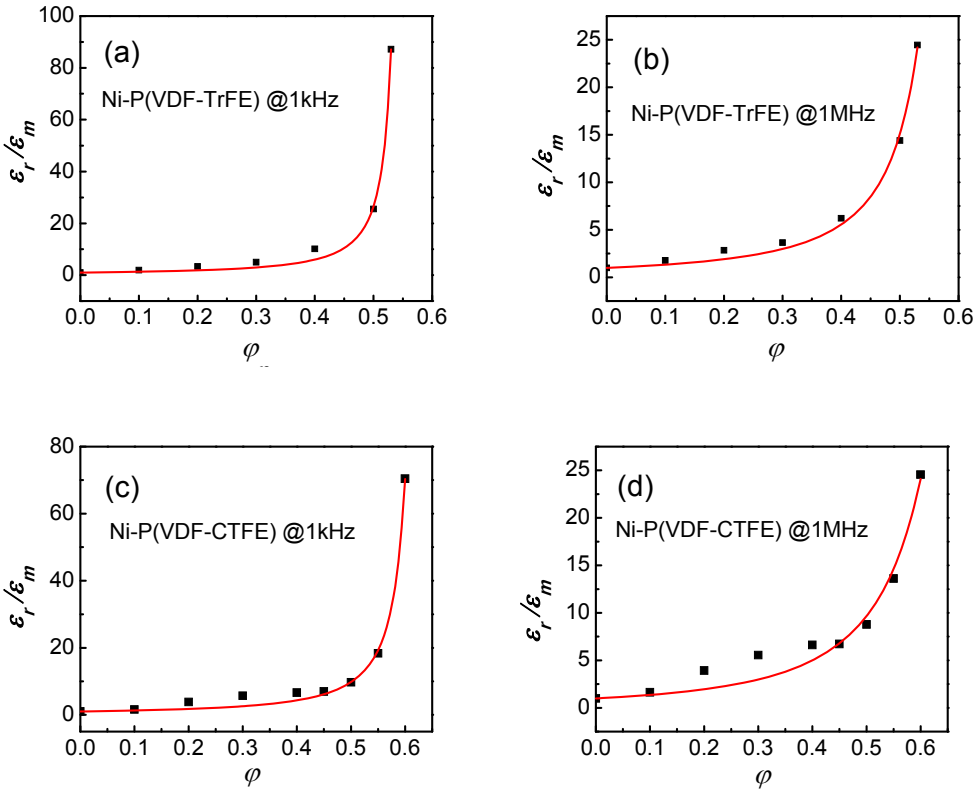

Figure 2-38. Variation of the dielectric constant of the Ni-P(VDF-TrFE) and Ni-P(VDF-CTFE) composites at room temperature with Ni volume fraction in comparison with fitting at 1 kHz and 1 MHz.

Table 2-9 φ_c and s vs. different frequencies of Ni-P(VDF-CTFE) and Ni-P(VDF-TrFE) composites

Composites	Frequency (Hz)	$\frac{\varepsilon_r}{\varepsilon_m} = \left(\frac{\varphi_c - \varphi_{filler}}{\varphi_c}\right)^{-s}$				
		φ_c	φ_c error	s	s error	R^2
Ni-P(VDF-CTFE)	100	0.62592	0.00327	1.53004	0.0494	0.9992
	501	0.63034	0.00448	1.46202	0.0587	0.9983
	1000	0.63464	0.00566	1.46278	0.0681	0.9975
	5001.8	0.64654	0.00888	1.47912	0.0888	0.9950
	10000	0.65372	0.01076	1.50235	0.0992	0.9937
	50118.7	0.67689	0.01738	1.60305	0.1339	0.9900
	100000	0.69096	0.02165	1.67316	0.1551	0.9884
	501187.2	0.74328	0.03870	1.96119	0.2386	0.9849
	1000000	0.77920	0.05117	2.17117	0.3000	0.9840
Ni-P(VDF-TrFE)	100	0.54543	0.00508	1.42138	0.1029	0.9959
	501	0.54945	0.00593	1.38936	0.1021	0.9948
	1000	0.55210	0.00659	1.38824	0.1045	0.9941
	5001.8	0.55959	0.00854	1.38943	0.1123	0.9928
	10000	0.56379	0.00967	1.39508	0.1169	0.9923
	50118.7	0.57716	0.01301	1.43490	0.1295	0.9922
	100000	0.58507	0.01485	1.46969	0.1365	0.9925
	501187.2	0.60735	0.01916	1.57968	0.1509	0.9940
	1000000	0.61763	0.02058	1.63257	0.1541	0.9948

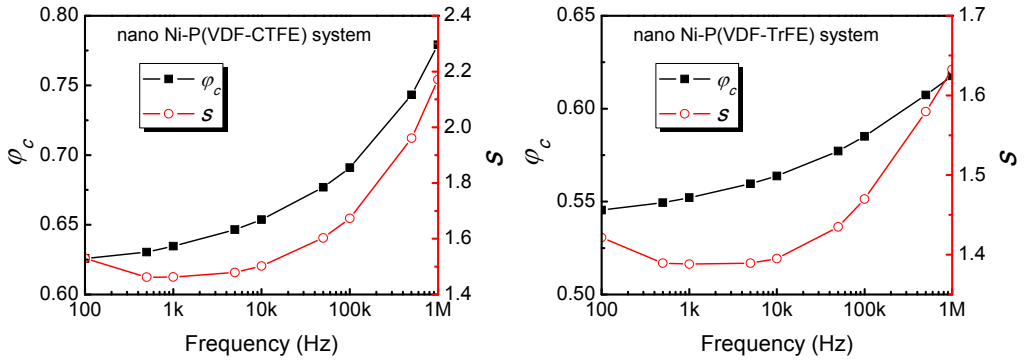

Figure 2-39. φ_c and s for different frequencies of Ni-P(VDF-CTFE) and Ni-P(VDF-TrFE).

The results shown in **Figure 2-39** indicated that the φ_c of both systems increased with increasing frequency. Two systems also showed the same trend of s vs.

frequency. That is, the *s* slightly decreased at low frequency then increased at high frequency with increasing frequency.

2.5.2. Percolative Behavior of Ni-Polymer Composites at Different Temperature

As discussed in Section 2.3, P(VDF-TrFE) and P(VDF-CTFE) have totally different temperature dependence of their dielectric properties. The φ_c and s of both composites at some frequencies at different temperatures are studied. The variation of $\varepsilon_r/\varepsilon_m$ of the Ni-P(VDF-CTFE) and Ni-P(VDF-TrFE) composites for different frequency (1 kHz, 10 kHz, 100 kHz, and 1 MHz) at -40 ^oC, 0^oC, 40 ^oC, 80 ^oC and 130 ^oC were studied. The variation of $\varepsilon_r/\varepsilon_m$ for both composites at -40 ^oC and 80 ^oC as examples are shown in **Figure 2-40**. At different temperature, the $\varepsilon_r/\varepsilon_m$ had the similar trend with increasing volume fraction of Ni. Before 50 vol.% Ni in Ni-P(VDF-CTFE) and 40 vol% Ni in Ni-P(VDF-TrFE), the $\varepsilon_r/\varepsilon_m$ did not change much with different frequencies.

The fitting results are listed in **Table 2-10** and **Table 2-11**, and the normalized $\varphi_c/\varphi_{-40^oC}$ and s/s_{-40^oC} are plotted in **Figure 2-41** and **Figure 2-42**. At different temperatures, the φ_c and s were different, which means the fitted φ_c and s are dependent on temperature. The φ_c always increased with frequency at each temperature for both systems. The $\varphi_c/\varphi_{-40^oC}$ and s/s_{-40^oC} varied with temperature were very similar to the curve of temperature dependence of the dielectric constant. For Ni-P(VDF-CTFE) system, the $\varphi_c/\varphi_{-40^oC}$ and s/s_{-40^oC} firstly increased then slightly decreased with temperature. At high temperature, the s always increases with frequency. For Ni-P(VDF-TrFE) system, the $\varphi_c/\varphi_{-40^oC}$ and s/s_{-40^oC} may have a peak

value between 80 °C and 130 °C, which was similar to the phase transition temperature.

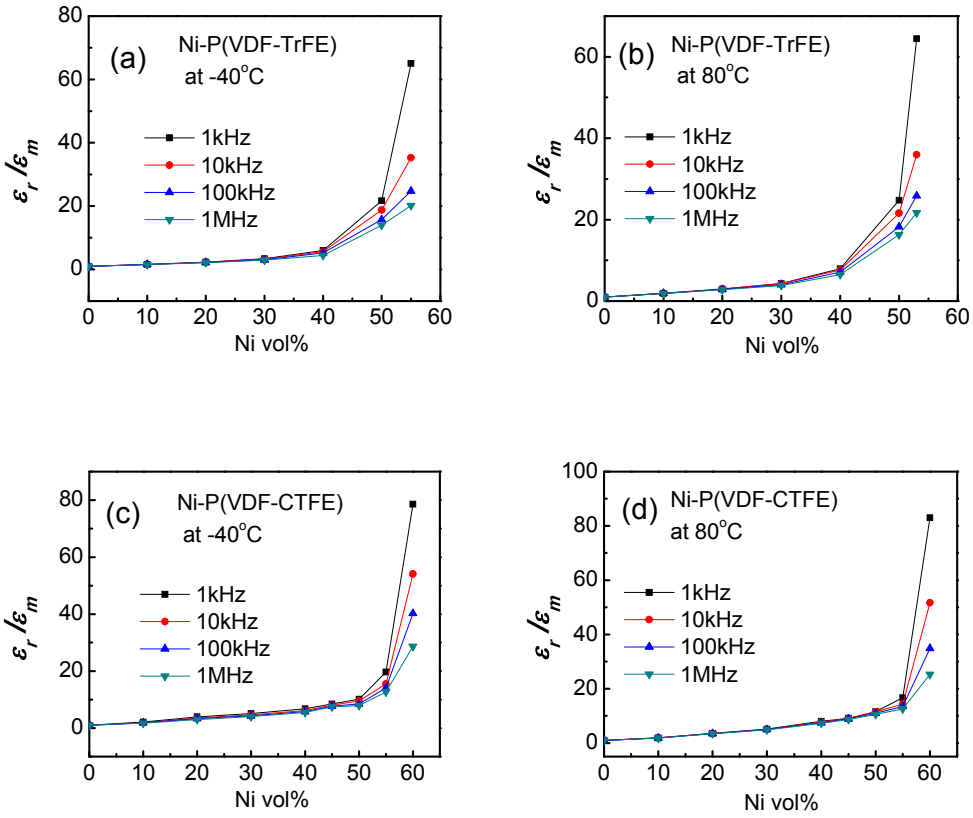

Figure 2-40. Variation of $\varepsilon_r/\varepsilon_m$ of the composites with different frequency 1 kHz, 10 kHz, 100 kHz, and 1 MHz: at Ni-P(VDF-TrFE) (a) -40 °C and (b) 80 °C, Ni-P(VDF-CTFE) at (c) 40 °C and (d) 80 °C.

Table 2-10 φ_c and s vs. different selected frequency and temperature of Ni-P(VDF-TrFE)

Temperature (°C)	Frequency (Hz)	$\frac{\varepsilon_{eff}}{\varepsilon_m} = \left(\frac{\varphi_c - \varphi_{filler}}{\varphi_c}\right)^{-s}$				
		φ_c	φ_c error	s	s error	R^2
-40	1k	0.5534	0.0015	1.3196	0.0217	0.9996
	10k	0.5894	0.0034	1.5535	0.0318	0.9996
	100k	0.6242	0.0091	1.6983	0.0675	0.9990
	1M	0.6364	0.0228	1.6845	0.1548	0.9953
0	1k	0.5531	9.22E-4	1.2779	0.0131	0.9998
	10k	0.5893	0.0027	1.5045	0.0239	0.9998
	100k	0.6250	0.0089	1.6849	0.0655	0.9991
	1M	0.6438	0.0234	1.7526	0.1581	0.9958
40	1k	0.5566	0.0012	1.3408	0.0169	0.9998
	10k	0.5969	0.0034	1.5893	0.0301	0.9997
	100k	0.6359	0.0102	1.7446	0.0718	0.9991
	1M	0.6438	0.0204	1.7011	0.1332	0.9969
80	1k	0.5647	0.0048	1.4928	0.0611	0.9977
	10k	0.6420	0.0150	2.0492	0.1199	0.9981
	100k	0.7335	0.0301	2.5368	0.1989	0.9983
	1M	0.7803	0.0499	2.7105	0.3050	0.9972
130	1k	0.5484	0.0020	0.9442	0.0246	0.9989
	10k	0.6038	0.0027	1.2714	0.0175	0.9998
	100k	0.6197	0.0040	1.2435	0.0223	0.9998
	1M	0.6430	0.0138	1.2795	0.0681	0.9986

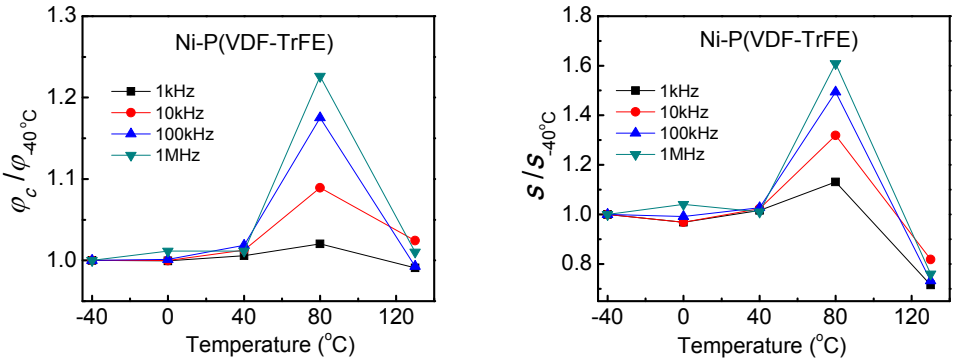

Figure 2-41. $\varphi_c/\varphi_{-40^oC}$ *and* s/s_{-40^oC} vs. different selected frequency and temperature for Ni-P(VDF-TrFE) composites.

Table 2-11 φ_c and s vs. different selected frequency and temperature of Ni-P(VDF-CTFE)

Temperature (°C)	Frequency (Hz)	$\frac{\varepsilon_r}{\varepsilon_m} = \left(\frac{\varphi_c - \varphi_{filler}}{\varphi_c}\right)^{-s}$				
		φ_c	φ_c error	s	s error	R^2
-40	1k	0.6356	0.0072	1.5138	0.0878	0.9946
	10k	0.6420	0.0103	1.4607	0.1102	0.9923
	100k	0.6545	0.0142	1.4854	0.1276	0.9891
	1M	0.6903	0.0258	1.6460	0.1830	0.9831
0	1k	0.6399	0.0117	1.5293	0.1339	0.9868
	10k	0.6610	0.0213	1.6179	0.1944	0.9723
	100k	0.6973	0.0340	1.8227	0.2543	0.9673
	1M	0.7539	0.0532	2.0883	0.3331	0.9691
40	1k	0.6372	0.0114	1.5191	0.1363	0.9866
	10k	0.6626	0.0229	1.6316	0.2063	0.9695
	100k	0.7318	0.0532	2.0258	0.3591	0.9567
	1M	0.9497	0.1818	3.1618	0.9764	0.9551
80	1k	0.6280	0.0088	1.4206	0.1175	0.9901
	10k	0.6495	0.0181	1.5304	0.1799	0.9735
	100k	0.7094	0.0437	1.8897	0.3122	0.9572
	1M	0.9037	0.1565	2.9342	0.8592	0.9508
130	1k	0.6191	0.0056	1.2166	0.0822	0.9941
	10k	0.6334	0.0115	1.3092	0.1271	0.9823
	100k	0.6754	0.0281	1.6176	0.2213	0.9642
	1M	0.7864	0.0834	2.2391	0.4906	0.9514

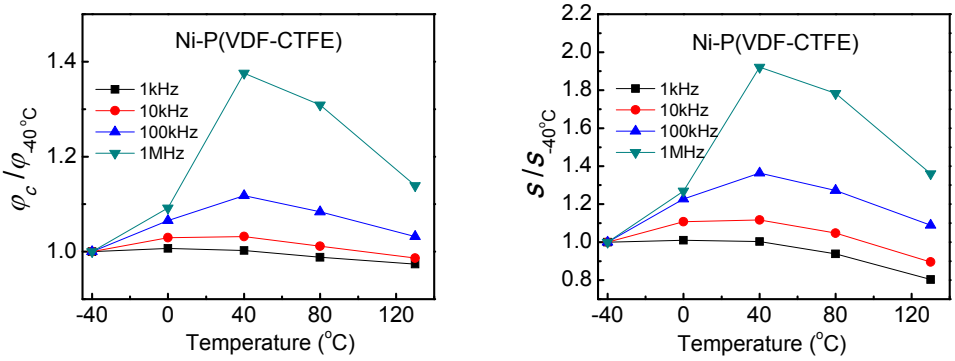

Figure 2-42. $\varphi_c/\varphi_{-40^oC}$ *and* s/s_{-40^oC} vs. different selected frequency and temperature for Ni-P(VDF-CTFE) composites.

2.5.3. γ Fitting Close to the Percolation Threshold

As discussed in Section 1.4.1, the effective dielectric constant of a conductor-dielectric composite, especially when $\varphi \approx \varphi_c$, was strongly dependent on the frequency. For example, if $\varphi \approx \varphi_c$, it was shown that:

$$\varepsilon_{eff} \propto \omega^{\gamma-1} \tag{2-8}$$

where γ (<1) is a constant and ω is the angular frequency. In these Ni based composites, the composites with 60 vol.% of Ni and 53 vol.% of Ni were the closest one for Ni-P(VDF-CTFE) and Ni-P(VDF-TrFE). The dielectric constant and the fitting curve by Eq.(2-8) are shown in **Figure 2-43**. Because it was a nonlinear curve in log-log scale, the fitting curve is separated to 2 parts, before 3 kHz and after 3 kHz. The γ_1=0.7234 γ_2=0.8155 is for Ni-P(VDF-CTFE) and γ_1=0.7327 γ_2=0.7573 is for Ni-P(VDF-TrFE). The results were close to the normal value from the percolation theory which is discussed in section 1.4.1.

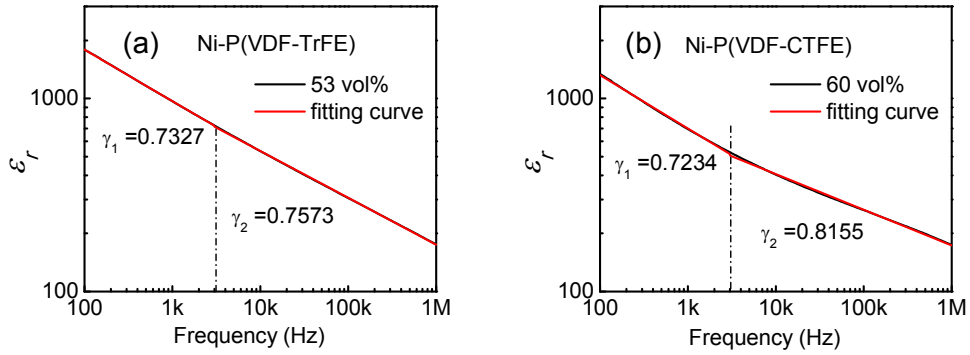

Figure 2-43. Dielectric constant vs. frequency of composites and fitting curve for (a) Ni-P(VDF-TrFE) with 53 vol.% of Ni and (b) Ni-P(VDF-CTFE) with 60 vol.% of Ni.

2.6. Conclusions

1. By combining solution casting and hot-pressed processing, metal-polymer composites with high φ_c were developed. This was due to a uniform dispersion of nanoparticles in nanocomposite and was experimentally proven by Ni-P(VDF-TrFE) and Ni-P(VDF-CTFE) composite systems.
2. Compared to the composites with low percolation threshold, composites with high percolation threshold had a wider volume fraction range for the percolation threshold concentration, making the material reproducible for practical applications.
3. Dielectric constants of more than 1000 were obtained in both systems with a low loss. A higher loading of the nano Ni at the percolation threshold gave the higher value of dielectric constant for Ni-P(VDF-CTFE) composite, but moderate loss. The dielectric loss for the composite film containing 50 vol% Ni was smaller than 0.2 at 100 Hz which is attractive for practical use.
4. The new dielectric process observed in the composites was a relaxation process with a very low relaxation frequency. There are three mechanisms in this conductor-polymer composite: 1) the dielectric relaxation process from the polymer matrix, 2) the new dielectric relaxation process from the composite, and 3) the conductivity of the conducting filler (Ni).
5. Ni had very different contributions to dielectric properties in different polymer matrix. For Ni-P(VDF-TrFE) system, Ni introduced may cause the size of crystal becoming smaller or crystallization of composite decreasing. For

Ni-P(VDF-CTFE) system, Ni introduced may cause the peak-like phenomenon in temperature dependence of dielectric constant at high temperature.

6. The percolation behavior in Ni-polymer composites was investigated and it was found that the percolation threshold and critical value were dependent on the selected frequency and temperature.

References of Chapter 2

1. Wei Wang, Novel Metal-Polymer Composite with High Percolation Threshold, M. S. Thesis, Auburn University, 2012.
2. L. Zhang, X. B. Shan, P. X. Wu and Z.-Y. Cheng, *Appl. Phys. A* **107**, 597 (2012).
3. X. B. Shan, L. Zhang, X. Q. Yang and Z.-Y. Cheng, *J. Adv. Ceramics*, **1(4)**, 310 (2012).
4. Z.-Y. Cheng, Q.M. Zhang, F.B. Bateman, *J. Appl. Phys*. **92**, 6749 (2002).
5. C. Ang and Z. Yu, *Appl. Phys. Lett.* **84**, 2145 (2004).

CHAPTER 3

All-Organic Nanocomposites with High Dielectric Constant

3.1. Introduction

Because of the tunable conductivity, low elastic modulus, flexibility and good compatibility with the dielectric polymer matrix, conducting polymers are good candidates for dielectric composite applications. In this chapter, a new all-organic composite system is introduced that is flexible with a high dielectric constant. The newly developed 2-D nanoclip conducting polymer polypyrrole (PPy) is used as filler. The dielectric properties and behavior of this system are studied.

3.2. Materials and Preparation

3.2.1. Materials

The conducting polymers were prepared at Dr. Xinyu Zhang's group in Department of Polymer and Fiber Engineering, Auburn University. A facile, one-step, general "oxidative template assembly" (OTA) approach was proposed to synthesize bulk quantities of electronic conducting polymers such as polyaniline (PANI), polypyrrole (PPy) and poly (3, 4-ethylenedioxythiophene) (PEDOT), which have an unusual nanoclip-like morphology [1, 2]. The as-produced conducting polymers possessed 2-dimensional nanostructures instead of granular structures without the templates.

For the preparation, 0.01 M cetrimonium bromide ($(C_{16}H_{33})N(CH_3)_3Br$) (CTAB)

was dispersed in 60 mL 1 M HCl under ice bath. After being magnetically stirred 10 min, 0.03 M ammonium peroxydisulfate (APS) was added into the solution and keep stirring for 10 min resulting in a reactive template in the form of white precipitates. All solutions were cooled to 0-3 ºC. Pyrrole (0.12 M) was added into the as-prepared reactive template solution and self-assembly was conducted at 0-3 ºC for 24 hrs. The resulting black precipitate of polypyrrole was suction filtered, washed with copious amounts of aq. 1 M HCl (3 x 100 mL) and acetone (3 x 100 mL) and freeze for 12 hrs. The structure of polypyrrole nanoclips is shown in **Figure 3-1**. The length of nano clips is around 1 μm and width is around 0.5 μm. The rectangular area in each clips is very small and the diameter is around 100-200 nm. The bulk electrical conductivity of the conducting polymer nanoclips was measured by a linear four probe measurement setup. The conductivity of PPy clips was 2.89 S/cm.

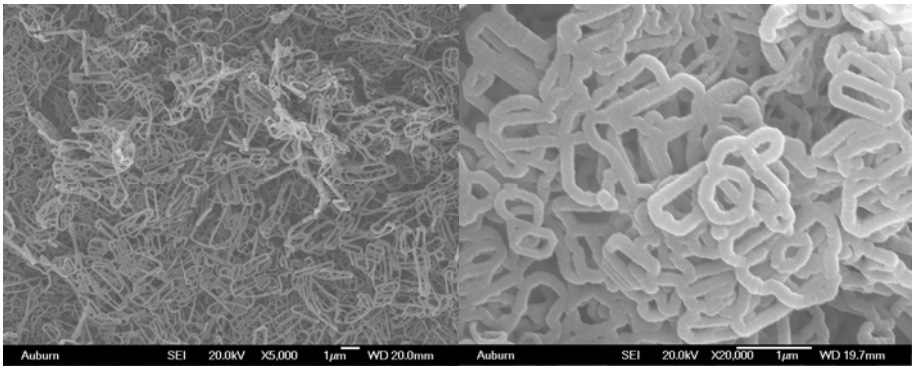

Figure 3-1. The structure of PPy clips.

3.2.2. Preparation of Composite

The P(VDF-TrFE) 70/30 mol% and P(VDF-CTFE) 88/12 mol% copolymer were used as a dielectric polymer matrix. The PPy-P(VDF-TrFE) and PPy-P(VDF-CTFE) composites with different PPy weight concentrations (0, 0.03, 0.04, 0.05, 0.06, 0.07, 0.08 and 0.09) were prepared. A weight ratios table for PPy-P(VDF-TrFE) and

PPy-P(VDF-CTFE) samples is given in **Table 3-1**.

Table 3-1 Weight ratios in PPy-matrix composites samples

PPy wt.%	3 wt.%	4 wt.%	5 wt.%	6 wt.%	7 wt.%	8 wt.%	9 wt.%
PPy	0.009g	0.012g	0.015g	0.018g	0.021g	0.024g	0.027g
Matrix*	0.3g	0.3g	0.3g	0.3g	0.3g	0.3g	0.3g

*Matrix: P(VDF-TrFE) 70/3 0mol.% or P(VDF-CTFE) 88/12 mol.% copolymer

The preparation is the same as Ni-polymer nano-composites in Section 2.2. Initially, either P(VDF-TrFE) or P(VDF-CTFE) copolymer was dissolved in dimethyl formamide (DMF) using magnetic stir bar for 8 hours. This was followed by the dispersion of PPy clips into the solution. They were sonicated about 30 mins firstly, stirred for 8 hours and sonicated about 30 mins. The final PPy-P(VDF-TrFE) or PPy-P(VDF-CTFE) solution was cast on a glass plate at 70 ºC for 8 hours. The morphologies and the uniformity of the PPy-polymer composite films were examined by JEOL JSM 7000F FE-SEM (Scanning Electron Microscopy). As shown in **Figure 3-2**, the PPy clips can be observed from the top and there are some holes on the top due to the solvent evaporation.

To improve the uniformity, the solution cast film was then hot pressed at 150^{o}C. During the HP process, four layers of the same as-cast layer were stacked using a so-called “sandwich” configuration described in Section 2.2.2, and preheated to 150^{o}C for 2 min then hot-pressed at 10 tons for 20 seconds, which is similar to the preparation of the Ni-polymer composites. All hot-pressed samples were annealed at 125ºC to enhance homogeneity and dielectric behavior. The thickness of one layer as-cast film was around 30-40 μm. After the four layers were hot pressed, the

thickness was around 80-110 μm. **Figure 3-3** shows the cross-section of PPy-P(VDF-TrFE) hot-pressed composites with 5 wt.%. From the cress-section, it is difficult to recognize the PPy and matrix separately because it is an all-polymer composite.

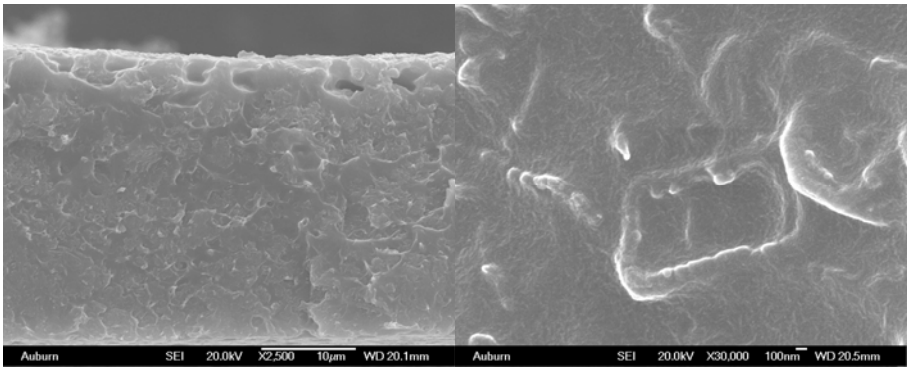

Figure 3-2. The structure of one layer 5 wt.% PPy-P(VDF-TrFE): cross-section and top surface.

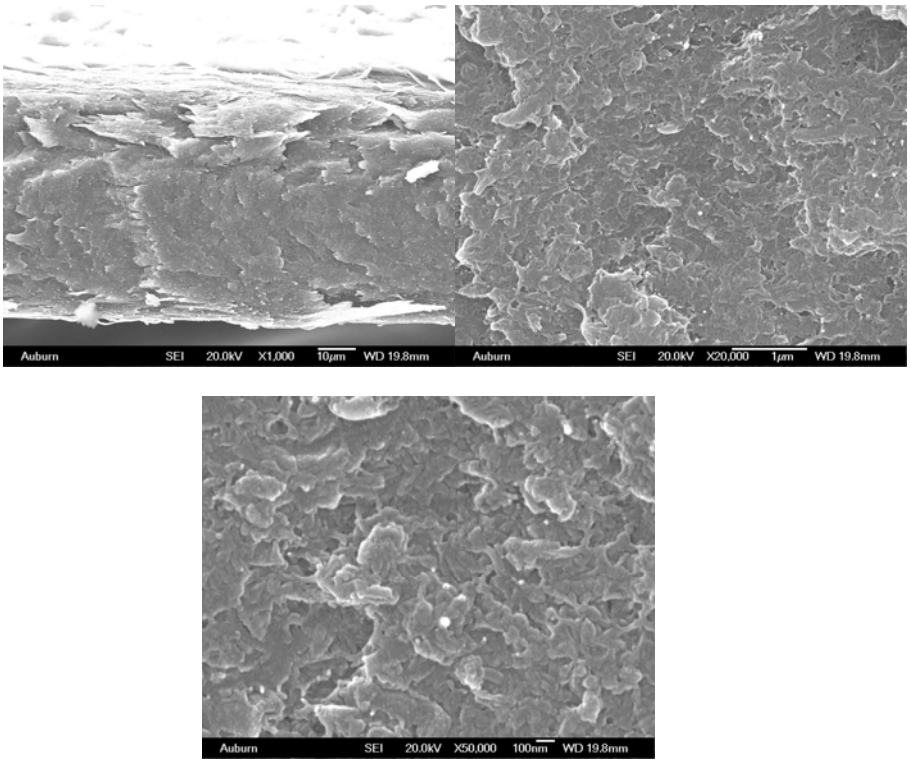

Figure 3-3. The cross-section of 4 layers 5 wt.% PPy-P(VDF-TrFE) composites.

3.2.3. Materials Characterization

For dielectric study, all samples were sputtered with gold on the top and bottom surfaces as electrodes using a PelcoSC-6 sputter coater as described in Section 2.3.2. The Agilent 4294A impedance analyzer was employed to measure the dielectric property of the samples over a frequency range of 100 Hz to 1 MHz using the Cp~D function. In order to characterize the temperature dependence of the dielectric response, the dielectric properties of the samples were characterized at frequencies of 1 kHz, 10 kHz, 100 kHz and 1 MHz over a temperature range from -60 ºC to 140 ºC using an impedance analyzer (Agilent 4294A) in Xi'an Jiaotong University, China.

3.3. Dielectric Behavior of PPy-P(VDF-TrFE) Composites

3.3.1. PPy-P(VDF-TrFE) Composites at Room Temperature

The dielectric properties and conductivity of the PPy-P(VDF-TrFE) nano-composites with different PPy concentration from 0 % to 9 wt.% at room temperature are shown in **Figure 3-4**. The dielectric constant of the composites increases with increasing filler concentration. A high dielectric constant (>1000) with a loss (<2) was observed at 1 kHz in the composite with 8 wt.% of PPy. This dielectric constant is about 100 times that of the dielectric constant for the polymer matrix itself. The composites with low PPy content showed a similar frequency dependence of the dielectric constant with the polymer matrix. For the composites with high PPy concentration, a stronger frequency dependence of the dielectric constant was observed. From 5 wt.%, the dielectric constant increased abruptly in low frequency, from 46 with 4 wt.% to 156 with 5 wt.% at 100 Hz. By increasing the filler

content, the dependence of the dielectric properties on frequency becomes stronger. However, at 7 wt.% and 8 wt.%, the dielectric constant can be considered as two dielectric processes: almost independent of frequency from 100 Hz to 3 kHz and very dependent on frequency with a sharp decrease from 3 kHz to 1MHz.

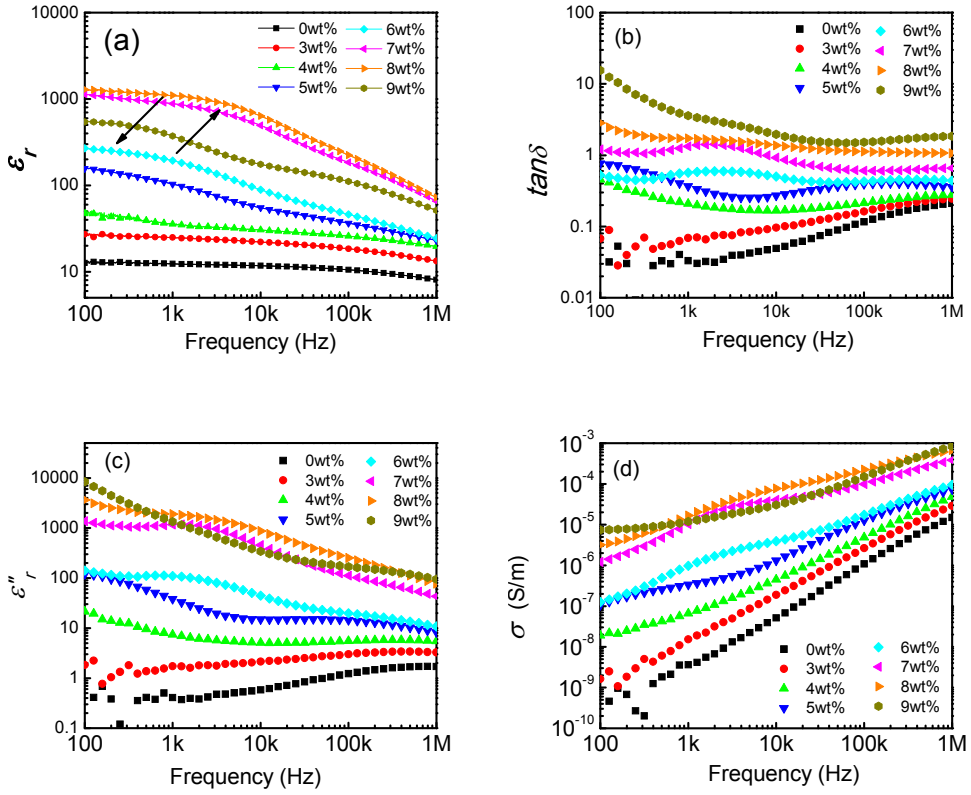

Figure 3-4. Dielectric responses (a) dielectric constant, (b) dielectric loss, (c) imaginary part of dielectric constant, (d) conductivity as a function of frequency for PPy-P(VDF-TrFE) composites with different PPy concentrations.

From **Figure 3-4 (b)** and **(c)**, it can be found that both $tan\delta$ and ε''_r increase with increasing frequency for polymer matrix. However, $tan\delta$ and ε''_r observed in the composites showed a different frequency dependence. At low frequencies, they decreased with increasing frequency, while at high frequencies, they increased with increasing frequency. That is, there is a certain frequency, where they reached their

minimum. This frequency separated the frequency range into two regimes: low and high frequency. This certain frequency for $tan\delta$ was lower than that for ε''_r. All these indicate that there was a new dielectric process in the composites. The contribution of this new dielectric process to the dielectric response of the composites increased with increasing PPy content. Moreover, there was a peak of this new dielectric process in $tan\delta$ and ε''_r which shifted to high frequency with increasing PPy content. As discussed for the Ni-polymer composites, the new dielectric process observed in the composites is a relaxation process with a very low frequency. There are three mechanisms in this conductor-polymer composite: 1) the dielectric relaxation process from the polymer matrix, 2) the new dielectric relaxation process from the composite, and 3) the conductivity of the conducting filler (PPy). The new dielectric relaxation process shows stronger influence in the PPy-P(VDF-TrFE) system than for the Ni-P(VDF-TrFE) system. This was due to the surface area of the conducting filler. For nano-sized Ni powder, the average diameter of Ni particle is 100 nm, then the surface area is around $\pi \cdot 10^4$ nm^2 for one particles. For PPy clips, the length is around 1μm, width is around 0.5 μm and the diameter is around 100-200 nm. The the surface area is no less than $3\pi \cdot 10^5$ nm^2 for one clip, which is more than 30 times of Ni nanoparticles. That is the smaller amount of PPy can have an extraordinary effect on the dielectric properties.

Figure 3-5 shows the dielectric constant and loss with different PPy concentrations. The dielectric constant raises gradually with increasing filler contents in the composites until the filler content reaches 4 wt.%. Subsequently, the dielectric

constant increases abruptly from 4 wt.% to 6 wt.%. In particular, when the PPy wt.% increases from 6 wt.% to 8 wt.%, the dielectric constant at 100 Hz rises steeply from 286 to 1289 about 100 times higher than the dielectric constant of pure P(VDF-TrFE) at 100 Hz. As shown in the **Figure 3-5** (b), the loss of composites with 0 to 6 wt.% of PPy are smaller than 0.5.

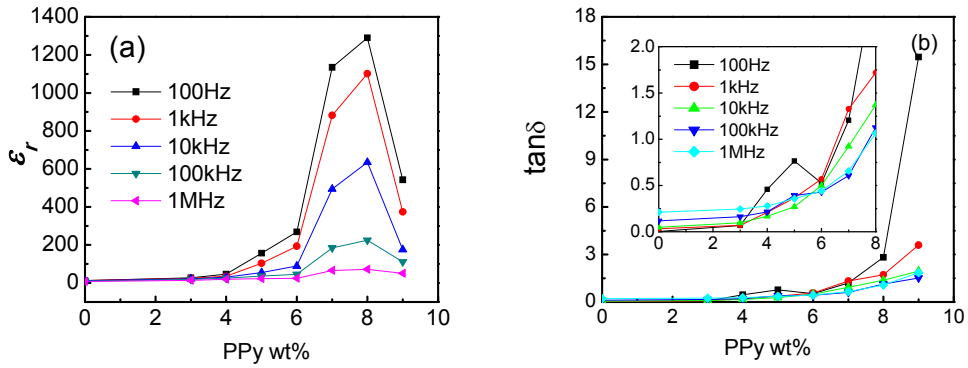

Figure 3-5. Dependence the dielectric properties (a) dielectric constant (b) loss for PPy-P(VDF-TrFE) composites on PPy concentrations at different frequency.

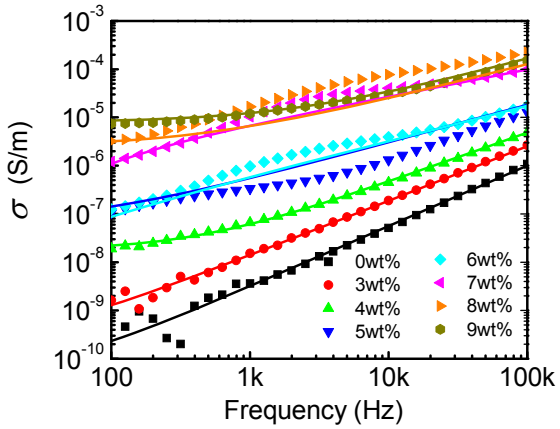

Figure 3-6. Conductivity of PPy-P(VDF-TrFE) composites vs. frequency with concentrations from 0% to 9wt% and the fitting curve of Johnscher's universal dielectric response law.

To study this new dielectric process, the real part of electric conductivity of the composites is plotted in **Figure 3-4(d)**, where the real part of the conductivity from

the imaginary part of the permittivity using Eq. (1-9). When Johnscher's universal dielectric response law is used to fit the experimental data, it is found that the fitting curve is not very well matched with the data due to this new relaxation process. The equation is shown in Section 2.3. **Figure 3-6** shows the conductivity of composites and fitting curve of Eq. (2-1) to the conductivity data for all of samples from 100 Hz to 100 kHz. The symbols represent the experimental data and the solid line represents the fitted data employing Jonscher's law. The corresponding parameters are listed in **Table 3-2**.

Table 3-2 Parameters of Johnscher's universal dielectric response law for fitting the conductivity of composites

PPy wt.%	Parameter in $\sigma_{ac} = \sigma_0 + A\omega^n$						
	σ_0	σ_0 error	A	A error	n	n error	R^2
0	1.67E-10	1.78E-11	5.89E-14	2.25E-15	1.2390	3.50E-3	0.9968
3	2.61E-10	5.53E-11	7.08E-13	3.11E-14	1.1301	2.99E-3	0.9971
4	1.80E-8	1.82E-10	5.81E-12	1.15E-13	1.0206	1.08E-3	0.9996
5	8.18E-8	2.80E-9	1.12E-10	5.95E-12	0.7895	3.92E-3	0.9973
6	2.49E-8	3.21E-9	1.44E-9	3.64E-11	0.7518	1.83E-3	0.9996
7	3.19E-7	5.71E-8	2.87E-9	6.79E-11	0.7348	2.56E-3	0.9985
8	2.41E-6	6.63E-7	6.69E-9	9.54E-9	0.7369	9.10E-2	0.9990
9	7.87E-6	4.56E-8	5.11E-9	1.27E-10	0.7744	1.84E-3	0.9987

The parameters σ_0, A, and n changed with PPy concentrations from 0% to 9wt% in **Table 3-2** are plotted in **Figure 3-7**. Compared with **Figure 2-8** and **Figure 3-7**, n changes from bigger than 1 to smaller than 1. The trends of these three are similar with the Ni-polymer composites, σ_0 and A increase with the increasing of conducting filler while n decreases. This means that the contribution of the new dielectric process in the composite to the dielectric response increases with the PPy content. This is

consistent with the direct observation of the dielectric loss discussed previously. There were some abnormal changes from 5 wt.% to 7 wt.% which may be due to the relaxation peak.

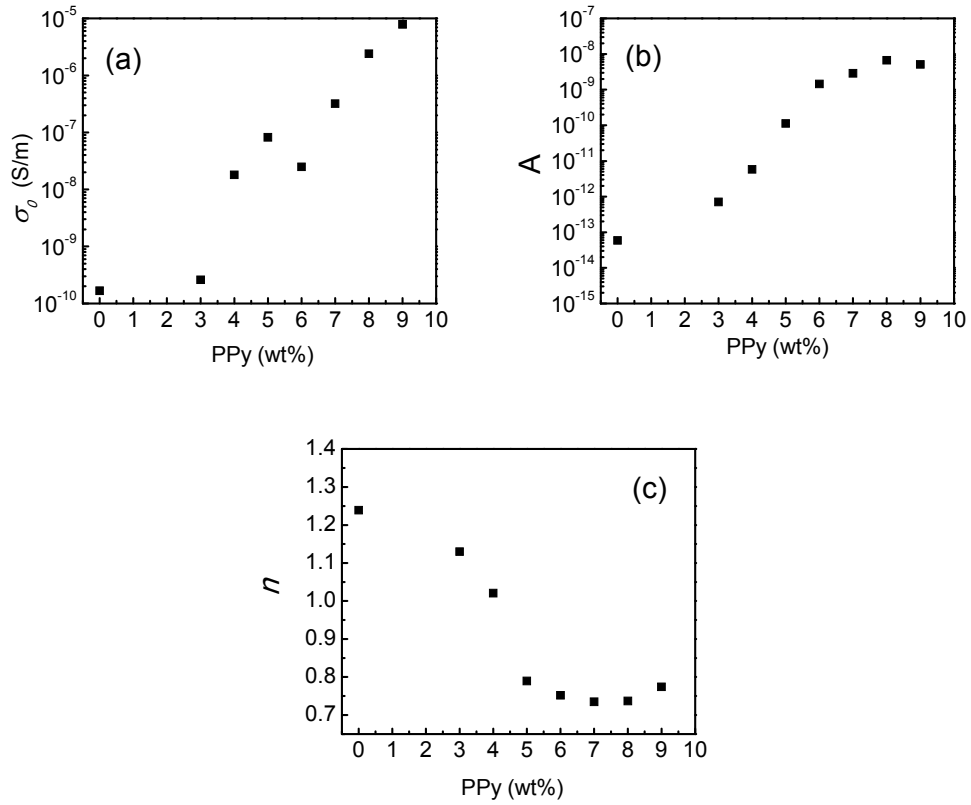

Figure 3-7. σ_0, A, and n change from Table 3-2 for PPy-P(VDF-TrFE).

3.3.2. PPy-P(VDF-TrFE) Composites at Different Temperature

Figure 3-8 to **Figure 3-15** show temperature dependence of the dielectric properties for PPy-P(VDF-TrFE) composites with different contents of PPy at 1 kHz, 10 kHz, 100 kHz, and 1 MHz.

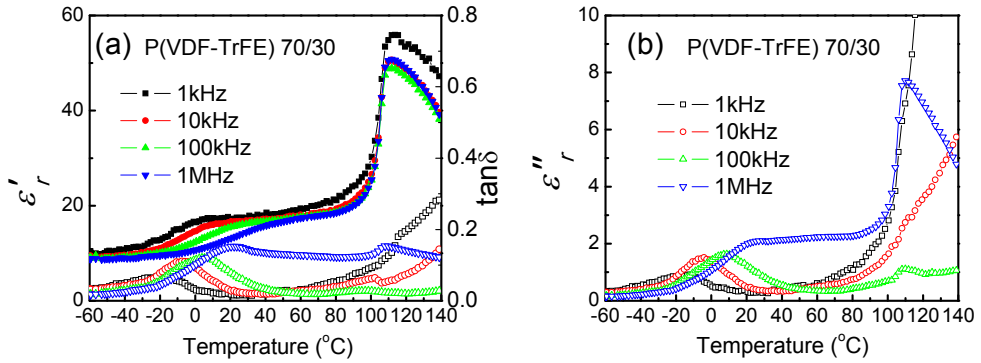

Figure 3-8. Temperature dependence of dielectric properties of pure P(VDF-TrFE): (a) real part(solid) and loss(open), (b) imaginary part.

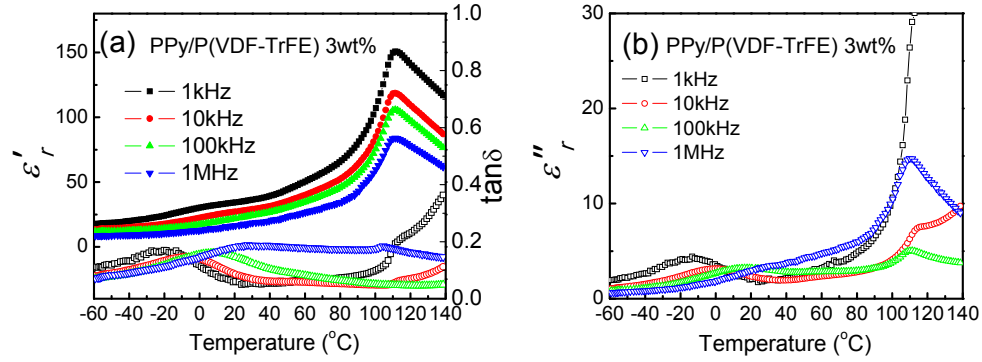

Figure 3-9. Temperature dependence of dielectric properties of PPy-P(VDF-TrFE) 3 wt.%: (a) real part(solid) and loss(open), (b) imaginary part.

The dielectric constant of the composite with 3 wt.% PPy shows the similar temperature dependence as the polymer matrix. However, this differed from the Ni-polymer composites which the composite exhibiting a higher loss across the whole temperature range. Regarding the glass transition process, similar to the polymer matrix, the higher the frequency, the higher the peak temperature for $tan\delta$ and ε''_r. However, the peak value of glass transition process at 1kHz increased and is close to that at 1MHz. Around the T_{max}, the dielectric constant increased dramatically from 21 (at 80 °C) to 53 (at 109 °C) at 1 kHz for polymer matrix, however, the dielectric constant increased continuously and gradually from 66 (at 80 °C) to 150 (at 111 °C) at

1kHz for 3 wt.% PPy. As discussed in **Figure 1-6** and Ni-P(VDF-TrFE) composites, PPy introduced may cause the size of crystal becoming smaller or crystallization of composite decreasing.

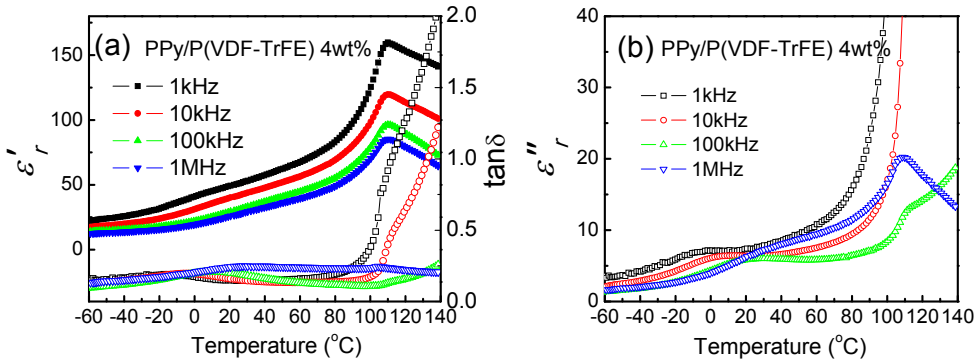

Figure 3-10. Temperature dependence of dielectric properties of PPy-P(VDF-TrFE) 4 wt.%: (a) real part(solid) and loss(open), (b) imaginary part.

The dielectric constant of the composite with 4 wt.% PPy showed similar temperature dependence as the composites with 3 wt.% PPy. The ε'_r, $tan\delta$,ε''_r were all higher than that of the composite with 3 wt.% PPy. The loss at 1kHz and 10kHz had a large increased at 1MHz for high temperatures compared with 3 wt.% PPy. All these may be the results of the new relaxation process. This is consistent with the data shown in **Table 3-2**. The conductivity had a 70 times increase from 3 wt.% PPy to 4 wt.% PPy. The T_g shifted to high temperature compared to the ε''_r of 4 wt.% and 3 wt.% PPy. In ε''_r for 3 wt.%, the ε''_r at 100kHz decreased with temperature when temperature was higher than T_{max}, However, the ε''_r at 100 kHz continuously increased with temperature when the temperature was higher than T_{max}, which was also due to the high loss at 100 kHz for high temperature.

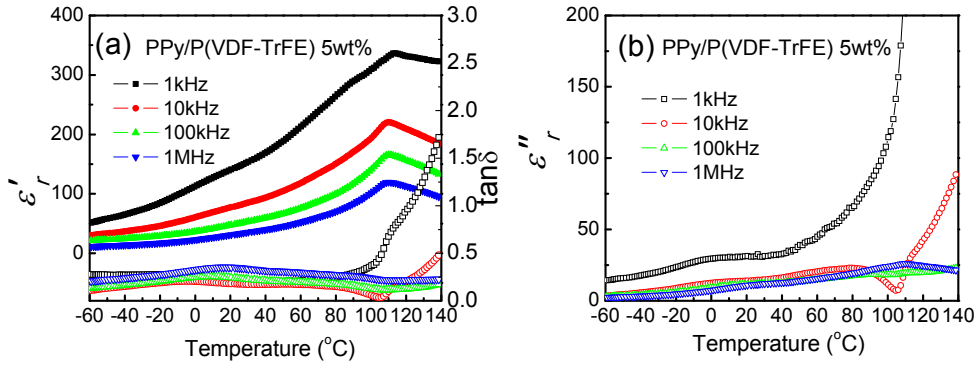

Figure 3-11. Temperature dependence of dielectric properties of PPy-P(VDF-TrFE) 5 wt.%: (a) real part(solid) and loss(open), (b) imaginary part.

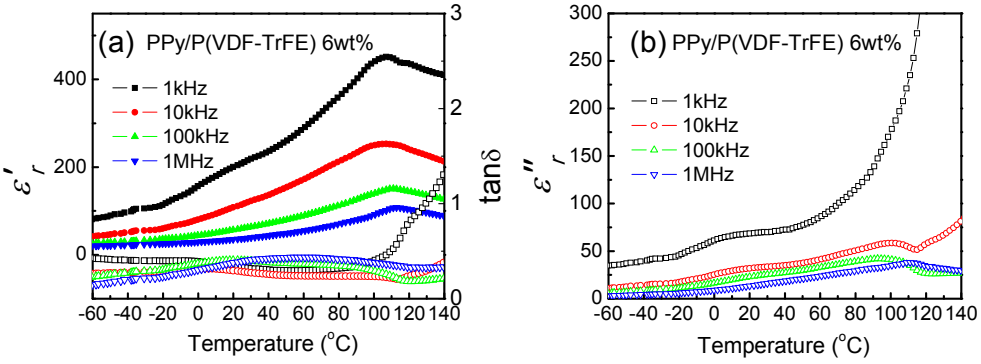

Figure 3-12. Temperature dependence of dielectric properties of PPy-P(VDF-TrFE) 6 wt.%: (a) real part(solid) and loss(open), (b) imaginary part.

The dielectric constant of the composite with 5 wt.% PPy showed similar temperature dependence as the composite with 4 wt.% PPy. The $\varepsilon_r^{'}$, $tan\delta$,$\varepsilon_r^{''}$ awere all high than that of the composite with 4 wt.% PPy. The T_g shifts to high temperature compared to the $\varepsilon_r^{''}$ of 5 wt.% and 4 wt.% PPy. The dielectric properties and conductivity of the composite with 5 wt.% and 6 wt.% PPy showed some interesting phenomenon. As shown in **Table 3-2**, the conductivity of 6 wt.% was smaller than 5 wt.% and 7 wt.% PPy due to the new dielectric relaxation. The value of $tan\delta$ and $\varepsilon_r^{''}$ of 5 wt.% and 6 wt.% were very close. For example, the composite with 5 wt.% PPy exhibited a lower loss at high temperature than 6 wt.%. The composite with 5 wt.%

PPy exhibited a lower dielectric constant at low temperature at 1 MHz than for the 6 wt.%. For 6 wt.% composites, the dielectric constant was larger than 450 at T_{max} (~107°C) and the loss was around 0.45.

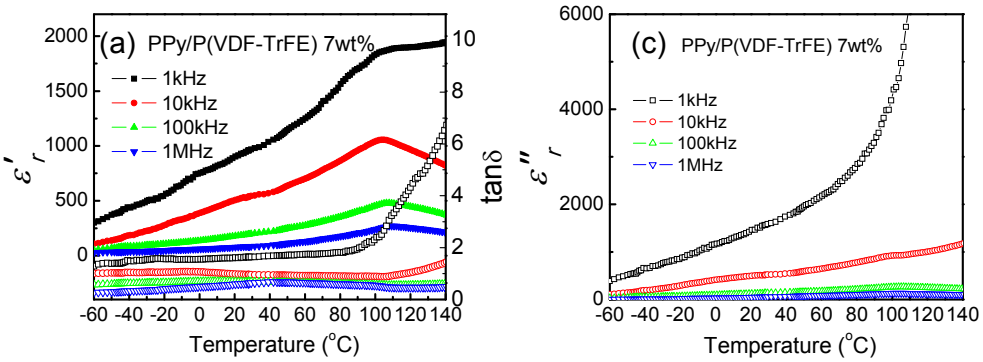

Figure 3-13. Temperature dependence of dielectric properties of PPy-P(VDF-TrFE) 7 wt.%: (a) real part(solid) and loss(open), (b) imaginary part.

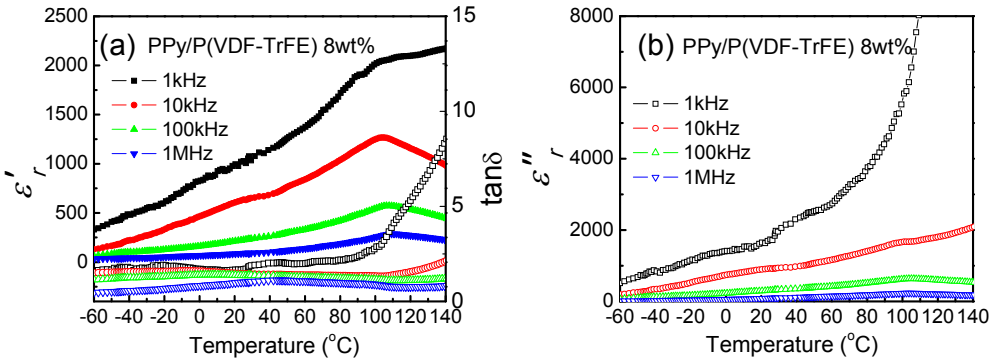

Figure 3-14. Temperature dependence of dielectric properties of PPy-P(VDF-TrFE) 8 wt.%: (a) real part(solid) and loss(open), (b) imaginary part.

From the pure matrix to 6 wt.%, it is easy to identify the glass transition temperature from imaginary part of dielectric constant. However, from 7 wt.% to the high volume fraction, the value of the "shoulder" between the peak of glass transition temperature and FE-to-PE phase transition temperature increased due to the new relaxation process. It was difficult to find the peak of glass transition temperature at high frequencies. Even for the FE-to-PE phase transition peak, the dielectric constant

still increased when the temperature was higher than T_{max}. For 8 wt.% composite, the dielectric constant was larger than 2000 at T_{max} (~103°C) and the loss was around 2.8.

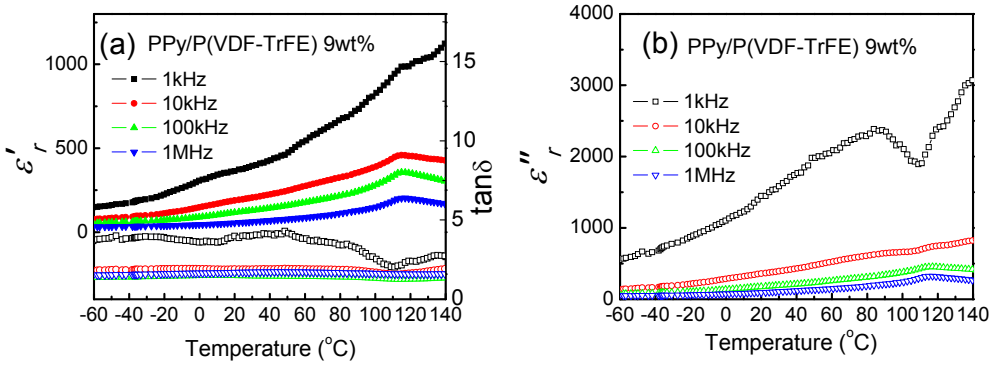

Figure 3-15. Temperature dependence of dielectric properties of PPy-P(VDF-TrFE) 9 wt.%: (a) real part(solid) and loss(open), (b) imaginary part.

The dielectric constant of the composite with 9 wt.% PPy showed similar temperature dependence as with the 9 wt.% PPy, but smaller than that of 8wt.%. It is interesting to find the loss firstly increased with temperature then decreased before T_{max} at 1 kHz, which means there was a new dielectric process at low frequency.

To compare the dielectric properties with different PPy volume fraction clearly, the ε'_r, ε''_r and $tan\delta$ at 1 kHz and 1MHz are shown in **Figure 3-16**. As a short summary, ε'_r, and ε''_r increased with the increasing PPy content. The loss at low temperature increased with the increasing PPy content, while decreased from 4 wt.% to 6 wt.% with the increasing PPy content then increased due to the high conductivity at high temperature. The peak of glass transition temperature of ε''_r slightly shifted to high temperature from 0 wt.% to 6 wt.%. However, it was difficult to quantify the change of shifts for glass transition temperature.

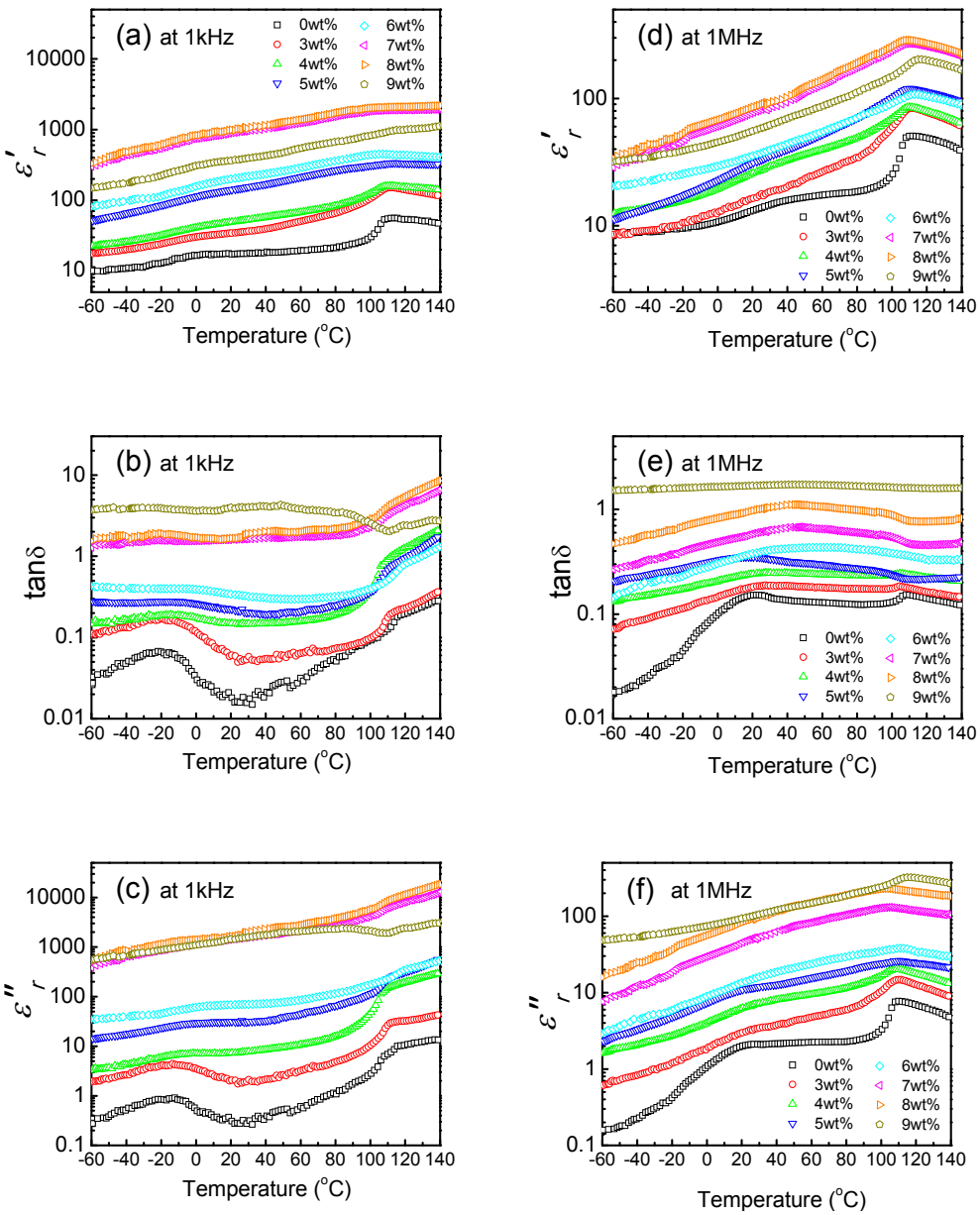

Figure 3-16. Temperature dependence of ε'_r, ε''_r and *tanδ* of composites: (a) to (c) at 1kHz and (d) to (f) at 1MHz.

Table 3-3 The peak positions of T_{max} of composites at different frequencies.

Freq.	0 %	3 wt.%	4 wt.%	5 wt.%	6 wt.%	7 wt.%	8 wt.%	9 wt.%
1kHz	113.53	113.34	111.96	114.36	107.71	-	-	-
10kHz	112.30	112.66	112.53	111.45	106.84	104.47	104.47	114.23
100kHz	112.65	112.63	111.50	111.35	111.81	107.82	107.81	114.79
1MHz	113.04	112.98	111.51	111.31	112.23	110.63	111.08	115.63

To study the effect of PPy on the T_{max} of composites, the T_{max} at different frequencies are fitted from **Figure 3-8** to **3-15**. The results are listed in Table 3-3. Because of high loss at 1 kHz, the T_{max} in 10 kHz is plotted in **Figure 3-17**. In each composite, the peak positions slightly increased with frequency when PPy wt% increasing. Compared with Ni-P(VDF-TrFE) composite, the PPy-P(VDF-TrFE) composites are much more complex because PPy filler may have a large effect on the polymer matrix. With the wt.% of PPy increasing, the peak positions of T_{max} slightly decreased. This phenomenon also can be explained by there being less crystals or there are smaller crystals, and more amorphous with increasing the conducting polymer.

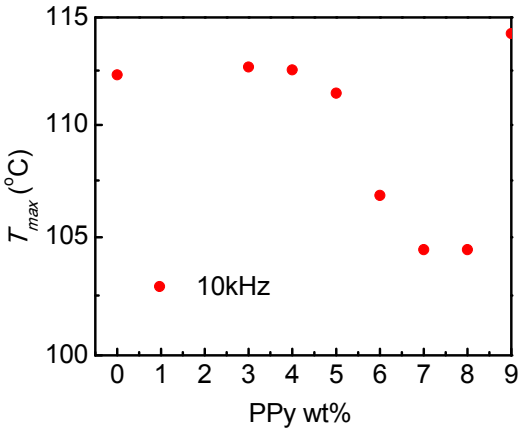

Figure 3-17. The T_{max} of composites at 10 kHz.

3.4. Dielectric Behavior of PPy-P(VDF-CTFE) Composites

3.4.1. PPy-P(VDF-CTFE) Composites at Room Temperature

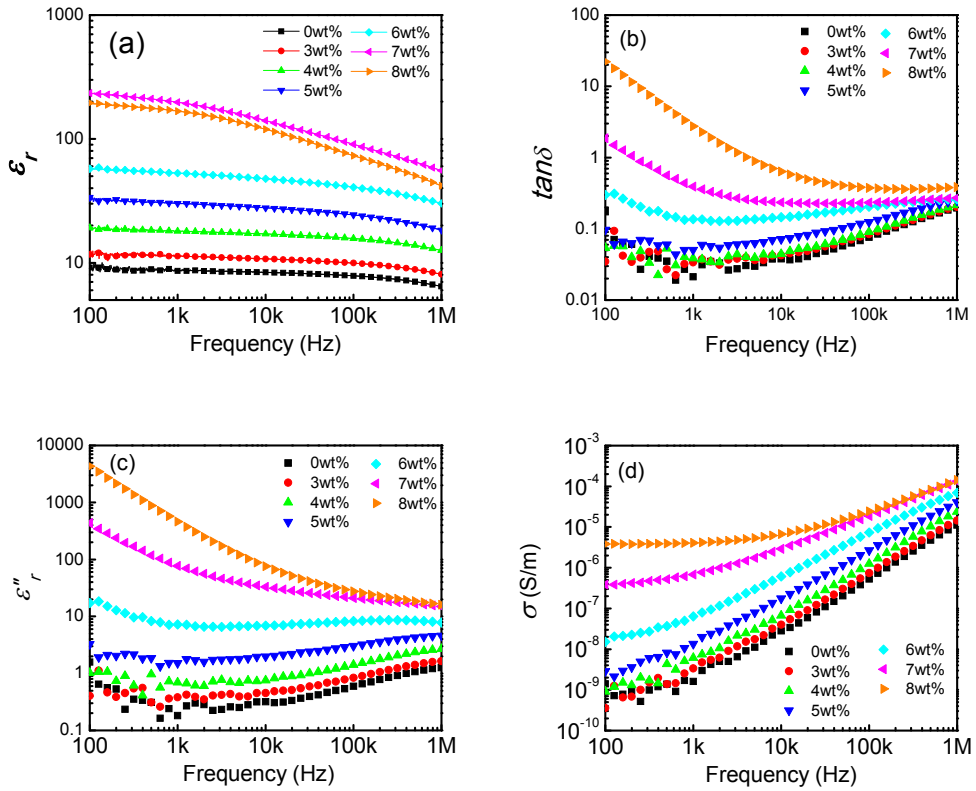

Figure 3-18. Dielectric responses (a) dielectric constant, (b) dielectric loss, (c) imaginary part of dielectric constant, (d) conductivity as a function of frequency for PPy-P(VDF-CTFE) composites with different PPy concentrations.

As shown in **Figure 3-18 (a)**, the dielectric constant of the composites raises with increasing filler concentration in matrix. The dielectric constant slightly decreased with frequency in the low frequency (100 to 100 kHz) with PPy concentration smaller than 6 wt.%. From 7 wt.%, the dielectric constant increased abruptly due to the increasing of the filler content. The dielectric constant of a composite with 7 wt.% was more than 25 times higher than that of the P(VDF-CTFE), rising to 250 at room temperature at 100Hz. Compared with PPy-P(VDF-TrFE), the maximum value of dielectric constant for P(VDF-CTFE) was smaller than that of PPy-P(VDF-TrFE). As

shown in **Figure 3-18 (b)**, the dielectric loss also increased with increasing of filler. The loss changed with PPy content of PPy-P(VDF-CTFE) was much more simple and clear than for the PPy-P(VDF-TrFE). There were no relaxation peaks observed and the loss increased dramatically at low frequency then gradually at high frequency.

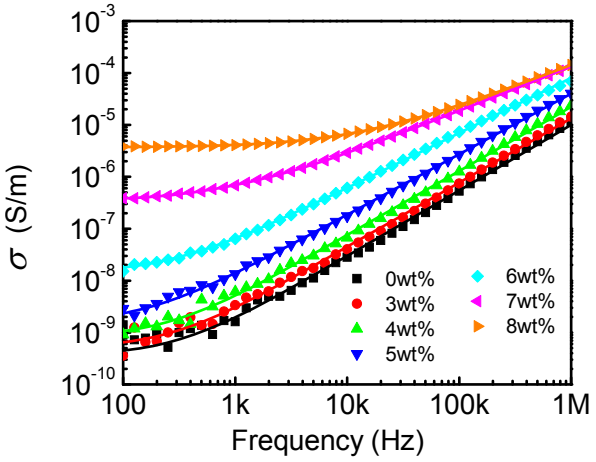

Figure 3-19. Conductivity of PPy-P(VDF-CTFE) composites vs. frequency with concentrations from 0% to 8 wt.% and the fitting curve of Johnscher's universal dielectric response law.

In order to study further, the Johnscher's universal dielectric response law was used to explain this phenomenon. The equation is shown in Section 2.3. **Figure 3-19** shows the conductivity of composites and fitting curve of Eq. (2-1) to the conductivity data for all of samples from 100 Hz to 100 kHz. The symbols represent the experimental data and the solid line represents the fitted data employing Jonscher's law. There is a close agreement between the experimental and fitted data. The corresponding parameters are listed in **Table 3-4**.

The parameters σ_0, A, and n changed with PPy concentrations from 0% to 9 wt.% in **Table 3-4** are plotted in **Figure 3-20**. From the fitting results, it was found that the σ_0 of composites increased slowly and continuously with increasing PPy content for

the composites. When the PPy concentration was higher than 6wt.%, the σ_0 increased with the PPy concentration rapidly. For example, the σ_0 of the composites with 6 wt.%, 7 wt.% and 8 wt.% of PPy was more than 9, 220, and 2400 times, respectively, higher than that of composite with 5 wt.% of PPy. The composites with 8 wt.% of PPy exhibited a high conductivity which was almost independence of frequency at low frequency. This means that the composite was around the percolation threshold. The value of A increases with increasing PPy concentration. This means that the contribution of the new dielectric process in the composite to the dielectric response increased with the PPy concentration. This is consistent with the direct observation of the dielectric loss discussed above. n changed from 1 to smaller than 1 at 6 wt.% to 7 wt.%, which was higher than 4 wt.% to 5 wt.% for PPy-P(VDF-TrFE).

Table 3-4 Parameters of Johnscher's universal dielectric response law for fitting the conductivity of composites

PPy wt.%	Parameter in $\sigma_{meas} = \sigma_0 + A\omega^n$						
	σ_0	σ_0 error	A	A error	n	n error	R^2
0	5.23E-10	1.85E-11	1.18E-14	7.56E-16	1.2503	5.53E-3	0.9969
3	5.61E-10	2.12E-11	5.01E-14	3.05E-15	1.2397	4.90E-3	0.9940
4	8.18E-10	2.55E-11	8.76E-14	3.84E-15	1.2364	3.52E-3	0.9969
5	1.49E-9	5.10E-11	4.57E-13	1.55E-14	1.1685	2.75E-3	0.9979
6	1.35E-8	1.11E-10	4.64E-12	5.83E-14	1.0652	9.97E-4	0.9997
7	3.33E-7	4.32E-10	1.99E-10	7.67E-13	0.8568	2.93E-4	0.9999
8	3.67E-6	1.86E-9	3.17E-10	1.61E-12	0.8298	3.60E-4	0.9999

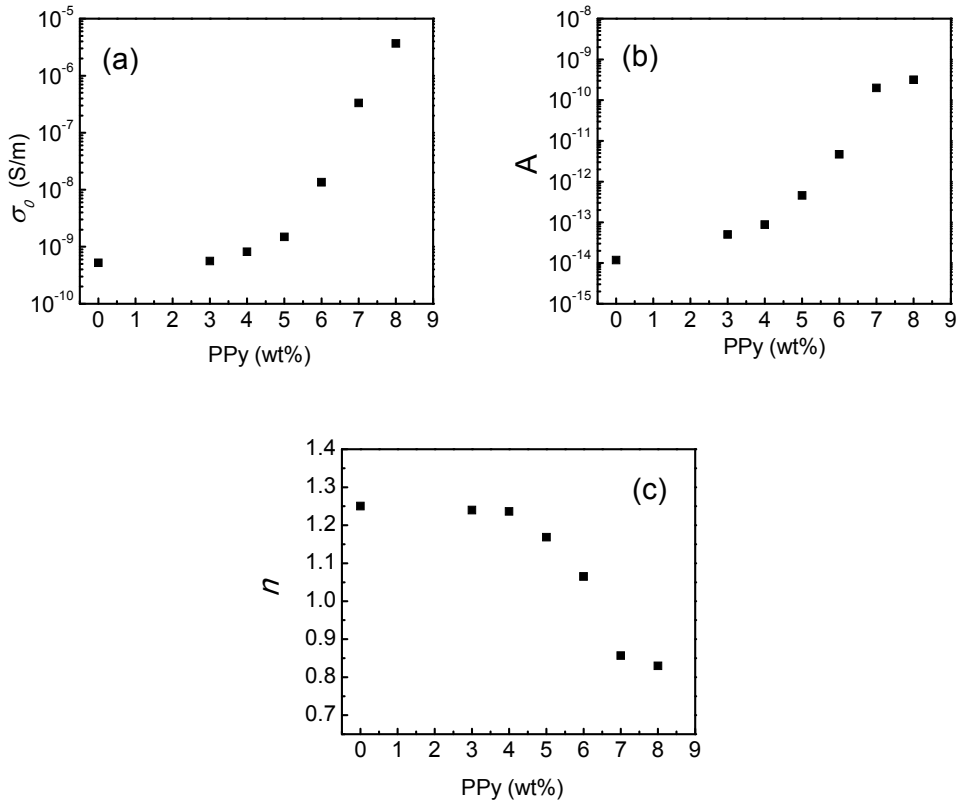

Figure 3-20. σ_0, A, and n change with PPy concentrations from 0 % to 8 wt.% for PPy-P(VDF-CTFE).

3.4.2. PPy-P(VDF-CTFE) Composites at Different Temperature

The polymer matrix effects on dielectric properties are shown with their temperature dependence issue from **Figure 3-21** to **Figure 3-27**. These figures show the temperature dependence of the dielectric properties for PPy-P(VDF-CTFE) composites with different contents of PPy at 1 kHz, 10 kHz, 100 kHz, and 1 MHz.

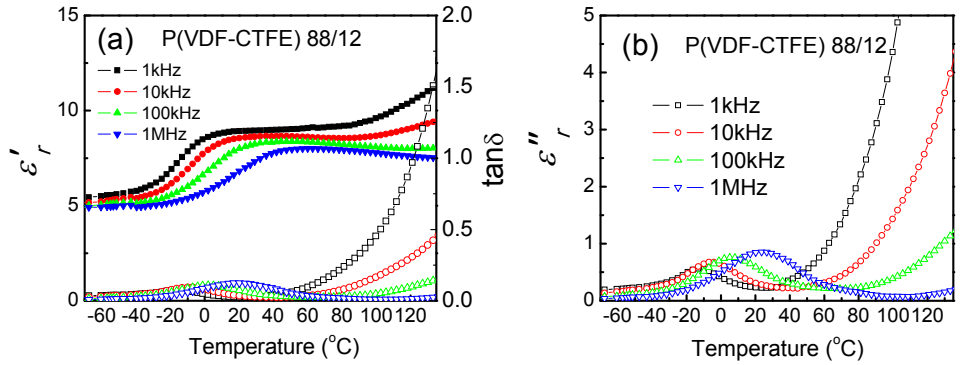

Figure 3-21. Temperature dependence of dielectric properties of pure P(VDF-CTFE): (a) real part(solid) and loss(open), (b) imaginary part.

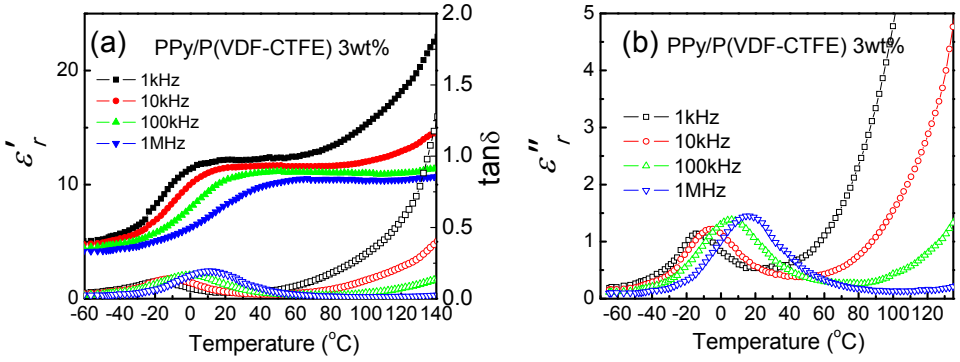

Figure 3-22. Temperature dependence of dielectric properties of PPy-P(VDF-CTFE) 3 wt.%: (a) real part, (b) loss and (c) imaginary part.

The dielectric constant of the composite with 3 wt.% of PPy showed a similar temperature dependence to the polymer matrix. However, the composite exhibits a lower loss at high temperature. Regarding the glass transition process, similar to the polymer matrix, the higher the frequencies, the higher the peak temperature for $tan\delta$ and ε''_r. However, the frequency dependence of the peak value higher than polymer matrix. Moreover, at high frequency, the peak position shifted to low temperature.

The dielectric constant of the composite with 4 wt.% PPy showed the similar temperature dependence to the polymer matrix and for composites with 3 wt.% PPy. Again, the composite exhibited a lower loss at high temperature than the polymer

matrix. Regarding glass transition process, although the ε''_r for the composite was higher than the composite with 3 wt.% PPy, the increase at low frequency was clearly smaller than it at high frequency. For example, the peak of ε''_r at 1 MHz was 1.45 and 4.0, for the composites with 3 wt.% and 4 wt.% respectively, while at 1 kHz it was 1.14 and 3.20, respectively. And the ε''_r of the composite at high temperature was also higher than the composite with 3 wt.% PPy. All these may be the results of new relaxation process. This is consistent with the data shown in **Table 3-4**.

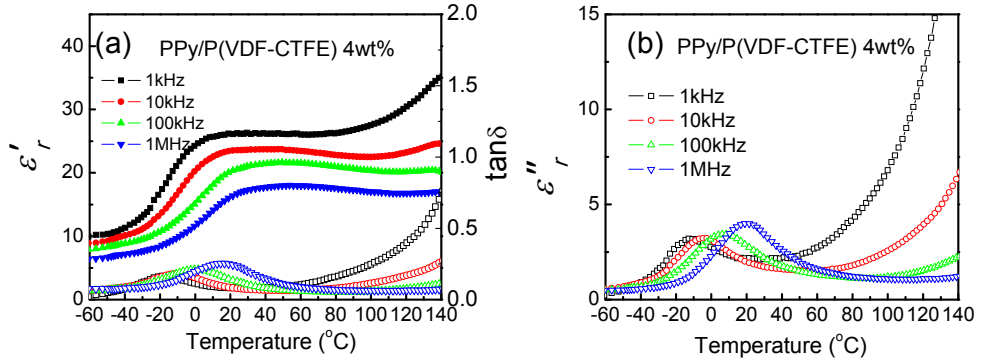

Figure 3-23. Temperature dependence of dielectric properties of PPy-P(VDF-CTFE) 4 wt.%: (a) real part, (b) loss and (c) imaginary part.

The dielectric constant of the composite with 5 wt.% PPy showed similar temperature dependency compared to the polymer matrix and composites with 4 wt.% PPy. Again, the composite exhibits a lower loss at high temperatures compared to the polymer matrix. Regarding the glass transition process, the ε''_r for the composite was higher than for the composite with 4 wt.% PPy at 1 kHz, and had very small change at 1 MHz. The increase at low frequency was clearly lager than at high frequency. Moreover, the ε''_r at 1kHz was higher than other frequencies across the whole temperature range. All these may have been the results of an increase in the

conductivity. This is consistent with the data shown in **Table 3-4**.

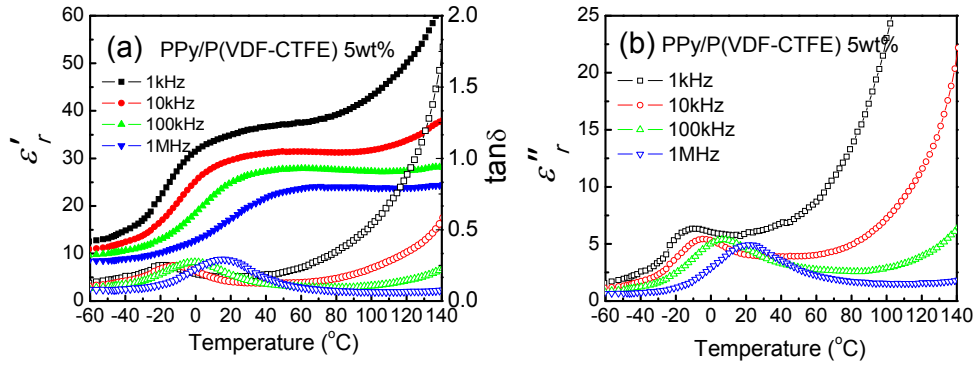

Figure 3-24. Temperature dependence of dielectric properties of PPy-P(VDF-CTFE) 5 wt.%: (a) real part, (b) loss and (c) imaginary part.

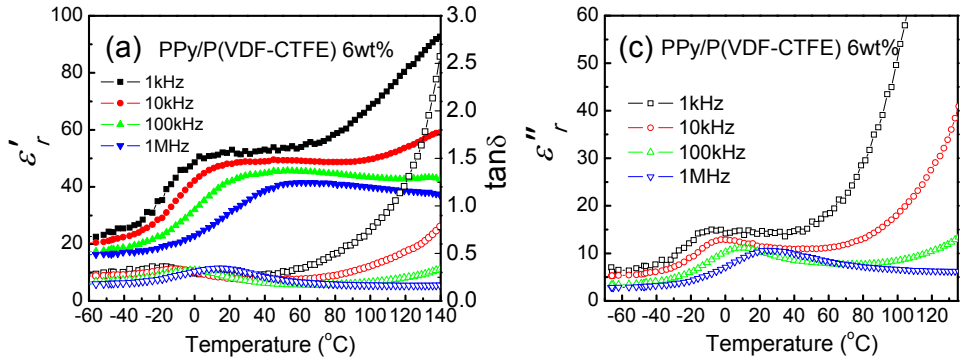

Figure 3-25. Temperature dependence of dielectric properties of PPy-P(VDF-CTFE) 6 wt.%: (a) real part, (b) loss and (c) imaginary part.

The dielectric constant of the composite with 6 wt.% PPy showed similar temperature dependence as the composites with 5 wt.% PPy. However, the composite exhibited a higher loss across the whole temperature range compared to polymer matrix and composites with less PPy content. Regarding the glass transition process, the ε''_r for the composite was much higher than the composite with 5 wt.% PPy at 1 MHz. Moreover, the ε''_r at 1 kHz was higher than other frequencies across the whole temperature range. All these may have been due to the new relaxation process.

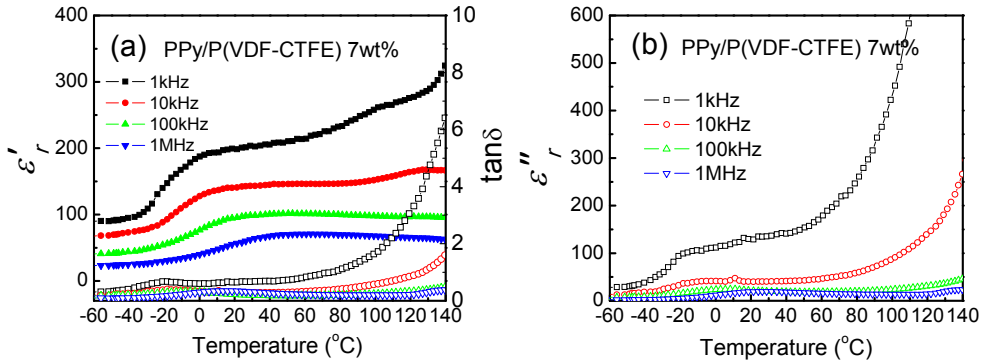

Figure 3-26. Temperature dependence of dielectric properties of PPy-P(VDF-CTFE) 7 wt.%: (a) real part, (b) loss and (c) imaginary part.

From a pure matrix to 6 wt.%, it was easy to identify the glass transition temperature from imaginary part of dielectric constant. However, for composites with 7 wt.% and 8 wt.% of PPy, it was difficult to find the peak at high frequency due to the new relaxation process dominating the dielectric response. The $\varepsilon_r^{'}$, $tan\delta$,$\varepsilon_r^{''}$ of the composite with 7 wt.% PPy were all high than that of the composite with 6 wt.% PPy. The T_g shifted to high temperatures compared to the $\varepsilon_r^{''}$ of 5 wt.% and 6 wt.% PPy. However, it was not easy to quantify the value of T_g. In the composites with 7 wt.% PPy, it was the first time the loss at 1 kHz was larger than other frequencies across the whole temperature range. The difference of dielectric constant among the four different frequencies was larger than that of composites with 3 wt.% to 6 wt.%.

The dielectric constant of the composite with 8 wt.% PPy showed similar temperature dependence as the composite with 7 wt.% PPy. The $\varepsilon_r^{'}$ of the composite with 8 wt.% PPy were smaller to that of the composite with 7 wt.% PPy. The loss of the composite with 8 wt.% PPy were higher than that of the composite with 7 wt.% PPy at 1 kHz to 100 kHz, but slightly smaller than that at 1 MHz. The T_g shifted to

high temperature slightly after compared the ε''_r of 8 wt.% and 7 wt.% PPy. However, which is not easy to quantify the value of T_g.

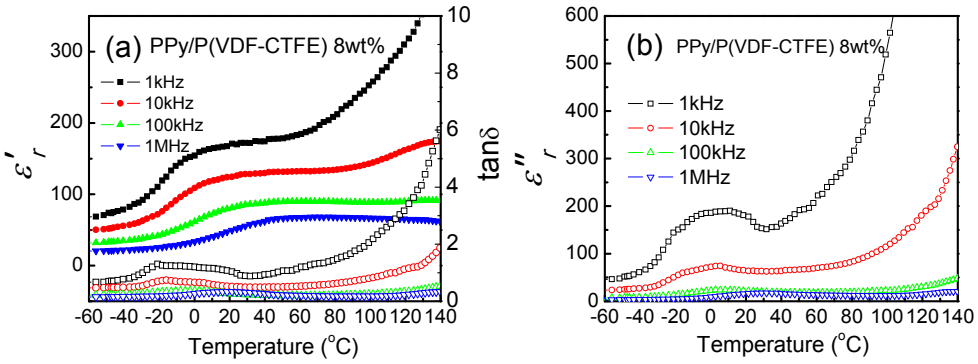

Figure 3-27. Temperature dependence of dielectric properties of PPy-P(VDF-CTFE) 8 wt.%: (a) real part, (b) loss and (c) imaginary part.

To compare the dielectric properties with different PPy concentrations clearly, the ε'_r, ε''_r and *tanδ* at 1 kHz and 1 MHz are shown in **Figure 3-28** and **Figure 3-29**. As a short summary, ε'_r, and ε''_r increased with the increasing PPy concentration from 3 wt.% to 7 wt.% then decreasing. The loss at low temperature increased with the increasing PPy content, while decreased initially with the increasing PPy concentration (from 0 wt.% to 4 wt.%) then increased due to the high conductivity at high temperatures at 1 kHz. The relationship between $\ln\varepsilon''_r$ and 1000/T is shown in **Figure 3-28 (d)** and the parameter is shown in **Table 3-5**. Compared with polymer matrix, it indicates that there are new dielectric relaxation process contributing to the ε''_r and conductivity. With the increasing PPy concentration, the $\ln\varepsilon''_{r0}$ increased from 4 wt.% to 8 wt.%, which was related to the conductivity. Compared with **Table 3-4**, the conductivity of composites at room temperature is from the new relaxation process not the conductivity of filler.

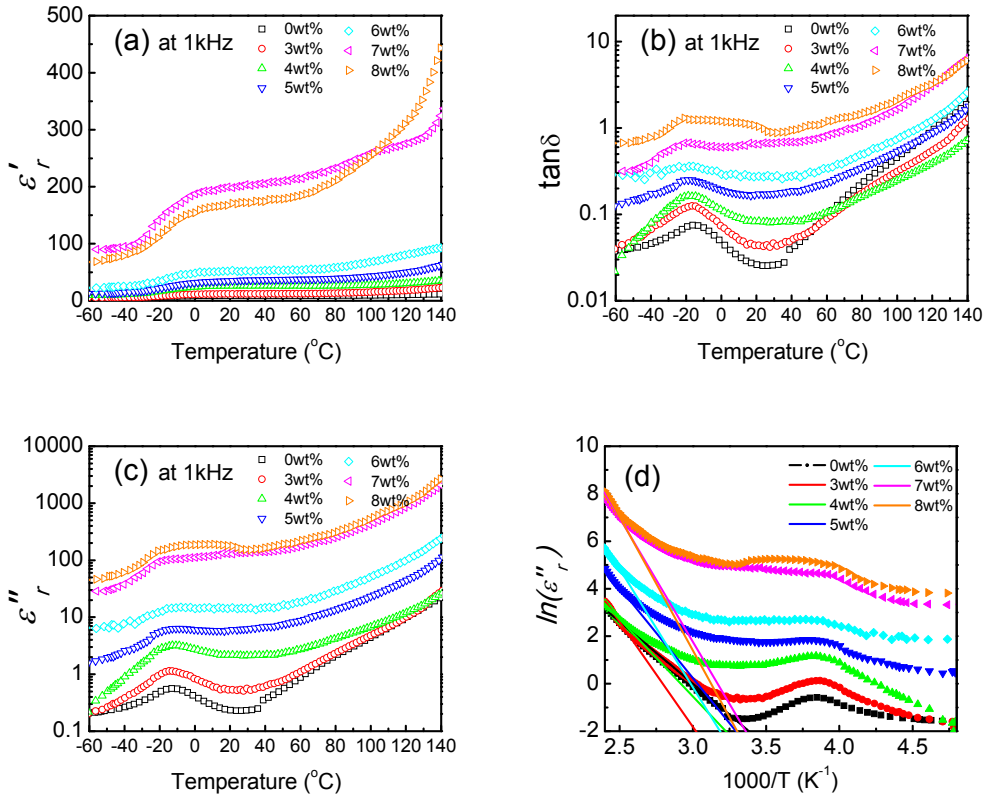

Figure 3-28. Temperature dependence of dielectric properties of composites: (a) ε'_r, (b) *tanδ*, (c) ε''_r and (d) $\ln\varepsilon''_r$ vs. 1000/T.

Table 3-5. Parameters given by Eq. (2-4) fitting at 1 kHz for composites

PPy wt.%	$ln\varepsilon''_{r0}$	σ_0 (S/m)	E_a (eV)	$ln\varepsilon''_{r0}$ at RT (S/m)	σ_0 at RT (S/m)	R^2
0	19.291	13.263	0.5775	-1.476	9.563×10^{-10}	0.9999
3	23.721	1.14×10^{3}	0.7624	-0.624	4.356×10^{-10}	0.9916
4	22.234	2.51×10^{2}	0.5609	0.767	3.497×10^{-9}	0.9934
5	23.073	5.83×10^{2}	0.6561	1.809	5.184×10^{-9}	0.9878
6	29.790	4.81×10^{5}	0.8603	2.671	1.628×10^{-9}	0.9526
7	33.139	1.37×10^{7}	0.9015	4.901	9.403×10^{-9}	0.9531
8	35.235	1.12×10^{8}	0.9721	5.052	4.966×10^{-9}	0.9949

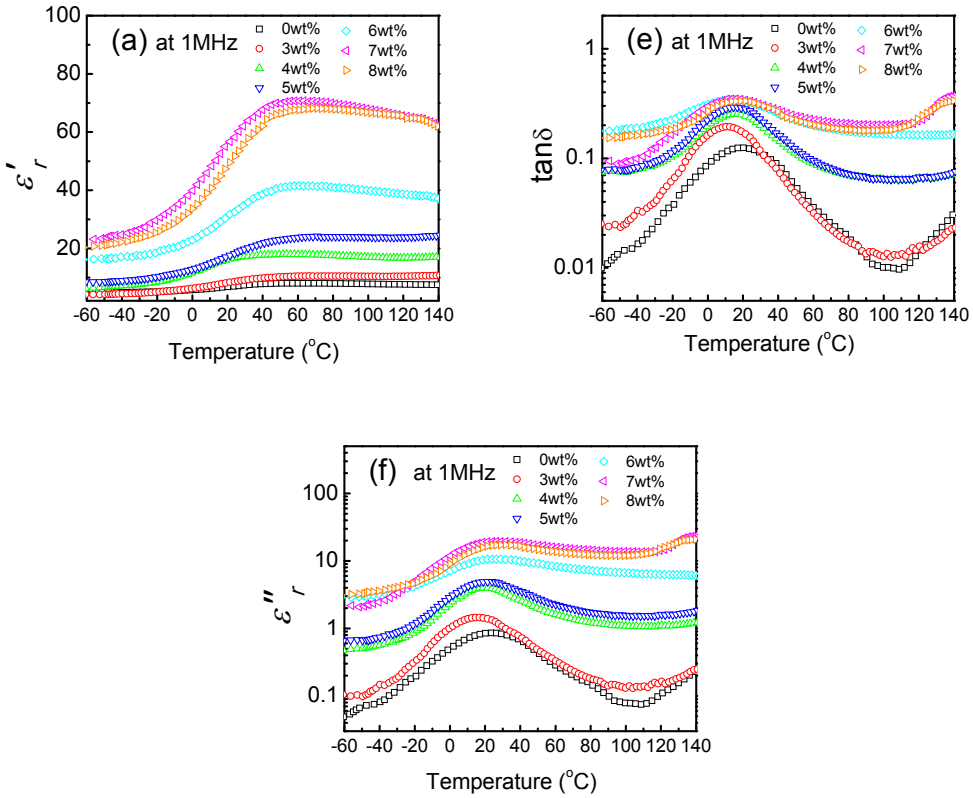

Figure 3-29. Temperature dependence of dielectric properties of composites: (a) ε'_r, (b) *tanδ*, and (c) ε''_r.

Table 3-6 Glass transition temperature of PPy-P(VDF-CTFE) composites with different frequencies (in K unit)

	0 wt.%	3 wt.%	4 wt.%	5 wt.%	6 wt.%
1kHz	260.24	260.63	261.98	263.63	267.31
10kHz	267.72	267.63	269.24	269.84	274.34
100kHz	278.99	279.0	280.42	280.64	283.6
1MHz	293.13	291.16	295.06	294.6	298.51

Regarding the glass transition temperature, it was of interest to know whether the filler had some influence on the T_g. The peak position of ε''_r shifted to high temperature at all four frequencies. The peak of relaxation shifted to high temperature with the increased frequency. To quantify the analysis, the peak temperature of ε''_r was determined for all composites as shown in **Table 3-6**. All of the peak positions were

fitted by peak fitting over a small temperature range from the imaginary parts of the dielectric constant. The log*f* versus $1000/T_g$ is shown in **Figure 3-30**.

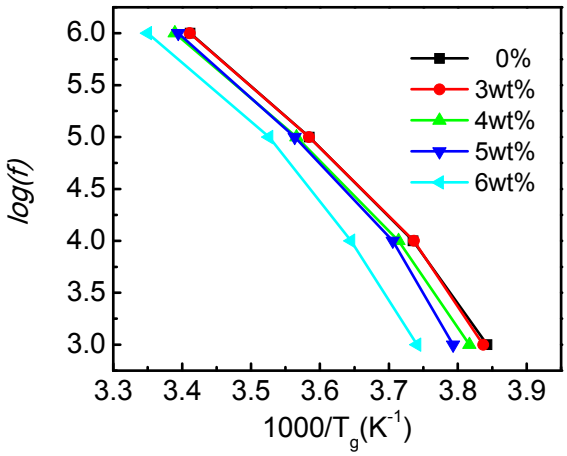

Figure 3-30. Relationship between log*f* and $1000/T_g$ of PPy-P(VDF-CTFE) composites.

A nonlinear relationship between log*f* and $1/T_g$ was reported and a more accurate fitting result was obtained by the Vogel–Fulcher (VF) relationship. The parameters of VF fitting are listed in **Table 3-7** and **Figure 3-31**. From the parameters given by fitting using Vogel–Fulcher equation, it indicates the activation energy almost continuously decreases from 0% to 5 wt.%, meanwhile, the T_f increases. It is different from the Ni-P(VDF-TrFE) composites which had a critical value at 30 vol%. The T_f increase can be explained by the crystallinity.

Table 3-7 Parameters given by fitting using Vogel–Fulcher equation

PPy wt.%	f_0 (Hz)	E_a (eV)	T_f(K)	R^2
0	1.22×10^{10}	0.037	205.5	0.9984
3	2.29×10^{10}	0.032	212.6	0.9968
4	2.30×10^{10}	0.031	213.4	0.9985
5	4.23×10^{9}	0.022	225.5	0.9878
6	7.92×10^{9}	0.024	227.0	0.9995

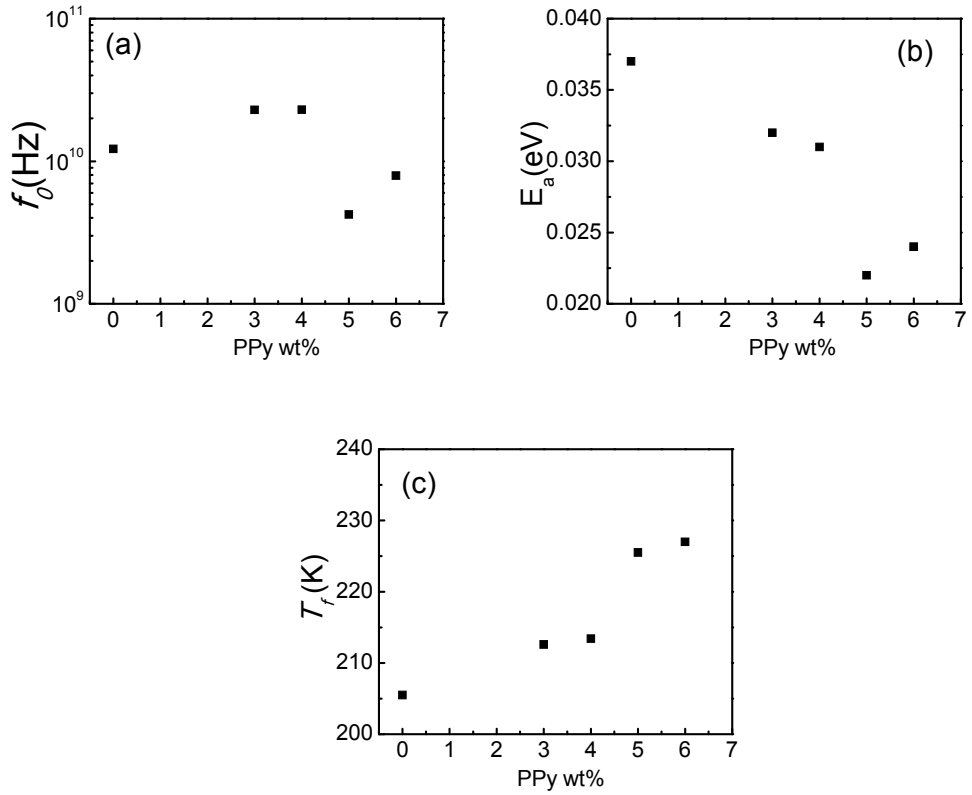

Figure 3-31. f_0, E_a, and T_f change with PPy concentrations from 0% to 6 wt.%.

3.5. Percolative Behavior of PPy-Polymer Composites

3.5.1. Percolation Behavior of PPy-Polymer Composites at Room Temperature

The dependence of $\varepsilon_r/\varepsilon_m$ of the PPy-P(VDF-TrFE) and PPy-P(VDF-CTFE) composites on PPy weight fraction are plotted in **Figure 3-32**. There are two main differences between the two composites which had a large effect on percolation behavior. First, the dielectric constant or $\varepsilon_r/\varepsilon_m$ of PPy-P(VDF-TrFE) was much higher than for PPy-P(VDF-CTFE). Second, there was a strong relaxation behavior in the PPy-P(VDF-TrFE) composites. From 1 kHz to 100 kHz, the dielectric constant decreased with frequency dramatically. In order to study the percolative behavior of the Ni-polymer composites at room temperature, the φ_c and s of both composites are listed in **Table 3-8** and plotted in **Figure 3-33**.

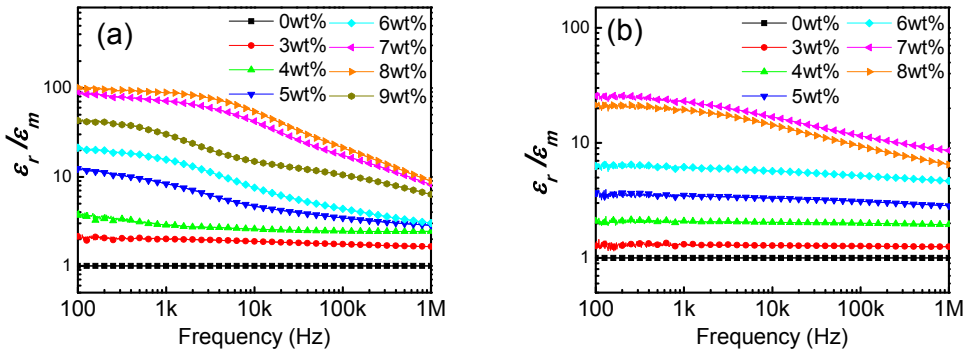

Figure 3-32. $\varepsilon_r/\varepsilon_m$ vs. frequency with different PPy weight fraction of (a) PPy-P(VDF-TrFE) and (b) PPy-P(VDF-CTFE) composites at room temperature.

For both composites, the φ_c is between 7 wt.% to 8 wt.%. However, the φ_c decreased with increasing frequency strongly from 1 kHz to 100 kHz in the PPy-P(VDF-TrFE) composites. The φ_c and s both decreased with frequency and the curve was similar to the dependence of dielectric constant on frequency at φ_c. For PPy-P(VDF-CTFE) composites, this case is similar to Ni-polymer composites. The φ_c and s both increased with frequency from 1 kHz to 1 MHz. before 1 kHz, the φ_c may decrease slightly. That is, the φ_c and s are not constant but dependent on the selected different frequency. The φ_c and s of PPy-P(VDF-CTFE) and PPy-P(VDF-TrFE) showed the very different trends, which was different from the case for the Ni-polymer composites.

Table 3-8 φ_c and s vs. different frequencies of PPy-P(VDF-TrFE) and PPy-P(VDF-CTFE)

Composites	Frequency (Hz)	$\frac{\varepsilon_r}{\varepsilon_m} = \left(\frac{\varphi_c - \varphi_{filler}}{\varphi_c}\right)^{-s}$				
		φ_c	φ_c error	s	s error	R^2
PPy-P(VDF-TrFE)	100	0.08278	2.49E-3	2.4066	0.1980	0.9972
	501	0.08046	1.55E-3	2.1222	0.1243	0.9985
	1000	0.07841	1.16E-3	1.9099	0.0969	0.9989
	5001.8	0.07420	4.60E-4	1.3842	0.0444	0.9996
	10000	0.07332	4.48E-4	1.2084	0.0442	0.9994
	50118.7	0.07315	7.98E-4	0.9803	0.0667	0.9973
	100000	0.07318	9.81E-4	0.9126	0.0759	0.9954
	501187.2	0.07399	1.89E-3	0.8028	0.1106	0.9827
	1000000	0.07550	3.10E-3	0.7998	0.1448	0.9658
PPy-P(VDF-CTFE)	100	0.07383	6.30E-4	1.0925	0.0544	0.9986
	501	0.07397	7.17E-4	1.0835	0.0586	0.9982
	1000	0.07424	6.88E-4	1.0876	0.0556	0.9983
	5001.8	0.07511	8.94E-4	1.0929	0.0638	0.9974
	10000	0.07578	1.06E-3	1.0961	0.0702	0.9967
	50118.7	0.07809	1.66E-3	1.1273	0.0896	0.9941
	100000	0.07901	2.02E-3	1.1413	0.1004	0.9925
	501187.2	0.08085	2.98E-3	1.1529	0.1265	0.9879
	1000000	0.08282	3.34E-3	1.1556	0.1349	0.9861

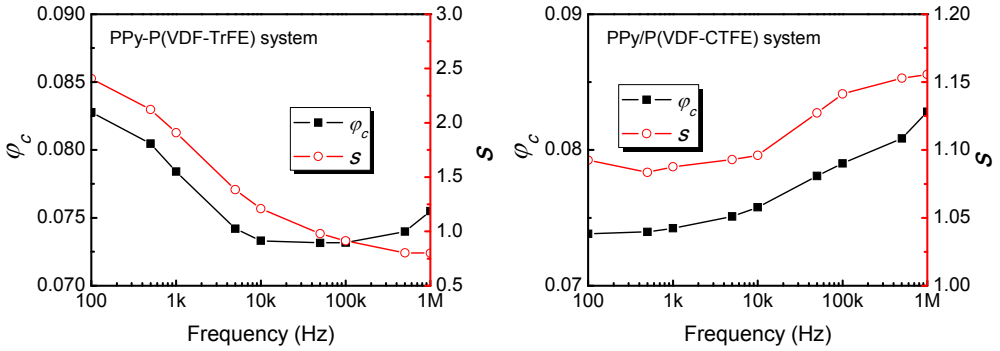

Figure 3-33. φ_c and s of the dielectric data to equation for (a) PPy-P(VDF-TrFE) and (b) PPy-P(VDF-CTFE) composites with different frequency at room temperature.

3.5.2. Percolative Behavior of PPy-Polymer Composites at Different Temperature

As discussed in Section 3.3 and 3.4, P(VDF-TrFE) and P(VDF-CTFE) have totally different temperature dependencies for their dielectric properties. The φ_c and s of both composites at some frequencies and temperatures were studied. The variation of $\varepsilon_r/\varepsilon_m$ of the PPy-P(VDF-TrFE) and PPy-P(VDF-CTFE) composites at different frequency (1 kHz, 10 kHz, 100 kHz, and 1 MHz) at temperatures of -40 ^oC, 0 ^oC, 40 ^oC, 80 ^oC and 130 ^oC are studied. The variation of $\varepsilon_r/\varepsilon_m$ for both composites at -40 ^oC and 80 ^oC as examples are shown in **Figure 3-34**. At each temperature, the $\varepsilon_r/\varepsilon_m$ had the similar trend with increasing weight fraction of PPy. At lower than 4 wt.% PPy in PPy-P(VDF-TrFE) and 6 wt.% PPy in PPy-P(VDF-CTFE), the $\varepsilon_r/\varepsilon_m$ did not change much with different frequencies.

The fitting results with frequency at different temperature are listed in **Table 3-9** and **Table 3-10**, and the normalized $\varphi_c/\varphi_{-40^oC}$ and s/s_{-40^oC} are plotted in **Figure 3-35** and **Figure 3-36**. At different temperatures, $\varphi_c/\varphi_{-40^oC}$ only changes for wt.% smaller than 8% and 6% for PPy-P(VDF-TrFE) and PPy-P(VDF-CTFE) respectively, which can be considered as independent on the selected temperature. The critical value is different, which means the fitted critical value is dependent on the selected temperature. The case was similar as Ni-polymer composites. The $\varphi_c/\varphi_{-40^oC}$ and s/s_{-40^oC} varies with temperature were very similar to the curve of temperature dependence of dielectric constant. For the PPy-P(VDF-TrFE) system, the $\varphi_c/\varphi_{-40^oC}$ and s/s_{-40^oC} had a peak value between 80 ^oC and 130 ^oC, which is similar to the phase transition temperature. For PPy-P(VDF-CTFE) system, the $\varphi_c/\varphi_{-40^oC}$ and s/s_{-40^oC} first

increased then slightly decreased with temperature. However, there was an abnormality for 1 MHz in s/s_{-40^oC} which continuously decreased with temperature.

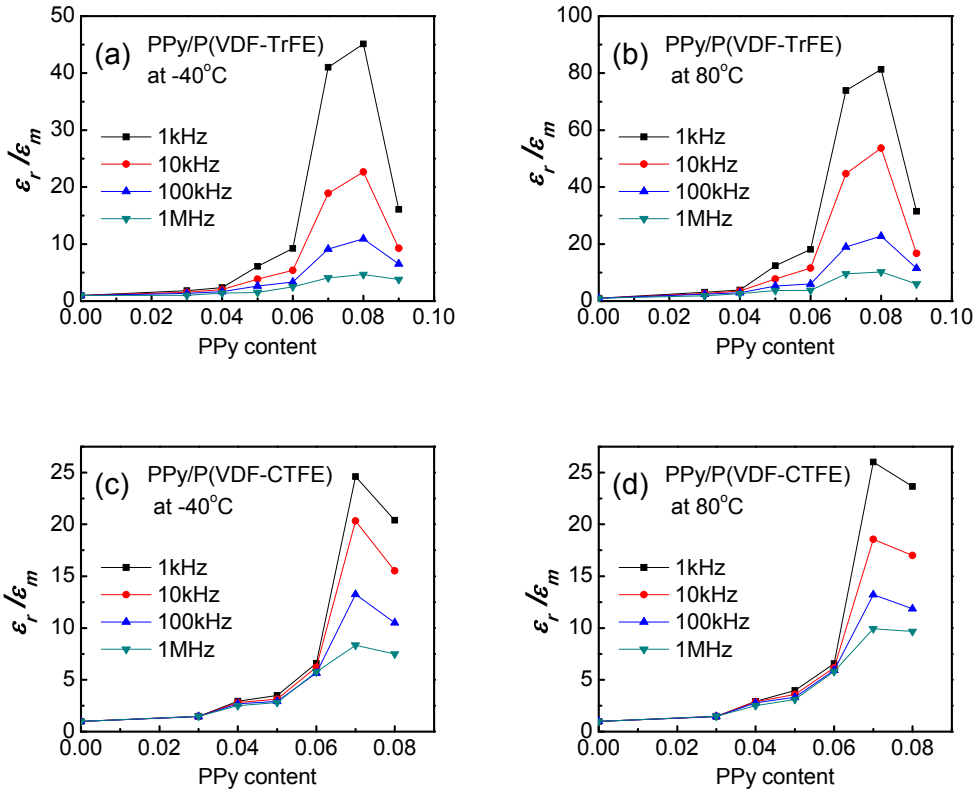

Figure 3-34. Variation of $\varepsilon_r/\varepsilon_m$ of the composites with (a) different frequency different frequency 1 kHz, 10 kHz, 100 kHz, and 1 MHz: PPy-P(VDF-CTFE) at (a) -40 °C and (b) 80 °C, PPy-P(VDF-TrFE) at (c) 40 °C and (d) 80 °C.

Table 3-9 φ_c and s vs. different selected frequency and temperature of PPy-P(VDF-TrFE)

Temperature (°C)	Frequency (Hz)	$\frac{\varepsilon_r}{\varepsilon_m} = \left(\frac{\varphi_c - \varphi_{filler}}{\varphi_c}\right)^{-s}$				
		φ_c	φ_c error	s	s error	R^2
-40	1k	0.07585	1.23E-3	1.4497	0.0996	0.9975
	10k	0.07465	9.26E-4	1.0588	0.0644	0.9974
	100k	0.07372	9.12E-4	0.7402	0.0516	0.9956
	1M	0.07451	2.64E-3	0.5015	0.0873	0.9667
0	1k	0.07775	1.40E-3	1.6576	0.1079	0.9978
	10k	0.07422	6.29E-4	1.1440	0.0504	0.9989
	100k	0.07417	8.94E-4	0.8307	0.0526	0.9966
	1M	0.07688	1.69E-3	0.7224	0.0607	0.9927
40	1k	0.07972	2.33E-3	1.9121	0.1773	0.9957
	10k	0.07672	1.01E-3	1.4361	0.0736	0.9984
	100k	0.07541	1.58E-3	0.9719	0.9911	0.9925
	1M	0.07745	3.32E-3	0.7553	0.1180	0.9745
80	1k	0.07992	3.61E-3	2.3419	0.2726	0.9940
	10k	0.07977	2.07E-3	1.8094	0.1489	0.9963
	100k	0.07931	3.87E-3	1.3721	0.2180	0.9813
	1M	0.08064	5.93E-3	1.1102	0.2446	0.9580
130	1k	0.07649	1.69E-3	1.4676	0.1297	0.9955
	10k	0.07474	1.59E-3	1.0827	0.1117	0.9925
	100k	0.07595	3.08E-3	0.8825	0.1506	0.9713
	1M	0.07434	2.21E-3	0.5836	0.0879	0.9730

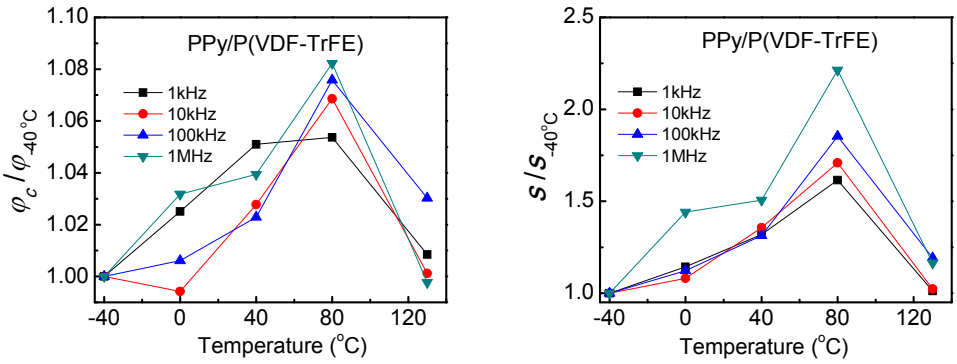

Figure 3-35. $\varphi_c/\varphi_{-40^oC}$ *and* s/s_{-40^oC} vs. different selected frequency and temperature for PPy-P(VDF-TrFE) composites.

Table 3-10 φ_c and s vs. different selected frequency and temperature of PPy-P(VDF-CTFE)

Temperature (°C)	Frequency (Hz)	$\frac{\varepsilon_r}{\varepsilon_m} = \left(\frac{\varphi_c - \varphi_{filler}}{\varphi_c}\right)^{-s}$				
		φ_c	φ_c error	s	s error	R^2
-40	1k	0.07479	6.67E-4	1.1655	0.0582	0.9977
	10k	0.07538	8.71E-4	1.1414	0.0591	0.9950
	100k	0.07924	1.91E-3	1.2030	0.0944	0.9830
	1M	0.09063	1.26E-2	1.7976	0.5355	0.9690
0	1k	0.07398	1.08E-3	1.1786	0.0797	0.9971
	10k	0.07705	1.16E-3	1.2278	0.0705	0.9976
	100k	0.07931	1.61E-3	1.2932	0.0795	0.9972
	1M	0.09464	7.97E-3	1.6839	0.2802	0.9873
40	1k	0.07525	1.28E-3	1.2046	0.0930	0.9961
	10k	0.07768	1.40E-3	1.2557	0.0282	0.9968
	100k	0.07958	2.13E-3	1.3876	0.0968	0.9966
	1M	0.09314	5.25E-3	1.6729	0.1916	0.9938
80	1k	0.07465	6.92E-4	1.1740	0.0533	0.9987
	10k	0.07683	1.02E-3	1.2068	0.0621	0.9980
	100k	0.07967	2.05E-3	1.3369	0.0949	0.9964
	1M	0.09102	6.01E-3	1.5715	0.2202	0.9899
130	1k	0.07562	4.84E-4	1.1680	0.0327	0.9995
	10k	0.07655	6.59E-4	1.1748	0.0404	0.9991
	100k	0.07988	1.70E-3	1.2904	0.0783	0.9973
	1M	0.09110	4.88E-3	1.5148	0.1716	0.9934

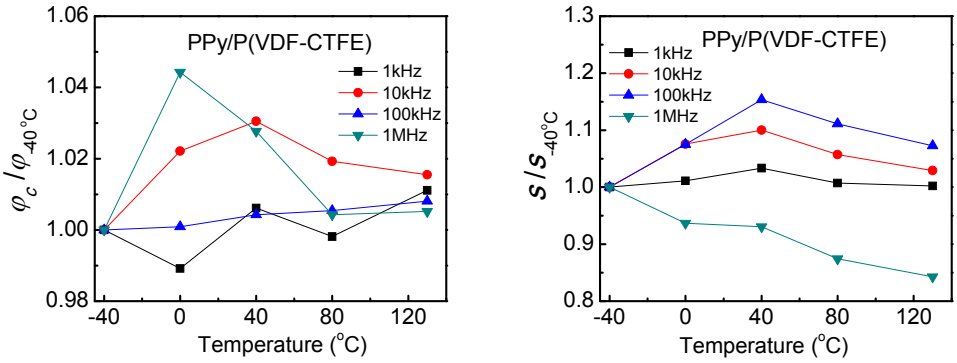

Figure 3-36. $\varphi_c/\varphi_{-40^oC}$ *and* s/s_{-40^oC} vs. different selected frequency and temperature for PPy-P(VDF-CTFE) composites.

3.5.3. γ Fitting Close to the Percolation Threshold

After the percolation threshold was determined, the γ was obtained from the composite which was the closest to the percolation threshold. In these PPy based composites, the composites with 7 wt.% of PPy were closest one for both PPy-P(VDF-CTFE) and PPy-P(VDF-TrFE). The dielectric constant and the fitting curve by Eq. (2-7) are shown in **Figure 3-37**. Because it is a nonlinear curve in log-log scale, the fitting curve is separated to 2 parts, before 3 kHz and after 3 kHz. The γ_1=0.8807 γ_2=0.5821 was determined for PPy-P(VDF-CTFE) and γ_1=0.9134 γ_2=0.8119 is for PPy-P(VDF-TrFE). The results are close to the normal value from the percolation theory which was discussed in Section 1.4.1.

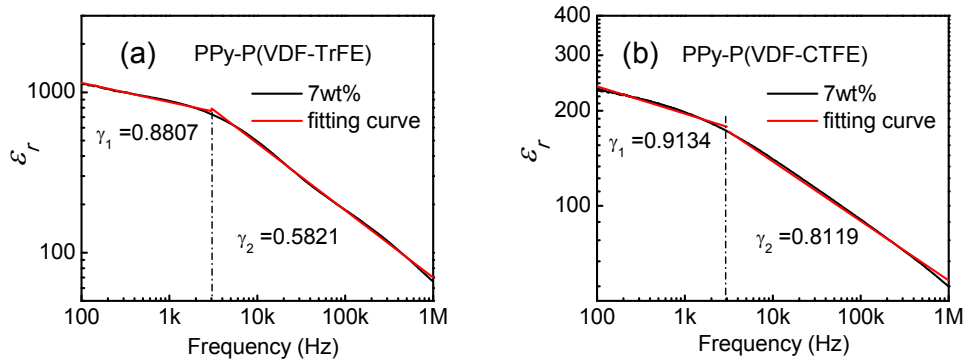

Figure 3-37. Dielectric constant vs. frequency of composites and fitting curve for (a) PPy-P(VDF-TrFE) and (b) PPy-P(VDF-CTFE).

3.6. Conclusions

1. All-organic dielectric composites based on PPy nanoclips were prepared by solution casting and hot-pressed processing. Low percolation threshold (φ_c<8 wt.%) were achieved in both systems. Compared to the composites with high percolation threshold, composites with low percolation threshold only needed very small amounts of filler with the composites maintaining their flexibility.
2. A dielectric constant of more than 1000 was obtained for PPy-P(VDF-TrFE) with 8 wt.%, which was more than 100 times higher than that of the P(VDF-TrFE) matrix. It has found that the observed relaxation peak shifted to lower frequency with increasing weight fraction of PPy. This indicated the PPy filler has much effect on polymer matrix, even in very small amounts.
3. There are two main differences between the two composites, which had a large effect on the percolation behavior. First, the dielectric constant or $\varepsilon_r/\varepsilon_m$ of PPy-P(VDF-TrFE) was much higher than PPy-P(VDF-CTFE). Second, there was a very strong relaxation behavior in the PPy-P(VDF-TrFE) composites. From 1 kHz to 100 kHz, the dielectric constant decreased with frequency dramatically.
4. Similar to the Ni-polymer composites, there were three mechanisms in this conductor-polymer composite: 1) the dielectric relaxation process from the polymer matrix, 2) the new dielectric relaxation process from the composite, and 3) the conductivity of the conducting filler (PPy).

5. Percolation theory in these composites was investigated. It is noted that the percolation threshold was almost independent on the selected frequency and temperature, while the critical value was dependent on the selected frequency and temperature.

References of Chapter 3

1. X. Zhang and S. K. Manohar, *J. Am. Chem. Soc*., **126**, 12714(2004).
2. Z. Liu, X. Y. Zhang, S. Poyraz, S. P. Surwade and S. K. Manohar, *J. Am. Chem. Soc*., **132**, 13158(2010).

CHAPTER 4

Further Study of Percolation Behavior of Polymer-based Composites

4.1. Introduction

In this chapter, the percolation behavior of six conductor-polymer composite systems, which were reported in literature, will be studied [1-6]. As discussed in Section 1.4.1, The Eq. (1-24) and (1-25) can be written as Eq. (4-1) and (4-2), respectively,

$$\varepsilon_{eff} = k(\varphi_c - \varphi)^{-s} \tag{4-1}$$

$$\frac{\varepsilon_{eff}}{\varepsilon_m} = \left(\frac{\varphi_c - \varphi_{filler}}{\varphi_c} \right)^{-s} \tag{4-2}$$

By physics and the nature of the composites, the φ_c and s are independent of the data selection at different frequencies and temperature. Eq. (4-1) and (4-2) were used to fit the data obtained at different frequencies. For the fitting data, two methods were used. For Method A, the fitting equation Eq. (4-1) or (4-2) was used with the same data points used in original articles. For Method B, the Eq. (4-2) was used as the fitting equation and more experimental data were included in the fitting. According to Eq. (4-2), the dielectric constant of the matrix must be in the fitting. It was found that both methods gave the same conclusion that the percolation threshold (φ_c) and critical value (s) are both dependent on frequency.

4.2. Percolation Behavior of Six Systems of Conductor-Polymer Composites

4.2.1. System-I: MWNT-PVDF Composites [1]

Wang *et. al* reported the dielectric properties of the untreated multiwall carbon-nanotubes/ poly(vinylidenefluoride) (MWNT/PVDF) composites with a very low percolation threshold. The MWNT/PVDF composites were prepared by simple physical blending with a hot-molding process. The MWNT were ultrasonically dispersed in DMF for as long as 2 h then the PVDF was dissolved in the DMF solvent at 50 °C. These two solutions were mixed and stirred by further ultrasonic treatment for 10 min. Then, the solution was heated to 60 °C for 8 h and consequently molded by hot-pressing at about 200 °C and 15 MPa. The final samples were disk-shaped with a 12 mm diameter and a 1 mm thickness. The low percolation threshold was explained due to the large aspect ratio and the high conductivity of the MWNT. The author's fitted data in the log–log plots of the power law gave φ_c=0.0161 and s=0.31 according to Eq.(4-1). The data selected for fitting data were dielectric constant at 1 kHz for composites φ_{MWNT}=0, 0.004, 0.008, 0.012 and 0.016.

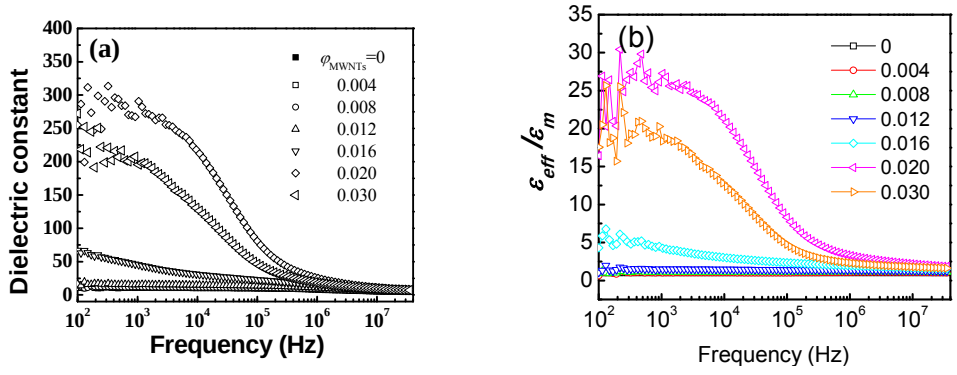

Figure 4-1. Dependence of (a) the dielectric constant, (b) $\varepsilon_{eff}/\varepsilon_m$ of the MWNT-PVDF composites on frequency at room temperature.

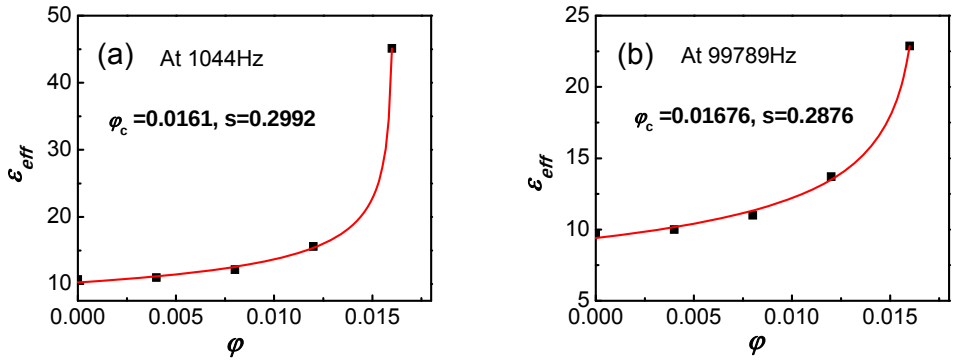

Figure 4-2. ε_{eff} vs. volume fraction φ and the fitting curve by Method A at different frequencies: (a) at 1044 Hz and (b) 99789 Hz.

Table 4-1 φ_c and s vs. different frequencies of System I by Method A

Frequency (Hz)	$\varepsilon_{eff} = k(\varphi_c - \varphi)^{-s}$ φ_{MWNT}=0, 0.004, 0.008, 0.012 and 0.016						
	φ_c	φ_c error	s	s error	k	k error	R^2
100	0.01611	2.42E-4	0.3519	0.1188	2.4416	1.4034	0.9948
477	0.01610	5.64E-5	0.3242	0.0271	2.5969	0.3998	0.9997
1044	0.01611	9.17E-5	0.2993	0.0384	2.9750	0.5499	0.9990
2002	0.01618	1.45E-4	0.3070	0.0486	2.8219	0.6543	0.9981
4984	0.01630	2.04E-4	0.3096	0.0512	2.7545	0.6640	0.9971
10892	0.01639	2.46E-4	0.3046	0.0510	2.7969	0.6637	0.9965
20895	0.01648	2.88E-4	0.2990	0.0514	2.8471	0.6745	0.9959
52017	0.01662	3.45E-4	0.2913	0.0503	2.8997	0.6624	0.9952
99789	0.01676	3.81E-4	0.2876	0.0477	2.9001	0.6204	0.9952
476563	0.01728	2.52E-4	0.2830	0.0215	2.7043	0.2510	0.9988
1041451	0.01769	1.93E-4	0.2857	0.0136	2.4411	0.1397	0.9995
4973664	0.01825	5.98E-4	0.2654	0.0317	2.0294	0.2610	0.9972
10869148	0.01827	3.19E-4	0.2445	0.0154	1.9138	0.1194	0.9992
35113424	0.01808	7.36E-4	0.2127	0.0328	1.8332	0.2454	0.9949

The dependence of the dielectric constant and $\varepsilon_{eff}/\varepsilon_m$ on the frequency for the MWNT-PVDF composites at room temperature is shown in **Figure 4-1**. In Method A, the fitting equation and selected fitting data were the same as the article selected: φ_{MWNT}=0, 0.004, 0.008, 0.012 and 0.016 and Eq. (4-1) were used as the fitting equation. **Figure 4-2** and **Table 4-1** show the fitting results. In Method B, the fitting

equation is used Eq. (4-2) and the selected fitting data included the peak position: φ_{MWNT}=0, 0.004, 0.008, 0.012, 0.016 and 0.02. **Figure 4-3** and **Table 4-2** show the fitting results. This fitting must start from the 0 vol.% point according to the percolation equation.

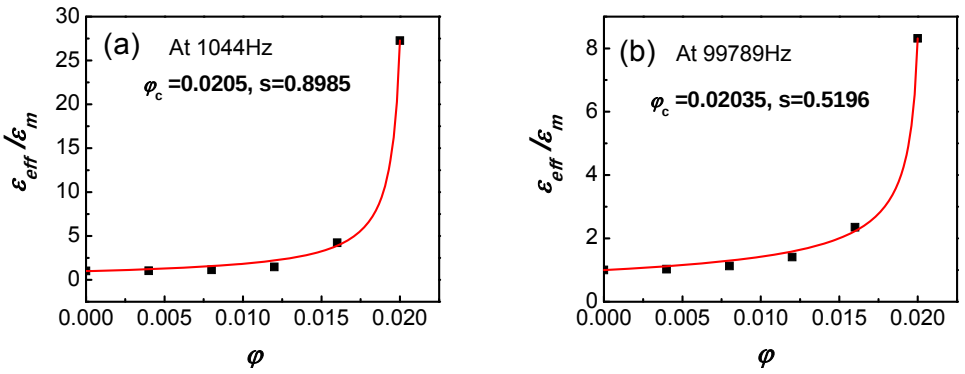

Figure 4-3. $\varepsilon_{eff}/\varepsilon_m$ vs. volume fraction φ and the fitting curve by Method B at different frequencies: (a) at 1044 Hz and (b) 99789 Hz.

Table 4-2 φ_c and s vs. different frequencies of System I by Method B

Frequency (Hz)	$\frac{\varepsilon_{eff}}{\varepsilon_m}=\left(\frac{\varphi_c-\varphi_{filler}}{\varphi_c}\right)^{-s}$ φ_{MWNT}=0, 0.004, 0.008, 0.012, 0.016 and 0.02				
	φ_c	φ_c error	s	s error	R^2
100	0.02142	5.01E-4	1.2580	0.1390	0.9969
477	0.02091	3.65E-4	1.0823	0.1173	0.9975
1044	0.02052	2.59E-4	0.8985	0.0993	0.9980
2002	0.02041	2.11E-4	0.8228	0.0864	0.9984
4984	0.02026	1.47E-4	0.7236	0.0695	0.9989
10892	0.02022	1.42E-4	0.6730	0.0680	0.9990
20895	0.02020	1.18E-4	0.6181	0.0553	0.9990
52017	0.02023	1.27E-4	0.5514	0.0450	0.9984
99789	0.02035	1.60E-4	0.5196	0.0470	0.9975
476563	0.02118	3.61E-4	0.4855	0.0440	0.9946
1041451	0.02196	4.94E-4	0.4901	0.0426	0.9947
4973664	0.02363	9.37E-4	0.4761	0.0506	0.9933
10869148	0.02429	1.33E-3	0.4481	0.0599	0.9905
35113424	0.02521	2.74E-3	0.3973	0.0953	0.9753

The dependence of φ_c and s on frequency for the results obtained by using Method A and B are plotted in **Figure 4-4**. In Method A, the φ_c=0.01611 and s=0.2992 at 1 kHz were very close to the results from the article (φ_c=0.0161 and s=0.31). For example, the φ_c increased from 0.01611 at 100 Hz to 0.01827 at 3.5 MHz then slightly decreased; the s decreased continuously from 0.3519 at 100 Hz to 0.2127 at 4 MHz, except the value at 1 kHz. Comparing with Method A, Method B gave a larger change in the φ_c and s. The φ_c firstly decreased slightly from 0.02142 at 100 Hz to 0.02020 at 20895Hz then increased with increasing frequency, a φ_c of 0.02521 was obtained at 3.5 MHz. The s decreased quickly from 1.2580 at 100 Hz to 0.4885 at before 500 kHz then slowly decreased with increasing frequency. Both of the fitting methods indicated that the percolation threshold and critical constant were change with frequency.

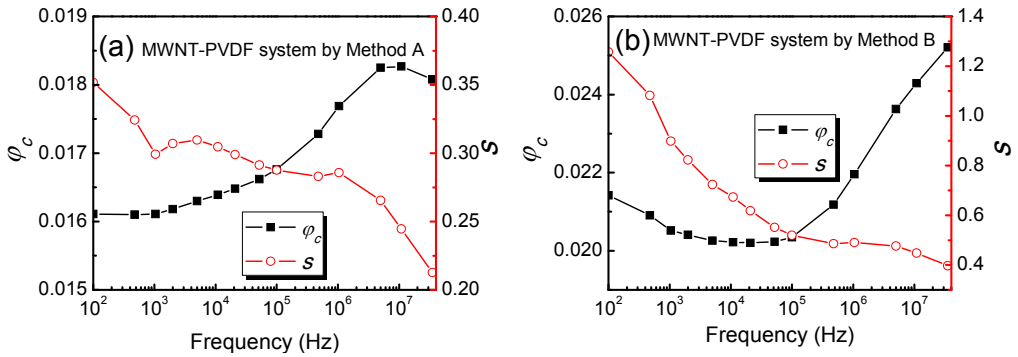

Figure 4-4. Dependence of percolation threshold (φ_c) and critical constant (s) on frequency by different fitting method: (a) Method A and (b) Method B.

4.2.2. System-II: CB-BT-VMQ Composites [2]

Dang *et. al* studied three-component high-elasticity nanocomposites, methyl vinyl silicone rubber (VMQ) as a matrix and nano-sized BT and carbon black (CB) as fillers. In this composite system, the volume fraction of BT was 0.40 and the diameter

was 100 nm. The size of CB was about 50 nm and surface area was about 60-70 mm^2/g^{-1}. A silane coupling agent (KH550) was used to modify the surface of both BT and CB particles. Then the CB and BT were mixed with VMQ in tetrahydrofuran solvent and hot pressed to a disk shape. The dielectric properties of the composites are shown in **Figure 4-5**. The dielectric constant had a giant enhancement in the composites near the percolation threshold of around 0.035. To determine the φ_c and s, dielectric constant of the composites for φ=0.04 is not considered because the dielectric constant increased dramatically between 0.035 and 0.0375. It was obtained that φ_c=0.0375 and s=0.289 using dielectric constant at 1 kHz.

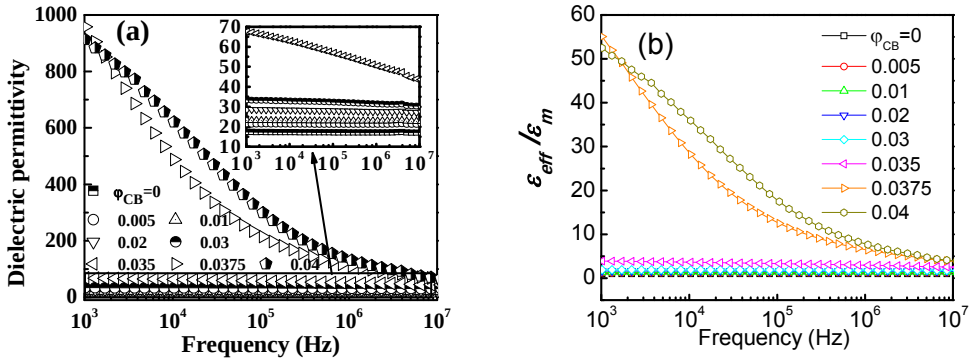

Figure 4-5. Dependence of (a) the dielectric constant, (b) $\varepsilon_{eff}/\varepsilon_m$ of the MWNT/PVDF composites on frequency at room temperature.

In Method A, the data selected were the same as used in the article selected: φ_{CB}=0, 0.005, 0.01, 0.02, 0.03 and 0.035. **Figure 4-6** and **Table 4-3** show the fitting results at select different frequencies. In Method B, the fitting equation was used Eq. (4-2) and selected fitting data including the peak position φ_{CB}=0, 0.005, 0.01, 0.02, 0.03, 0.035 and 0.0375. **Figure 4-7** and **Table 4-4** show the fitting results at selected frequencies by Method B.

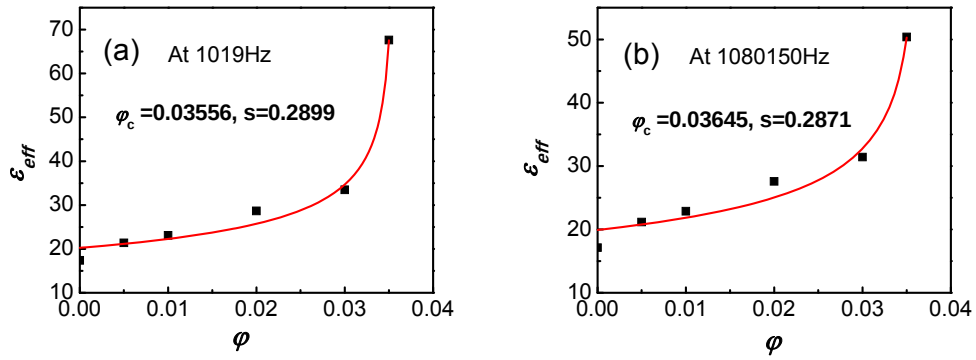

Figure 4-6. ε_{eff} vs. volume fraction φ and the fitting curve by Method A at different frequencies: (a) at 1019 Hz and (b) 1080150 Hz.

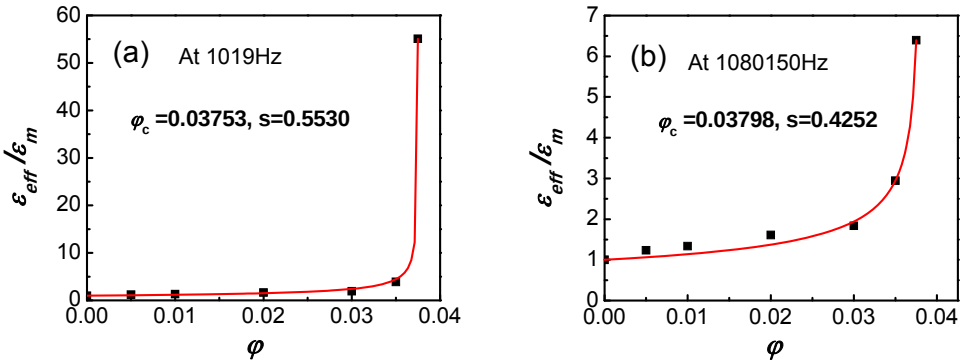

Figure 4-7. $\varepsilon_{eff}/\varepsilon_m$ vs. volume fraction φ and the fitting curve by Method B at different frequencies: (a) at 1019 Hz and (b) 1080150 Hz.

Table 4-3 φ_c and s vs. different frequencies of System II by Method A

Frequency (Hz)	$\varepsilon_{eff} = k(\varphi_c - \varphi)^{-s}$ φ_{CB}=0, 0.005, 0.01, 0.02, 0.03 and 0.035						
	φ_c	φ_c error	s	s error	k	k error	R^2
100	0.03541	4.56E-4	0.2748	0.0627	8.3842	2.1759	0.9858
470	0.03553	5.79E-4	0.2911	0.0715	7.6782	2.2516	0.9823
1019	0.03556	6.01E-4	0.2899	0.0722	7.6957	2.2732	0.9814
4793	0.03561	6.67E-4	0.2863	0.0739	7.7750	2.3356	0.9790
10393	0.03568	7.18E-4	0.2873	0.0750	7.7292	2.3442	0.9776
48864	0.03584	8.67E-4	0.2870	0.0788	7.7201	2.4255	0.9734
105952	0.03595	9.74E-4	0.2873	0.0814	7.7044	2.4793	0.9707
498149	0.03624	1.27E-3	0.2871	0.0879	7.6927	2.6161	0.9638
1080150	0.03645	1.49E-3	0.2871	0.0928	7.6950	2.7251	0.9589
3923640	0.03702	2.14E-3	0.2916	0.1063	7.7162	3.0263	0.9481
11011690	0.03791	3.21E-3	0.3044	0.1275	7.3210	3.2959	0.9370

The φ_c and s obtained at different frequencies using Method A and B are plotted in **Figure 4-8**. In Method A, the φ_c=0.03556 and s=0.2899 at 1 kHz were very close to the results from the article (φ_c=0.0375 and s=0.289). Both methods resulted in that the φ_c increased slightly with increasing frequency selected. However, the s value obtained using Method A was almost independent of frequency, while the s changed a lot in Method B, decreasing from 0.5917 at 100 Hz to 0.4272 around 3.9 MHz.

Table 4-4 φ_c and s vs. different frequencies of System II by Method B

Frequency (Hz)	$\frac{\varepsilon_{eff}}{\varepsilon_m}=\left(\frac{\varphi_c-\varphi_{filler}}{\varphi_c}\right)^{-s}$ φ_{CB}=0, 0.005, 0.01, 0.02, 0.03, 0.035 and 0.0375				
	φ_c	φ_c error	s	s error	R^2
100	0.03753	1.23E-4	0.5917	0.0634	0.9994
470	0.03753	1.07E-4	0.5877	0.0540	0.9995
1019	0.03753	8.07E-5	0.5530	0.0401	0.9997
4793	0.03753	4.74E-5	0.4964	0.0222	0.9998
10393	0.03753	4.53E-5	0.4747	0.0202	0.9997
48864	0.03758	5.62E-5	0.4551	0.0201	0.9993
105952	0.03763	6.84E-5	0.4464	0.0206	0.9989
498149	0.03782	1.20E-4	0.4303	0.0233	0.9970
1080150	0.03798	1.90E-4	0.4252	0.0285	0.9924
3923640	0.03842	3.85E-4	0.4181	0.0373	0.9842
11011690	0.03925	8.46E-4	0.4272	0.05337	0.9716

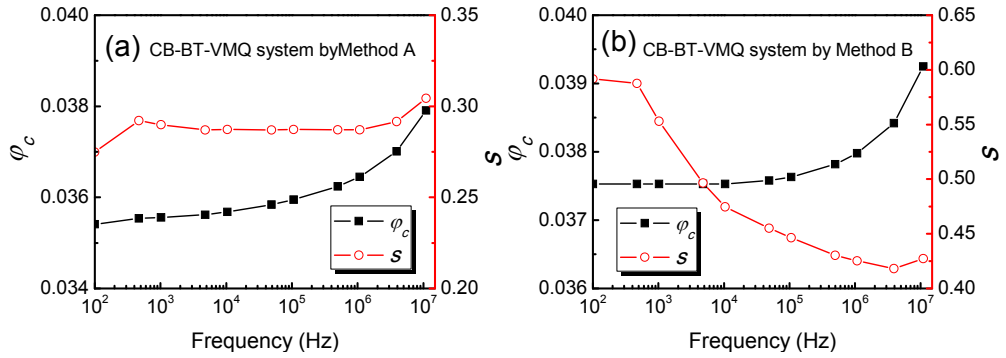

Figure 4-8. Dependence of percolation threshold (φ_c) and critical constant (s) on frequency by different fitting method: (a) Method A and (b) Method B.

4.2.3. System-III: PANI-PVDF Composites [3]

Yuan *et. al* investigated the dielectric properties of all-organic polyaniline/poly(vinylidene fluoride) (PANI/PVDF) composites with a wide range of PANI loading. The average diameter and conductivity of PANI particles was 0.1 μm and 6.7 S/m, respectively. PANI/PVDF composites were prepared via a solution-grinding and hot-molding route. **Figure 4-9** shows the dependence of the dielectric constant ε_{eff} and $\varepsilon_{eff}/\varepsilon_m$ on frequency at room temperature. According to Eq. (4-1), the φ_c=0.045 and s=0.167 were obtained from fitting the data at 100Hz.

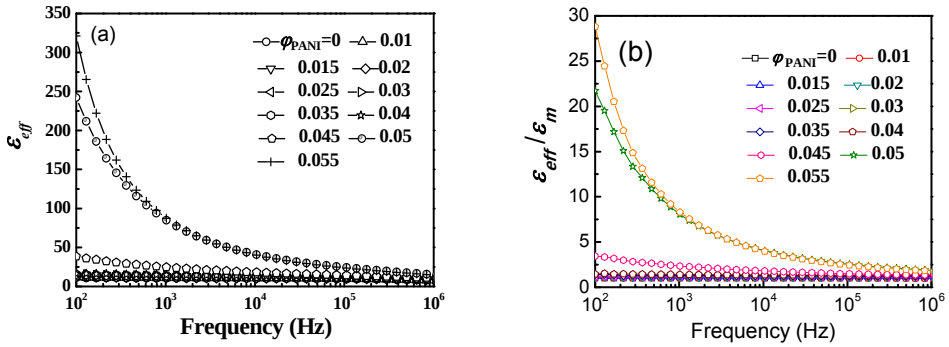

Figure 4-9. Dependence of (a) the dielectric constant, (b) $\varepsilon_{eff}/\varepsilon_m$ of the PANI-PVDF composites on frequency at room temperature.

In Method A, the selected data were the same as the article selected: φ_{PANI}=0, 0.01, 0.015, 0.02, 0.025, 0.03, 0.035, 0.04 and 0.045. **Figure 4-10** and **Table 4-5** show fitting results at select different frequencies. According the Method A in this case, the results in 498149Hz and 1080150Hz are shown in **Figure 4-11**. It indicates the dielectric constant without including the φ_{PANI}=0.05 was not in agreement with the percolation theory at very high frequencies. In this case, dielectric constant at φ_{PANI}=0.05 must be considered as the abrupt point in the percolation theory.

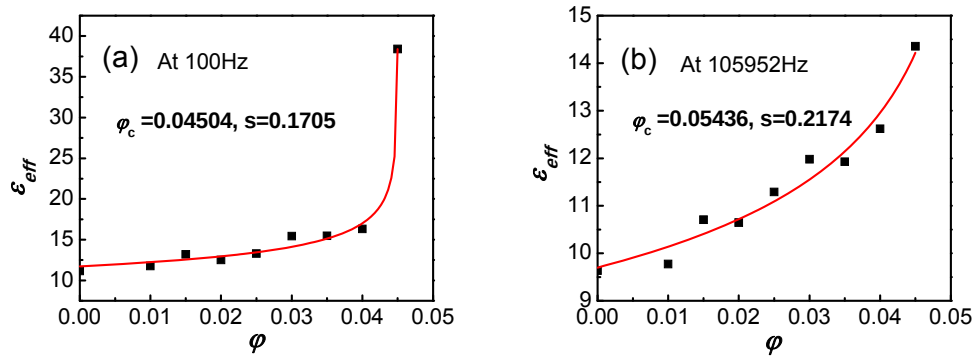

Figure 4-10. ε_{eff} vs. volume fraction φ and the fitting curve by Method A at different frequencies: (a) at 100 Hz and (b) 105952 Hz.

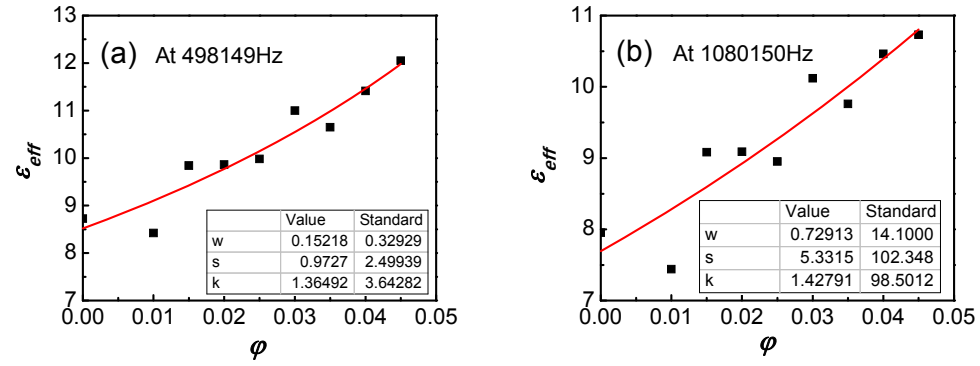

Figure 4-11. ε_{eff} vs. volume fraction φ and the fitting curve by Method A at different frequencies: (a) at 498149 Hz and (b) 1080150 Hz.

Table 4-5 φ_c and s vs. different frequencies of System III by Method A

Frequency (Hz)	$\varepsilon_{eff} = k(\varphi_c - \varphi)^{-s}$ φ_{PANI}=0, 0.01, 0.015, 0.02, 0.025, 0.03, 0.035, 0.04 and 0.045						
	φ_c	φ_c error	s	s error	k	k error	R^2
100	0.04504	1.50E-4	0.1700	0.0292	6.9212	0.8316	0.9918
470	0.04513	1.46E-4	0.1610	0.0189	6.6779	0.5124	0.9933
1019	0.04522	1.82E-4	0.1559	0.0179	6.6583	0.4797	0.9917
4793	0.04565	3.85E-4	0.1506	0.0200	6.5919	0.5113	0.9841
10393	0.04608	6.07E-4	0.1494	0.0221	6.5560	0.5462	0.9784
48864	0.04884	2.24E-3	0.1693	0.0370	6.0141	0.7358	0.9619
105952	0.05438	6.39E-3	0.2177	0.0714	5.1465	1.0449	0.9522
498149	0.15218	0.32929	0.9727	0.2499	1.3649	3.6428	0.8781
1080150	0.72913	14.1000	5.3315	102.35	1.4279	98.501	0.8023

In Method B, selected data are φ_{PANI}=0, 0.01, 0.015, 0.02, 0.025, 0.03, 0.035, 0.04, 0.045 and 0.05. **Figure 4-12** and **Table 4-6** shows fitting results in at select different frequencies by Method B.

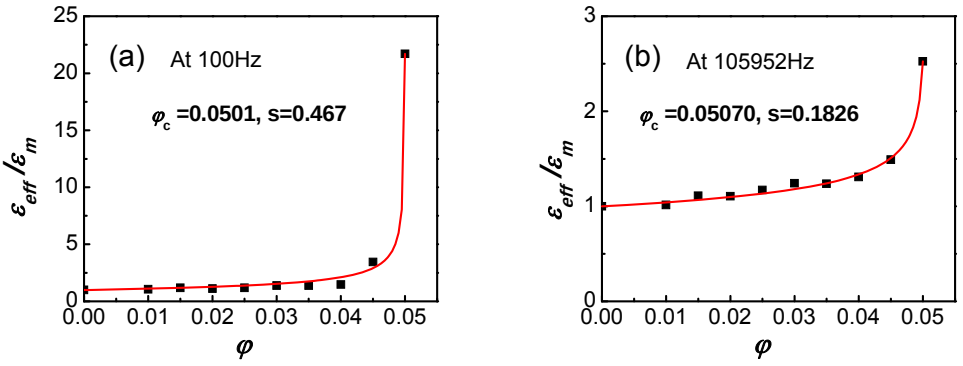

Figure 4-12. $\varepsilon_{eff}/\varepsilon_m$ vs. volume fraction φ and the fitting curve by Method B at different frequencies: (a) at 100 Hz and (b) 105952 Hz.

Table 4-6 φ_c and s vs. different frequencies of System III by Method B

Frequency (Hz)	$\frac{\varepsilon_{eff}}{\varepsilon_m}=\left(\frac{\varphi_c-\varphi_{filler}}{\varphi_c}\right)^{-s}$ φ_{PANI}=0, 0.01, 0.015, 0.02, 0.025, 0.03, 0.035, 0.04, 0.045 and 0.05				
	φ_c	φ_c error	s	s error	R^2
100	0.05007	1.53E-4	0.4670	0.0469	0.9972
470	0.05007	1.35E-4	0.3640	0.0343	0.9955
1019	0.05007	1.23E-4	0.3205	0.0280	0.9950
4793	0.05011	9.76E-5	0.2618	0.0166	0.9955
10393	0.05014	8.47E-5	0.2360	0.0121	0.9963
48864	0.05023	7.98E-5	0.1972	0.0076	0.9969
105952	0.05032	1.17E-4	0.1826	0.0087	0.9942
498149	0.05078	4.39E-4	0.1693	0.0170	0.9647
1080150	0.05145	9.78E-4	0.1735	0.0249	0.9252

The φ_c and s at frequency by Fitting Method A and B are plotted in **Figure 4-13**. In Fitting Method A, the φ_c=0.04504 and s=0.1705 at 100 Hz were very close to the results from the article (φ_c=0.045 and s=0.167). In Method A, from 100 Hz to 100

kHz, both φ_c and s both increased slightly. However, in Method B, the φ_c value is almost independent of frequency. The s continuously decreased from 0.467 at 100 Hz to 0.1735 around 1 MHz.

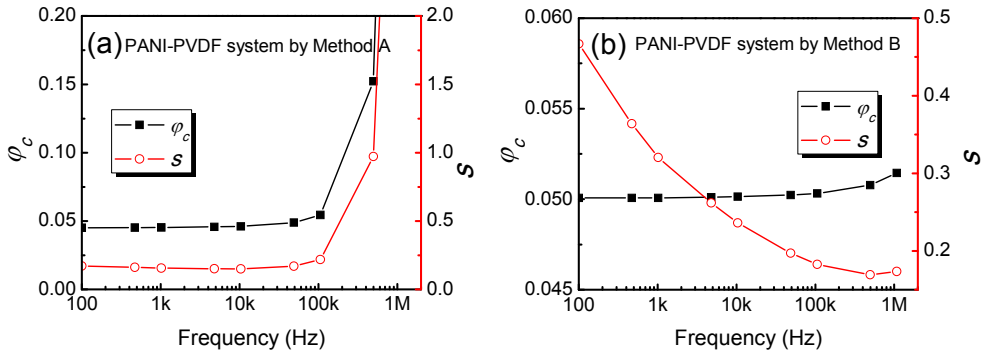

Figure 4-13. Dependence of percolation threshold (φ_c) and critical constant (s) on frequency by different fitting methods: (a) Method A and (b) Method B.

4.2.4. System-IV: Ag-PI Composites [4]

Dang investigated Ag/polyimide (PI) composite by simple ultrasonic dispersion and subsequent in situ polymerization processing. The Ag particles (0.5 μm in diameter), 4,4-diamino-diphenyl ether (ODA) and N, N-dimethylacetamide (DMAc) were placed in a flask. After 0.5 hours ultrasonic dispersion, pyromellitic dianhydride and more DMAc were subsequently added. Finally, the yellow-colored transparent Ag/PI hybrid films with a 30 μm thickness were obtained after the mixture stirred for 3 hours at room temperature. **Figure 4-14** shows the dependence of the dielectric constant ε_{eff} and $\varepsilon_{eff}/\varepsilon_m$ on frequency at room temperature. The dielectric constant of the Ag/PI composite films agree with Eq.(4-1) very well, with $\varphi_c \approx 0.122$ and $s \approx 0.27$ at 1kHz.

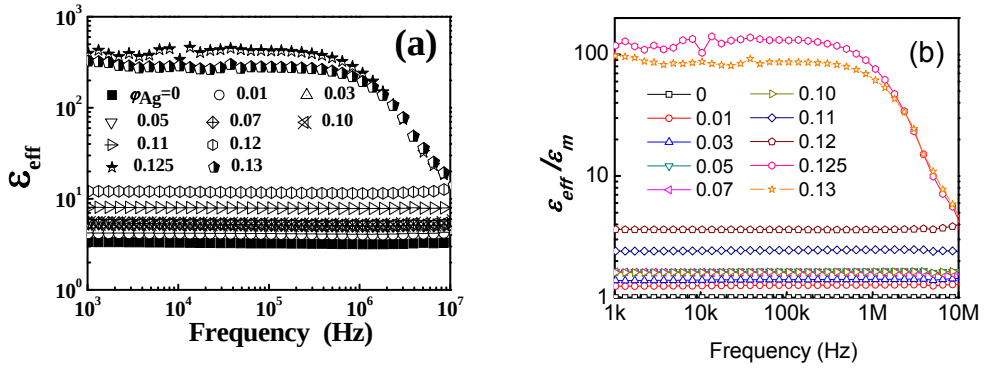

Figure 4-14. Dependence of (a) the dielectric constant, (b) $\varepsilon_{eff}/\varepsilon_m$ of the Ag-PI composites on frequency at room temperature.

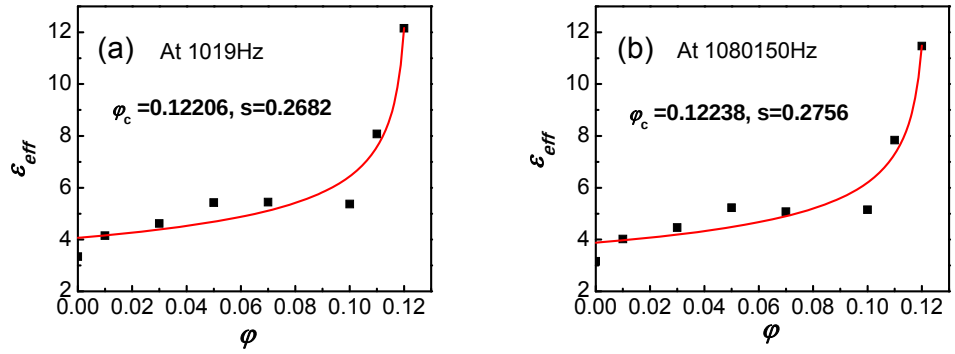

Figure 4-15. ε_{eff} vs. volume fraction φ and the fitting curve by Method A at different frequencies: (a) at 1019 Hz and (b) 1080150 Hz.

Table 4-7 φ_c and s vs. different frequencies of System IV by Method A

Frequency (Hz)	$\varepsilon_{eff} = k(\varphi_c - \varphi)^{-s}$ φ_{Ag}=0, 0.01, 0.03, 0.05, 0.07, 0.1, 0.11, and 0.12						
	φ_c	φ_c error	s	s error	k	k error	R^2
1019	0.12206	2.43E-3	0.2682	0.0768	2.3144	0.5442	0.9336
4793	0.12208	2.45E-3	0.2683	0.0768	2.2960	0.5393	0.9335
10393	0.12212	2.49E-3	0.2690	0.0774	2.2833	0.5398	0.9326
48864	0.12220	2.59E-4	0.2708	0.0790	2.2501	0.5411	0.9305
105952	0.12225	2.63E-3	0.2719	0.0796	2.2311	0.5398	0.9299
498149	0.12235	2.75E-3	0.2746	0.0813	2.1896	0.5386	0.9281
1080150	0.12238	2.78E-3	0.2756	0.0818	2.1747	0.5381	0.9277
2342110	0.12234	2.72E-3	0.2754	0.0811	2.1827	0.5366	0.9289
5078441	0.12194	2.26E-3	0.2664	0.0740	2.2594	0.5149	0.9380
8507712	0.12152	1.87E-3	0.2604	0.0695	2.3367	0.5092	0.9456

In Method A, the data selected were the same as the article selected: φ_{Ag}=0, 0.01, 0.03, 0.05, 0.07, 0.1, 0.11, and 0.12. **Figure 4-15** and **Table 4-7** show the fitting results at select different frequencies. In Method B, the data selected were φ_{Ag}=0, 0.01, 0.03, 0.05, 0.07, 0.1, 0.11, 0.12 and 0.125. **Figure 4-16** and **Table 4-8** show the fitting results at select different frequencies by Method B.

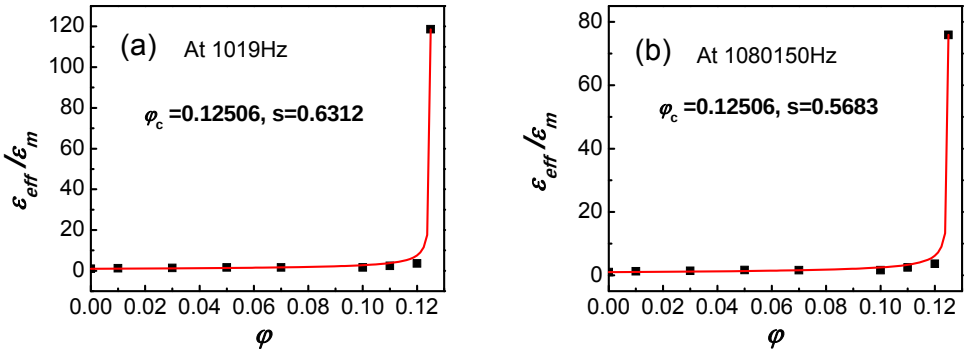

Figure 4-16. $\varepsilon_{eff}/\varepsilon_m$ vs. volume fraction φ and the fitting curve by Method B at different frequencies: (a) at 1019 Hz and (b) 1080150 Hz.

Table 4-8 φ_c and s vs. different frequencies of System IV by Method B

Frequency (Hz)	$\frac{\varepsilon_{eff}}{\varepsilon_m}=\left(\frac{\varphi_c-\varphi_{filler}}{\varphi_c}\right)^{-s}$ φ_{Ag}=0, 0.01, 0.03, 0.05, 0.07, 0.1, 0.11, 0.12 and 0.125				
	φ_c	φ_c error	s	s error	R^2
1019	0.12506	4.82E-4	0.6312	0.0779	0.9982
4793	0.12506	4.67E-4	0.6191	0.0750	0.9983
10393	0.12507	4.71E-4	0.6209	0.0755	0.9979
48864	0.12507	5.15E-4	0.6594	0.0845	0.9981
105952	0.12508	5.22E-4	0.6639	0.0856	0.9979
498149	0.12508	4.93E-4	0.6375	0.0794	0.9978
1080150	0.12506	3.97E-4	0.5683	0.0614	0.9981
2342110	0.12506	2.17E-4	0.4619	0.0304	0.9986
5078441	0.12546	2.92E-4	0.4094	0.0237	0.9930
8507712	0.12837	1.54E-3	0.4745	0.0458	0.9680

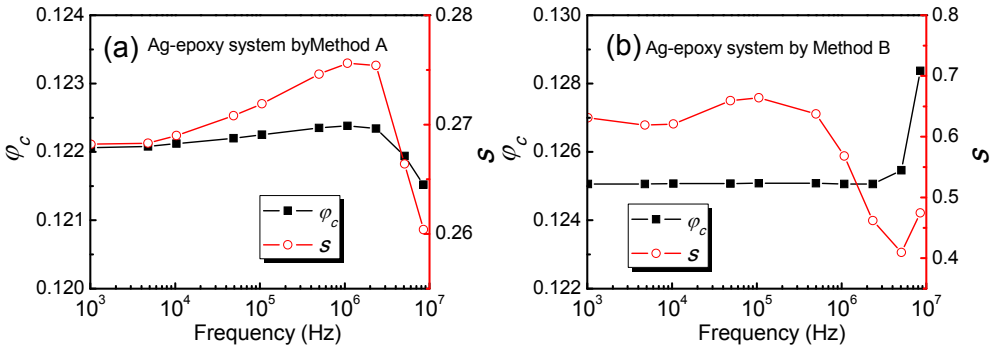

Figure 4-17. Dependence of percolation threshold (φ_c) and critical constant (s) on frequency by different fitting methods: (a) Method A and (b) Method B.

The φ_c and s at different frequencies by Method A and B are plotted in **Figure 4-17**. In Method A, the φ_c=0.12206 and s=0.2682 at 1 kHz were very close to the results from the article (φ_{Ag} ≈0.122 and s≈0.27). The φ_c and s both increased from 100 Hz to 1 MHz slightly then dramatically decreased after 1 MHz. This was due to the unstable dielectric constant at the φ_{Ag}=0.11. In Method B, the φ_c value was almost independent of frequency from 1 kHz to 5 MHz. For the critical value, the s almost kept as a constant value around 0.65 then decreased at high frequency due to the dielectric constant abruptly decreasing at the φ_{Ag}=0.125.

4.2.5. System-V: CF-PVDF Composites [5]

Dang *et. al* investigated untreated conductive short carbon fiber (CF)/PVDF composites with low concentrations of CF. The CF was the conducting filler with an average length and diameter, 100 and 8μm, respectively. **Figure 4-18** shows the dependence of the dielectric constant ε_{eff} and $\varepsilon_{eff}/\varepsilon_m$ on frequency at room temperature. According to Eq. (4-2), the percolation threshold φ_c=0.066 and critical value s=0.87 were obtained at 1 kHz, which was very low due to the large slenderness ratio and upright shape of the CF.

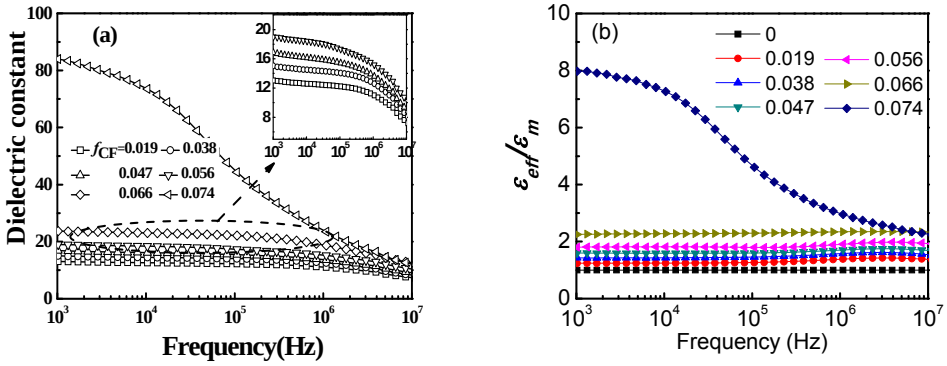

Figure 4-18. Dependence of (a) the dielectric constant, (b) $\varepsilon_{eff}/\varepsilon_m$ of the CF-PVDF composites on frequency at room temperature.

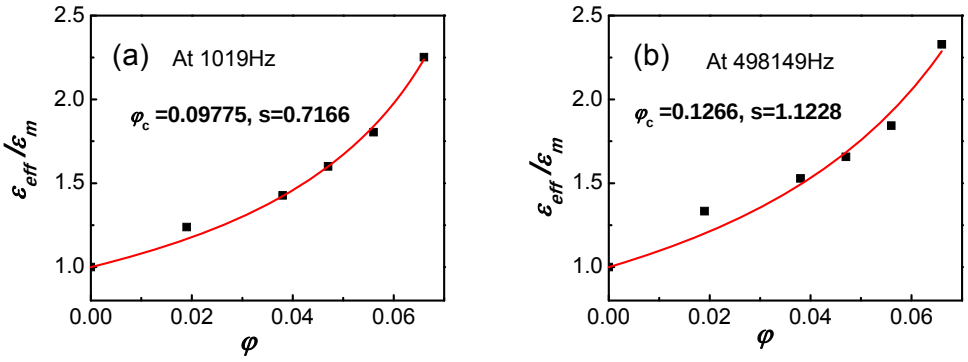

Figure 4-19. $\varepsilon_{eff}/\varepsilon_m$ vs. volume fraction φ and the fitting curve by Method A at different frequencies: (a) at 1019 Hz and (b) 498149 Hz.

The fitting equation used by authors was the same as Eq. (4-2). In Method A and B, the same fitting equation was used and the only difference was the selected fitting data. In Method A, the selected fitting data were the same as the article selected: φ_{CF}=0, 0.019, 0.038, 0.047, 0.056, and 0.066. **Figure 4-19** and **Table 4-9** show the fitting results at selected frequencies. In Method B, selected fitting data including the peak position φ_{CF}=0, 0.019, 0.038, 0.047, 0.056, 0.066 and 0.074. **Figure 4-20** and **Table 4-10** show the fitting results at selected frequencies.

Table 4-9 φ_c and s vs. different frequencies of System IV by Method A

Frequency (Hz)	$\frac{\varepsilon_{eff}}{\varepsilon_m}=\left(\frac{\varphi_c-\varphi_{filler}}{\varphi_c}\right)^{-s}$ φ_{CF}=0, 0.019, 0.038, 0.047, 0.056, and 0.066				
	φ_c	φ_c error	s	s error	R^2
1019	0.09775	9.28E-3	0.7166	0.1151	0.9918
4793	0.09629	8.79E-3	0.7061	0.1112	0.9916
10393	0.09563	8.52E-3	0.6972	0.1079	0.9916
48864	0.09582	0.01045	0.7029	0.1329	0.9875
105952	0.09638	0.01296	0.7115	0.1647	0.9815
498149	0.1266	0.04642	1.1228	0.5729	0.9657
1080150	0.2435	0.2898	2.6264	3.5658	0.9612

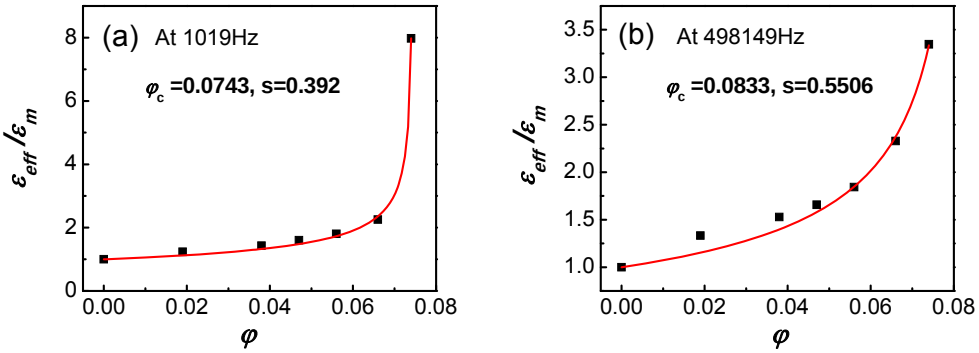

Figure 4-20. $\varepsilon_{eff}/\varepsilon_m$ vs. volume fraction φ and the fitting curve by Method B at different frequencies: (a) at 1019 Hz and (b) 498149 Hz.

Table 4-10 φ_c and s vs. different frequencies of System IV by Method B

Frequency (Hz)	$\frac{\varepsilon_{eff}}{\varepsilon_m}=\left(\frac{\varphi_c-\varphi_{filler}}{\varphi_c}\right)^{-s}$ φ_{CF}=0, 0.019, 0.038, 0.047, 0.056, 0.066 and 0.074				
	φ_c	φ_c error	s	s error	R^2
1019	0.07437	1.72E-4	0.3924	0.0202	0.9982
4793	0.07445	1.84E-4	0.3981	0.0202	0.9981
10393	0.07452	1.97E-4	0.3993	0.0201	0.9979
48864	0.07517	3.35E-4	0.4130	0.0222	0.9961
105952	0.07825	5.74E-4	0.4329	0.0258	0.9943
498149	0.08511	0.00349	0.5895	0.0697	0.9819
1080150	0.11059	0.01624	0.9658	0.2383	0.9760

In Method A, the φ_c=0.07437 and s=0.3924 at 1 kHz were far from the results

from the article (φ_c=0.066 and s≈0.87). In this case, the same equation Eq. (4-2) was used in both Method A and B. The φ_c and s were both kept as a constant before 100 kHz then increased at high frequency with increasing frequency.

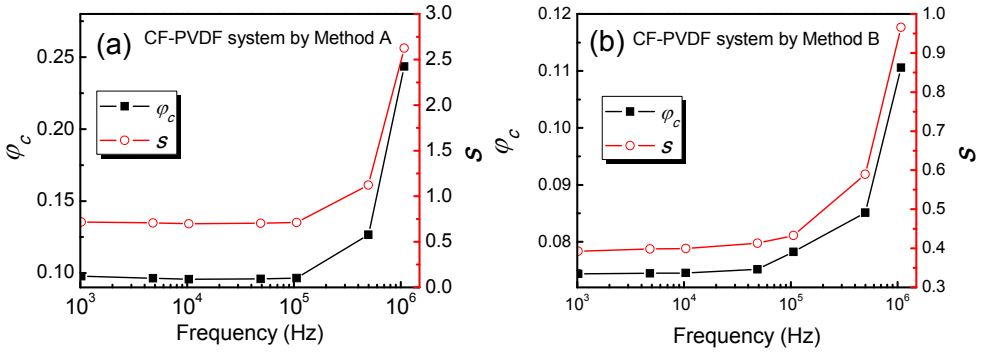

Figure 4-21. Dependence of percolation threshold (φ_c) and critical constant (s) on frequency by different fitting methods: (a) Method A and (b) Method B.

4.2.6. System-VI: TFP-MWNT-PVDF Composites [6]

In this section, trifluorophenyl(TFP)-functionalized MWNTs and PVDF nanocomposites were studied. MWNTs were modified with 3,4,5-trifluorobromobenzene (TFBB) to improve the dispersal. The strong interaction between the trifluorophenyl (TFP)-functionalized MWNTs and PVDF was obtained because of the number of fluoride groups existing on the surface of the TFP-MWNTs. The film was folded and hot pressed at 200 ^{o}C into a disk-shaped sample and further strengthened the preferred orientation of the TFP-MWNT in the matrix. **Figure 4-22** shows the dependence of the dielectric constant ε_{eff} and $\varepsilon_{eff}/\varepsilon_m$ on frequency at room temperature. The fitting values of dielectric constant were in agreement with percolation theory, with φ_c=0.08 and s=1.63 at 1 kHz.

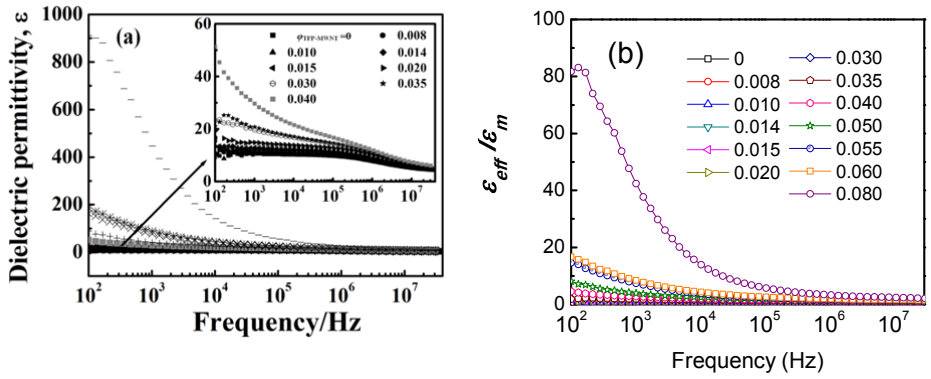

Figure 4-22. Dependence of (a) the dielectric constant, (b) $\varepsilon_{eff}/\varepsilon_m$ of the TFP-MWNT-PVDF composites on frequency at room temperature.

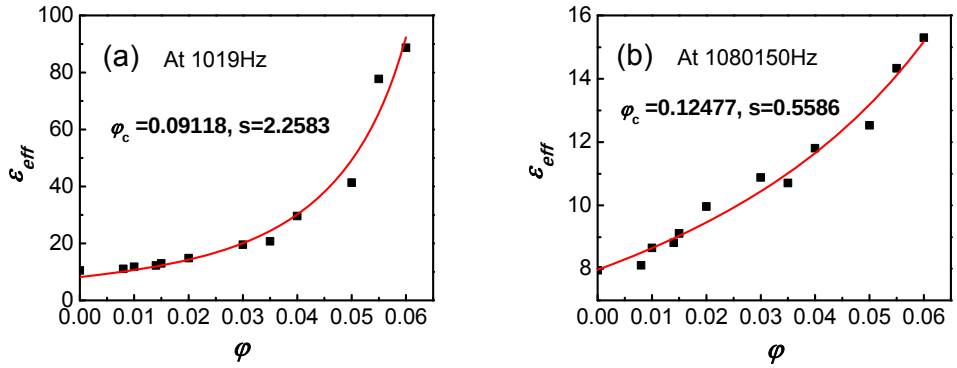

Figure 4-23. ε_{eff} vs. volume fraction φ and the fitting curve by Method A at different frequencies: (a) at 1019 Hz and (b) 1080150 Hz.

In Method A, the selected data were the same as the article selected: $\varphi_{TFP\text{-}MWNT}$ =0, 0.008, 0.01, 0.014, 0.015, 0.02, 0.03, 0.035, 0.04, 0.05, 0.055 and 0.06. **Figure 4-23** and **Table 4-11** show the fitting results at selected frequencies. As shown in Figure 4-24, it is difficult to determine the φ_c range for the fitting. Therefore, in Method B, two groups of data were used. One with $\varphi_{TFP\text{-}MWNT}$=0, 0.008, 0.01, 0.014, 0.015, 0.02, 0.03, 0.035, 0.04, 0.05, 0.055, 0.06 and 0.08, and another including more data with $\varphi_{TFP\text{-}MWNT}$=0, 0.008, 0.01, 0.014, 0.015, 0.02, 0.03, 0.035, 0.04, 0.05, 0.055, 0.06, 0.08, 0.09, 0.11 and 0.12. After the error was compared for φ and s, the fitting equation was used Eq. (4-2) and selected data included $\varphi_{TFP\text{-}MWNT}$ =0, 0.008, 0.01,

0.014, 0.015, 0.02, 0.03, 0.035, 0.04, 0.05, 0.055, 0.06 and 0.08. **Figure 4-25** and **Table 4-12** show the fitting results in at selected frequencies.

Table 4-11 φ_c and s vs. different frequencies of System VI by Method A

Frequency (Hz)	$\varepsilon_{eff} = k(\varphi_c - \varphi)^{-s}$ $\varphi_{\text{TFP-MWNT}}$=0, 0.008, 0.01, 0.014, 0.015, 0.02, 0.03, 0.035, 0.04, 0.05, 0.055 and 0.06						
	φ_c	φ_c error	s	s error	k	k error	R^2
100	0.23053	0.54598	12.132	30.012	9.42E-8	1.78E-6	0.9654
407	0.10395	0.0427	3.2762	2.2751	4.31E-3	0.0183	0.9644
1019	0.09118	0.02443	2.2583	1.1784	0.0366	0.0910	0.9634
4793	0.08153	0.0124	1.3418	0.4606	0.0317	0.0338	0.9701
10393	0.07940	9.74E-3	1.0820	0.3093	0.6289	0.4575	0.9700
48864	0.08050	9.03E-3	0.8135	0.2017	1.2849	0.5881	0.9811
105952	0.08409	0.01110	0.7646	0.2050	1.4821	0.6529	0.9813
498149	0.10396	0.02695	0.8426	0.3477	1.3138	0.7861	0.9787
1080150	0.12477	0.05039	0.9822	0.5586	1.0306	0.8234	0.9765
2342110	0.13941	0.07221	1.0207	0.7051	0.9393	0.8398	0.9743
11011690	0.13747	0.07695	0.8319	0.6247	1.0237	0.8199	0.9684
30904320	0.07575	0.01627	0.2598	0.1332	2.4621	0.7705	0.8937

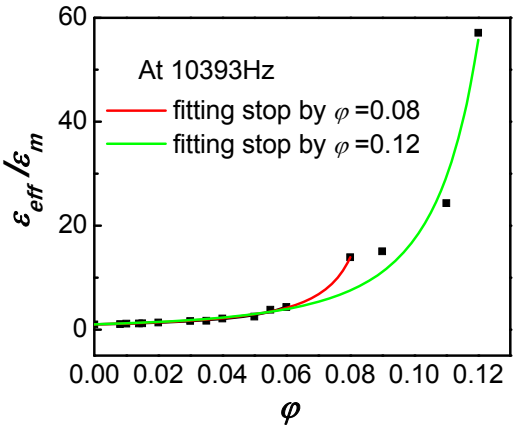

Figure 4-24. $\varepsilon_{eff}/\varepsilon_m$ vs. volume fraction φ and the fitting curve by Method B for different data selected.

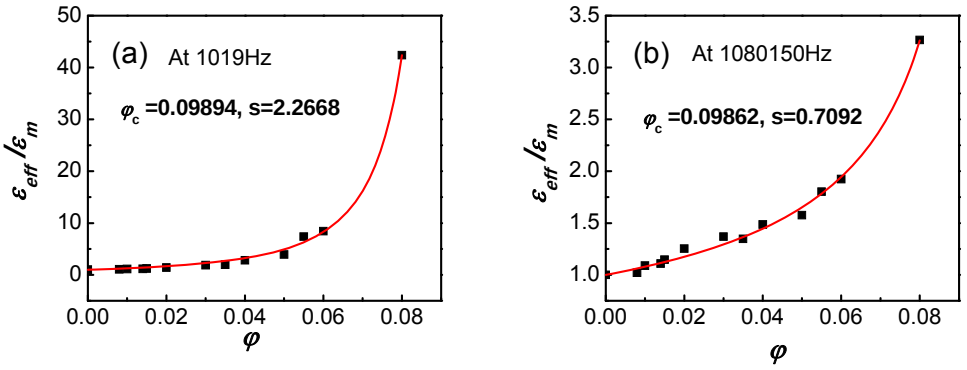

Figure 4-25. $\varepsilon_{eff}/\varepsilon_m$ vs. volume fraction φ and the fitting curve by Method B at different frequencies: (a) at 1019 Hz and (b) 1080150 Hz.

Table 4-12 φ_c and s vs. different frequencies of System VI by Method B

Frequency (Hz)	$\frac{\varepsilon_{eff}}{\varepsilon_m}=\left(\frac{\varphi_c-\varphi_{filler}}{\varphi_c}\right)^{-s}$ $\varphi_{TFP\text{-}MWNT}$=0, 0.008, 0.01, 0.014, 0.015, 0.02, 0.03, 0.035, 0.04, 0.05, 0.055, 0.06 and 0.08				
	φ_c	φ_c error	s	s error	R^2
100	0.12637	7.53E-3	4.3920	0.5196	0.9982
470	0.10205	3.01E-3	2.6752	0.1771	0.9980
1019	0.09894	2.66E-3	2.2668	0.1477	0.9976
4793	0.09597	2.17E-3	1.6736	0.0999	0.9970
10393	0.09551	1.98E-3	1.4494	0.0805	0.9969
48864	0.09596	1.71E-3	1.1156	0.0517	0.9971
105952	0.09667	1.71E-3	0.9918	0.0445	0.9971
498149	0.09839	2.17E-3	0.7972	0.0417	0.9956
1080150	0.09862	2.46E-3	0.7092	0.0413	0.9944
2342110	0.09753	2.48E-3	0.6129	0.0372	0.9936
11011690	0.10012	3.52E-3	0.5580	0.0433	0.9900
30904320	0.08642	2.67E-3	0.2800	0.0361	0.9613

In **Table 4-11**, the parameters had a large error at very low and very high frequencies. The φ_c=0.09121 and s=2.26 at 1 kHz were far from the results from the article (φ_c=0.08 and s=1.63). As shown in **Figure 4-26**, the φ_c firstly decreased at low frequency then increased at high frequency in both Method A and B. The difference is the φ_c had the similar values at 100 Hz and 1 MHz. The critical constant s

continuously decreased from 4.392 at 100 Hz to smaller than 1 at high frequency. The R^2 and error of parameter of the fitting results indicated Method B was in good agreement with the data.

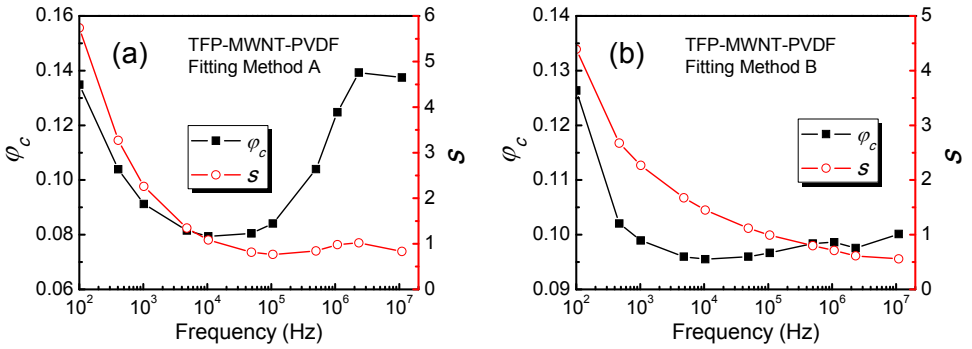

Figure 4-26. Dependence of percolation threshold (φ_c) and critical constant (s) on frequency by different fitting method: (a) Method A and (b) Method B.

4.3. Summary of Six System and Further Study

Six systems of conductor-polymer composites were studied based on percolation theory. These included: System I (MWNT-PVDF), System II (CB-BT-VMQ), System III (PANI-PVDF), System IV (Ag-PI), System V (CF-PVDF) and System VI (TFP-MWNT-PVDF). In general, it was found that the φ_c and s obtained at different frequencies were different. To make this clear about how the φ_c and s changed with frequency, the normalized values of the φ_c and s: φ_c/φ_0 and s/s_0 are shown in **Figure 4-27** and **Figure 4-28**, where φ_0 and s_0 was the first value of φ_c and s in each system, such as φ_c and s at 100 Hz in system I or at 1 kHz in System IV. As discussed before, the percolation threshold and critical constant obtained by fitting changed with selected frequency. The percolation threshold and critical constant also had a relationship with the shape of filler. In these six systems, the filler of System II (diameter of CB: 50 nm), System III (diameter of PANI: 0.1μm) and System IV

(diameter of Ag: 0.5μm) are sphere. The corresponding φ_c in **Figure 4-27** is weekly dependent on frequency. The filler of System V (CF-PVDF) had a high aspect ratio ≈12 (W:8 μm and L:100 μm) which may have resulted in the φ_c and s both increasing for high frequency. The filler of System I (MWNT-PVDF) and System VI (TFP-MWNT-PVDF) were both multiwall carbon-nanotubes. The size in system VI was 10-30 nm in width and 5-15 μm in length. It was found that the φ_c of both system decreased with as increasing frequency then increased for high frequency, even higher than 1.

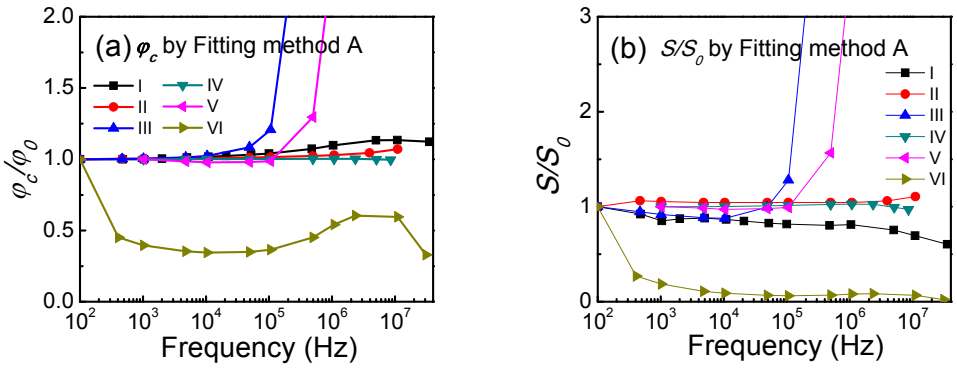

Figure 4-27. Dependence of (a) percolation threshold (φ_c) and (b) critical constant (s) on frequency of six systems by Method A.

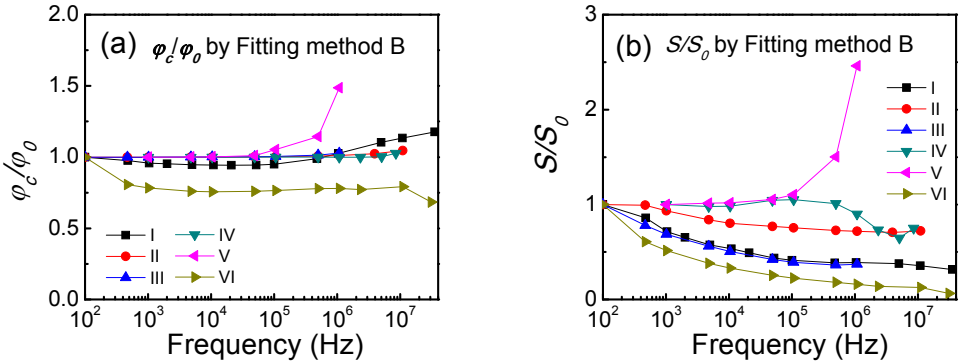

Figure 4-28. Dependence of (a) percolation threshold (φ_c) and (b) critical constant (s) on frequency of six systems by Method B.

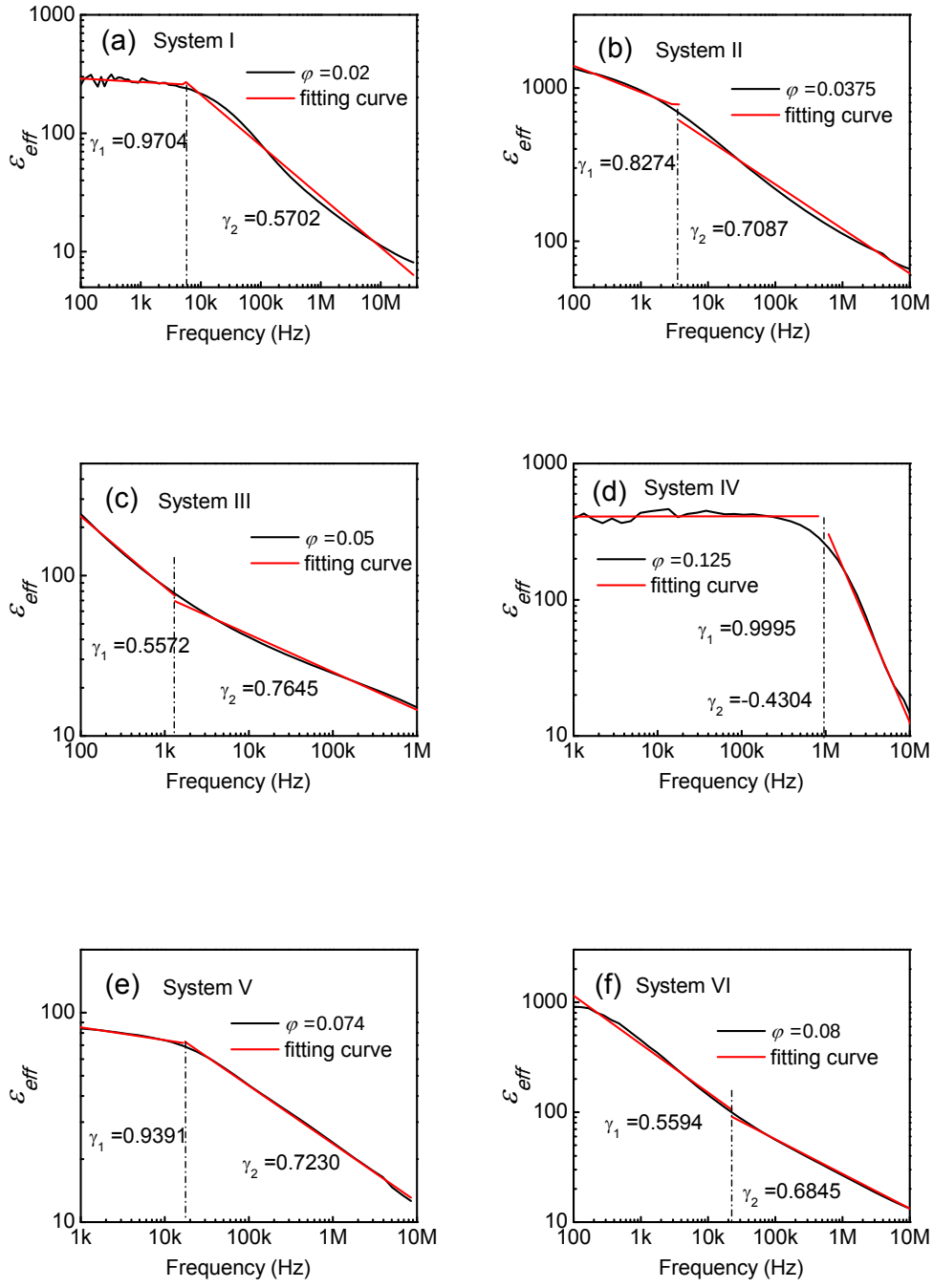

Figure 4-29. Dielectric constant vs. frequency of composites and fitting curve for six systems.

The γ from articles and calculated from this chapter are shown in **Table 4-13**.

Some γ from articles were obtained from conductivity. In these six different systems,

the γ of the composites were close to the percolation threshold of 0.6-0.8 which is close to the normal value from the percolation theory discussed in Section 1.4.1. Because the dielectric constant was very "flat" in low frequency, the curve was fitted in two separated parts. The fitting results for six systems are shown in **Figure 4-29**.

Table 4-13 The φ and γ from articles and from this chapter

		I	II	III	IV	V	VI
From articles	φ	0.016	0.035	-	0.125	0.074	-
	γ	0.805	1.1469	-	1.22	0.82	-
From this Chapter	φ	0.02	0.0375	0.05	0.125	0.074	0.08
	γ_1	0.9704	0.8274	0.5572	0.9995	0.9391	0.5594
	γ_2	0.5702	0.7087	0.7645	-0.4304	0.7230	0.6845

4.4. Simulation

In order to find the reason why the φ_c & s are dependent on the frequency selection, a new conductor-polymer composite based on Debye Equation and percolation theory was introduced. The Debye Equation is expressed as:

$$\varepsilon_{eff} = \varepsilon_\infty + \frac{\varepsilon_s - \varepsilon_\infty}{1+\omega^2\tau_0^{\,2}} = \varepsilon_\infty + \frac{\varepsilon_s - \varepsilon_\infty}{1+4\pi^2 f^2\tau_0^{\,2}} \tag{4-3}$$

where ε_s is the static dielectric constant, ε_∞ is the dielectric constant at high frequency limit and τ_0 is the characteristic relaxation time. For the case of conductor-polymer composite, ε_s is considered as the ε_{eff} obtained from percolation theory. Wagner considered a sphere-like conductor with conductivity σ in a non-conducting matrix of dielectric constant ε_m. From the Wagner's formula [7], there is:

$$\varepsilon_\infty = \frac{2\varepsilon_m(1-\varphi)}{2+\varphi} \tag{4-4}$$

$$\tau = \frac{\varepsilon_0 \varepsilon_m (2+\varphi)}{\sigma(1-\varphi)} \tag{4-5}$$

Then Eq. (4-3) can be written as:

$$\varepsilon_{eff} = \frac{2\varepsilon_m(1-\varphi)}{2+\varphi} + \frac{\varepsilon_m\left(\frac{\varphi_c-\varphi}{\varphi_c}\right)^{-s} - \frac{2\varepsilon_m(1-\varphi)}{2+\varphi}}{1+4\pi^2 f^2\left(\frac{\varepsilon_0\varepsilon_m(2+\varphi)}{\sigma(1-\varphi)}\right)^2} \tag{4-6}$$

The $\varepsilon_{eff}/\varepsilon_m$ vs. volume fraction is φ always used as the fitting function, then Eq.(4-6) can be as:

$$\frac{\varepsilon_{eff}}{\varepsilon_m} = \frac{2(1-\varphi)}{2+\varphi} + \frac{\left(\frac{\varphi_c-\varphi}{\varphi_c}\right)^{-s} - \frac{2(1-\varphi)}{2+\varphi}}{1+\left(\frac{\varepsilon_0\varepsilon_m}{\sigma}\frac{(2+\varphi)}{(1-\varphi)}\right)^2 4\pi^2 f^2} \tag{4-7}$$

Therefore, let φ_c=10 vol.%, s= 0.7 and $2\pi\varepsilon_0\varepsilon_m/\sigma$ is chosen as 10^{-5}, the curves under this condition are plotted in **Figure 4-30**.

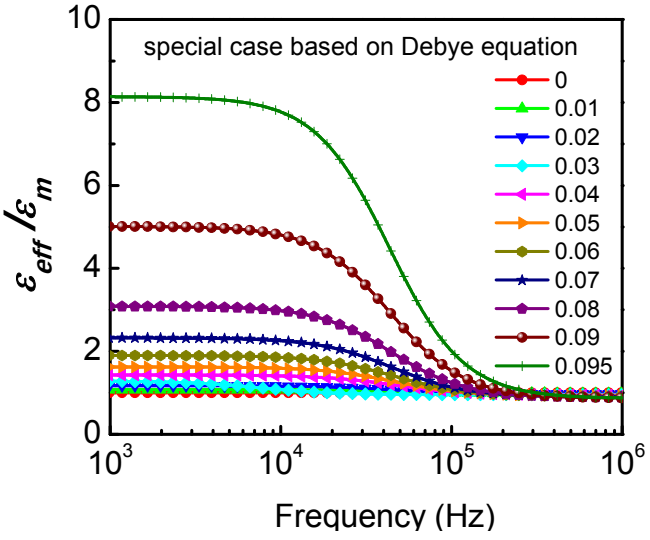

Figure 4-30. Dependence of $\varepsilon_{eff}/\varepsilon_m$ of the special case based on Debye equation.

The dielectric constant of this artificial conductor-polymer composite is shown in **Figure 4-30**. The selected volume fraction is from 0 vol.% to 9.5% and the step is 1

vol.%. The dielectric constant of the composite with all volume fractions are independent of frequency at low frequency then decrease dramatically with increasing frequency. At very high frequencies, all of the curve are close to 0 vol.% which is similar to the reality.

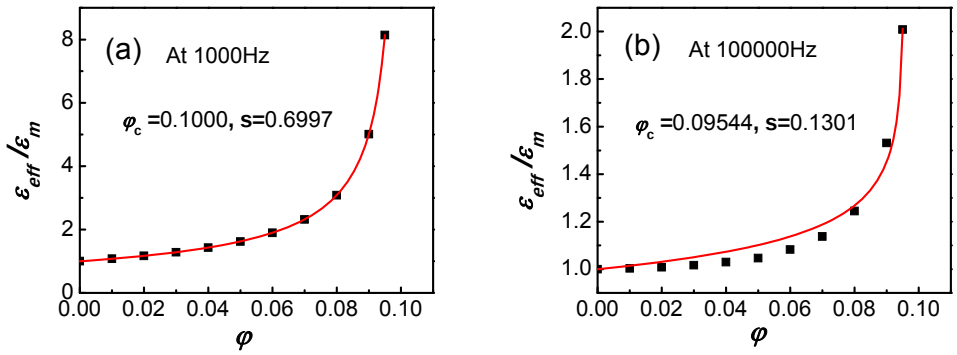

Figure 4-31. $\varepsilon_{eff}/\varepsilon_m$ vs. volume fraction φ and the fitting curve at different frequencies: (a) at 1000Hz and (b) at 100000Hz.

The $\varepsilon_{eff}/\varepsilon_m$ vs. volume fraction φ and the fitting results are shown in **Figure 4-31** at select different frequencies. The corresponding data are listed in **Table 4-14** and plotted in **Figure 4-32**. According to the Eq. (4-9), at low frequency, the fitting can have a very good result, such as φ is 0.1 and s is very close to 0.7. When the frequency is lower than relaxation range (ω_0), the φ_c and s can be considered as independence of frequency. In the range of relaxation, the φ_c decreases from 0.0978 to 0.09544 and the change is smaller than 5%. It means the percolation threshold almost independent on frequency. For critical constant, the value is 0.1301 at 100 kHz, which is smaller than 1/5 of 0.7 at very low frequency. For very high frequency, the dielectric constant of composites is very close to the dielectric constant of the pure matrix, which is not in agreement with percolation theory.

Table 4-14 φ_c and s vs. different frequencies of the special case based on Debye equation

Frequency (Hz)	$\frac{\varepsilon_{eff}}{\varepsilon_m} = \left(\frac{\varphi_c - \varphi_{filler}}{\varphi_c}\right)^{-s}$				
	φ_c	φ_c error	s	s error	R^2
1000	0.10000	2.74E-7	0.6997	1.03E-5	1.0000
2600	0.09998	1.85E-6	0.6983	6.98E-5	1.0000
5012	0.09994	6.80E-6	0.6935	2.56E-4	1.0000
10000	0.09978	2.61E-5	0.6750	9.77E-4	1.0000
16032	0.09947	6.25E-5	0.6392	2.31E-3	1.0000
20184	0.09920	9.28E-5	0.6084	3.40E-3	0.9999
30200	0.09848	1.70E-4	0.5238	6.07E-3	0.9996
40272	0.09775	2.37E-4	0.4377	8.26E-3	0.9987
50119	0.09714	2.85E-4	0.3619	9.68E-3	0.9974
60256	0.09662	3.17E-4	0.2955	1.05E-2	0.9953
75858	0.09601	3.36E-4	0.2144	1.09E-2	0.9905
100000	0.09544	3.31E-4	0.1301	1.05E-2	0.9785

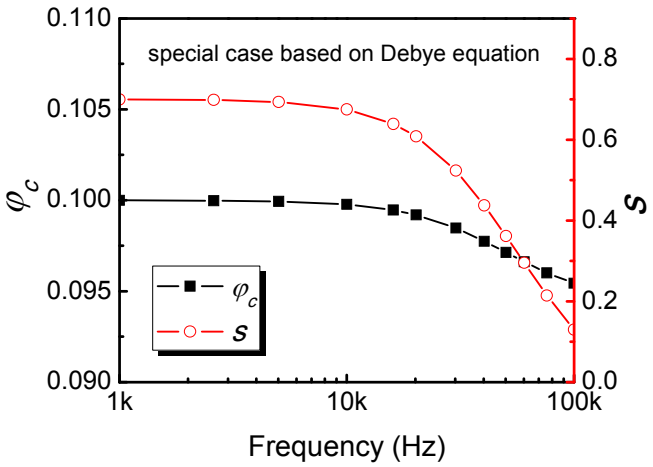

Figure 4-32. Dependence of percolation threshold (φ_c) and critical constant (s) with frequency of the special case based on Debye equation.

The Debye Equation did not fit the experimental results for most of the dielectric materials that have a set of relaxation time. Therefore, there are many empirical relaxation equations that have been introduced to describe the relaxation phenomena. For example, Cole-Cole equation is shown as [8]:

$$\varepsilon^*_r(\omega) = \varepsilon_{r\infty} + \frac{\varepsilon_{rs} - \varepsilon_{r\infty}}{1 + (j\omega\tau_0)^{1-\alpha}} \tag{4-8}$$

where α varies $0<\alpha<1$, and the maximum ε''_r occurs at $\omega\tau_0=1$. Some experimental results agree well with Cole-Cole equation with $\alpha > 0$. The real part of the dielectric constant can be shown as:

$$\varepsilon_{eff}(\omega) = \varepsilon_\infty + (\varepsilon_s - \varepsilon_\infty)\frac{1 + (\omega\tau_0)^{1-\alpha}\sin\frac{1}{2}\alpha\pi}{1 + 2(\omega\tau_0)^{1-\alpha}\sin\frac{1}{2}\alpha\pi + (\omega\tau_0)^{2(1-\alpha)}} \tag{4-9}$$

After combined with Eq.(4-4), (4-5) and (4-9),

$$\frac{\varepsilon_{eff}}{\varepsilon_m} = \frac{2(1-\varphi)}{2+\varphi} + \frac{\left[\left(\frac{\varphi_c-\varphi}{\varphi_c}\right)^{-s} - \frac{2(1-\varphi)}{2+\varphi}\right]\left\{1 + \left[2\pi f\frac{\varepsilon_0\varepsilon_m(2+\varphi)}{\sigma(1-\varphi)}\right]^{1-\alpha}\sin\frac{1}{2}\alpha\pi\right\}}{1 + 2\left[2\pi f\frac{\varepsilon_0\varepsilon_m(2+\varphi)}{\sigma(1-\varphi)}\right]^{1-\alpha}\sin\frac{1}{2}\alpha\pi + \left[2\pi f\frac{\varepsilon_0\varepsilon_m(2+\varphi)}{\sigma(1-\varphi)}\right]^{2(1-\alpha)}} \tag{4-10}$$

The α is around 0.5 for some PVDF-based polymer [9, 10]. For a special case, if α=0.5, φ_c=10vol.% and s=0.7, $2\pi\varepsilon_0\varepsilon_m/\sigma$ is chose as 10^{-5}, the dielectric constant of this special conductor-polymer composite based on Cole-Cole equation is shown in **Figure 4-33**. The selected volume fraction is from 0 vol.% to 9.5 vol.% and the step is 1 vol.%. The dielectric constant of the composite with all volume fractions decreases with frequency continuously according to the Cole-Cole Equation.

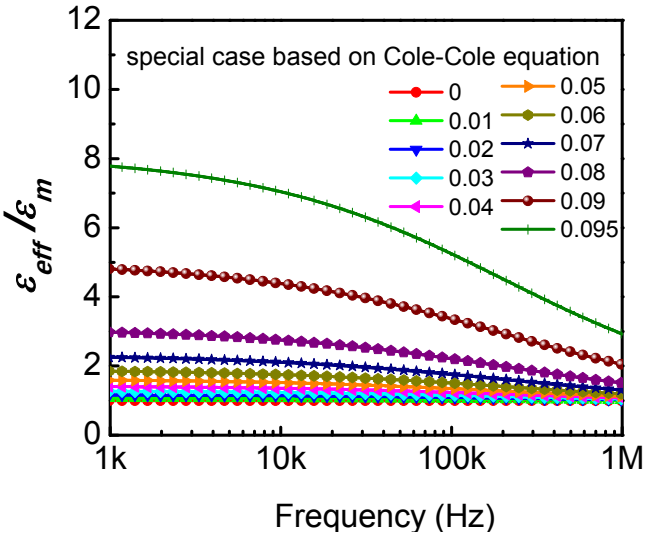

Figure 4-33. Dependence of $\varepsilon_{eff}/\varepsilon_m$ of the special case based on the Cole-Cole equation.

The corresponding data are listed in **Table 4-15** and plotted in **Figure 4-34**. According to the Eq. (4-10), at low frequency, the fitting result is not as good as Debye Equation, such as s is 0.6742 which is not very close to 0.7. Because the relaxation frequency covers a wide range for the Cole-Cole equation, the φ_c and s decrease gradually with frequency.

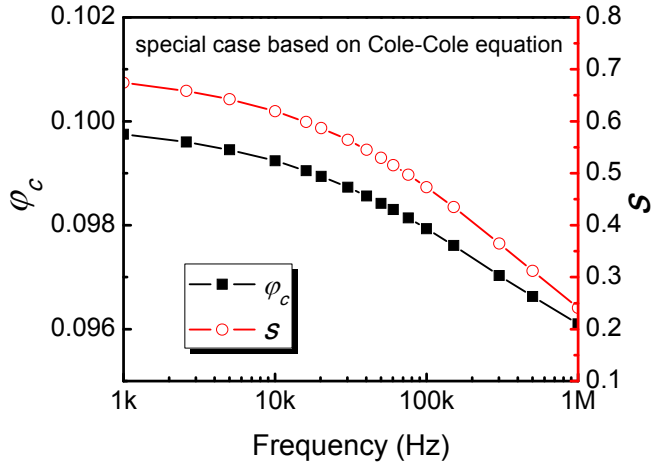

Figure 4-34. Dependence of percolation threshold (φ_c) and critical constant (s) with frequency of the special case based on Cole-Cole equation.

Table 4-15 φ_c and s vs. different frequencies of the special case based on Cole-Cole equation

Frequency (Hz)	$\frac{\varepsilon_{eff}}{\varepsilon_m} = \left(\frac{\varphi_c - \varphi_{filler}}{\varphi_c}\right)^{-s}$				
	φ_c	φ_c error	s	s error	R^2
1000	0.09975	3.59E-5	0.6742	1.34E-3	1.0000
2600	0.09960	5.70E-5	0.6584	2.13E-3	1.0000
5012	0.09945	7.79E-5	0.6424	2.90E-3	1.0000
10000	0.09924	1.07E-4	0.6193	3.97E-3	0.9999
16032	0.09905	1.31E-4	0.5987	4.87E-3	0.9998
20184	0.09894	1.45E-4	0.5870	5.36E-3	0.9997
30200	0.09873	1.71E-4	0.5639	6.29E-3	0.9996
40272	0.09856	1.91E-4	0.5451	6.99E-3	0.9995
50119	0.09842	2.07E-4	0.5295	7.55E-3	0.9993
60256	0.09830	2.20E-4	0.5155	8.03E-3	0.9992
75858	0.09814	2.37E-4	0.4969	8.63E-3	0.9990
100000	0.09793	2.58E-4	0.4731	9.34E-3	0.9987
151356	0.09761	2.89E-4	0.4350	1.04E-2	0.9980
301995	0.09703	3.31E-4	0.3646	1.17E-2	0.9962
501187	0.09663	3.55E-4	0.3121	1.24E-3	0.9942
1000000	0.09610	3.68E-4	0.2409	1.28E-2	0.9898

According to further studies based on the Debye Equation and Cole-Cole Equation, the change of φ_c and s is strongly dependent on frequency selection.

4.5. Conclusions

From the six systems and further study based on the Debye Equation and Cole-Cole Equation,

1) The percolation threshold (φ_c) and critical constant (s) are dependent on the selection of frequency.
2) Compared with the Method A and B, selected different data have strong effect on the φ_c and s. The maximum value of dielectric constant obtained in the composites very close to φ_c should be included in fitting data.

3) The percolation threshold and critical constant also have the relationship with the shape of the filler. The change in φ_c and s for the composite with sphere-like fillers are less than that with a fiber or tube. High aspect ratio may cause much difference in φ_c and s with respect to frequency.

4) According to further study based on the Debye Equation and Cole-Cole Equation, the change in φ_c and s with frequency is very similar to the change of dielectric constant of composite ($\varphi \rightarrow \varphi_c$) with frequency.

References of Chapter 4

1. L. Wang and Z. M. Dang, *Appl. Phys. Lett.* **87**, 042903 (2005).

2. Z. M. Dang, B. Xia, S. H. Yao, M. J. Jiang, H. T. Song, L. Q. Zhang, and D. Xie, *Appl. Phys. Lett*. **94**, 042902 (2009).

3. J. K.Yuan, Z. M. Dang and J. B Bai, *Phys. Stat. Sol.* **2**, 233 (2008).

4. Z. M. Dang, B. Peng, D.Xie, S. H. Yao, M. J. Jiang, and J. B. Bai, *Appl. Phys. Lett.* **92**, 112910 (2008).

5. Z. M. Dang J. P.Wu, H. P. Xu, S. H.Yao, M. J. Jiang and J. B. Bai, *Appl. Phys. Lett.* **91**, 072912 (2007).

6. Z. M. Dang, L. Wang, Y. Yin, Q. Zhang and Q. Q. Lei, *Adv. Mater.* **19**, 852 (2007).

7. B. K. P. Scaife, Principles of Dielectrics, Clarendon Press, Oxford, 1989.

8. K. C. Kao, Dielectric Phenomena in Solids. Elsevier Academic Press: San Diego, CA, 2004.

9. X. B. Shan, Ph. D. Dissertation, Auburn University, 2008.

10. H. L. W. Chan, Q. Q. Zhang, W. Y, Ng and C. L. Choy, *IEEE Trans. Dielectr. Electr. Insul.* **7**, 204 (2000).

CHAPTER 5

Complex Dielectric Constant of Composite Introduced Dielectric loss

5.1. Introduction

In current research, many theoretical models/methods have been introduced to simulate the ε_{eff} of a composite using ε_m, ε_f, φ and may had one parameter related to the shape/size of the filler [1-6]. However, more and more experimental results are reported and cannot be explained using these models. The interfacial layer was introduced as a new phase to explain the experimentally observed results. The results may be well fitted/explained, but the interfacial layer, which had the same composition as the polymer matrix, had a very high dielectric constant (10^2 to 10^3 times higher than the ε_m). Based on the physics of dielectrics, this high dielectric constant for the interfacial layer is unreasonable. One of important issue was the dielectric loss should be taken into account. In this Chapter, the loss of both constituents is included in the simulation of the ε_{eff} for a composite in three different models. As discussed in Section 1.5.1, the series model is for 2-2 composite, Maxwell model is for 0-3 composite and Lichtenecker's logarithmic mixing model is more like for 0-0 composite.

5.2. The Series Model Introduced Dielectric Loss

For a two-layer composite (2-2 connection), as **Figure 1-12** and **Figure 1-13** in Section 1.5.1 shown, the relationship of capacity with series connection can be given by

$$\frac{1}{C_s^*} = \frac{1}{C_1^*} + \frac{1}{C_2^*} \quad C_s^* = \frac{\varepsilon_0 \varepsilon_s^* A}{d_1 + d_2} \tag{5-1}$$

$$\varepsilon_s^* = \varepsilon_s' - i\varepsilon_s'' \qquad \frac{\varepsilon_s''}{\varepsilon_s'} = \tan\delta_s \tag{5-2}$$

$$d = d_1 + d_2 \qquad \varphi = \frac{d_1}{d} \quad 1 - \varphi = \frac{d_2}{d} \tag{5-3}$$

From these equations, the real and imaginary part of dielectric constant of the composite can be obtained as:

$$\varepsilon_s' = \varepsilon_1'\varepsilon_2' \left(\frac{\varphi[\varepsilon_2'(1+\tan^2\delta_2) - \varepsilon_1'(1+\tan^2\delta_1)] + \varepsilon_1'(1+\tan^2\delta_1)}{[\varepsilon_1' - \varphi(\varepsilon_1' - \varepsilon_2')]^2 + [\varepsilon_1'\tan\delta_1 - \varphi(\varepsilon_1'\tan\delta_1 - \varepsilon_2'\tan\delta_2)]^2} \right) \tag{5-4a}$$

$$\varepsilon_s'' = \varepsilon_1'\varepsilon_2' \left(\frac{\varphi[\varepsilon_2'\tan\delta_1(1+\tan^2\delta_2) - \varepsilon_1'\tan\delta_2(1+\tan^2\delta_1)] + \varepsilon_1'\tan\delta_2(1+\tan^2\delta_1)}{[\varepsilon_1' - \varphi(\varepsilon_1' - \varepsilon_2')]^2 + [\varepsilon_1'\tan\delta_1 - \varphi(\varepsilon_1'\tan\delta_1 - \varepsilon_2'\tan\delta_2)]^2} \right) \tag{5-4b}$$

$$\tan\delta_s = \frac{\varepsilon_s''}{\varepsilon_s'} = \frac{\varphi[\varepsilon_2'\tan\delta_1(1+\tan^2\delta_2) - \varepsilon_1'\tan\delta_2(1+\tan^2\delta_1)] + \varepsilon_1'\tan\delta_2(1+\tan^2\delta_1)}{\varphi[\varepsilon_2'(1+\tan^2\delta_2) - \varepsilon_1'(1+\tan^2\delta_1)] + \varepsilon_1'(1+\tan^2\delta_1)} \tag{5-4c}$$

In these equations, the three dielectric parameters are expressed as the function of $F(\varepsilon'_1, \varepsilon'_2, tan\delta_1, tan\delta_2, \varphi)$.

5.2.1 The Relationship Between $tan\delta_1$, $tan\delta_2$ and $tan\delta_s$

Because the dielectric was taken into account, it was necessary to check how the dielectric loss effected on the dielectric properties of the composite.

$$\frac{\tan\delta_s}{\tan\delta_1} = \frac{\varepsilon_s''}{\varepsilon_s'} = \frac{\varphi[\varepsilon_2'(1+\tan^2\delta_2) - \varepsilon_1'\frac{\tan\delta_2}{\tan\delta_1}(1+\tan^2\delta_1)] + \varepsilon_1'\frac{\tan\delta_2}{\tan\delta_1}(1+\tan^2\delta_1)}{\varphi[\varepsilon_2'(1+\tan^2\delta_2) - \varepsilon_1'(1+\tan^2\delta_1)] + \varepsilon_1'(1+\tan^2\delta_1)} \tag{5-5a}$$

$$= 1 + \frac{\varepsilon_1'(1 - \frac{\tan\delta_2}{\tan\delta_1})(1+\tan\delta_1^{\,2})(\varphi - 1)}{\varphi\varepsilon_2'(1+\tan\delta_2^{\,2}) + (1-\varphi)\varepsilon_1'(1+\tan\delta_1^{\,2})}$$

$$\frac{\tan\delta_s}{\tan\delta_2} = 1 + \frac{\varphi\varepsilon_2'(\frac{\tan\delta_1}{\tan\delta_2} - 1)(1+\tan^2\delta_2)}{\varphi\varepsilon_2'(1+\tan\delta_2^{\,2}) + (1-\varphi)\varepsilon_1'(1+\tan\delta_1^{\,2})} \tag{5-5b}$$

if $tan\delta_1 > tan\delta_2$, $0<\varphi<1$, then $\frac{\tan\delta_s}{\tan\delta_1} < 1$, $\frac{\tan\delta_s}{\tan\delta_2} > 1$

$$\tan\delta_2 < \tan\delta_s < \tan\delta_1$$

Vice versa for $tan\delta_1 < tan\delta_2$, $\tan\delta_1 < \tan\delta_s < \tan\delta_2$

So $Min(\tan\delta_1, \tan\delta_2) < \tan\delta_s < Max(\tan\delta_1, \tan\delta_2)$ (5-6)

From this model, the dielectric loss of the composite must be in between the value of dielectric loss of two materials. Especially, when $tan\delta_1 = tan\delta_2$, there is $tan\delta_s = tan\delta_1 = tan\delta_2$, and $\varepsilon'_s = \varepsilon'_1 \cdot \varepsilon'_2 / [(1-\varphi)\cdot\varepsilon'_1 + \varphi\cdot\varepsilon'_2]$, which is consistent with classic series model. That is, the dielectric loss does not have any influence on the ε'_s. This is because that when $tan\delta_1 = tan\delta_2$, there is no charge accumulation on the interface.

5.2.2 The Relationship Between ε'_1, ε'_2 and ε'_s

Case 1: When $\varepsilon'_1 = \varepsilon'_2$ & $tan\delta_1 = 0$ or $tan\delta_2 = 0$

As we known, if the loss is not considered, ε'_s will be the same value whatever the φ when $\varepsilon'_1 = \varepsilon'_2$. However, if the loss is considered, the effective dielectric constant of composite ε'_s and $tan\delta_s$ can be rewritten as follow:

$$\varepsilon'_s = \varepsilon' \left(\frac{(1+\tan^2\delta_1) - \varphi(\tan^2\delta_1 - \tan^2\delta_2)}{1+[\tan\delta_1 - \varphi(\tan\delta_1 - \tan\delta_2)]^2} \right) \quad (5\text{-}7)$$

$$\tan\delta_s = \frac{\tan\delta_2(1+\tan^2\delta_1) - \varphi[\tan\delta_2(1+\tan^2\delta_1) - \tan\delta_1(1+\tan^2\delta_2)]}{(1+\tan^2\delta_1) - \varphi[\tan^2\delta_2 - \tan^2\delta_1]} \quad (5\text{-}8)$$

ε'_s and $tan\delta_s$ are the function of the dielectric loss of both materials, and changes with the various of φ.

When one of materials does not have the dielectric loss, the dielectric constant of composites can be larger than the dielectric constant of both materials under this

condition. **Figure 5-1(a)** shows the dielectric constant and loss of composites with different $tan\delta_1$ and $tan\delta_2$ when $\varepsilon'_1 = \varepsilon'_2$. Due to the symmetry, it assumes $tan\delta_1$=0 and $tan\delta_2$ various. It is easy to find that there is a peak for certain vol.% concentration due to the dielectric constant is the same value for φ =0 and φ=100%. That means: if the matrix is an ideal dielectric material without the loss and the filler has the same value of dielectric constant as matrix but has very high dielectric loss, the dielectric constant of composites will be strongly affected by the value of dielectric loss of the filler. The dielectric constant of composites will increase firstly then decrease. This trend is very similar with the phenomenon of conducting filler-polymer composites which can be explained by percolation theory. **Figure 5-1 (b)** shows the information of the peak of $\varepsilon'_s/\varepsilon'_1$ in details extracted from **Figure 5-1 (a)**. When the dielectric loss of filler approaches to very high values, the dielectric constant of composites will quickly reach to the maximum value and the value will very large.

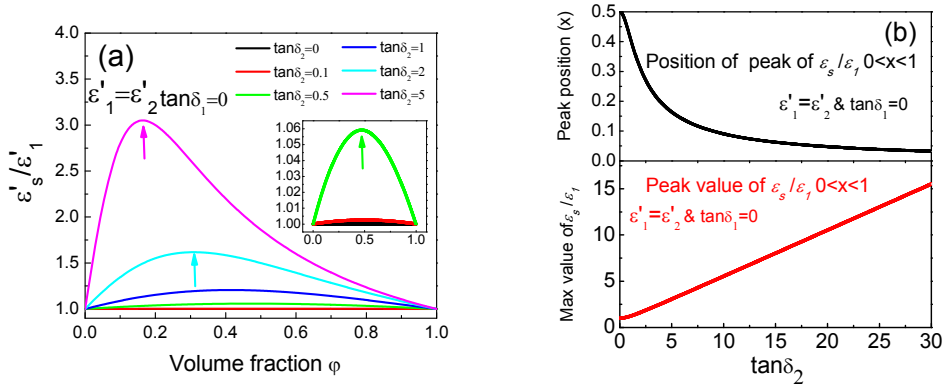

Figure 5-1. (a) The ratio of dielectric constant of composites and constituent-1 various with φ for different dielectric loss. (b) The position and maximum value of peak of dielectric constant ratio various with dielectric loss of constituent-2.

Case 2: When $\varepsilon'_1 = \varepsilon'_2$ & $tan\delta_1 \neq tan\delta_2 \neq 0$

This condition means the two materials have the same relative dielectric constant but have different dielectric loss. As shown in **Figure 2 (a)-(b)**, when the dielectric loss is very small, the maximum peak position of $\varepsilon'_s/\varepsilon'_1$ is very close to φ=0.5 and the value of $\varepsilon'_s/\varepsilon'_1$ is slight larger than 1. When dielectric loss is relative large, the value of $\varepsilon'_s/\varepsilon'_1$ increases, and if $tan\delta_1/tan\delta_2$ is very larger than 1 or very smaller than 1, the peak position will be far away from φ =0.5.

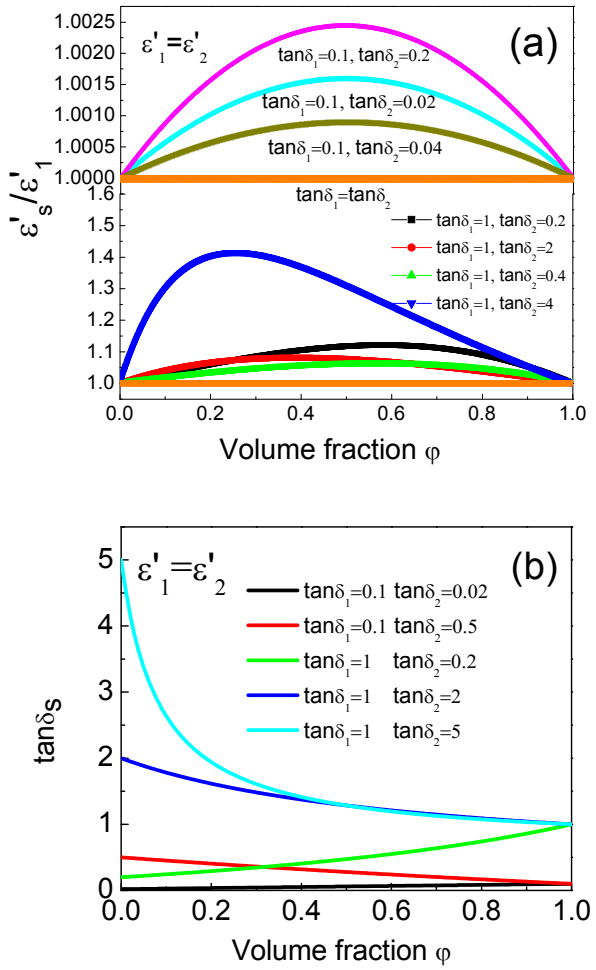

Figure 5-2. The dielectric properties of composites varies with vol% content for different dielectric constant and loss of constituent-1 and constituent-2 when $\varepsilon'_1 \neq \varepsilon'_2$: (a) effective dielectric constant of composite, (b) dielectric loss of composite.

Case 3: When $\varepsilon'_1 \neq \varepsilon'_2$ & $tan\delta_1 \neq tan\delta_2 \neq 0$

The equation for dielectric constant of composites is shown as

$$\varepsilon'_s = \varepsilon'_1\varepsilon'_2\left(\frac{\varphi[\varepsilon'_2(1+\tan^2\delta_2)-\varepsilon'_1(1+\tan^2\delta_1)]+\varepsilon'_1(1+\tan^2\delta_1)}{[\varepsilon'_1-\varphi(\varepsilon'_1-\varepsilon'_2)]^2+[\varepsilon'_1\tan\delta_1-\varphi(\varepsilon'_1\tan\delta_1-\varepsilon'_2\tan\delta_2)]^2}\right) \quad (5\text{-}9)$$

As discussed before, the dielectric constant of composites can be larger than each material when $\varepsilon'_1 = \varepsilon'_2$. If the matrix and filler have totally different dielectric constant and loss, the situation will be more complex. However, it is still easy to find that for certain parameters of ε'_1, ε'_2, $tan\delta_1$, $tan\delta_2$, x, one can find the conclusion:

$$\varepsilon'_{eff} > Max(\varepsilon'_1, \varepsilon'_2) \text{ and } \varepsilon'_{eff} > \varepsilon'_{series} \quad (5\text{-}10)$$

For the common case, it is very different to predict the peak value and position of $F(\varepsilon'_1, \varepsilon'_2, tan\delta_1, tan\delta_2, \varphi)$. In this section, 2 special cases are checked. Special Case I: If ε'_1=10, ε'_2=20, $tan\delta_1$=0.1, $tan\delta_2$=0.05, 0.1, 1, 3, 5, 10, 20 etc, it means the constituent-1 only has a low dielectric constant while the constituent-2 has higher dielectric constant. **Figure 5-3** shows the dielectric properties of composites under this condition: ε'_1=10, ε'_f=20, $tan\delta_1$=0.1: (a) ε'_s with φ, (b) $tan\delta_s$ with φ, (c) ε'_s with $tan\delta_2$ changes at different φ, and (d) $tan\delta_s$ with $tan\delta_2$ changes at different φ. The peak of ε'_s increases with increasing $tan\delta_2$ and the peak position shifts to high volume fraction which is very close to 1. If the ε'_f is very large (>100), the peak position is larger than 99%. In real dielectric-dielectric composites, the dielectric constant is very high and loss is lower than 1 for dielectrics, which results no peak is observed. For loss part, the $tan\delta_s$ increases with volume fraction and the value is between $tan\delta_1$ and $tan\delta_2$. However, as shown in **Figure 5-3 (d)**, at a fixed volume fraction, the $tan\delta_s$ increases then decreases with the $tan\delta_2$ increasing. From **Figure 5-3**, it is very

important to see that there is a way to prepare the composite with a higher dielectric constant but lower loss.

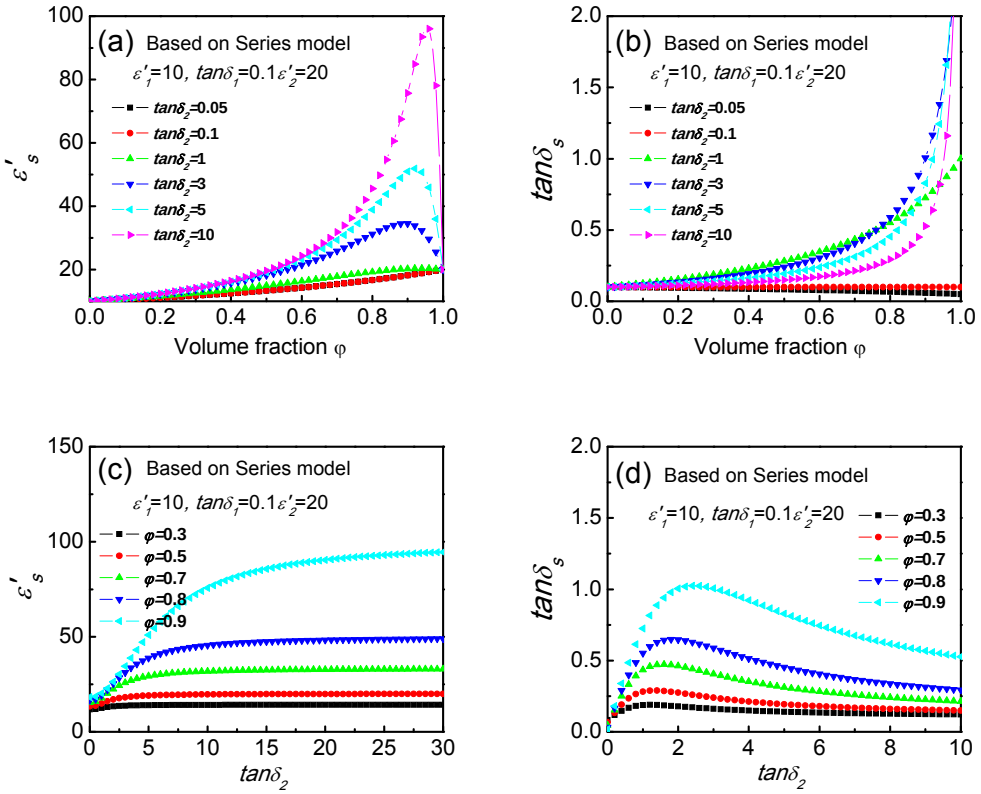

Figure 5-3. The dielectric properties of composites under this condition: ε'_1=10, ε'_f=20, $tan\delta_1$=0.1: (a) ε'_s with φ, (b) $tan\delta_s$ with φ, (c) ε'_s with $tan\delta_2$ changes at different φ, and (d) $tan\delta_s$ with $tan\delta_2$ changes at φ.

Special Case II: If ε'_1=10, ε'_2=1, $tan\delta_1$=0.1, $tan\delta_2$=0.05, 0.1, 1, 3, 5, 10, 20 etc. This means the matrix only has a low dielectric constant while the filler also has low dielectric constant but with large dielectric loss. This situation is about the same as the conductive-filler which has a larger dielectric loss introduced in polymer matrix. **Figure 5-4 (a)** shows the dielectric constant of composites various with φ different dielectric loss of constituent-2. At first, the $tan\delta_2$ increases from 0.1 to 3, the ε'_s decreases with the vol.% increasing because the ε'_2 *is* smaller than ε'_1. When the $tan\delta_2$

is larger than 3, the curve of ε'_s changes and the ε'_s will first increase then decrease. This is similar to the percolation theory describes the conductive-filler polymer-based composite. It is means the ε'_s cannot only be larger than $\varepsilon'_{parallel}$, but also larger than either ε'_1 or ε'_2. Compared with Special Case I, the peak position of ε'_s in Special Case I can start from very low volume fraction. The corresponding ε'_s of composite with $tan\delta_2$ increasing is shown in **Figure 5-4 (c)** It is much complex that the ε'_s increases in different curve. This case indicates that the dielectric loss of constituent-2 can have tremendous influence on the dielectric properties of final composite, and there is a way to prepare the composite with a higher dielectric constant but lower loss.

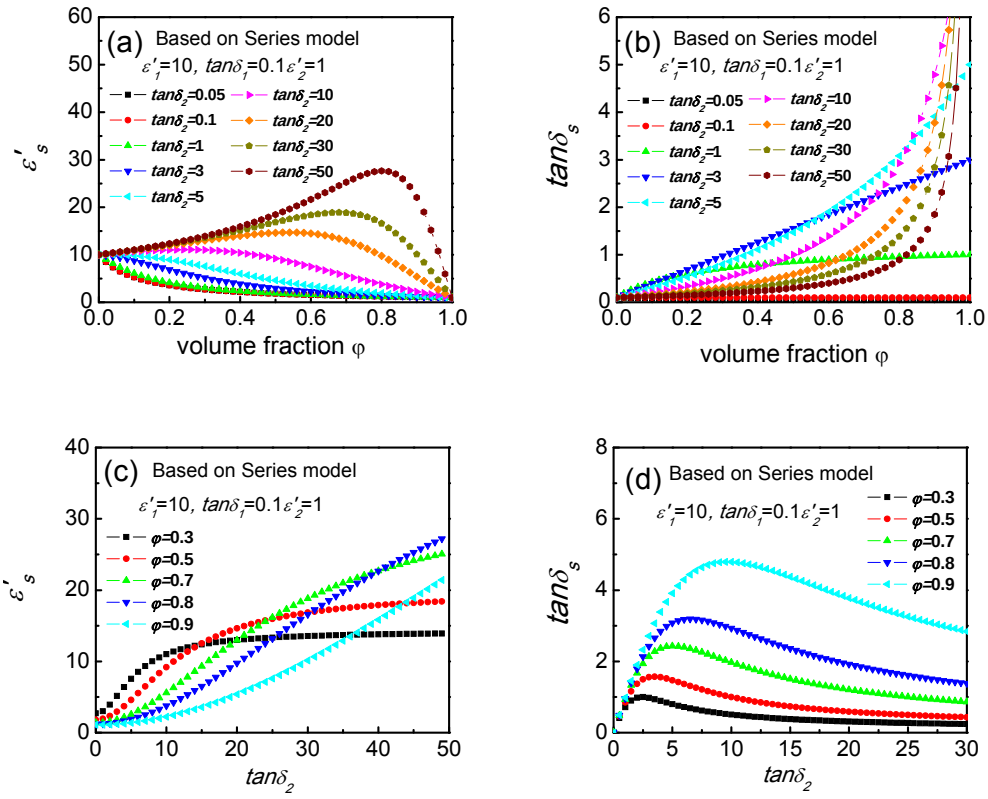

Figure 5-4. The dielectric properties of composites under this condition: ε'_1=10, ε'_2=1, $tan\delta_1$=0.1: (a) ε'_s with φ, (b) $tan\delta_s$ with φ, (c) ε'_s with $tan\delta_2$ changes at different φ, and (d) $tan\delta_s$ with $tan\delta_2$ changes at different φ.

5.3. The Maxwell-Wagner Model Introduced Dielectric Loss

The series model is too simple to express the dielectric properties vs. volume fraction of filler. As discussed before, the Maxwell-Wagner (also named as Maxwell-Garnett) mixing rule, which has been widely employed for calculation of the dielectric constant of 0-3 composites [7-9]. If filler particles are spherical in shape, as mentioned in Section 1.5.1, Maxwell-Wagner model is much better for further simulation. This rule is effective for infinite dilution of the dispersed phase. That is, the spherical filler particles are well separated by distances greater than their characteristic size. If filler particles are spherical in shape, the following equation is obtained for the effective dielectric constant of the composite,

$$\begin{aligned}\varepsilon_{eff} &= \varepsilon_m \frac{2\varepsilon_m + \varepsilon_f + 2\varphi(\varepsilon_f - \varepsilon_m)}{2\varepsilon_m + \varepsilon_f - \varphi(\varepsilon_f - \varepsilon_m)} \\ &= \varepsilon_m\left[1 + \frac{3\varphi(\varepsilon_f - \varepsilon_m)}{(2+\varphi)\varepsilon_m + (1-\varphi)\varepsilon_f}\right] = \varepsilon_m\left[1 + \frac{\varphi}{\varepsilon_m/(\varepsilon_f - \varepsilon_m) + (1-\varphi)/3}\right]\end{aligned} \tag{5-11}$$

If the $\varepsilon_m^{\,*} = \varepsilon'_m - i\varepsilon''_m = \varepsilon'_m(1 - i\tan\delta_m)$ and $\varepsilon_f^{\,*} = \varepsilon'_f - i\varepsilon''_f = \varepsilon'_f(1 - i\tan\delta_f)$ are used to replace ε_m and ε_s.

$$\begin{aligned}\varepsilon'_{eff} = {} & \frac{\left[(-2\varphi^2 - 2\varphi + 4)\varepsilon'^{\,3}_m + (4\varphi^2 + \varphi + 4)\varepsilon'^{\,2}_m\varepsilon'_f + (-2\varphi^2 + \varphi + 1)\varepsilon'_m\varepsilon'^{\,2}_f\right]}{\left[(2+\varphi)\varepsilon'_m + (1-\varphi)\varepsilon'_f\right]^2 + \left[(2+\varphi)\varepsilon''_m + (1-\varphi)\varepsilon''_f\right]^2} \\ & + \frac{\left[(-2\varphi^2 - 2\varphi + 4)\varepsilon'_m\varepsilon''^{\,2}_m + (4\varphi^2 + \varphi + 4)\varepsilon'_m\varepsilon''_m\varepsilon''_f + (-2\varphi^2 + \varphi + 1)\varepsilon'_m\varepsilon''^{\,2}_f\right] + 9\varphi(\varepsilon''^{\,2}_m\varepsilon'_f - \varepsilon'_m\varepsilon''_m\varepsilon''_f)}{\left[(2+\varphi)\varepsilon'_m + (1-\varphi)\varepsilon'_f\right]^2 + \left[(2+\varphi)\varepsilon''_m + (1-\varphi)\varepsilon''_f\right]^2}\end{aligned} \tag{5-12a}$$

$$\begin{aligned}\varepsilon''_{eff} = {} & \frac{\left[(-2\varphi^2 - 2\varphi + 4)\varepsilon''_m\varepsilon'^{\,2}_m + (4\varphi^2 + \varphi + 4)\varepsilon'_m\,\varepsilon'_f\varepsilon''_m + (-2\varphi^2 + \varphi + 1)\varepsilon'^{\,2}_f\varepsilon''_m\right]}{\left[(2+\varphi)\varepsilon'_m + (1-\varphi)\varepsilon'_f\right]^2 + \left[(2+\varphi)\varepsilon''_m + (1-\varphi)\varepsilon''_f\right]^2} \\ & + \frac{\left[(-2\varphi^2 - 2\varphi + 4)\varepsilon''^{\,3}_m + (4\varphi^2 + \varphi + 4)\varepsilon''^{\,2}_m\varepsilon''_f + (-2\varphi^2 + \varphi + 1)\varepsilon''_m\varepsilon''^{\,2}_f\right] - 9\varphi(\varepsilon'_m\varepsilon''_m\varepsilon'_f - \varepsilon'^{\,2}_m\varepsilon''_f)}{\left[(2+\varphi)\varepsilon'_m + (1-\varphi)\varepsilon'_f\right]^2 + \left[(2+\varphi)\varepsilon''_m + (1-\varphi)\varepsilon''_f\right]^2}\end{aligned} \tag{5-12b}$$

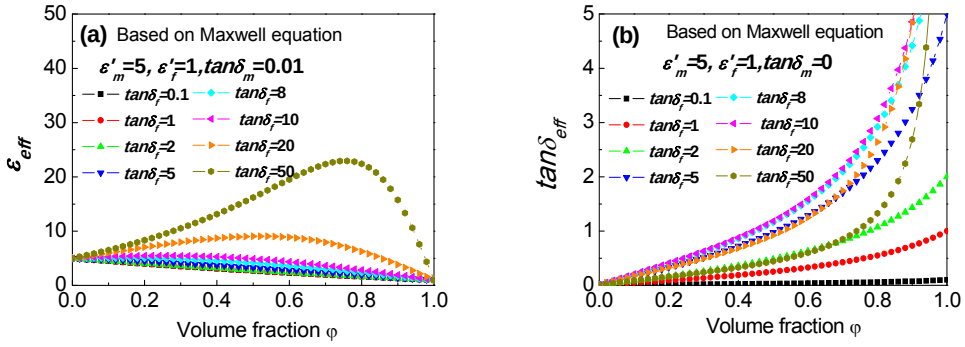

Figure 5-5. The dielectric constant of composites varies with vol.% content for different dielectric constant and loss of matrix and filler under this condition: ε'_m =5, ε'_f=1 & $tan\delta_m$=0.01, $tan\delta_f$=0.1, 1, 2, 5, 8, 10, 20 and 50: (a) effective dielectric constant of composite, (b) dielectric loss of composite.

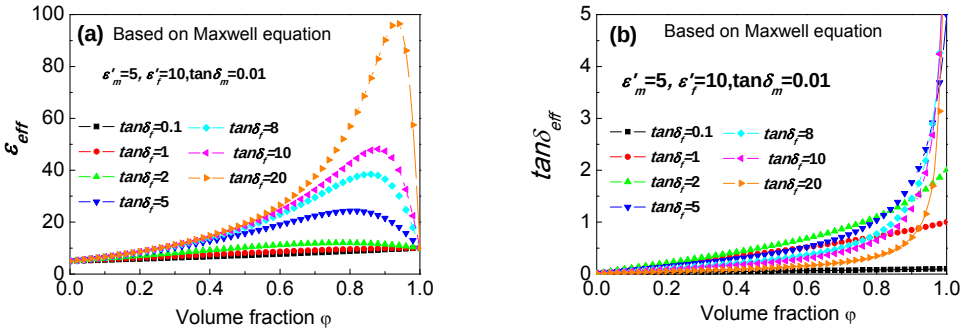

Figure 5-6. The dielectric properties of composites varies with vol.% content for different dielectric constant and loss of matrix and filler under this condition: ε'_m =5, ε'_f=10 & $tan\delta_m$=0.01, $tan\delta_f$=0.1, 1, 2, 5, 8, 10 and 20: (a) effective dielectric constant of composite, (b) dielectric loss of composite.

The result of simulation is similar to the simulation of series model. When ε'_m = ε'_f, if the dielectric loss of matrix and filler are taken into account, the dielectric constant of composite can be larger than the dielectric constant of matrix and filler, which is the same as series model. **Figure 5-5 and 5-6** show the dielectric constant of composites various with vol.% content for different dielectric constants and loss for the matrix and filler under this condition: ε'_m =5 ε'_f=1 or 10 & $tan\delta_m$=0.01, $tan\delta_f$=0.1, 1, 2, 5, 8, 10, 20 and 50. The results are similar to Series Model introduced the dielectric loss. If the dielectric loss of the filler is very larger that means the filler can

be considered as conducting filler, the dielectric constant of the composite is the similar to percolative behavior.

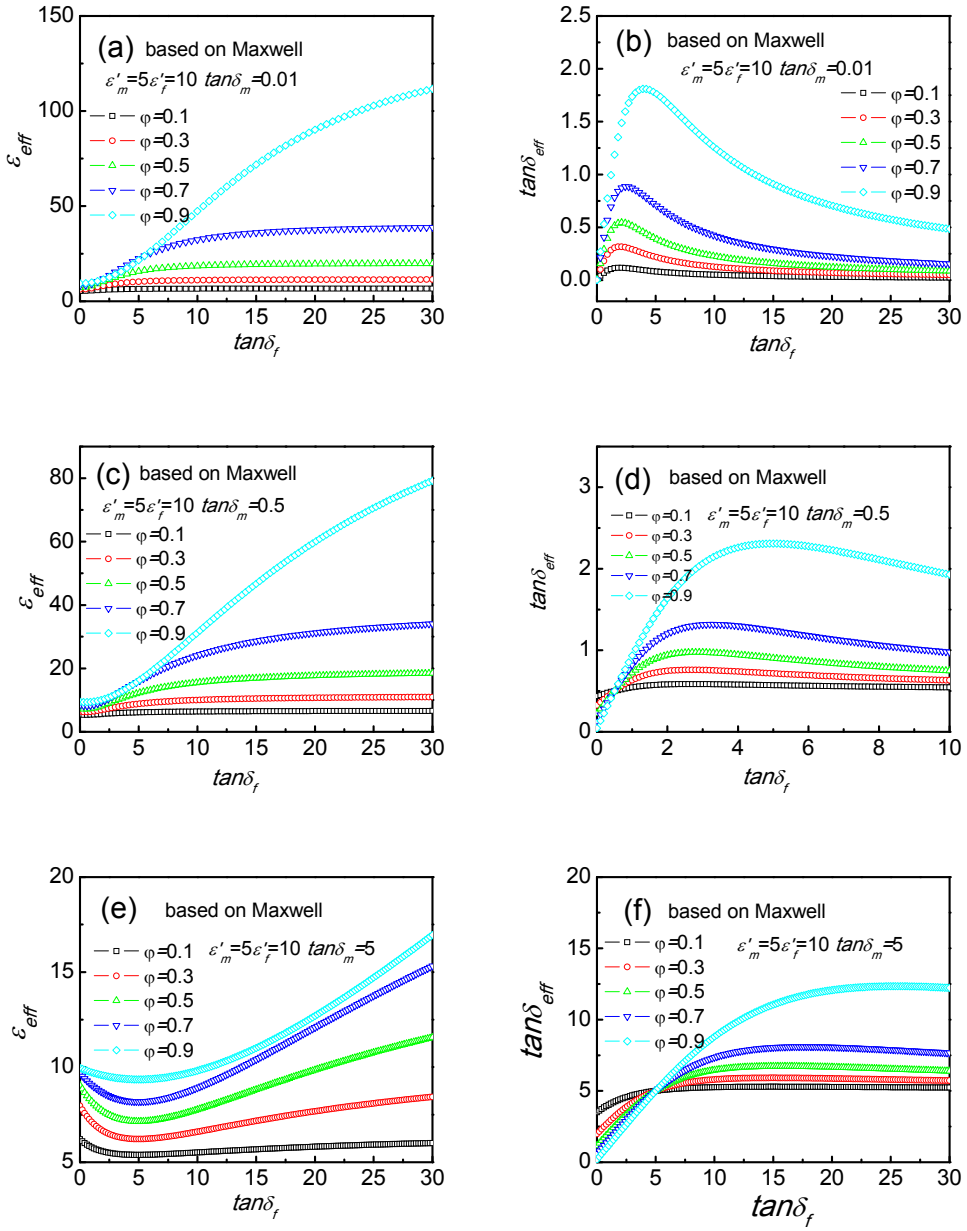

Figure 5-7. The dielectric properties of composites varies with $tan\delta_f$ under this condition: ε'_m =5 ε'_f=10, $tan\delta_f$=0.01, 0.05, 0.1, 0.5, 1, 5, 10 and 20: (a) and (b) $tan\delta_m$=0.01, (c) and (d) $tan\delta_m$=0.5, (e) and (f) $tan\delta_m$=5.

The effect of dielectric loss of filler and matrix on ε'_{eff} and $tan\delta_{eff}$ are shown in **Figure 5-7**. For ε'_{eff} part, the ε'_{eff} at different volume fractions of filler always

decreases first then increases with increasing $tan\delta_f$. The minimum point is the $tan\delta_m=tan\delta_f$. Compared **Figure 5-7 (a), (c)** and **(e)**, for the same $tan\delta_f$($tan\delta_m<tan\delta_f$), the value of ε'_{eff} decreases with increasing $tan\delta_m$. For loss part, when dielectric loss of matrix is small, the trend is similar to Series Model. The peak value of $tan\delta_{eff}$ increases with increasing $tan\delta_f$ and the peak position shifts to high $tan\delta_f$ with increasing volume fraction of filler. If the $tan\delta_m$ increases, there is a cross point in the figure for $tan\delta_{eff}$, which is the point that is the same as the minimum value of $tan\delta_{eff}$, that is, $tan\delta_m=tan\delta_f$.

5.4. The Logarithmic Model Introduced Dielectric Loss

Lichtenecker's logarithmic mixing model has been used in various literatures and generally considered as a quasi-empirical formula. Recently, Lichtenecker treated mixtures/composites using statistics as discussed in Section 1.5.1. If the dielectric loss of two phases is considered into Lichtenecker's logarithmic model, it can be written as,

$$\varepsilon_{eff} = \varepsilon_1^{\varphi_1} \cdot \varepsilon_2^{\varphi_2} \tag{5-13}$$

Then the complex dielectric constant can be expressed as,

$$\varepsilon_1^* = \varepsilon_1' - i\varepsilon_1'' = \varepsilon_1'(1 - i\tan\delta_1) = \frac{\varepsilon_1'}{\cos\delta_1}(\cos\delta_1 - i\sin\delta_1) = \frac{\varepsilon_1'}{\cos\delta_1}e^{-i\delta_1} \tag{5-14a}$$

$$\varepsilon_2^* = \varepsilon_2' - i\varepsilon_2'' = \varepsilon_2'(1 - i\tan\delta_2) = \frac{\varepsilon_2'}{\cos\delta_2}(\cos\delta_2 - i\sin\delta_2) = \frac{\varepsilon_2'}{\cos\delta_2}e^{-i\delta_2} \tag{5-14b}$$

$$\begin{aligned}\varepsilon_{eff}^* &= \left(\frac{\varepsilon_1'}{\cos\delta_1}e^{-i\delta_1}\right)^{\varphi} \cdot \left(\frac{\varepsilon_2'}{\cos\delta_2}e^{-i\delta_2}\right)^{1-\varphi} \\ &= \left(\frac{\varepsilon_1'}{\cos\delta_1}\right)^{\varphi} e^{-i\varphi\delta_1} \cdot \left(\frac{\varepsilon_2'}{\cos\delta_2}\right)^{1-\varphi} e^{-i(1-\varphi)\delta_2}\end{aligned} \tag{5-15}$$

$$\varepsilon'_{eff} = \left(\frac{\varepsilon'_1}{\cos\delta_1}\right)^{\varphi}\left(\frac{\varepsilon'_2}{\cos\delta_2}\right)^{1-\varphi}\cos[\varphi\delta_1 + (1-\varphi)\delta_2] \quad \text{(5-16a)}$$

$$\varepsilon''_{eff} = \left(\frac{\varepsilon'_1}{\cos\delta_1}\right)^{\varphi}\left(\frac{\varepsilon'_2}{\cos\delta_2}\right)^{1-\varphi}\sin[\varphi\delta_1 + (1-\varphi)\delta_2] \quad \text{(5-16b)}$$

$$\tan\delta_{eff} = \tan[\varphi\delta_1 + (1-\varphi)\delta_2] \quad \tan\delta_2 < \tan\delta_{eff} < \tan\delta_1 (\text{if} \tan\delta_2 < \tan\delta_1) \quad \text{(5-16c)}$$

Eq.(5-16) shows the real and imaginary parts of dielectric constant, and the dielectric loss for Lichtenecker's logarithmic model. From Eq.(5-16c), the loss has some contribution to ε'_{eff} but the ε'_1 and ε'_2 do not have any contribution to the $tan\delta_{eff}$, which is different from the Series and Maxwell-Wagner models.

The dielectric properties of composites various with φ for different dielectric constant and loss of two constituents under different conditions are shown in **Figure 5-8 and 5-9**. Similar to the Series and Maxwell-Wagner model, the dielectric constant of composites first increases then decreases with volume fraction. With the loss of constituent-1 increases from 0.05 to 1, the peak value of dielectric constant decreases. For loss part, since the dielectric constant cannot have effect on loss of composite, the **Figure 5-8(b)**, **(d)** and **(f)** are very similar.

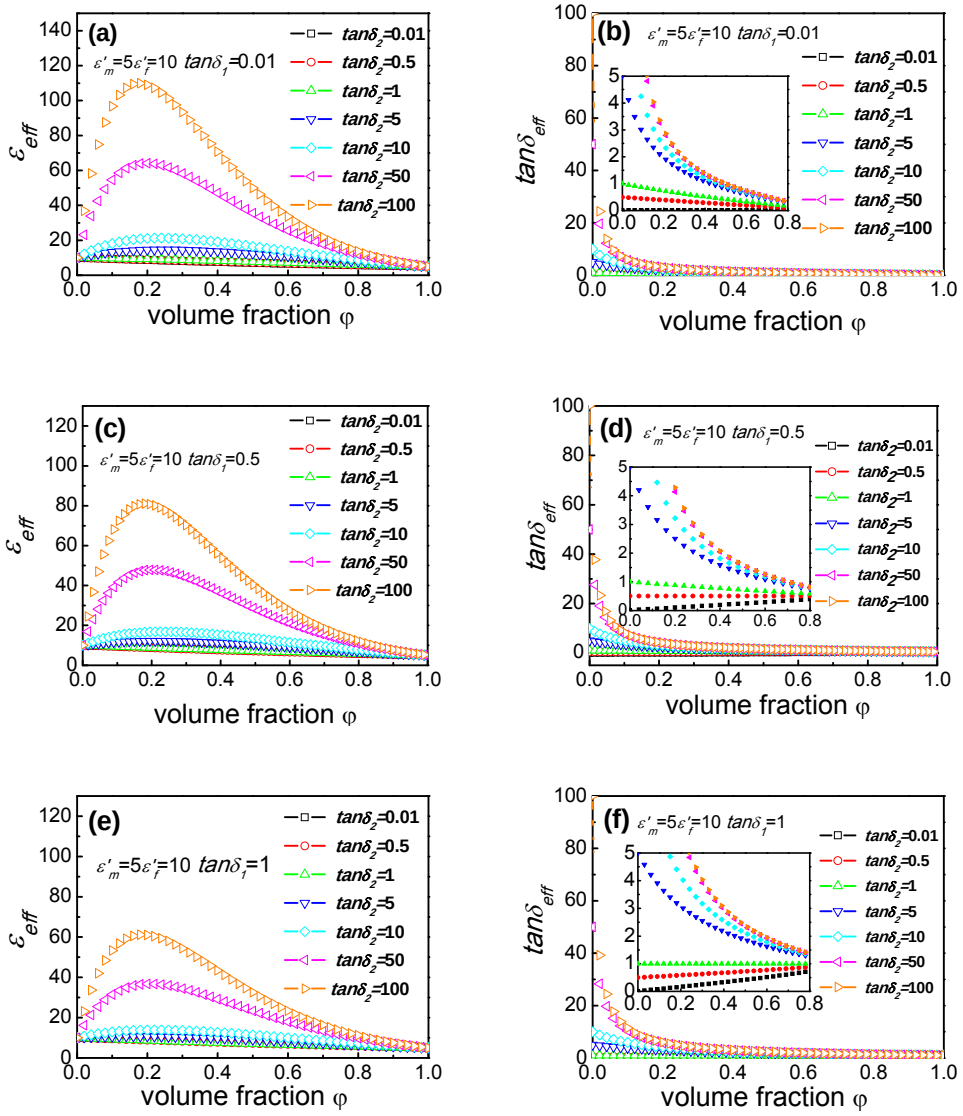

Figure 5-8. The dielectric properties of composites varies with vol.% content for different dielectric constant and loss of matrix and filler under this condition: $\varepsilon'_1=5$ $\varepsilon'_2=10$& $tan\delta_2$=0.01, 0.5, 1, 5, 10, 50 and 100: (a) and (b) $tan\delta_1$=0.01, (c) and (d) $tan\delta_1$=0.5, (e) and (f) $tan\delta_1$=1.

Compared to Series and Maxwell model, the Lichtenecker's logarithmic model is relatively simple. At each volume fraction, the dielectric constant ε'_{eff} and $tan\delta_{eff}$ always increase with the $tan\delta_2$ increasing, as shown in **Figure 5-8**. For conducting filler concern, as shown in **Figure 5-10**, the peak position also can start from very low

volume fraction. When the $tan\delta_2$ is high, close to 100, the peak position is still around 60 vol.%.

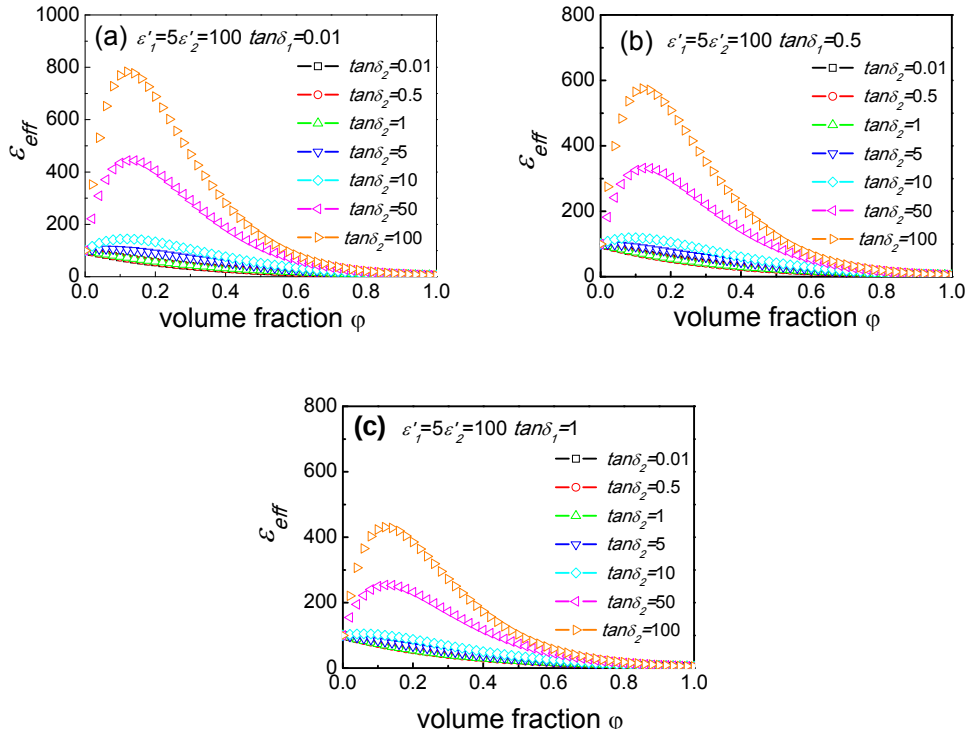

Figure 5-9. The dielectric constant of composites varies with φ for different dielectric constant and loss of matrix and filler under this condition: ε'_1=5 ε'_2=100& $tan\delta_2$=0.01, 0.5, 1, 5, 10, 50 and 100: (a) $tan\delta_1$=0.01, (b) $tan\delta_1$=0.5, (c) $tan\delta_1$=1.

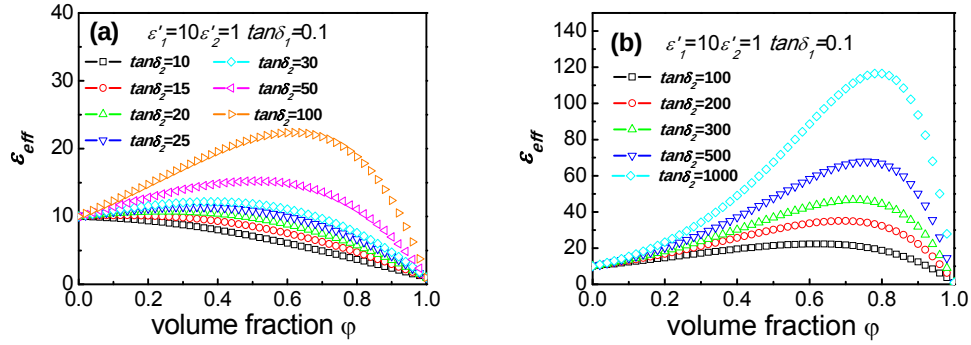

Figure 5-10. The dielectric constant of composites varies with φ for different dielectric constant and loss of matrix and filler under this condition: ε'_1=10, ε'_2=1, $tan\delta_1$=0.1and different $tan\delta_2$: (a) $tan\delta_2$=10 to 100, (b) $tan\delta_2$=100 to 1000.

5.5. The Maxwell-Wagner Model Introduced Conductivity

If the dielectric loss is considered, a composite can have a higher dielectric constant than the dielectric constant of both constituents. This would break the Wiener limits, Eq. (1-34). However, we currently believe that the dielectric loss of a composite is between the dielectric losses of two constituents. The above discussion is based on ideal dielectrics where the conductivity is zero. Actually, all dielectrics have a nonzero conductivity.

It is well known that for a homogenous dielectric the conductivity σ contributes to the measured imaginary part of the complex relative permittivity as

$$\varepsilon''_{con} = \frac{\sigma}{\varepsilon_0 \cdot \omega} \tag{5-17}$$

where ε_0 and ω are the permittivity of vacuum and the angular frequency. Therefore, the experimentally measured dielectric loss in a dielectric actually has two parts: one is the real dielectric loss (the imaginary part of the permittivity) and another is due to the electrical conductivity. For a composite, the conductivity of its constituents would make the dielectric response of a composite much more complicated. For a composite under an electric field, the electric field is not uniform and its distribution is dependent on the dielectric property of each constituent. An electric current is induced in each constituent due to the electrical conductivity. The difference in the current density between two constituents would result in a charge accumulation around the boundary between the two constituents. The charge accumulation would redistribute the electric field in the composite, which would change the current density in each constituent. Here, the electrical conductivity of each constituent is considered and the

influence of their conductivities on the ε'_{eff} is studied using Maxwell model.

5.5.1. Conductivity Introduced for Special Case: ε''_m=0

If ε''_m=0, the Eq.(5-16) can be simplified as below:

$$\varepsilon'_{eff}=\frac{\left[(-2\varphi^2-2\varphi+4)\varepsilon_m'^3+(4\varphi^2+\varphi+4)\varepsilon_m'^2\varepsilon_f'+(-2\varphi^2+\varphi+1)\varepsilon_m'\varepsilon_f'^2\right]+\left[+(-2\varphi^2+\varphi+1)\varepsilon_m'\varepsilon_f''^2\right]}{\left[(\varphi^2+4\varphi+4)\varepsilon_m'^2+(-2\varphi^2-2\varphi+4)\varepsilon_m'\varepsilon_f'+(\varphi^2-2\varphi+1)\varepsilon_f'^2\right]+\left[(\varphi^2-2\varphi+1)\varepsilon_f''^2\right]} \quad (5\text{-}18a)$$

$$\varepsilon''_{eff}=\frac{9\varphi\varepsilon_m'^2\varepsilon_f''}{\left[(\varphi^2+4\varphi+4)\varepsilon_m'^2+(-2\varphi^2-2\varphi+4)\varepsilon_m'\varepsilon_f'+(\varphi^2-2\varphi+1)\varepsilon_f'^2\right]+(\varphi^2-2\varphi+1)\varepsilon_f''^2} \quad (5\text{-}18b)$$

The imaginary part of filler can be expressed as:

$$\varepsilon''_f=\frac{\sigma_f}{\varepsilon_0\omega}=\frac{\lambda_f}{\omega} \text{ and } \lambda_f=\frac{\sigma_f}{\varepsilon_0} \quad (5\text{-}19)$$

Then the complex equation can be rewritten as the form of Debye Equation:

$$\varepsilon'(\omega)=\varepsilon_\infty+\frac{\varepsilon_s-\varepsilon_\infty}{1+(\omega\tau)^2}=\varepsilon'_m\frac{2(1-\varphi)\varepsilon'_m+(2\varphi+1)\varepsilon'_f}{(2+\varphi)\varepsilon'_m+(1-\varphi)\varepsilon'_f}-\frac{\frac{(2\varphi+1)\varepsilon'_m}{(1-\varphi)}-\varepsilon'_m\frac{2(1-\varphi)\varepsilon'_m+(2\varphi+1)\varepsilon'_f}{(2+\varphi)\varepsilon'_m+(1-\varphi)\varepsilon'_f}}{1+(\frac{\omega\left[(2+\varphi)\varepsilon'_m+(1-\varphi)\varepsilon'_f\right]}{(1-\varphi)\lambda})^2} \quad (5\text{-}20a)$$

$$\varepsilon''(\omega)=\frac{(\varepsilon_s-\varepsilon_\infty)\omega\tau}{1+(\omega\tau)^2}=\frac{\left[\frac{(2\varphi+1)\varepsilon'_m}{(1-\varphi)}-\varepsilon'_m\frac{2(1-\varphi)\varepsilon'_m+(2\varphi+1)\varepsilon'_f}{(2+\varphi)\varepsilon'_m+(1-\varphi)\varepsilon'_f}\right]\frac{\left[(2+\varphi)\varepsilon'_m+(1-\varphi)\varepsilon'_f\right]}{(1-\varphi)\lambda}\omega}{1+(\frac{\omega\left[(2+\varphi)\varepsilon'_m+(1-\varphi)\varepsilon'_f\right]}{(1-\varphi)\lambda})^2} \quad (5\text{-}20b)$$

$$\varepsilon_\infty==\varepsilon'_m\frac{2(1-\varphi)\varepsilon'_m+(2\varphi+1)\varepsilon'_f}{(2+\varphi)\varepsilon'_m+(1-\varphi)\varepsilon'_f}$$

$$\varepsilon_s==\frac{(2\varphi+1)\varepsilon'_m}{(1-\varphi)} \quad (5\text{-}20c)$$

$$\tau=\frac{(2+\varphi)\varepsilon'_m+(1-\varphi)\varepsilon'_f}{(1-\varphi)\lambda}$$

Under this condition, we can check different volume fractions and how it effects on the dielectric properties of the composites. **Figure 5-11** shows parameters from Eq. (5-20c) change with volume fraction of filler. ε_∞ is the Maxwell equation (Eq.(1-45)) and the plot with different ε'_f is shown in **Figure 5-11(a)**. The ε_∞ is only related to the ε'_m and increases slowly before φ=0.8 then fast at higher volume fractions. The τ is much more complex because both of ε'_f and λ can effect on the value of τ. As shown in **Figure 5-11(c)** and **(d)**, the τ always increases with increasing φ. With different ε'_f, the τ varies slightly difference at low φ. For a certain volume fraction, if λ=10^3, 10^4 and10^5. φ=0.6, the curve can be expresses as Debye Equation as shown in **Figure 5-12**.

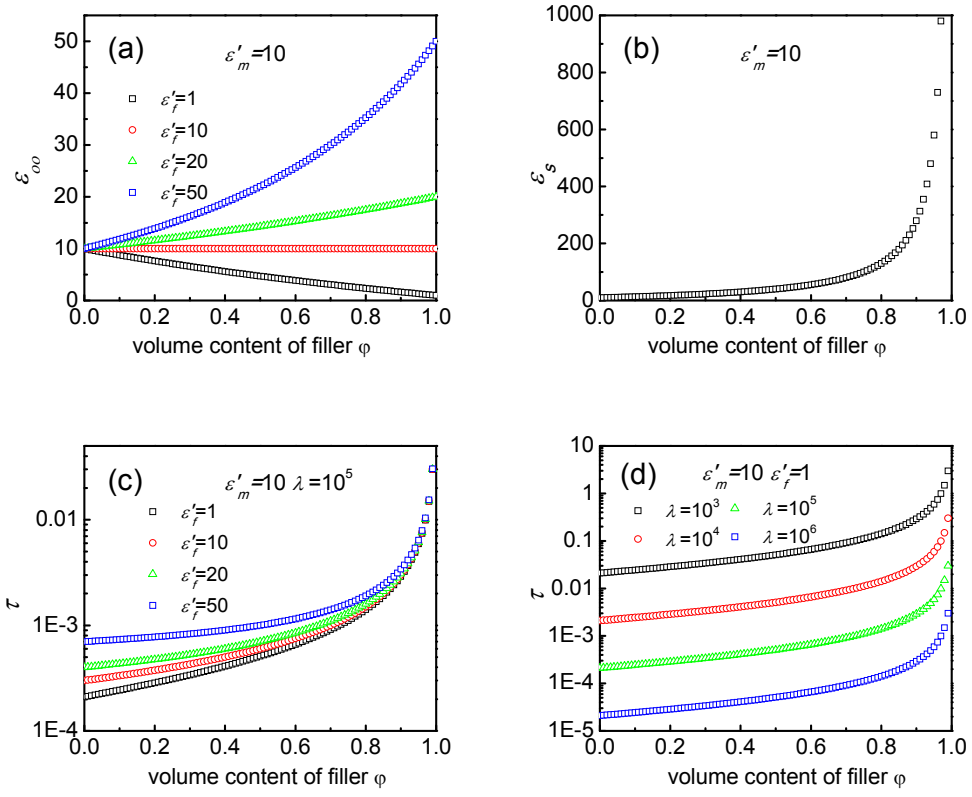

Figure 5-11. Parameters from Eq. (5-20c) change with volume fraction of filler: (a) ε_∞, (b) ε_s, (c) τ with different ε'_f, and (d) τ with different λ.

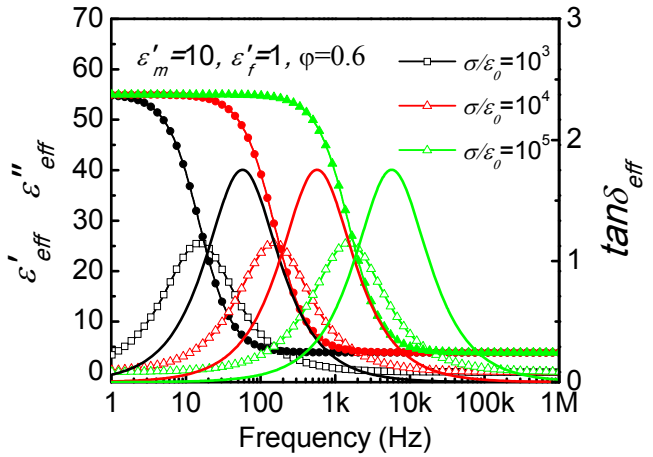

Figure 5-12. Simulation of conductivity introduced for special case: ε'_m=10, $\lambda=10^3$, 10^4 and10^5, φ=0.6. (Solid, open and solid line are real part, imaginary part and loss of dielectric properties).

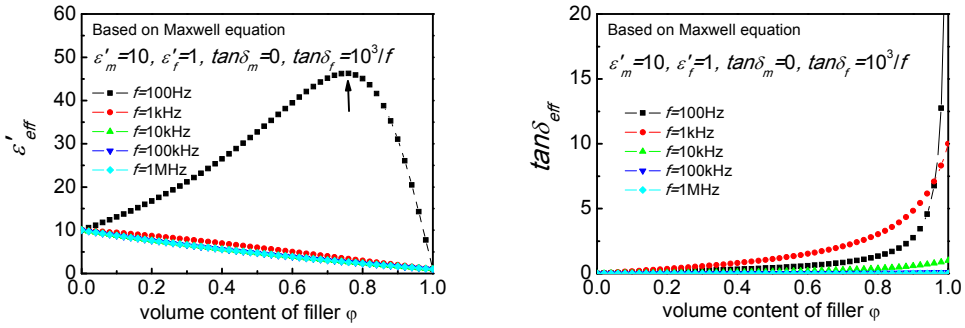

Figure 5-13. Simulation of conductivity introduced for special case: ε'_m=10, ε'_f=1, $\lambda=10^3$, with different frequency.

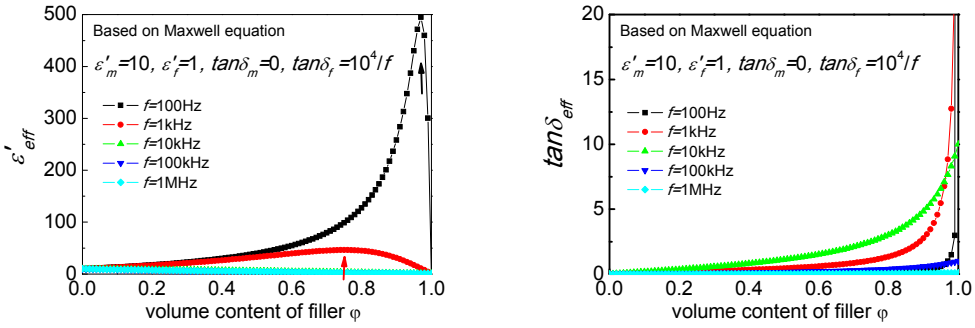

Figure 5-14. Simulation of conductivity introduced for special case: ε'_m=10, ε'_f=1, $\lambda=10^4$, with different frequency.

The dielectric properties vs. volume fraction under these conditions are also

checked and shown in **Figure 5-13** and **5-14**. There is a peak showing maximum value of ε'_{eff}, as marked by the arrow. It is clear that the dielectric properties are strongly dependent on frequency, especially at low frequency.

5.5.2. Nonideal Dielectric Material of Matrix and Filler

For the general case, the matrix and filler are both non-ideal dielectric material which means the high conductivity of the filler and matrix are introduced in the Maxwell model. A special case is presented for study. It is assumed $\lambda_m = \frac{\sigma_m}{\varepsilon_0} = 10$ and $\lambda_f = \frac{\sigma_f}{\varepsilon_0} = 10^5$. As shown in **Figure 5-15**, the curve of real, imaginary and loss of composite are similar as **Figure 5-12** at high frequencies. The only difference between both cases is in low frequency. The loss of composites is very high due to the loss of the matrix. As shown in **Figure 6-16 (b)**, the loss at 1 Hz is almost the same as the value of the relaxation peak when the σ_m is very small (λ=10).

The conductivity of the matrix and filler both have a much larger effect on the dielectric constant and loss. As shown in **Figure 5-16** and **Figure 5-17**, the dielectric constant of the matrix and filler are fixed. With the conductivity of the filler increasing, the relaxation peaks of composites shifts to high frequencies. With the conductivity of matrix increasing, the relaxation peaks of composites do not shift, only effects on low frequencies. When λ_m is close to λ_f, the relaxation peaks disappear.

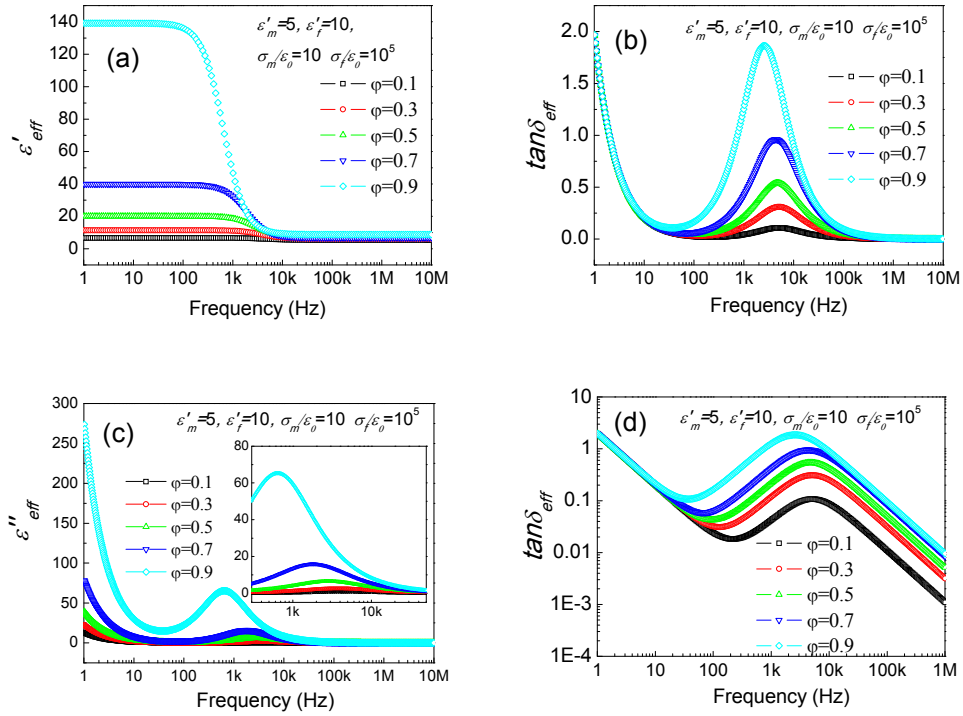

Figure 5-15. Simulation of conductivity introduced for special case: ε'_m=5, ε'_f=10 λ_m=10^5, λ_f=10^5, φ =0.1, 0.3, 0.5, 0.7 and 0.9: (a) real part, (b) loss, (c) imaginary part and (d) loss in log-log scale.

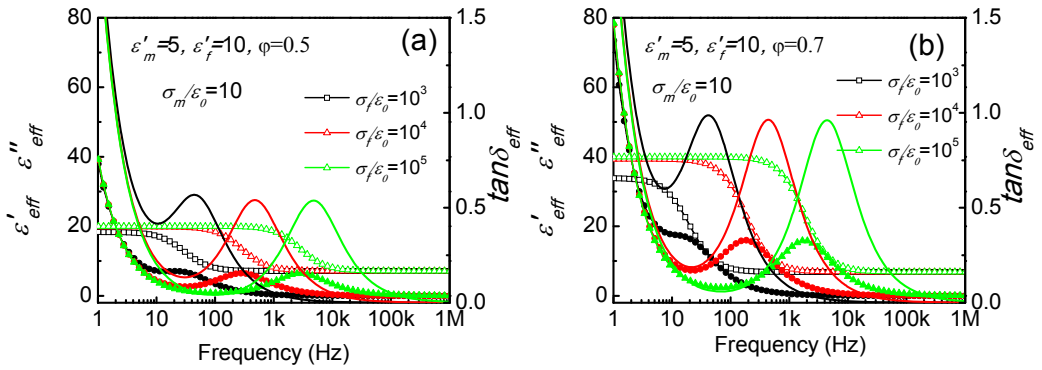

Figure 5-16. Simulation of conductivity introduced for special case: ε'_m=5, ε'_f=10, λ_m=10, λ_f=10^3,10^4 and10^5, (a) φ=0.5 and (b) φ=0.7 (Solid, open and solid line are real part, imaginary part and loss of dielectric properties).

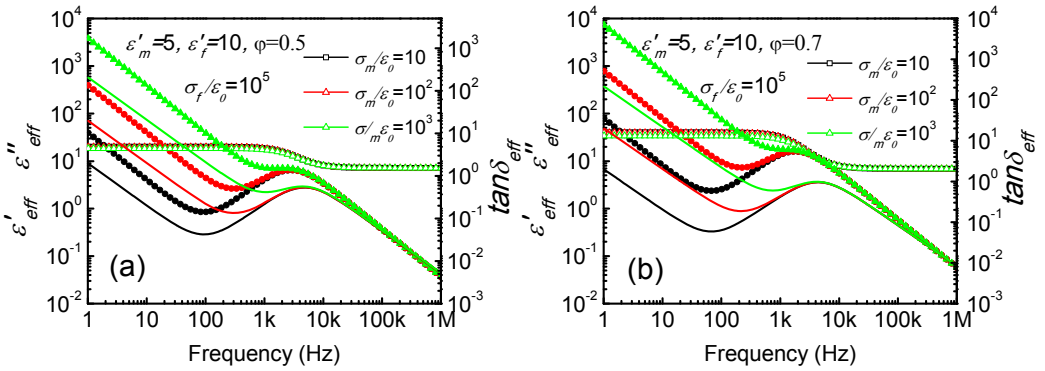

Figure 5-17. Simulation of conductivity introduced for special case: ε'_m=5, ε'_f=10, λ_f=10^5, λ_m=10,10^2 and10^3, (a) φ=0.5 and (b) φ=0.7 (Solid, open and solid line are real part, imaginary part and loss of dielectric properties).

5.6. Conclusions

In this chapter, the dielectric loss including the electrical conductivity of each constituent in a composite is considered. The influence of the loss on the ε'_{eff} is examined using three models, which corresponding three types of microstructure of the composite. The following conclusions are obtained:

1. The difference in the dielectric loss of the constituent had a strong influence on ε'_{eff}, which makes the ε'_{eff} higher than the results without considering loss. The contribution of the loss to the ε'_{eff} is dependent on the microstructure of the composite (i.e. the model used in the simulation).
2. Based on the Series and Maxwell model, if the loss difference is high enough, there is a maximum peak obtained in the filler content which is dependent on the ε'_{eff}. If the difference in the loss is zero, the ε'_{eff} is the same as the classic model and the loss of the composite is the same as the loss of its constituents. If the loss if different, as the loss difference increases, the loss of the

composite increases initially and then decreases, while the ε'_{eff} increases monotonically. That is, if the loss difference is high, a composite with a higher ε'_{eff} and a lower loss can be obtained. In other words, the loss of the composite does not change with the filler content monotonically if the loss difference is high. It is also found that the loss of the composite cannot be higher than loss of the constituent with a higher loss, and cannot be smaller/lower than the loss of the constituent with a lower loss.

$$\varepsilon'_{eff} > Max(\varepsilon'_1, \varepsilon'_2) \quad \text{and} \quad \varepsilon'_{eff} > \varepsilon'_{series} \tag{5-21}$$

$$Min(\tan\delta_1, \tan\delta_2) < \tan\delta_{eff} < Max(\tan\delta_1, \tan\delta_2) \tag{5-22}$$

3. Based on Lichtenecker's logarithmic model, if the loss difference is high, again a maximum peak is observed in the relationship between ε'_{eff} and filler content. However, the loss of the composite changes with the filler content monotonically.
4. The conductivity of matrix and filler both have a large effect on the dielectric constant and loss. In certain composite, the relaxation peak shifts to low frequency with the content of filler increasing. With the conductivity of filler increasing, the relaxation peaks of composites shifts to high frequency. With the conductivity of matrix increasing, the relaxation peaks of composites do not shift and only effects on low frequency.

References of Chapter 5

1. W. Jillek and W. K. C. Yung, *Int. Adv. J. Manuf. Technol.* **25**, 350(2005).

2. J. R. Yoon, J. W. Han, K. M. Lee and H. Y. Lee,Trans. *Electr. Electron. Mater.* **10**, 116 (2009).

3. M. T. Sebastian and H. Jantunen, *Int. J. Appl. Ceram. Technol.* **7**, 415(2010).

4. L. Zhang and Z.-Y. Cheng, *J. Adv. Dielectr*. **1** 389(2011).

5. Z. M. Dang, J. K. Yuan, J. W. Zha, T. Zhou, S. T. Li and G. H. Hu, *Prog. Mater. Sci.* **57**, 660(2012).

6. C. W. Nan, Y. Shen and J. Ma, *Annu. Rev. Mater. Res*. **40**, 131(2010).

7. B. K. P. Scape, *Principles of Dielectrics* (Clarendon Press, Oxford, 1989).

8. J. C. Maxwell, *Electricity and Magnetism* (Clarendon Press, Oxford, 1892).

9. K. W. Wagner, Die *Isolierstoffe der Elektrotechnik*, ed. H. Schering, Vol. 1 (Springer, Berlin, 1924) (in German).

CHAPTER 6

Conclusions and Future Work

6.1. Conclusions

1. Composites based on nano Ni particles and copolymers were prepared by solution casting and hot-pressed processing. Uniform dispersion of nanoparticles in nanocomposite materials was achieved by improvement of the processing conditions. By solution casting and hot-pressed processing, high percolation threshold (φ_c>50 vol.%) was achieved in both systems. Dielectric constant more than 1000 were obtained in both Ni-P(VDF-TrFE) and Ni-P(VDF-CTFE) systems. Compared to the composites with low percolation threshold, composites with high percolation threshold had a wider volume fraction range of the percolation threshold concentration, making the material reproducible for practical applications.
2. All-organic dielectric composites, PPy-P(VDF-TrFE) and PPy-P(VDF-CTFE) systems, based on PPy nanoclips were prepared by solution casting and hot-pressed processing. Low percolation threshold (φ_c<8 wt.%) were achieved in both systems. These composites with low percolation threshold only needed very small amount filler and the composites are still flexible. Dielectric constant of more than 1000 was got in PPy-P(VDF-TrFE). The dielectric constant of a composite with 8 wt.% was more than 100 times higher than that of the P(VDF-TrFE)70/30 matrix. There were two main differences between

the two composites, which have much effect on percolation behavior. First, the dielectric constant or $\varepsilon_{eff}/\varepsilon_m$ of PPy-P(VDF-TrFE) was much higher than PPy-P(VDF-CTFE). Second, there were strong relaxation behaviors in PPy-P(VDF-TrFE) composites. From 1 kHz to 100 kHz, the dielectric constant decreased with frequency dramatically.

3. In both conductor-polymer composites, the new dielectric process observed in the composites was a relaxation process with a very low relaxation frequency. There were three mechanisms in this conductor-polymer composite: 1) the dielectric relaxation process from the polymer matrix, 2) the new dielectric relaxation process from the composite, and 3) the conductivity of the conducting filler.
4. Percolation theory in these composites was investigated. It was noted that the percolation threshold and critical value were dependent on the selected frequency and temperature. In order to further study the percolation behavior, six systems of conductor-polymer composites, which were reported in literature, were studied based on the percolation theory. The φ_c and s were dependent on frequency. The different selected data have strong effect on the φ_c and s. The φ_c and s also had a relationship with the shape of filler. The change of φ_c and s of the composite with sphere-like filler were less than that with fibers or tubes. High length-to-width ratios may have caused large differences in φ_c and s with frequency.

5. In the last part, the dielectric loss (or conductivity) was used to explain the mechanism behind the dielectric properties of conductor-dielectric composites. Based on the Series and Maxwell models, if the loss difference was high enough, there would be a maximum peak obtained in the filler content dependent on the ε'_{eff}. A composite with a higher ε'_{eff} and a lower loss can be obtained. It was also found that the loss of the composite cannot be higher than the loss of the constituent with a higher loss, and could not be smaller/lower than the loss of the constituent with a lower loss. Based on Lichtenecker's logarithmic model, if the loss difference was high, again a maximum peak was observed in the relationship between ε'_{eff} and filler content. However, the loss of the composite changed with the filler content monotonically. The conductivity of matrix and filler both had a large effect on the dielectric constant and loss. In certain composites, the relaxation peak shifts to low frequency with increasing the content of filler. With increasing the conductivity of filler, the relaxation peaks of the composites shifted to high frequencies. With increasing the conductivity of the matrix, the relaxation peaks of the composites did not shift, only effected on low frequencies.

6.2. Future Work

1. The conductor-dielectric composites exhibited a high dielectric constant when the filler concentration was close to the percolation threshold, which resulted in the composites having a high dielectric loss and a low E_b. Investigating

approaches for increasing the E_b and reducing the dielectric loss in conductor-dielectric composites would be interesting.

2. The shape and size of filler have strong influence on dielectric properties and percolation behavior. Also the core-shell particles show some promises and further research is needed. The thickness of the shell layer has to be optimized based on the desired dielectric constant and loss.
3. The creation of model to explain both the dielectric-dielectric composite and conductor-dielectric composite is a challenge, but a worthwhile pursuit to fully understanding the mechanisms occurring in dielectric composites.